RESOURCE OPTIMIZATION IN COOPERATIVE NOMA-BASED 5G SYSTEMS WITH CONSIDERATION OF COGNITIVE RADIO AND SECURITY

———

DISSERTATION

for the Degree of

DOCTOR OF PHILOSOPHY
(Electrical Engineering)

———

CARLA ESTEFANÍA GARCÍA MORETA

MAY 2023

Resource Optimization in Cooperative NOMA-based 5G Systems with consideration of Cognitive Radio and Security

DISSERTATION

Submitted in Partial Fulfillment
of the Requirements for the
Degree of

DOCTOR OF PHILOSOPHY
(Electrical Engineering)

at the

UNIVERSITY OF ULSAN

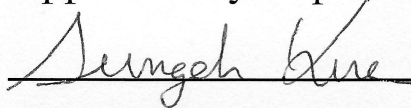by

Carla Estefanía García Moreta
May 2023

Publication No._____

Resource Optimization in Cooperative NOMA-based 5G Systems with consideration of Cognitive Radio and Security

Approved by Supervisory Committee:

_____

Prof. Sungoh Kwon, Chair

_____
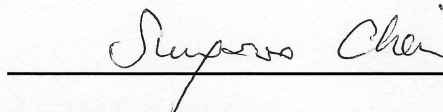
Prof. In-Soo Koo, Supervisor

_____

Prof. Hee-Youl Kwak

_____

Dr. Chiho Lee

_____

Dr. Sungsoo Choi

Department of Electrical, Electronic and Computer Engineering
University of Ulsan, South Korea
Date: May, 2023

VITA

Carla Estefanía García Moreta was born in Quito, Ecuador. She received the B.E in Electronics and Telecommunication Engineering from the Escuela Politécnica Nacional (EPN), Quito, Ecuador, in 2016. She received the M.S. degree in Electrical Engineering from the University of Ulsan, Ulsan, South Korea, in 2020.

Since 2020, she is pursuing her Ph.D. degree from the University of Ulsan, South Korea, under the guidance of Professor In-Soo Koo. Her current research interests include artificial intelligence, machine learning, optimizations, wireless security and multi-antenna communications.

Dedicated to my beloved parents,

Silvia Moreta and Nelson García

ACKNOWLEDGMENTS

ABSTRACT
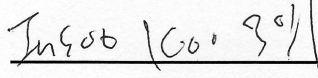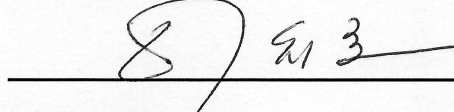
Resource Optimization in Cooperative NOMA-based 5G Systems with consideration of Cognitive Radio and Security

by

Carla Estefanía García Moreta

Supervisor: Prof. In-Soo Koo

Submitted in Partial Fulfillment of the Requirements for the Degree of

Doctor of Philosophy (Electrical Engineering)

May 2023

Currently, the deployment of fifth-generation (5G) networks is underway in numerous countries and regions, and it is expected to bring about a new era of innovation and connectivity in the upcoming years. However, to satisfy the increasing demands for high data speed, minimal delay, and pervasive computing in 5G and future wireless communication technologies, there is a critical request for advanced communication system design. In particular, the primary challenge is the efficient assignment of resources, which refers to managing limited quantities such as bandwidth, power, and time in wireless communications. Furthermore, advancements in technologies accompany the progress of wireless communication systems to enable faster data transfer rates, lower latency, and more effective use of network resources. Based on the above observations, this thesis explores and investigates efficient resource allocation strategies for promising 5G and beyond 5G candidate technologies in terms of non-orthogonal multiple access (NOMA), beamforming, and mobile edge computing (MEC). To further enhance the throughput and extend the coverage of the 5G networks, in this thesis, we utilize collaborative communication techniques including relay selection, cognitive radio (CR), and power allocation schemes.

In addition, to address the problem of limited battery life in energy-constrained wireless devices, energy harvesting (EH) techniques from ambient radio frequency (RF) signals have emerged as a promising solution. EH techniques provide a sustainable and eco-friendly manner to power devices, especially in remote locations where traditional power sources may not be available. In this respect, simultaneous wireless information and power transfer (SWIPT) offers another option in EH methods since it enables simultaneously both RF EH and information decoding for the user, utilizing the same RF signal. Moreover, SWIPT eliminates the need for separate power and data transmission systems, which reduces the complexity and cost of the overall system. Motivated by the benefits mentioned above, SWIPT, linear and non-linear EH models are part of the wireless network designs studied in this dissertation. Despite the potential of cooperative communications in NOMA systems along with CR and SWIPT technologies to meet the requirements of 5G networks, ensuring wireless security remains a significant challenge. In wireless transmission environments, confidential information is particularly at risk of being intercepted by eavesdroppers. Although industry and academia have proposed cryptographic encryption and decryption methods to overcome this issue, these techniques rely heavily on complex decoding/encoding algorithms and encryption key management, which require significant computing power and resource consumption. Furthermore, these complex algorithms can be compromised, as eavesdroppers nowadays have access to high computational power. Therefore, this thesis proposes an alternative approach to conventional security techniques by utilizing physical layer security (PLS) in our systems, which takes advantage of the characteristics of wireless channels. PLS provides security regardless of the computing ability of the communication equipment even if the eavesdropper has strong computing capability. Furthermore, resource allocation optimization is a crucial task in 5G networks, which aims to maximize the utilization of network resources while meeting the quality of service (QoS) requirements of the users. Nevertheless, resource allocation optimization is a complex problem, and solving it can be computationally intensive. Therefore, reducing computational complexity is an important

research field in wireless communications that brings several benefits. For instance, simplifying computational complexity ensures data is processed faster, preventing delays and ensuring smooth communication. Moreover, as the number of users in wireless communication systems increases, so does the computational load. By reducing the computational complexity, the system can scale easier without requiring additional resources. Hence, in this thesis, we investigate low-complexity algorithms that can significantly reduce the computational complexity of solutions that lead to resource allocation optimization in 5G networks. In particular, we study metaheuristics techniques that utilize a trade-off between randomization and local search to obtain an approximately optimal solution. In addition, machine learning (ML)-based schemes are considered in this thesis to reduce computational complexity by learning patterns in the data and optimizing the processing accordingly.

Firstly, we study the problem of secure computation efficiency (SCE) in a NOMA MEC system with a nonlinear EH user and a power beacon in the presence of an eavesdropper. To further provide a friendly environment resource allocation design, wireless power transfer is applied. The SCE problem is solved by jointly optimizing the transmission power, the time allocations for energy transfer, the computation time, and the central processing unit (CPU) frequency in the NOMA-enabled MEC system. The problem is non-convex and challenging to solve because of the complexity of the objective function in meeting constraints that ensure the required QoS, such as the minimum value of computed bits, limitations on total energy consumed by users, maximum CPU frequency, and minimum harvested energy and computation offloading times. Therefore, a low-complexity particle swarm optimization (PSO)-based algorithm is proposed to solve this optimization problem. For comparison purposes, time division multiple access and fully offloading baseline schemes are investigated. Simulation results show the superiority of the proposed approach over baseline schemes.

Secondly, we investigate a beamforming design with artificial noise (AN) to improve the security of a multi-user downlink, multiple-input single-output (MISO) NOMA-CR network with SWIPT. To further support power-limited, battery-driven devices, EH users are involved in the pro-

posed network. Specifically, we investigate the optimal AN, power-splitting ratios, and transmission beamforming vectors for secondary users and EH users to minimize the transmission power of the secondary network, subject to the following constraints: a minimum signal-to-interference-plus-noise ratio at the secondary users, minimum harvested energy by secondary users and EH users, maximum power at the secondary transmitter, and maximum permissible interference with licensed users. The proposed solution for the challenging non-convex optimization problem is based on the semidefinite relaxation method. Numerical results show that the proposed scheme outperforms the conventional scheme without AN, the zero-forcing-based scheme, and the space-division multiple-access-based method.

Thirdly, we consider a cooperative non-linear SWIPT-enabled NOMA system with a non-linear EH user. Specifically, we investigate two optimization problems. First, we minimize transmission power, and second, we maximize energy efficiency subject to meeting QoS constraints. Furthermore, we develop the optimal solution based on convex optimization and the exhaustive search (ES) method to validate the results of the proposed PSO-based framework. Afterward, we investigate the performance of five swarm intelligence-based baseline schemes and evaluate an additional low-complexity solution based on the cuckoo search technique. For comparison purposes, we use orthogonal multiple access (OMA), equal power splitting (EPS), and time-fixed (TF) baseline schemes. From the results in terms of total transmission power and energy efficiency, the proposed SWIPT NOMA network outperforms the benchmark schemes, and the proposed PSO-based framework achieves the nearest performance to the optimal scheme with lower complexity than obtained by the comparative swarm intelligence techniques and from convex optimization with the ES method.

Finally, we design a novel artificial intelligence (AI)-based framework for maximizing the secrecy energy efficiency (SEE) in FD cooperative relay underlay CR-NOMA systems with imperfect successive interference cancellation that are exposed to multiple eavesdroppers. First, we formulate

the non-convex SEE optimization problem as bi-level optimization, subject to constraints that satisfy the QoS requirements of secondary users. In particular, the outer problem is solved with ensemble learning (EL) to select the optimal relay. Regarding the inner problem, we propose a quantum particle swarm optimization (QPSO)-based technique to optimize power allocation. In addition, for comparison purposes, we describe a cooperative relay CR network with OMA, rate-splitting multiple access, and half-duplex technologies. Moreover, we evaluate comparative schemes based on machine learning algorithms and swarm intelligence baseline schemes. Furthermore, the proposed EL-aided QPSO-based framework achieves performance close to the optimal solutions, with a meaningful reduction in computation complexity.

Contents

List of Figures

List of Tables

Nomenclature

Notation Description

AI	Artificial Intelligence
ALO	Ant Lion Optimziation Algorithm
AN	Artificial Noise
AWGN	Additive White Gaussian Noise
BA	Bat Algorithm
BOA	Butterfly Optimization Algorihtm
CPU	Central Processing Unit
CR	Cognitive Radio
CS	Cuckoo Search
CSCG	Circularly Symmetric Complex Gaussian
DF	Decode-and-Forward
DNN	Deep Neural Network
EL	Ensemble Learning
EH	Energy-Harvesting
EPS	Equal Power Splitting
ES	Exhaustive Search
FA	Firefly Algorithm
FD	Full-duplex
ID	Information Decoding
IoT	Internet of Things
LOS	Line-of-Sight
MEC	Mobile Edge Computing
MIMO	Multiple-Input Multiple-Output
MISO	Multiple-Input Single-Output
NOMA	Non-Orthogonal Multiple Access
PB	Power Beacon
PLS	Physical Layer Security
PS	Power-Splitting
PSO	Particle Swarm Optimization
PU	Primary User
QoS	Quality of Service
QPSO	Quantum Particular Swarm Optimization
RF	Radio Frequency
RS	Rate-Splitting
RSMA	Rate-Splitting Multiple Access
SCA	Successive Convex Approximation
SCE	Secure Computation Efficiency
SEE	Secrecy Energy Efficiency
SSR	Secrecy Sum-Rate
SDMA	Space-Division Multiple Access
SDP	Semidefinite Programming
SDR	Semidefinite Relaxation
SIC	Successive Interference Cancellation
SINR	Signal-to-Interference-plus-Noise Ratio

SNR	Signal-to-Noise Ratio
SU	Secondary User
SWIPT	Simultaneous Wireless Information and Power Transfer
TDMA	Time-Division Multiple Access
TS	Time Switching
WPT	Wireless power transfer
ZF	Zero-forcing

Chapter 1

Introduction

1.1 Background

1.1.1 Non-orthogonal multiple access

Non-orthogonal multiple access (NOMA) is a multiple access technique used in wireless communication systems where multiple users share the same frequency band and time slot. Unlike orthogonal multiple access (OMA) techniques such as time division multiple access (TDMA) and frequency division multiple access (FDMA), NOMA allows multiple users to share the same frequency band and time slot simultaneously by using different power levels, codebooks, or signatures to distinguish between users. Indeed, the user with a stronger channel is assigned a lower power level, while the user with a weaker channel is assigned a higher power level so that all users can achieve a comparable quality of service (QoS) [1].

In NOMA, the base station transmits signals to multiple users simultaneously by applying superposition coding. Thus, NOMA relies on the use of advanced signal processing techniques, such as successive interference cancellation (SIC), to separate the signals of individual users at the receiver. With SIC, the receiver first decodes the strongest signal and then subtracts it from the received signal

to cancel out the interference from that user. The process is repeated for the remaining signals until all users' signals are decoded [2, 3].

1.1.2   Cooperative NOMA

Cooperative NOMA exploits the advantage of cooperative communications and the NOMA technique. In particular, NOMA can improve spectral and energy efficiency. Meanwhile, cooperative communications are able to solve the coverage problem in wireless communications and mitigate the impact of channel fading. In cooperative communications, the intermediate users are employed as relays to assist in the transmission of data between the transmitter and the receiver. For this purpose, amplify-and-forward (AF) or decode-and-forward (DF) protocols can be applied. In the AF protocol, the intermediate user receives the signal from the transmitter, amplifies it, and forwards it to the destination. Regarding DF protocol, the intermediate node receives the signal from the source, decodes it, and re-encodes it before forwarding it to the destination [4–6].

Figure 1.1 presents a simple system model of a cooperative NOMA system comprised of one source denoted by S, and two users, where a nearby user employs DF protocol. Assume that each node only has a single antenna and nearby user u_1 has better channel conditions than distant user u_2. Then, according to NOMA principles, the data transmission of this scheme involves two phases. In Phase 1, the source transmits nearby, and distant users' messages and then nearby user and distant user receive them. Formally, the source conveys the superimposed signal $x = \sqrt{p_1}x_1 + \sqrt{p_2}x_2$ where x_1, $x_2 \in$ are the information bearing messages with the corresponding transmit power p_1 and p_2 for nearby user u_1 and distant user u_2, respectively. Note that $p_2 > p_1$ since distant user u_2 has weaker channel conditions than nearby user u_1. Moreover, following NOMA fundamentals, SIC is performed at nearby user u_1. Specifically, user u_1 first decodes message x_2 of distant user u_2 by treating x_1 as noise and then subtracts this message x_2 from the received signal. Then, nearby user u_1 decodes its own message x_1. In Phase 2, u_1 retransmits message x_2 to distant user u_2. At the end of phase 2,
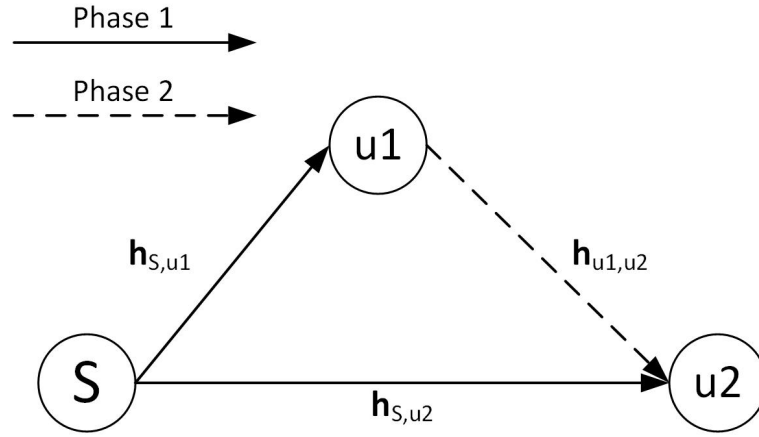
Figure 1.1: System model of cooperative NOMA communication.

distant user u_2 utilizes maximal-ratio combination (MRC) to merge the message x_2 received in the two phases (in Phase 1 from the source and in Phase 2 from the nearby user u_1) and then decodes it.

Accordingly, in Phase 1, the received signal at nearby user u_1 and at distant user u_2 can be given by (1.1) and (1.2), respectively.

$$y_{u1}^{(1)} = h_{S,u1} (p_1 x_1 + p_2 x_2) + z_1^{(1)}, \tag{1.1}$$

$$y_{u2}^{(1)} = h_{S,u2} (p_1 x_1 + p_2 x_2) + z_2^{(1)}, \tag{1.2}$$

where $h_{S,u1}$ is the channel coefficient between the source and user u_1, and $z_1^{(1)}$ is the additive white Gaussian noise (AWGN) at user 1. Similarly, $h_{S,u2}$ is the channel coefficient between the source and user u_2, and $z_2^{(1)}$ is the additive white Gaussian noise (AWGN) at user 2.

In Phase 2, the received signal at distant user u_2 can be given by

$$y_{u2}^{(2)} = h_{u1,u2} p_{u1} x_2 + z_2^{(2)}, \tag{1.3}$$

where $h_{u1,u2}$ is the channel coefficient between user u_1 and user u_2, p_{u1} is the transmitted power from user u_1, and $z_1^{(1)}$ is the AWGN at user 2.

1.1.3   Cognitive Radio

Cognitive radio (CR) allows radio devices to intelligently and dynamically access the radio frequency spectrum, which is the range of electromagnetic frequencies that wireless signals used to transmit data. In this sense, CR systems use software-defined radios (SDRs) that can detect and analyze the available frequency bands in the environment and automatically switch to the best available frequency band. This allows for more efficient use of the spectrum and increased data transmission rates [7]. CR systems use various techniques to detect and analyze the available frequency bands. For instance, the spectrum sensing technique involves analyzing the radio frequency spectrum to detect the presence of primary users (PUs) (e.g., licensed users such as TV stations) and avoiding their frequency bands. On the other hand, the spectrum decision technique selects the optimal frequency band based on the current environment and the user's communication requirements [8].

In addition to optimizing spectrum utilization, CR systems can also enhance communication security and reliability. For example, CRs can use techniques such as dynamic spectrum access, adaptive modulation and coding, and channel aggregation to provide better QoS and overcome interference from other wireless devices. In this sense, underlay and overlay CR are two different approaches for utilizing the spectrum in a dynamic and efficient way. Underlay CR is a technique where a secondary user (SU) operates in a spectral band that is already occupied by a primary user (PU). The SU uses the spectrum without interfering with the PU's transmission by carefully selecting the power level and modulation scheme. Underlay CR typically operates in a licensed spectrum, where the PU has priority access to the spectrum. On the other hand, overlay CR is a technique where the SU uses a spectrum that is not currently being used by any PU. The SU detects and utilizes spectrum holes or white spaces that are available in the frequency band. Overlay CR can operate in both licensed and unlicensed spectrum [8, 9].

1.1.4 Energy Harvesting

Energy harvesting (EH) is the process of capturing and storing energy from natural or artificial sources such as solar, wind, thermal, kinetic, or electromagnetic sources and converting it into electricity that can be used to power electronic devices or systems. The goal of EH is to provide a sustainable and reliable source of power for devices that are not connected to the power grid or that require power in remote or hard-to-reach locations [6]. In this sense, simultaneous wireless information and power transfer (SWIPT) provides another choice in EH techniques since it allows simultaneous information decoding (ID) for the user and RF EH using the same RF signal. The most used types of SWIPT are power-splitting (PS) SWIPT and time-switching (TS) SWIPT. In PS SWIPT, the receiver splits the received signal into two parts according to a power splitting ratio - one part is used for ID, and the other part is used for EH. The power-splitting ratio determines the proportion of the received signal that is used for ID and EH. In TS SWIPT, the receiver alternates between two-time slots - one for ID and the other for EH. The duration of the time slots and the switching time is typically optimized to maximize the overall system performance [10, 11].

1.1.5 Physical Layer Security

Physical Layer Security (PLS) is a technique used to ensure the security of wireless communication systems by exploiting the physical properties of the communication medium. PLS has been considered a powerful alternative to the commonly utilized higher-layer encryption technique. Traditional encryption methods that rely on complex algorithms are susceptible to being broken by those with advanced computational skills. To overcome this challenge, PLS can achieve secure communications without relying on cryptographic techniques [12]. In PLS, the properties of the wireless channel, such as the signal-to-noise ratio, channel fading, and interference patterns, are exploited in such a way that the information is distorted or obfuscated for anyone who is not the intended receiver. In [13], Wyner stated that it is possible to have secure communication in a

wireless system, provided that the channel capacity of the intended recipient is higher than that of the eavesdropper. The secure capacity can be determined by assessing the achievable secrecy rate, which calculates the maximum amount of secure information that can be received by the intended receiver. In particular, PLS techniques include beamforming, artificial noise (AN) generation, and cooperative communication, among others.

1.2   Optimization Algorithms

1.2.1   Metaheuristic algorithms

Metaheuristic algorithms are used to solve complex optimization problems that are difficult to solve using conventional optimization techniques. These algorithms are inspired by natural processes such as evolution, swarm behavior, and the movement of particles, and they rely on heuristics or rules of thumb to guide their search for the approximately optimal solution. The general idea behind metaheuristic algorithms is to iteratively explore the search space in a way that balances exploration and exploitation. They start with an initial solution and then apply a set of rules to generate a new set of candidate solutions. These candidate solutions are evaluated using an objective function that quantifies how well they perform relative to the problem's constraints and goals. Then, according to this evaluation, the metaheuristic algorithm selects the best candidate solutions to continue the search process. One of the key advantages of metaheuristic algorithms is that they can be adapted to different problem settings, such as multi-objective optimization or dynamic optimization, by modifying the evaluation criteria or the search process [14, 15]. In particular, particle swarm optimization (PSO), and cuckoo search (CS) are two powerful metaheuristic algorithms that have been applied to a variety of problems, including scheduling, routing, design optimization, and machine learning (ML) [16, 17].

Particle Swarm Optimization

PSO is a metaheuristic optimization algorithm inspired by the social behavior of bird flocking or fish schooling. In PSO, a swarm of particles moves in a search space to find the approximately optimal solution. The PSO algorithm starts by initializing a population of particles in the search space. Each particle represents a potential solution to the optimization problem, and its position in the search space corresponds to a possible set of parameter values for the problem [16]. The particles move through the search space, updating their positions and velocities based on their own best-known position (personal best) and the best-known position of the swarm (global best). The movement of each particle is determined by two components: the cognitive component and the social component. The cognitive component represents the particle's own experience, while the social component represents the experience of the entire swarm. These two components guide the particles toward the best solution in the search space [18].

The velocity of each particle is updated at each iteration based on the following equation:

$$v_i(t+1) = w * v_i(t) + c1 * rand() * (pbest_i - x_i(t)) + c2 * rand() * (gbest - x_i(t)) \qquad (1.4)$$

where $v_i(t)$ is the velocity of particle i at iteration t, w is the inertia weight, $c1$ and $c2$ are acceleration coefficients, $pbest_i$ is the personal best position of particle i, $x_i(t)$ is the current position of particle i at iteration t, $gbest$ is the best-known position of the swarm, and $rand()$ is a random number between 0 and 1.

The position of each particle is updated based on its velocity:

$$x_i(t+1) = x_i(t) + v_i(t+1). \qquad (1.5)$$

The algorithm ends until a stopping criterion is met, such as a maximum number of iterations that achieves a satisfactory level of convergence. In a nutshell, PSO is a metaheuristic optimization algorithm that simulates the behavior of a group of particles moving in a search space to

find the optimal solution. A variant of PSO is quantum particle swarm optimization (QPSO) which utilizes the principles of quantum mechanics to enhance its performance. In QPSO, each particle is represented by a quantum state, which is a complex-valued function that can be expressed as a linear combination of basis states. The quantum state of each particle is updated using the principles of quantum mechanics [19].

Cuckoo search

CS is a metaheuristic optimization algorithm that is inspired by the behavior of cuckoo birds. It was proposed by Xin-She Yang and Suash Deb in 2009. The basic idea behind the algorithm is to mimic the brood parasitism behavior of cuckoo birds. In nature, cuckoo birds lay their eggs in the nests of other bird species and let them raise their offspring. The cuckoo bird's goal is to lay its eggs in the best nests with the highest quality hosts. In the CS algorithm, the nests correspond to the candidate solutions of an optimization problem and the quality of the nests is evaluated using an objective function. The algorithm tries to improve the quality of the nests by laying new eggs (i.e., generating new candidate solutions) and replacing the eggs in the nests with the poorest quality [20].

1.2.2   Ensemble Learning Algorithms

Ensemble learning (EL) is a ML technique that involves combining multiple models to improve the accuracy and robustness of predictions. The basic idea of EL is to train several models, each with different strengths and weaknesses, and then combine their predictions to make a final prediction that is more accurate than any individual model [21]. The two main types of EL are bagging and boosting. Specifically, in bagging, multiple models are trained on different random subsets of the training data, with replacement. Each model is trained independently and then their predictions are combined to make a final prediction. Bagging is particularly effective for reducing overfitting. On the other hand, in boosting, a series of weak models are trained sequentially, each one attempting

to correct the errors of the previous models. Boosting is particularly effective for improving the performance of weak models. Overall, EL can improve the accuracy and robustness of ML models, especially when individual models may have different biases or limitations. By combining multiple models, the overall performance can be improved, and overfitting can be reduced [22, 23].

The most common algorithms used for EL are:

Random Forest (RF): A type of bagging that combines multiple decision trees. RF can be applied for both classification and regression tasks. It works by creating multiple decision trees and combining them to produce a more accurate and stable prediction. In RF, each tree is built using a subset of the training data and a subset of the features. This helps to reduce overfitting and enhance the accuracy of the model. The subsets of data and features are chosen randomly for each tree. On the other hand, to make a prediction, each tree in the forest independently makes a prediction, and the final result is determined by taking the majority vote on the predictions made by all the decision trees for classification tasks, and the mean of all the predictions for regression tasks [24].

AdaBoost: A type of boosting that assigns weights to the training data to give more emphasis to misclassified data points. In particular, the AdaBoost algorithm works by iteratively training a sequence of weak models, each of which is assigned a weight that reflects its performance on the training data. In each iteration, the algorithm focuses on the instances that were misclassified by the previous models and assigns higher weights to those instances. This puts more emphasis on the difficult examples and forces the next weak model to focus on the areas where the previous models struggled. The final model is a weighted combination of the weak models, with higher weight given to the more accurate models [25].

Stagewise Additive Modeling (SAM): A technique used for constructing an additive model by sequentially adding one function at a time. SAM can be used for both regression and classification tasks. In classification tasks, SAM can use a Multi-class Exponential Loss Function to optimize the model [22]. The basic idea of the SAM algorithm is that each new function added

to the model corrects the errors made by the previous functions. The Multi-class Exponential Loss Function encourages the model to assign high scores to the correct class labels while penalizing incorrect assignments. In particular, the Multi-class Exponential Loss Function is a commonly used loss function that measures the difference between the predicted class probabilities and the true class labels. The goal is to minimize this loss function during training so that the predicted probabilities are as close as possible to the true probabilities. Accordingly, by minimizing the loss function at each iteration, the algorithm ensures that the model is optimized for classification performance [26].

1.2.3   Semidefinite Relaxation

Semidefinite relaxation solves quadratically constrained quadratic programs (QCQPs) that involve relaxing the problem by replacing the quadratic constraints with semidefinite constraints. The key idea is to reformulate the original QCQP as a semidefinite program (SDP), by introducing a new matrix variable $\mathbf{X} = \mathbf{x}\mathbf{x}^H$, where $\mathbf{X}$ is a rank-one symmetric positive semidefinite matrix. Then, by applying the SDR technique, the variable $\mathbf{x}$ is replaced to $\mathbf{X}$ and the constraints of $\mathbf{X} > 0$ and $\operatorname{rank}(\mathbf{X}) = 1$ are included. Finally, to obtain a semidefinite programming (SDP) problem, the rank-one constraint is removed, and the SDP problem is solved by a numerical method [27].

The optimal solution is achieved when $\mathbf{X}$ is rank-one. Otherwise, the penalty-based method [28] or the Gaussian randomization method [29] can aid to approximate the rank-one solution.

1.3   Motivation and Objective

At present, a significant challenge for the advancement of upcoming wireless technologies that allow for the widespread use of the Internet of Things (IoT), device-to-device (D2D) communication, spectrum sharing, and large-scale machine communication is the issue of restricted spectrum

and efficient energy utilization. To overcome this challenge, resource allocation optimization along with the application of potential fifth generation (5G) candidate technologies play a crucial role in wireless communication systems [3]. In this sense, NOMA is a promising technology for the 5G cellular networks and beyond 5G wireless networks that allows multiple users to share the same resources (frequency band and time slot) by using a superposition coding technique at the transmitter and a SIC technique at the receiver [2]. Therefore, NOMA can provide significant benefits in terms of spectral efficiency, user fairness, energy efficiency, and support for IoT and 5G networks. Moreover, cooperative wireless communications can also improve energy efficiency by allowing devices to share resources. This can extend the battery life of devices and reduce the overall energy consumption of wireless networks. Cooperative wireless communications permit reducing latency by allowing devices to relay data to each other and create shorter communication paths [5]. This can be particularly important in real-time applications, such as video conferencing or gaming, where even small delays can be noticeable. CR-inspired NOMA aims to address the shortage of spectrum resources by promoting smart utilization of spectrum sharing. In particular, CR systems aim to maximize the utilization of the available radio spectrum by enabling secondary users to access the unused spectrum bands that are assigned to primary users. By dynamically allocating resources based on the changing demands of the users, CR systems can provide better QoS guarantees while minimizing interference and maintaining network stability. In this sense, resource optimization techniques can be used to mitigate interference between primary and secondary users. For example, power control can be used to adjust the transmission power of secondary users to reduce interference with primary users [7]. Furthermore, the PLS strategy is of meaningful importance for upcoming wireless networks to improve the confidentiality of the transmitted information. Specifically, PLS uses techniques such as signal masking, AN generation, and beamforming to prevent eavesdroppers from intercepting and decoding the transmitted information. One of the main motivations for implementing PLS is to provide robustness to the communication system by designing the transmission schemes that are robust against

intentional interference, jamming attacks and interference from other signals. Moreover, by lever-
aging the inherent properties of the wireless channel, PLS techniques can be implemented without
requiring additional hardware or computational resources. To further enhance secure transmissions,
cooperative wireless communications provide reliability to wireless communication by increasing
signal strength and reducing the effects of fading and interference. By working together, devices can
share information and resources to overcome the limitations of individual devices [12]. In addition,
to address the problem of limited battery lifetime in energy-constrained wireless devices, RF EH
provides a means of harvesting energy from the environment and converting it into electrical energy,
which can be used to power low-power wireless devices. This eliminates the need for batteries, which
reduces the cost and complexity of the device, and also reduces the environmental impact of battery
disposal. Moreover, RF energy harvesting can be used to power devices in remote or hard-to-reach
locations, where it is difficult or impractical to replace batteries [8]. In this sense, SWIPT provides
another option in EH techniques. In particular, SWIPT allows a device can both receive data and
power at the same time by using the same radio frequency signal through a wireless connection.
SWIPT technology has the potential to enable a variety of applications, including wireless charging of
devices, powering sensors in remote locations, and enabling IoT devices to communicate and operate
without the need for external power sources. Hence, SWIPT is an area of ongoing research and
development, with many potential applications and challenges to overcome [10, 11]. In order to make
advanced wireless communication systems more efficient, there has been a growing interest in using
artificial intelligence (AI) solutions that incorporate ML and metaheuristic methods. These solutions
aim to decrease the amount of computational work required and effectively manage resources. In
this sense, an innovative and effective approach in wireless networks is to use an intelligent resource
allocation strategy, which can help to reduce complexity and minimize communication delays. As a
result, AI plays a meaningful role in designing resource allocation systems and addressing challenges
related to different aspects of wireless networks. ML is one of the most popular AI technologies and

is widely used in telecommunications engineering. For example, using ML to select relays in IoT networks can significantly simplify the selection process and reduce latency. ML algorithms can learn patterns from vast amounts of data and use this knowledge to make predictions or decisions. This ability makes ML particularly suitable for optimizing resource allocation in wireless networks, where complex interactions and constraints make traditional optimization techniques challenging [22]. In addition to relay selection in IoT networks, ML-based resource allocation has been applied to various aspects of wireless networks, including power control, scheduling, and interference management. These approaches have been shown to improve system performance and reduce latency compared to traditional methods. Regarding metaheuristic algorithms, these techniques are increasingly being used in wireless communications because they can efficiently solve complex optimization problems. These algorithms are designed to find near-optimal solutions to problems that are difficult or impossible to solve using traditional optimization techniques [14]. Wireless communication systems involve a wide range of complex and dynamic optimization problems, including resource allocation, power control, interference management, and routing. To this end, metaheuristic algorithms are capable of handling the complexity of these systems and can optimize solutions over multiple objectives. By using metaheuristic algorithms, researchers can design and optimize wireless communication systems to meet the increasing demands for higher data rates, more efficient use of spectrum, and more reliable and secure communications [15, 16].

1.4   Contribution and Thesis Outline

This dissertation investigates the resource optimization in cooperative NOMA-based systems with consideration of CR and security taking into account different technologies such as underlying CR and SWIPT with perfect and imperfect SCI. The thesis first proposes a close-optimal scheme based on the PSO algorithm to maximize the secure computation efficiency in a power

beacon-assisted wireless-powered mobile edge computing (MEC) NOMA System. Then, joint beamforming and AN optimization are considered for secure transmissions in the MISO-NOMA CR system with SWIPT, where the idea of minimizing transmit power for the SUs and EH users is to use the rest of the available power at the secondary transmitter to maximize AN and protect transmitted messages against an eavesdropper. Later, linear and non-linear EH models are considered in the SWIPT NOMA system to optimize the transmission problem and energy efficiency subject to meeting quality-of-service (QoS) constraints. After that, a FD cooperative relay CR-NOMA system with imperfect SIC is investigated with the aim of maximizing the secrecy energy efficiency (SEE) to prevent multiple-eavesdropper wiretapping, where close-optimal and low complexity schemes based on ML and metaheuristics algorithms are proposed to solve the non-convex problems. The rest of the thesis is organized into five chapters as follows:

- **Chapter 2**: the purpose of this chapter is to improve user connectivity and security when offloading computation tasks. The study focuses on a wireless-powered NOMA MEC system with a nonlinear EH user and a power beacon, in the presence of an eavesdropper, where wireless power transfer is applied to provide a resource allocation design that is friendly to the environment. The problem of secure computation efficiency (SCE) is addressed by optimizing the transmission power, energy transfer time allocations, computation time, and CPU frequency in the NOMA-enabled MEC system. However, this problem is complex and non-convex, making it challenging to solve while meeting the necessary constraints for quality of service. To address this, a low-complexity particle swarm optimization (PSO)-based algorithm is investigated. The proposed approach is compared to time division multiple access and fully offloading baseline schemes, with simulation results demonstrating the superiority of the proposed approach.

- **Chapter 3**: proposes a beamforming design with AN to enhance the security of the network in

a multi-user downlink, MISO NOMA-CR network with SWIPT and EH users. The solution optimizes AN, power-splitting ratios, and transmission beamforming vectors for secondary users and EH users to minimize the transmission power of the secondary network while satisfying several constraints, including minimum signal-to-interference-plus-noise ratio (SINR), minimum harvested energy, and maximum power at the secondary transmitter. The proposed approach uses the SDR method to solve the non-convex optimization problem. Numerical results demonstrate that the proposed scheme outperforms other conventional schemes such as the zero-forcing-based scheme and the space-division multiple-access (SDMA)-based method.

- **Chapter 4**: proposes a low-complexity PSO-based approach to address the resource allocation problem in a cooperative non-linear SWIPT-enabled NOMA system. We consider two optimization problems: minimizing transmission power and maximizing energy efficiency while meeting QoS requirements. The effectiveness of the proposed system design compared with the traditional OMA, equal power splitting (EPS), and time-fixed (TF) baseline schemes is proved through numerical simulations under different scenarios. Moreover, six swarm intelligence-based baseline schemes are investigated including: CS, the ant lion optimization (ALO) method, the butterfly optimization algorithm (BOA), the firefly algorithm (FA), and the bat algorithm (BA). The proposed SWIPT NOMA network outperforms benchmark schemes, and the proposed PSO-based optimization solution achieves performance closest to the optimal method with lower complexity than other swarm intelligence techniques or convex optimization with the ES method.

- **Chapter 5**: investigates an innovative AI-based framework that focuses on maximizing the secrecy energy efficiency (SEE) in full-duplex (FD) cooperative relay underlay CR-NOMA systems that are vulnerable to multiple eavesdroppers. Initially, the non-convex SEE optimization problem is transformed into a bi-level optimization, while ensuring that the QoS

requirements of secondary users are met. The outer problem is resolved with EL, which selects the optimal relay, while the inner problem is solved using a QPSO-based method that optimizes power allocation. We also provide a comparison of this framework to a cooperative relay CR network with orthogonal multiple access (OMA), rate-splitting multiple access (RSMA), and half-duplex technologies, as well as evaluate comparative schemes based on ML algorithms and swarm intelligence baseline schemes. Simulation results show that EL-aided QPSO-based framework performs close to optimal solutions, while reducing computation complexity considerably.

- **Chapter 6**: summarizes the thesis contributions and gives a discussion on future research directions.

Chapter 2

Paticle Swarm Optimization-Based Secure Computation-Efficiency Maximization in a Power Beacon–Assisted Wireless-Powered Mobile Edge Computing NOMA System[1]

2.1 Introduction

The rapid advances in 5G wireless networks have improved cutting-edge technology requirements, such as support for massive connectivity due to the proliferation of IoT devices and growth in the amount of data in modern society [1]. In this sense, recent technological breakthroughs for next-generation wireless networks have promoted the use of smart applications, such as virtual

---

[1]The study in this chapter is published in Energies [30]

reality, augmented reality, mobile online games, face recognition, and so on. However, latency sensitivity and high computation intensity are two main features of these applications that represent a challenging task for mobile devices, which have low computing capabilities and a limited battery capacity. To tackle these issues, MEC appears to be a technology that can remarkably decrease the computing burden and improve the computing capabilities of mobile devices [31]. In a MEC system, servers are used by mobile devices to offload tasks for low-latency computing, which can be executed in partial or binary modes. In partial mode, computation tasks can be processed into two parts; one part is executed locally at the mobile device and the other is offloaded to the nearby MEC server. In binary mode, the complete task is executed locally, or the entire task is offloaded to a close-proximity MEC server via uplink [31, 32]. Furthermore, future wireless networks should be able to support massive connectivity of devices because of the rapid advancements in the IoT. However, this fact entails the spectrum scarcity issue, which can be handled by the application of a NOMA transmission strategy that works in the power domain and employs superposition coding and successive interference cancellation techniques. Therefore, NOMA with MEC has aroused attention in recent research work that pointed out the superiority of NOMA in comparison with the conventional OMA baseline scheme [33–36]. In [34], the authors applied NOMA to offload tasks from each user to a MEC server, with the aim being to improve the resource allocation problem in an ultra-dense network. They demonstrated that NOMA outperforms the conventional TDMA technique in terms of energy consumption and task delay. A NOMA-based optimization scheme was investigated in [35] to minimize energy consumption by users in a MEC network through an efficient heuristic algorithm. The simulation results showed significant energy-consumption lowering by applying the NOMA framework. Energy-efficiency maximization in NOMA-enabled massive IoT networks based on resource allocation strategies was investigated by Liu et al. [36]. The paper concluded that NOMA for offloading can save a considerable amount of energy, in comparison with existing baseline schemes such as OMA.

In [31], Lin et al. considered a NOMA-enabled MEC network in which several users perform partial offloading under the presence of an eavesdropper. The authors investigated the maximization of the secure computation efficiency subject to the constraints of minimum computation rate, maximum transmission power allowed by the users, and maximum CPU frequency, where the solution was based on the successive convex approximation (SCA) technique. In [32], Wu et al. considered a MEC system with NOMA composed of two users and one eavesdropper. The authors used a partial offloading setup with the aim to minimize the weighted sum-energy consumption of the users subject to the constraints of secrecy offloading rates, channel capacity, and maximum tolerable secrecy outage probability. The solution was based on the exhaustive search method and semi-closed form expressions. In [37], Wu et al. studied a multiuser MEC system with NOMA under the presence of an eavesdropper. The partial offloading mode was used and the authors investigated the minimization of the weighted sum-energy consumption subject to the constraints of required bits securely offloaded, channel capacity, and maximum tolerable secrecy outage probability. The solution was based on the bisection method and semi-closed form expressions. However, none of the previous three references have considered a wireless power transfer phase, a PB device, and the presence of an energy harvesting user with its corresponding minimum EH constraint. Therefore, several new variables and constraints are included in the optimization problem proposed in this chapter, compared with those in [31, 32, 37] where the solutions proposed in these references are not suitable for the problem investigated in this chapter. For instance, the variable to define the time for the wireless power transfer phase is coupled with the transmission power variables and the variable to define the local computing time is coupled with the variable of the local computing CPU frequency. In addition, the works in [32, 37] considered the minimization of the weighted sum-energy consumption which is different to the proposed SCE maximization in this chapter. In [37], Wu et al. considered a NOMA-enabled multi-access MEC system where a single mobile user can offload part of its task to a group of edge-servers. The authors investigated the minimization of the delay in

completing the task required by the mobile user under the constraints of maximum available energy at the mobile user and the maximum allowed energy at the edge-server to process the task requirement. However, the authors did not study the physical layer security under the presence of an eavesdropper and did not consider a wireless power transfer phase, a PB device, and the presence of an energy harvesting user with its corresponding minimum EH constraint. Then, the solution proposed in [37] can not be used in the problem proposed in this chapter.

Furthermore, wireless power transfer (WPT) has been investigated as a promising solution to deal with the limited battery capacity of wireless devices in MEC networks. WPT can steadily reload the batteries of a large number of low-power wireless devices through a dedicated RF transmitter. The foremost benefits from WPT are focused on prolonging the wireless network lifetime, reaching sustainability in network operations, and improving the communications capacity in edge wireless devices. In a WPT-aided MEC network, the access point (AP) sends RF energy to customers on downlink. Then, the customers use the harvested energy to perform computation tasks in partial or binary offloading modes. The integration of WPT with MEC is denominated as a wireless-powered MEC system, which has been studied in recent work [38–42] to extend the operational lifetime of the battery in both partial [38] and binary [39, 40] offloading modes. In [40, 41], the authors approached energy-effecient computation offloading for a cooperative MEC network where a user near a hybrid AP helps to offload tasks from a distant user, and both users benefit by receiving energy from the hybrid AP through WPT. In [42], a wireless-powered MEC network was studied for local computing and offloading by jointly optimizing energy and task allocation. In addition, the wireless signal experiences attenuation as the distances increase and in the presence of obstacles, where the integration of a power beacon (PB) provides a solution to satisfy EH requirements of the users. The PB is a low-cost and low-complexity device that provides wireless energy to users, and it does not need high computational capabilities. In [43], a wireless information and power transfer system aided by a PB was proposed, with the objective being to minimize total transmit power under

constraints for QoS and EH requirements. The results showed the benefits from the PB in satisfying

the EH requirements of the users.

Although the application of a NOMA system in MEC networks increases the possibilities

of meeting 5G requirements, wireless security is still a challenging issue to solve. In particular,

confidential information's vulnerability to being trapped by eavesdroppers increases when compu-

tation tasks are offloaded from mobile devices to MEC servers over wireless channels. PLS has

been considered an alternative to the conventional higher-layer encryption techniques that utilize key

management and complex algorithms, and risk being broken by high computational capabilities of

the eavesdropper. On the other hand, PLS keeps information safe under wireless communications

by exploiting physical layer features of wireless channels, such as noise, interference, fading, and

so on, without the use of cryptographic keys, and regardless of the computing capability of the

eavesdropper. In the literature, there are some recent researches that encompass PLS in NOMA-MEC

networks to accomplish a boost in secrecy transmission and to improve energy-efficient resource

allocation. In this sense, green communication is an essential topic that has been considered for

suitable development in future wireless networks due to excessive energy consumption that will

bring plenty of environmental problems [31, 32, 44]. For instance, in [44], the authors maximized the

computation efficiency of the NOMA-MEC network in both partial and binary offloading modes.

The paper concluded that the computation efficiency achieved by using partial offloading can exceed

the performance obtained by applying binary offloading mode. Moreover, this article pointed out the

superiority of NOMA over the TDMA scheme. Although this study did not consider PLS, it opened

doors for computation-efficiency maximization in different next-generation MEC networks. On the

other hand, PLS in a NOMA-enabled MEC system in the presence of a malicious eavesdropper was

studied [31, 32]. The results demonstrated that partial offloading mode with NOMA outperforms

fully offloading mode with NOMA and other the baseline schemes, such as OMA. Moreover, Lin

et al. [31] highlighted the concept of computation energy-efficiency, which is defined as the ratio

of total computation bits to energy consumption. Different from the uplink transmission schemes proposed in [31, 32], our proposed scheme consists of uplink and downlink transmission to further optimize the energy efficiency of the system through the application of WPT service of the AP and the energy transmitted from the PB.

None of the research articles discussed above considered the study of PLS in a PB-assisted wireless-powered NOMA-MEC network with a practical non-linear EH user. In this chapter, we demonstrate through simulations that by employing a PB in the proposed MEC network, the secrecy computation efficiency (SCE) is enhanced. The main advantage of PBs is that they can be densely deployed without a backhaul link installation or complex computational capabilities [45]. We investigate the design of a proper low-complexity resource-allocation scheme to block an eavesdropper in a wireless-powered NOMA-enabled MEC network with a practical non-linear EH user and PB. From this, we provide a solution based on the particle swarm optimization (PSO) algorithm to maximize the SCE while satisfying the QoS requirements of NOMA users in order to successfully compute their tasks in a safe manner under partial offloading mode. Moreover, the optimization problem is subject to minimum EH by the non-linear EH user. In the literature, PSO is considered a powerful optimization method since it has demonstrated high performance in solving optimization problems. For instance, in our previous works [1, 46], the PSO technique has been investigated and applied for maximizing the secrecy sum rate and the secrecy energy efficiency of a cooperative NOMA network, respectively. In both cases, the results showed that the proposed PSO-based method accomplished yield very close to that obtained by the optimal exhaustive search method, but with the benefit of low computational complexity. Furthermore, analytical solutions that provide close-form expressions are unflexible for new system model designs. Particularly when the system model includes a new network element such as mobile device or transmitter, we have to reformulate the optimization problem and find a new solution. Moreover, the procedures to transform non-convex problems into convex problems are not the same for all the cases and depend on the

constraints and variables of the optimization problem, case by case basis. Therefore, most of the solutions offered in related references can not be applied to the proposed problem in this chapter. Next, we analyze the optimization problems in related references and the reason why those approaches can not be used in this chapter. This motivated us to introduce PSO as a potential optimization solution in an innovative wireless-powered NOMA-enabled MEC system with a practical non-linear EH user. Different from [1, 46], where the downlink transmission from the transmitter to the receivers is only considered to carry messages, in this chapter an uplink-downlink transmission scheme is studied where the AP integrates a MEC server to alieve the burden of the users. Moreover, the AP provides the WPT service and practical non-linear EH and PB are integrated into the network.

The main contributions of this chapter are as follows.

- We focus on PLS to study the SCE maximization problem in a wireless-powered NOMA-enabled MEC network assisted by a PB under partial offloading mode. Moreover, a practical non-linear EH and power amplifier coefficient are considered in the design of our proposed scheme.

- We aim to reduce computational complexity. Therefore, we provide a low-complexity PSO-based solution for the proposed challenging non-convex optimization problem, which maximizes SCE by satisfying the QoS requirements of NOMA users and meeting the minimum energy harvested by non-linear EH users. In particular, we jointly optimize the local computing frequency, the computation time for local computing, and the power allocation variables involved in the network. Moreover, we obtain the limits of the search range of each variable to be optimized through mathematical procedures to properly find the global best particle´s position.

- We further investigate SCE maximization for the conventional TDMA-MEC system under partial offloading mode (and for NOMA-MEC system, fully offloading) in order to compare

them with our proposed scheme. Numerical results to assess the performance of each scheme show that the SCE obtained under our proposed wireless-power NOMA-enabled MEC scheme is superior to that of other baseline schemes. Moreover, the numerical results show that a system with a PB improves SCE performance.

The rest of the chapter is organized as follows. Section 2.2 presents the proposed system model and two baseline schemes for comparison purposes. Section 2.3 describes the problem formulation. Section 2.4 explains the proposed PSO-based solution. The numerical results are given in Section 2.5. Finally, the conclusions are presented in Section 2.6.

2.2   System Model

We study a wireless-powered multi-user NOMA-enabled MEC system assisted by a PB in the presence of an eavesdropper, as illustrated in Figure 2.1, where the AP provides the WPT service for M users and a non-linear EH user. The AP integrates the MEC server and an RF energy transmitter. Moreover, each user device contains an energy-harvesting circuit and a rechargeable battery that is able to store the collected energy for its operations. It is assumed that the communications and power transferred from the PB and the AP are sent over the same frequency band, and that all nodes are equipped with a single antenna, similar to the research in [39, 47, 48]. In this chapter, we consider partial offloading. Note that local computations and the downlink WPT transmission from the AP and PB can be performed simultaneously, but the uplink offloading operation and downlink WPT cannot be simultaneously executed [39, 49–52].

The transmission frame duration, T, illustrated in Figure 2.2, is based on four phases. First, the AP and the PB broadcast the RF energy to charge the M users and the EH user during the first phase, with duration θT, $\theta \in (0, 1]$. Then, users offload tasks to the MEC server by employing NOMA during the second phase, over duration $(1 - \theta) T$. In the third and fourth phases, respectively,

(a) First phase (for wireless power transfer).   (b) Second phase (for offloading).
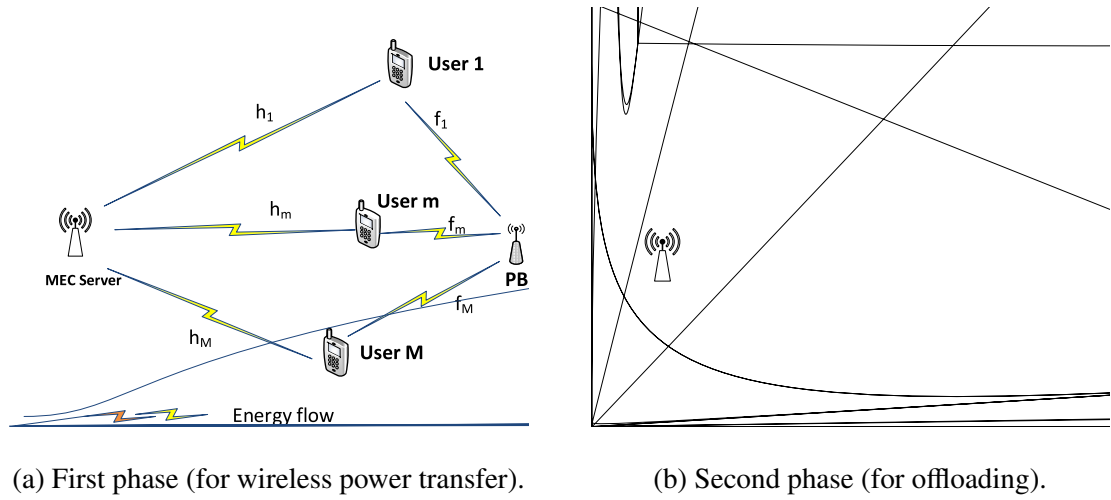
Figure 2.1: System model of the wireless-powered NOMA-enabled MEC system.
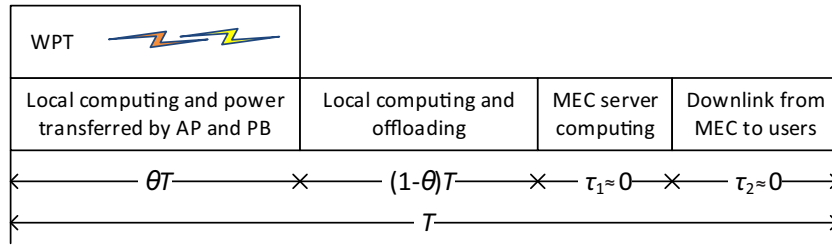
Figure 2.2: Frame scheme of the wireless-powered NOMA-MEC network.

the MEC server carries out the computation tasks and downloads the computation outcomes. To that end, computation time τ_1 and downloading time τ_2 belonging to the MEC server are omitted, since the MEC server is considered to have a stronger computation capability than the users, and the number of bits corresponding to the results of the tasks is negligible [44, 47–52], [19-24].

The baseband equivalent channels from the AP and PB to NOMA users are defined as $h_m \in \mathbb{C}$, and $f_m \in \mathbb{C}$, respectively. Meanwhile, the channel from each of the m users to the eavesdropper is defined as $g_m \in \mathbb{C}$. It is understood that the same channel, h_m, is used for both uplink and downlink due to channel reciprocity [39]. Moreover, we consider the noise variance of the MEC server and the eavesdropper to be the same, denoted as $\sigma^2 = \sigma_{mec}^2 = \sigma_{eav}^2$.

In this chapter, we consider a practical non-linear EH model based on the work in [44, 53], which was subjected to experimental evaluations to validate effectiveness. In particular, the proposed EH model satisfies the sensitivity property, which states that when the input RF power does not exceed the sensitivity boundary, the harvested energy is zero. This differs from the work in [38, 39, 39, 40, 49–52] that employed the ideally linear EH model. Accordingly, the energy harvested by the m–th user is given by

$$EH_m = \theta T \left[\left(\frac{P_{eh\_max}}{\exp(\lambda - \mu p_0)} \left(\frac{1 + \exp(\lambda - \mu p_0)}{1 + \exp\left(\lambda - \mu\left(P_{AP}|h_m|^2 + P_{PB}|f_m|^2\right)\right)} - 1 \right) \right) \right]^+, \qquad (2.1)$$

where P_{AP} and P_{PB} are the transmit power from the AP and the PB, respectively. P_{eh_max} represents the maximum harvested power of the m–th user, $m = 1, 2, 3, ..., M$; is the sensitivity boundary; μ and λ are the control parameters for the steepness of the function; and $[x]^+ = \max(x, 0)$ selects the bigger value of x and 0. Based on the work in [38, 51], the aforementioned parameters were set to $P_{eh\_max} = 0.004927\,\text{W}$, $p_0 = 0.000064\text{W}, \mu = 274$, and $\lambda = 0.29$.

In addition, we consider the EH user to be a sensor node that is regularly powered by a battery with a limited lifetime [54]. Similar to the m-th user, the EH device follows a non-linear EH model and is expressed as follows:

$$EH_{user} = \theta T \left[\left(\frac{P_{eh\_max}}{\exp(\lambda - \mu p_0)} \left(\frac{1 + \exp(\lambda - \mu p_0)}{1 + \exp\left(\lambda - \mu\left(P_{AP}|l_{AP}|^2 + P_{PB}|l_{PB}|^2\right)\right)} - 1 \right) \right) \right]^+, \qquad (2.2)$$

where $l_{AP} \in \mathbb{C}$ and $l_{PB} \in \mathbb{C}$ are the channels to the EH user from the AP and PB, respectively.

2.2.1   Local Computing Mode

Each m-th user is able to compute tasks and harvest energy simultaneously, since the computing unit and the energy harvesting circuit are separate [44, 55]. This means that the entire frame can be used for local computing. The number of CPU cycles required to compute one bit of raw data at the m-th user is denoted as C_m. Let q_m denote the CPU frequency (in cycles per second) of the m-th user, which should be lower than the maximum computation speed, i.e., $q_m \leq q_{max}$.

The effective capacitance coefficient of the processor's chip is denoted by α_m. Then, the energy consumption of the local computing mode can be expressed as $E_m^{loc} = \alpha_m q_m^3 t_m$, where t_m represents the computation time of the m-th user, $0 \leq t_m \leq T$. Thus, the number of locally computed bits for the m-th user in local computing mode is defined as the amount of bits processed in the time frame considered, given by

$$\gamma_m^{loc} = \frac{q_m t_m}{C_m}. \tag{2.3}$$

To secure sustainable operation for the m-th user, the utilized energy should not exceed that of the harvested energy, i.e., $E_m^{loc} \leq EH_m$.

2.2.2   Partial Offloading Mode with NOMA

Since we consider partial offloading to be separate from local computing, each user can offload tasks to the AP after completing the θT period for harvesting energy, so the $(1 - \theta) T$ period can be utilized for offloading. On uplink, multiple users apply the NOMA transmission strategy to offload their computation tasks simultaneously. Following the processes in [39, 44], included in the offloaded task of the m-th user is communications overhead (represented by δ), such as a packet header, and it is greater than 1, i.e., $\delta > 1$. Without loss of generality, the distance between the m-th user and the AP is considered to be sorted as follows: $d_{AP,u_1} \geq d_{AP,u_2} \geq ... \geq d_{AP,u_M}$, and then channel gain is in descending order: $h_1 < h_2 < ... < h_M$. According to NOMA principles for uplinks employing SIC techniques, the decoding process is in descending order of channel power, since the received signal power that belongs to the stronger channel's user corresponds to the M-th user, which is decoded first at the AP and contains interference from all users with relatively weaker channel conditions. Thus, the secrecy offloading computation of the m-th user is given by the total number of computed bits at the MEC server minus the total number of computed bits at the eavesdropper, and can be expressed as follows:

$$r_m^{off} = \tag{2.4}$$

$$
\begin{cases}
\dfrac{B}{\delta}\left(1-\theta\right)T\left[\log_2\left(1+\dfrac{p_m|h_m|^2}{\sum\limits_{j=1}^{m-1}p_j|h_j|^2+\sigma_{mec}^2}\right)-\log_2\left(1+\dfrac{p_m|g_m|^2}{\sigma_{eav}^2+\sum\limits_{j=1,j\neq m}^{M}p_j|g_j|^2}\right)\right]^+ &,2\leq m\leq M \\[4ex]
\dfrac{B}{\delta}\left(1-\theta\right)T\left[\log_2\left(1+\dfrac{p_m|h_m|^2}{\sigma_{mec}^2}\right)-\log_2\left(1+\dfrac{p_m|g_m|^2}{\sigma_{eav}^2+\sum\limits_{j=2}^{M}p_j|g_j|^2}\right)\right]^+ &,\ m=1,
\end{cases}
$$

where $[x]^+ \overset{\Delta}{=} \max(x,0)$ means the higher value between x and zero, B represents the channel bandwidth, σ denotes the power of AWGN, and p_m denotes the transmission power for the m–th user.

The offloading consumed power indicated in equation (2.5) considers the amplifier coefficient, the consumed power during the first phase for receive-signal processing, and the constant circuit power consumption for transmit signal processing, which are denoted as ϑ, p_r, and p_c, respectively [44]:

$$
E_m^{off} = p_{r,m}\theta T + \vartheta\left(p_m + p_c\right)\left(1-\theta\right)T. \tag{2.5}
$$

The SCE of the proposed NOMA-enabled MEC WPT system is defined as the ratio of total computed bits to power consumption in both modes, i.e., local computing and offloading mode [31, 44], as follows:

$$
S_c = \frac{\sum\limits_{m=1}^{M}\left[r_m^{off}+\gamma_m^{loc}\right]}{\sum\limits_{m=1}^{M}\left[p_{r,m}\theta T+\vartheta\left(p_m+p_c\right)\left(1-\theta\right)T+\alpha_m q_m^3 t_m\right]}. \tag{2.6}
$$

2.2.3   Offloading Mode with TDMA

For comparison purposes, we describe the system model of the TDMA benchmark scheme in which time resource $(1-\theta)T$ has to be divided among the M users. Let the offloading time for the m-th user be denoted as w_m. Then, the corresponding secrecy computed bits can be given by

$$
r_{m\_tdma}^{off} = \frac{B}{\delta}w_m T\log_2\left(1+\frac{p_m|h_m|^2}{\sigma_{mec}^2}\right)-\frac{B}{\delta}w_m T\log_2\left(1+\frac{p_m|g_m|^2}{\sigma_{eav}^2}\right). \tag{2.7}
$$

Consequently, the partial offloading SCE of each user is given by

$$S_{c\_OMA} = \frac{\sum\limits_{m=1}^{M} \left[r_{m\_tdma}^{off} + \gamma_m^{loc} \right]}{\sum\limits_{m=1}^{M} \left[p_{r,m}\theta T + \vartheta \left(p_m + p_c \right) w_m T + \alpha_m q_m^3 t_m \right]}. \tag{2.8}$$

2.3 SCE Maximization in Wireless-Powered MEC Systems with an EH User

2.3.1 Problem Formulation of Partial Offloading Mode in the NOMA-MEC System

In this chapter, we develop a low-complexity resource-allocation scheme based on the PSO algorithm for SCE maximization in a wireless-powered NOMA-MEC system with a non-linear EH user and in the presence of an eavesdropper. Specifically, period θ, local computing CPU frequency q_m, computation time t_m, and power allocation p_m are jointly optimized variables subject to the following constraints:

$$P1 : \max_{\theta, \{p_m, t_m, q_m\}} S_c \tag{2.9a}$$

$$\text{s.t. } C1 : \frac{B}{\delta} (1 - \theta) T \log_2 \left(1 + \frac{p_m |h_m|^2}{\sum\limits_{j=1}^{m-1} p_j |h_j|^2 + \sigma_{mec}^2} \right) + \frac{q_m t_m}{C_m} \geq r_{\min,m}, \forall m \tag{2.9b}$$

$$C2 : p_{r,m}\theta T + \vartheta \left(p_m + p_c \right) \left(1 - \theta \right) T + \alpha_m q_m^3 t_m \leq EH_m, \forall m \tag{2.9c}$$

$$C3 : 0 \leq q_m \leq q_m^{\max}, \forall m \tag{2.9d}$$

$$C4 : p_m \geq 0, \forall m \tag{2.9e}$$

$$C5 : EH_{User} \geq \xi_{EH} \tag{2.9f}$$

$$C6 : 0 < t_m \leq T, \forall m \tag{2.9g}$$

$$C7 : 0 < \theta \leq 1, \tag{2.9h}$$

where constraint C1 indicates the minimum computed bits required by the m-th user, and this value is targeted by $r_{\min}$. Constraint C2 indicates that the total consumed energy by the m-th user for partial offloading cannot exceed the harvested energy. Constraint C3 establishes the maximum CPU frequency for each user, while constraint C4 indicates that power allocation should be higher than zero. Constraint C5 indicates the minimum harvested energy by the EH user, and this target value is represented by ξ_{EH}. Constraints C6 and C7 define the boundaries for the local and offloading computing times, respectively.

2.3.2   Problem Formulation of Fully Offloading Mode in the NOMA-MEC System

For comparison purposes, the problem formulation for fully offloading was developed. In offloading mode, local computing is omitted, and problem formulation P2 is given as follows:

$$P2 : \max_{\theta, \{p_m\}} \quad \frac{\sum\limits_{m=1}^{M} r_m^{off}}{\sum\limits_{m=1}^{M} \left[p_{r,m}\theta T + \vartheta \left(p_m + p_c \right) \left(1 - \theta \right) T \right]} \tag{2.10a}$$

$$\text{s.t.} \quad C1 : \frac{B}{\delta} \left(1 - \theta \right) T \log_2 \left(1 + \frac{p_m |h_m|^2}{\sum\limits_{j=1}^{m-1} p_j \left| h_j \right|^2 + \sigma_{mec}^2} \right) \geq r_{\min,m}, \ \forall_m \tag{2.10b}$$

$$C2 : p_{r,m}\theta T + \vartheta \left(p_m + p_c \right) \left(1 - \theta \right) T \leq EH_m, \ \forall_m \tag{2.10c}$$

$$C3 : (2.9e), (2.9f), (2.9h), \tag{2.10d}$$

2.3.3   Problem Formulation of Partial Offloading Mode in the TDMA-MEC System

SCE maximization is formulated as follows when partial offloading mode is applied in the TDMA-MEC baseline scheme:

$$P3 : \max_{\theta, \{w_m, p_m, t_m, q_m\}} \quad \frac{\sum\limits_{m=1}^{M} \left[r_{m\_tdma}^{off} + \gamma_m^{loc} \right]}{\sum\limits_{m=1}^{M} \left[p_{r,m}\theta T + \vartheta \left(p_m + p_c \right) w_m T + \alpha_m q_m^3 t_m \right]} \tag{2.11a}$$

$$\text{s.t.} \ \ C1 : \frac{B}{\delta} w_m T \log_2\left(1 + \frac{p_m |h_m|^2}{\sigma_{mec}^2}\right) + \frac{q_m t_m}{C_m} \geq r_{\min,m}, \ \forall_m \tag{2.11b}$$

$$C2 : p_{r,m}\theta T + \vartheta\left(p_m + p_c\right)w_m T + \alpha_m q_m^3 t_m \leq EH_m, \forall_m, \ \forall_m \tag{2.11c}$$

$$C3 : \sum_{m=1}^{M} w_m \leq 1 - \theta \tag{2.11d}$$

$$C4 : 0 \leq w_m < 1. \ \forall_m \tag{2.11e}$$

$$C5 : (2.9d), (2.9e), (2.9f), (2.9g), (2.9h), \tag{2.11f}$$

where constraints C3 and C4 define the limits for offloading time, which cannot be longer than $1 - \theta$, and cannot exceed 1.

2.4   PSO-based resource allocation scheme for SCE maximization

In this chapter, we consider a low-complexity resource-allocation scheme based on PSO to maximize the SCE in the proposed wireless-powered MEC network. The PSO-based algorithm has been applied to various optimization problems in the engineering field because it provides high precision and low computational complexity. This optimization technique focuses on achieving an approximately optimal solution by iteratively updating each particle's position, which leads to the global and local best positions. The position of each particle corresponds to the variables to be optimized. The global best position corresponds to the particle that achieves the best yield in the swarm, while the local best position corresponds to the position that achieves the best yield for that particle. In this context, the global best position is achieved by the particle position that gets the highest value for SCE.

In the following sections, we describe the development of the PSO algorithm for the proposed NOMA-MEC system and the baseline schemes, such as the TDMA-MEC system and the fully offloading MEC system.

2.4.1 PSO-based Algorithm for Partial Offloading in the NOMA-MEC System

In the proposed NOMA-MEC system, the s-th particle's position is given by the set of $1 + 3M$ variables to be optimized, as follows:

$$\mathbf{x}_s = \left\{ x_{\theta,s}, x_{\mathbf{p},s}, x_{\mathbf{q},s}, x_{\mathbf{t},s} \right\}, \tag{2.12}$$

where $s = 1, 2, ..., S$, in which S indicates the number of particles in the swarm, and $x_{\theta,s}, x_{\mathbf{p},s}, x_{\mathbf{q},s}, x_{\mathbf{t},s}$ represent the resource variables: θ, $\mathbf{p} = \{p_1, ..., p_M\}$, $\mathbf{q} = \{q_1, ..., q_M\}$, and $\mathbf{t} = \{t_1, ..., t_M\}$, respectively. Then, we define the search region of the s-th particle according to the boundaries belonging to each variable. For instance, the lower boundary for period θ is given by (2.13) and is calculated based on constraint (2.9f):

$$\theta_{\min} = \frac{\xi_{EH}}{T \times \left[\left(\frac{P_{eh\_\max}}{\exp(\lambda - \mu p_0)} \left(\frac{1 + \exp(\lambda - \mu p_0)}{1 + \exp(\lambda - \mu(P|l_{AP}|^2 + P_{PB}|l_{PB}|^2))} - 1 \right) \right) \right]^+}. \tag{2.13}$$

The lower boundary for transmission power variable p_m is given by (2.14) and is calculated based on constraint (2.9b):

$$p_{\min,m} = \left[2^{\frac{r_{\min,m} - \frac{q_{\max}T}{C_m}}{\frac{B}{\delta}(1 - \theta_{\min})T}} - 1 \right]^+ \frac{\sigma_{mec}^2}{|h_m|^2}. \tag{2.14}$$

The lower boundary for variables t_m and q_m are obtained based on constraint (2.9b) as follows:

$$t_{\min,m} = \left[\left(r_{\min,m} - \frac{B}{\delta} (1 - \theta_{\min}) T \log_2 \left(1 + \frac{p_{max}|h_m|^2}{\sigma_{mec}^2} \right) \right) \frac{C_m}{q_{\max}} \right]^+, \tag{2.15}$$

and

$$q_{\min,m} = \left[\left(r_{\min,m} - \frac{B}{\delta} (1 - \theta_{\min}) T \log_2 \left(1 + \frac{p_{max}|h_m|^2}{\sigma_{mec}^2} \right) \right) \frac{C_m}{T} \right]^+. \tag{2.16}$$

The upper boundary of variable θ is given by (2.17), based on constraint (2.9b).

$$\theta_{\max} = \min \left(\left[\min_{1 \leq m \leq M} \left(1 - \frac{r_{\min,m} - \frac{q_{\max}T}{C_m}}{\frac{BT}{\delta} \log_2 \left(1 + \frac{p_{max}|h_m|^2}{\sigma_{mec}^2} \right)} \right) \right]^+, 1 \right). \tag{2.17}$$

The upper boundary of power allocation variable p_m is denoted as $p_{\max}$, and the upper boundaries for q_m and t_m are $q_m^{\max}$ and T under constraints (9d) and (9g), respectively. Therefore, each particle's position represents a vector of $1 + 3M$ elements, $(\theta, \{p_m, q_m, t_m\})$, for which the limits are $[\theta_{\min}, \theta_{\max}]$, $[p_{\min,M}, p_{\max}]$, $[q_{\min,M}, q_m^{\max}]$, and $[t_{\min,M}, T]$, respectively. The initial values of the s-th particle's positions are randomly initialized based on the uniform distribution between these limits established for each particle's position.

Moreover, a penalty function based on objective function $f(\mathbf{x}_s) = f(\theta, p_m, q_m, t_m)$ of problem (2.9) is used to deal with the constraint as follows:

$$f(\mathbf{x}_s) = \frac{\sum\limits_{m=1}^{M} \left[r_m^{off} + \gamma_m^{loc} \right]}{\sum\limits_{m=1}^{M} \left[p_{r,m}\theta T + \vartheta (p_m + p_c)(1 - \theta) T + \alpha_m q_m^3 t_m \right]} - \gamma \sum_{i=1}^{2m+1} \rho(k_i), \qquad (2.18)$$

where the penalty value is denoted as γ, and k_i is the i-th constraint of problem (2.9) corresponding to (9b), (9c), and (9f). In addition, the function based on constraint $\rho(k_i) = 0$ means that the i-th constraint is satisfied; otherwise, $\rho(k_i) = 1$.

Furthermore, the procedures of the proposed PSO-based algorithm to solve SCE maximization problem (2.9) are described in Algorithm 1, where the input parameters for PSO are the maximum number of iterations, the number of particles in a swarm, the inertia weight for velocity updates, and the cognitive and social parameters, which are denoted as $I_{\max}$, S, I_w, c_1, and c_2, respectively. The initial values of the m-th particle's velocities are randomly initialized between the boundaries established for each particle's position: $[\theta_{\min}, \theta_{\max}]$, $[p_{\min,m}, p_{\max}]$, $[q_{\min,m}, q_m^{\max}]$, and $[t_{\min,m}, T]$. Accordingly, in each successive b-th iteration, the velocity of each m-th particle is updated towards the relative global best position, $\mathbf{gb}$, and the local best position, $\mathbf{pb}_s$, as follows:

$$v_{\theta,s}^{b+1} = I_w^{(b)} v_{\theta,s}^{(b)} + n_1 c_1 \left(pb_{\theta,s} - x_{\theta,s}^{(b)} \right) + n_2 c_2 \left(gb_\theta - x_{\theta,s}^{(b)} \right) \qquad (2.19a)$$

$$v_{p_m,s}^{b+1} = I_w^{(b)} v_{p_m,s}^{(b)} + n_1 c_1 \left(pb_{p_m,s} - x_{p_m,s}^{(b)} \right) + n_2 c_2 \left(gb_{p_m} - x_{p_m,s}^{(b)} \right), \; \forall m \qquad (2.19b)$$

$$v_{q_m,s}^{b+1} = I_w^{(b)} v_{q_m,s}^{(b)} + n_1 c_1 \left(pb_{q_m,s} - x_{p_m,s}^{(b)} \right) + n_2 c_2 \left(gb_{q_m} - x_{q_m,s}^{(b)} \right), \; \forall m \qquad (2.19c)$$

$$v_{t_m,s}^{b+1} = I_w^{(b)} v_{t_m,s}^{(b)} + n_1 c_1 \left(pb_{t_m,s} - x_{t_m,s}^{(b)} \right) + n_2 c_2 \left(gb_{t_m} - x_{t_m,s}^{(b)} \right), \; \forall m, \qquad (2.19\text{d})$$

where n_1 and n_2 are random numbers between zero and one.

The update of the particle's position is based on the current particle's position plus the corresponding updated velocity. Therefore, the m-th particle's position belonging to the set of elements pointed out in (2.20) is updated as follows:

$$x_{\theta,s}^{b+1} = x_{\theta,s}^b + v_{\theta,s}^{b+1} \qquad (2.20\text{a})$$

$$x_{p_m,s}^{b+1} = x_{p_m,s}^b + v_{p_m,s}^{b+1}, \; \forall m \qquad (2.20\text{b})$$

$$x_{q_m,s}^{b+1} = x_{q_m,s}^b + v_{q_m,s}^{b+1}, \; \forall m \qquad (2.20\text{c})$$

$$x_{t_m,s}^{b+1} = x_{t_m,s}^b + v_{t_m,s}^{b+1}, \; \forall m. \qquad (2.20\text{d})$$

In this chapter, the low-complexity PSO-based optimization technique allows us to find the best values of the variables θ, p_m, q_m, and t_m to maximize the SCE by iteratively updating the global and local best particle positions until reaching the stopping criterion.

Regarding the computational complexity of the PSO algorithm in solving problem (2.9), it is necessary to compute the number of iterations used and the number of particles in the swarm. Therefore, the total complexity is given by $O(I_{\max}S)$. We highlight the fact that matrix operations are not needed to solve the proposed optimization problem.

2.4.2   PSO-based Algorithm for Fully Offloading in the MEC

The procedure of the PSO-based algorithm in the fully offloading MEC system is developed in a way similar to that described in Algorithm 2.1. However, in this case, each particle's position represents a vector of $1 + M$ elements, $(\theta, \{p_m\})$, for which the limits are $\left[\theta_{\min}, \theta_{\max\_off}\right]$, $\left[p_{\min\_off,m}, p_{\max}\right]$, respectively. These boundaries are indicated as follows:

$$\theta_{\max\_off} = \min \left(\min_{1 \le m \le M} \left[1 - \frac{r_{\min,m}}{\frac{B}{\delta} T \log_2 \left(1 + \frac{p_{\max}|h_m|^2}{\sigma_{mec}^2} \right)} \right]^+, 1 \right), \qquad (2.21\text{a})$$

Algorithm 2.1 PSO-based algorithm to solve SCE problem P1.

1: **Input**: Set the PSO parameters: $I_{\max}$, S, I_w, c_1, and c_2.

2: Set iteration count $b=1$.

3: Initialize the position of particles $\mathbf{x}_s = \left(\theta, \mathbf{p}, \mathbf{q}, \mathbf{t} \right)$ which are randomly selected in $[\theta_{\min}, \theta_{\max}]$, $\left(p_{\min,m}, p_{\max} \right)$, $\left(q_{\min,m}, q_m^{\max} \right)$, and , $\left(t_{\min,m}, T \right)$, respectively. Then, evaluate $f(\mathbf{x}_s)$.

4: Find the index of the best particle position: $\mathbf{g}_{best} = \arg\max_{1 \leq s \leq S} f(\mathbf{x}_s)$.

5: Initialize the local best position: $\mathbf{pb}_s = \mathbf{x}_s, \forall s$ and the s-th particle's velocities: $v_s^{(b)} = \left(v_{\theta,s}^{(b)}, v_{\mathbf{p}_m,s}^{(b)}, v_{\mathbf{q}_m,s}^{(b)}, v_{\mathbf{t}_m,s}^{(b)} \right)$.

6: **For** $b = 1 : 1 : I_{max}$ **do**

7:     **For** each particle $s = 1, \ldots, S$ **do**

8:         From (2.19a) to (2.19d), update the particles' velocity.

9:         Update particle position by using equations (2.20a) to (2.20d): $\mathbf{x}_s^{b+1} \left(\mathbf{x}_s + \mathbf{v}_s^{b+1} \right.$.

10:         Restrict each particle's position for vector in accordance with boundaries $[\theta_{\min}, \theta_{\max}]$, $\left(p_{\min,m}, p_{\max} \right)$, $\left(q_{\min,m}, q_m^{\max} \right)$, and $\left(t_{\min,m}, T \right)$.

11:         Evaluate the local best position:

12:         **if** $f\left(\mathbf{x}_s^{(b+1)} \right) > f(\mathbf{pb}_s)$ **then** $\mathbf{pb}_s \left(\mathbf{x}_s^{(b+1)} \right.$

13:         **end if**

14:         Evaluate the global best position:

15:         **if** $f\left(\mathbf{x}_s^{(b+1)} \right) > f(\mathbf{g}_{best})$ **then** $\mathbf{g}_{best} \left(\mathbf{x}_s^{(b+1)} \right.$

16:         **end if**

17:     **end for**

18: **end for**

19: **Result:** Set $f(\mathbf{g}_{best})$ as the maximum SCE in the wireless-powered NOMA-enabled MEC system for problem (2.9).

$$p_{\min\_off,m} = \left[\left(2^{\frac{r_{\min,m}}{\frac{B}{\delta}(1-\theta_{\min})T}} - 1\right)\frac{\sigma^2_{mec}}{|h_m|^2}\right]^+.$$ (2.21b)

2.4.3   PSO-based Algorithm for Partial Offloading in the TDMA-MEC System

In the TDMA-MEC system, a particle's position is composed of the following $1 + 4M$ elements: $\theta, \{w_m, p_m, q_m, t_m\}$. Thereby, the search space is established according to the following limits:

$$0 \leq \theta \leq 1,$$ (2.22a)

$$\left[2^{\frac{r_{\min,m}-\frac{q_{\max}T}{C_m}}{\frac{B}{\delta}T}} - 1\right]^+ \frac{\sigma^2_{mec}}{|h_m|^2} \leq p_m \leq p_{\max}, \forall m$$ (2.22b)

$$\left[\left(r_{\min,m} - \frac{B}{\delta}T\log_2\left(1 + \frac{p_{max}|h_m|^2}{\sigma^2_{mec}}\right)\right)\frac{C_m}{q_{\max}}\right]^+ \leq t_m \leq T, \forall m$$ (2.22c)

$$\left[\left(r_{\min,m} - \frac{B}{\delta}T\log_2\left(1 + \frac{p_{max}|h_m|^2}{\sigma^2_{mec}}\right)\right)\frac{C_m}{T}\right]^+ \leq q_m \leq q_{\max}, \forall m$$ (2.22d)

$$0 \leq w_m < 1, \forall m.$$ (2.22e)

Then, the procedure to apply the PSO algorithm is similar to that expressed in Algorithm 2.1.

2.5   Numerical Results

In this section, we numerically evaluate the performance of our proposed wireless-powered NOMA-MEC system with an EH user and PB. The simulations were programmed in Matlab by utilizing a Core i7-6700K CPU with 16 GB of main memory. In addition, the application of TDMA and fully offloading mode are considered baseline schemes to be evaluated and compared with our proposed scheme. The results presented in this chapter were averaged over 50 independent channel realizations. In addition, the PSO algorithm was executed ten times for each channel realization, where the average value was used to evaluate the results.

In the considered work, the channels follow circularly symmetric, complex Gaussian random variables as follows: $h_m : CN\left(0, d_{AP-u_m}^{-v}\right)$, $f_m : CN\left(0, d_{PB-u_m}^{-v}\right)$, $g_m : CN\left(0, d_{Eav-u_m}^{-v}\right)$, $l_{AP} : CN\left(0, d_{AP-EH}^{-v}\right)$, and $l_{PB} : CN\left(0, d_{PB-EH}^{-v}\right)$, where d_{ij} denotes the distance between node i and j and the path-loss exponent is denoted by v. The distances between the nodes were $d_{AP-u_1}^{-v} = 10$, $d_{AP-u_2}^{-v} = 5$, $d_{PB-u_1}^{-v} = 6$, $d_{PB-u_1}^{-v} = 4$, $d_{Eav-u_1}^{-v} = 6$, $d_{Eav-u_2}^{-v} = 10$, $d_{AP-EH}^{-v} = 5$, and $d_{PB-EH}^{-v} = 3$, in meters. Moreover, the simulation parameters listed in Table 2.1 were chosen based on the work in [6, 44, 46, 53–58]. Specifically, the parameters for the non-linear EH model such as the maximum EH power, sensitivity threshold, circuit parameters were chosen based on [44, 53], the communication bandwidth, the minimum computation bits, the number of cycles for one bit, the amplifier coefficient, the constant circuit power were selected based on [44] and the maximum cycles per second was selected based on [54, 55].

The simulation parameters for PSO are selected based on [6, 46, 56–58], which frequently provide good converge behavior. In addition, simulations were carried out to set the suitable PSO parameters such as inertia weight for velocity update, cognitive and social parameters. Then, the cognitive and social parameters were set $c_1 = 2$ and $c_2 = 2$, and the inertia weight for velocity update was set $I_w = 0.7$. Figure 2.3 shows the convergence of the PSO algorithm of our proposed scheme in partial offloading mode with four different combinations of the inertia weight, cognitive and social parameters where typical values in the literature [6, 46, 56–58] are used. For instance, in [57], the linear decreasing inertia weight is established as $I_w(t) = I_{w,max} - \frac{I_{w,max} - I_{w,min}}{I_{max}} \times t$, where $I_{w,max} = 0.9$, $I_{w,min} = 0.4$, t is the current iteration and I_{max} is the maximum number of iteration. In addition, we set the number of particles $S = 40$, $q_{max} = 10^8$ cycles/s, $I_{max} = 200$, and the rest of the simulation parameters were as indicated in Table 2.1. We can observe that the case with $c_1 = c_2 = 2$ and $I_w = 0.7$ achieves the fastest convergence among all the cases. Then, we set $c_1 = c_2 = 2$ and $I_w = 0.7$ for the rest of the simulations.

In [59], the authors proposed some initialization strategies for the particles' positions in

Table 2.1: Simulation parameters.

Parameter	Notation	Value
Number of users	M	2
Communication bandwidth	B	2 MHz
Communication overhead	δ	1.1
Minimum computation bits	$r_{\min,m}$	10^4 bits
Minimum harvested energy by EH user	ξ_{EH}	0.0006 W
Number of cycles for one bit	C_m	10^3 cycles/bit
Maximum CPU frequency	$q_{\max}$	10^8 cycles/s
Transmission power from the AP and PB	P_{AP}, P_{PB}	0.2 W
Capacitance coefficient	α_m	10^{-24}
Amplifier coefficient	ϑ	3
Maximum transmission power of the user	$p_{\max}$	0.04 W
Consumed power for receive-signal processing	p_r	5 dBm
Constant circuit power	p_c	5 dBm
Path-loss exponent	v	4
Noise variance	σ^2	-80 dBm
Maximum EH power	$P_{eh\_\max}$	0.004927 W
Sensitivity threshold	p_0	0.000064 W
Circuit parameter	λ	0.29
Circuit parameter	μ	274
Constant circuit power	p_c	5 dBm
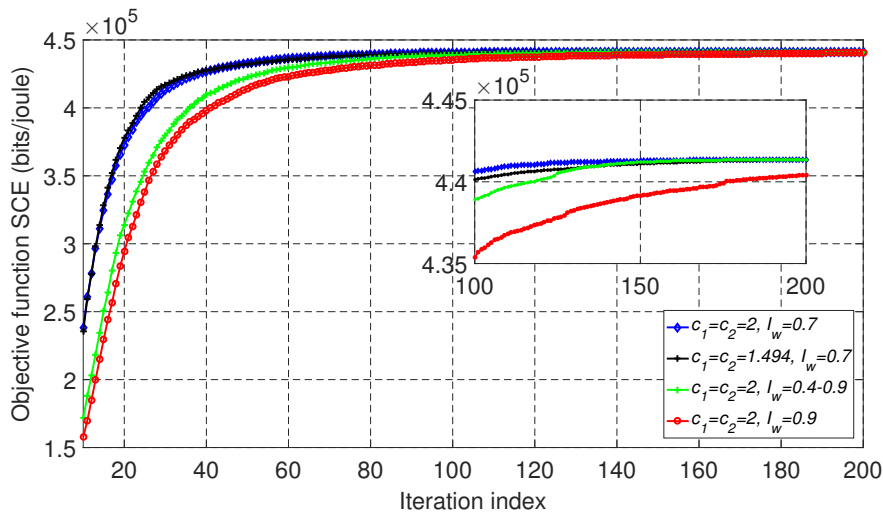
Figure 2.3: The convergence behavior of the proposed PSO-based algorithm for different combinations of the inertia weigh, cognitive and social parameters.

PSO, such as the logarithmic and normal distributions. In the case of the logarithmic, the position of the particle for the variable θ is initialized as $\exp\left(\ln\left(\theta_{min}\right) + \ln\left(\theta_{max}/\theta_{min}\right) \times rnd\right)$, where *rnd* is a random number from the uniform distribution in $[0, 1]$. In the case of the normal, the position of the particle for the variable θ is initialized based on the normal distribution with mean $\mu = \frac{\theta_{max} + \theta_{min}}{2}$ and the standard deviation between 1 to 5. From the numerical simulations with a number of particles $S = 40$ and $I_{max} = 200$, we obtain a SCE value of 441342.39 bits/joule for the uniform distribution (used in the proposed approached), a SCE value of 423160.11 bits/joule with the logarithmic strategy, and a SCE value of 436509.85 bits/joule for the normal distribution with a standard deviation of 5. We conclude that the uniform distribution strategy achieves a better SCE than the other initialization strategies.

Next, we present the PSO convergence behavior with ten runs of the PSO algorithm by using a different number of particles for each scheme, i.e., the TDMA baseline scheme and the wireless-powered NOMA-MEC system in partial offloading mode and fully offloading mode, with the simulation parameters indicated in Table 2.1.
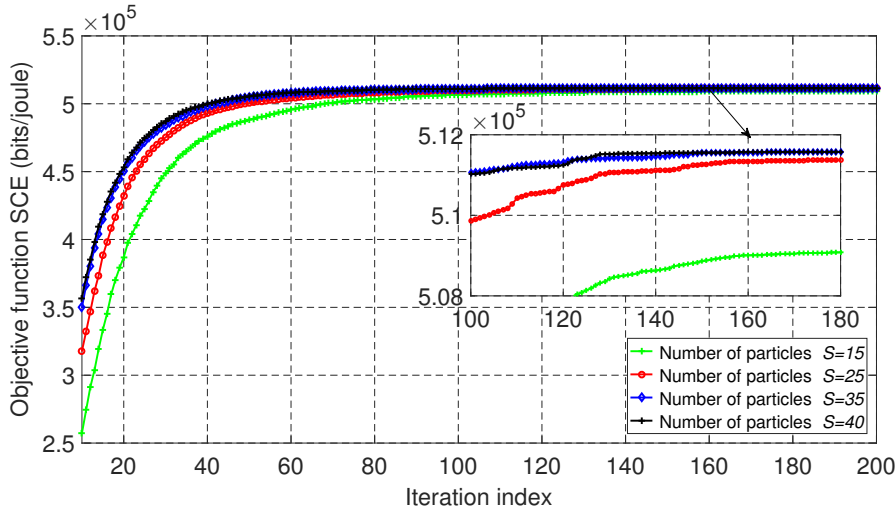
Figure 2.4: The convergence behavior of the proposed PSO-based algorithm with different numbers of particles, S, in the proposed wireless-powered NOMA-MEC system for partial offloading mode when $q_{max} = 4 \times 10^8$ cycles/s.

Figure 2.4 shows the convergence of the PSO algorithm given in Algorithm 1 for our wireless-powered NOMA-MEC system with an EH user and PB, based on four different numbers of particles, $S = \{15, 25, 30, 40\}$, and with $q_{max} = 4 \times 10^8$ cycles/s. The rest of the simulation parameters were as indicated in Table 2.1. We can see that the performance of the SCE was enhanced as the iteration index and the number of particles increased. Moreover, we observe that the SCE achieved steady behavior after about 100 iterations. However, as we reached a greater number of particles and iterations, the computational complexity increased, since each particle evaluated the objective function and constraints for a total time equal to the maximum number of iterations.

Similar to Figure 2.4, Figure 2.5 shows the convergence of the PSO algorithm of our proposed scheme in partial offloading mode with four different numbers of particles, $S = \{15, 25, 30, 40\}$. In this case, we set the value of the maximum CPU frequency parameter at $q_{max} = 10^8$ cycles/s to verify the convergence of our proposed scheme in a different scenario. From Figure 2.5, we can see that the SCE showed stable behavior from around 100 iterations, and its highest performance
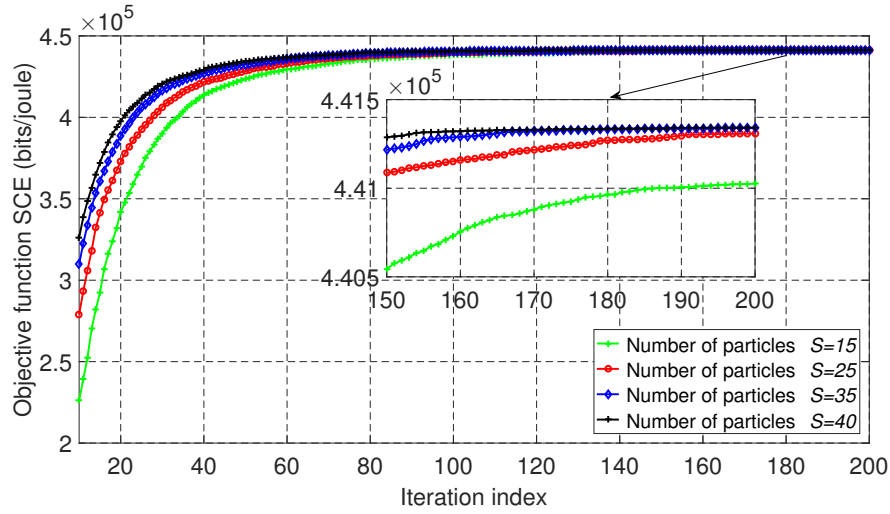
Figure 2.5: The convergence behavior of the proposed PSO-based algorithm with different numbers of particles, S, for the proposed wireless-powered NOMA-MEC system in partial offloading mode with $q_{\max} = 10^8$ cycles/s.

was achieved at $S = 40$. In order to select a suitable value for the number of particles and the maximum number of iterations, we have analyzed the computation time of the PSO algorithm and the other baseline schemes. Then, in Table 2.2, we have compared the incidence for the number of particles in terms of the relative error and computation time of our proposed scheme, NOMA-MEC in fully offloading mode, and those of TDMA-MEC system. To compute relative error, we set the one obtained by using $S = 40$ as the true value for each scheme since this value is correspondent to the highest SCE, and the computation time was calculated with 200 as the number of iterations for the proposed scheme and fully offloading mode. On the other hand, the computation time for the TDMA-based scheme was evaluated with 400 iterations. As a result, we can see that the higher number of particles entails the lower relative error at the expense of a longer computation time. Therefore, we set $I_{\max} = 170$ and $S = 35$ for further simulations of our proposed wireless-powered NOMA-MEC system.

Figure 2.6 shows the convergence of the PSO algorithm for the wireless-powered NOMA-

Table 2.2: Effects of the number of particles on PSO

	TDMA-MEC system in partial offloading mode				NOMA-MEC system in fully offloading mode				The proposed NOMA-MEC system in partial offloading mode			
Particles S	15	25	35	40	15	25	35	40	15	25	35	40
Time (ms)	80.43	134.77	158.65	208.99	27.44	45.68	57.45	72.12	30.99	48.63	58.97	79.63
Relative error (%)	8.631	6.750	5.740	—	0.0031	0.0012	0.0009	—	0.0708	0.0082	0.0020	—

MEC system in fully offloading mode in accordance with four different numbers of particles, $S = \{15, 25, 30, 40\}$ and with $q_{max} = 10^8$ cycles/s. From Figure 2.6, we can see that the SCE is converged after iteration 180, and its highest performance was achieved with 40 particles, followed slightly by using 35 particles. However, the larger number of particles, the longer the computation time required to complete the process of the PSO algorithm, as shown in Table 2.2. Therefore, we used $I_{max} = 180$ and $S = 35$ for the simulations performed in the NOMA-MEC system with the fully offloading scheme.

Figure 2.7 shows the convergence of the TDMA-MEC system baseline scheme in partial offloading mode. From Figure 2.7, it is observed that the SCE can be stable after 600 iterations. It is noteworthy that the required number of iterations for convergence of SCE in the TDMA-MEC scheme was higher than those of the previous schemes since an extra variable for offloading time, w_m, needs to be optimized to solve the optimization problem in the TDMA-MEC scheme, as shown in problem formulation (11). Moreover, the SCE performance reached a higher value with $S = 40$. Thus, we used the tradeoff values of $S = 40$ and $I_{max} = 250$ for simulations of the TDMA-MEC baseline system in partial offloading mode.
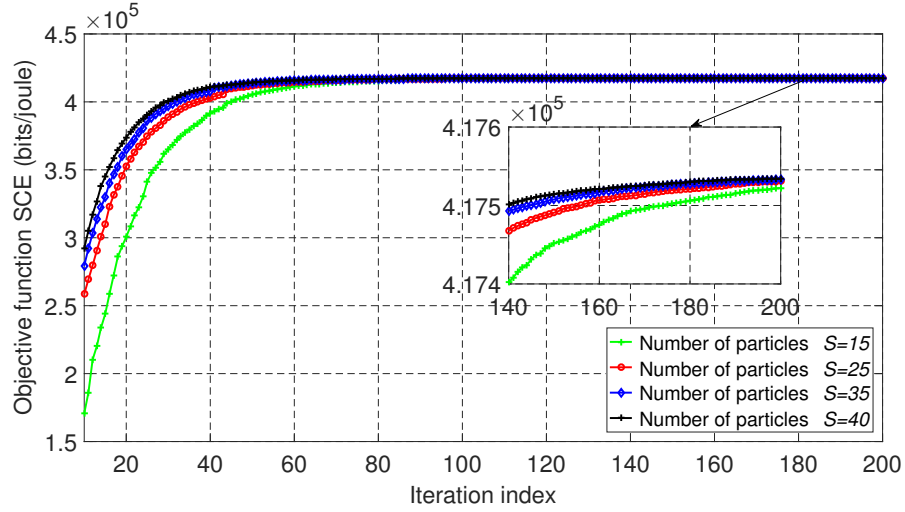
Figure 2.6: The convergence behavior of the proposed PSO-based algorithm with different numbers of particles, S, for the wireless-powered NOMA- MEC system in fully offloading mode when $q_{max} = 10^8$ cycles/s.
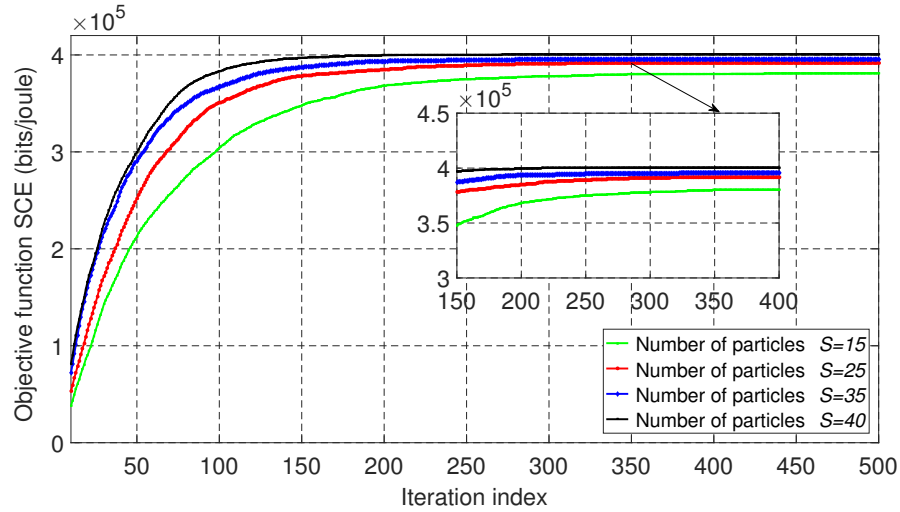
Figure 2.7: The convergence behavior of the proposed PSO-based algorithm with different numbers of particles, S, for the wireless-powered TDMA-MEC system in partial offloading mode when $q_{max} = 10^8$ cycles/s.
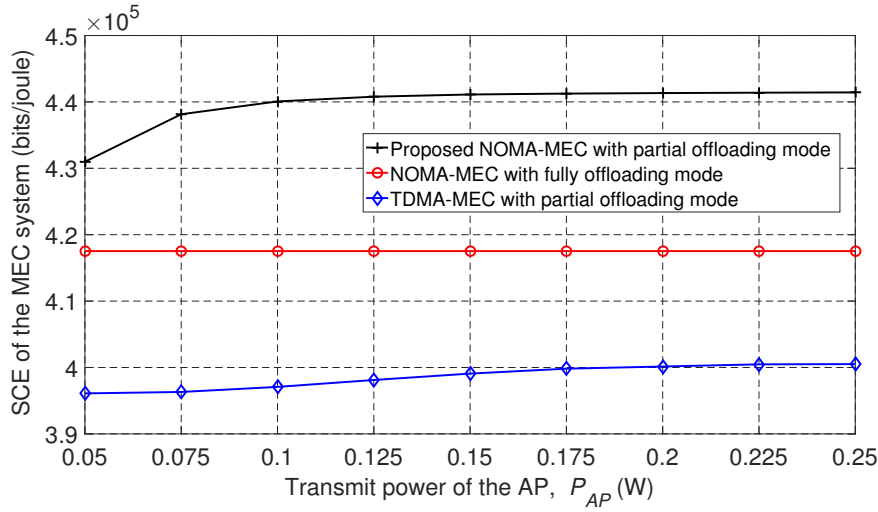
Figure 2.8: SCE based on the transmission power of the wireless AP.

Figure 2.8 shows a comparison of SCE performance from our proposed scheme applying NOMA in the wireless-powered MEC system in partial offloading mode, from the NOMA-enabled MEC system in fully offloading mode, and from the TDMA-MEC scheme in partial offloading mode. In Figure 2.8, observe that the NOMA-assisted MEC system outperformed the baseline schemes. We can particularly see that the proposed scheme had a much better SCE performance than that obtained by the conventional TDMA-MEC scheme. This is because only one phase is required to offload the tasks from the users to the MEC server in our proposed NOMA-MEC scheme, where the same time interval can be shared by all users. Thus, resources are efficiently used. Using TDMA in the MEC system, more resources are employed to complete offloading the computation tasks, since each user offloads to the MEC server at different times. Accordingly, the eavesdropper has more opportunities to trap messages that are transmitted in the wireless environment. Hence, the SCE in the TDMA-MEC system was lower than that achieved in the proposed NOMA-MEC system.

Figure 2.9 shows the SCE achieved with three different values for transmission power P_{PB}. We can see that the SCE performance increased as the transmission power of the AP and PB increased. This is because when transmission power increases, users can harvest a greater amount of
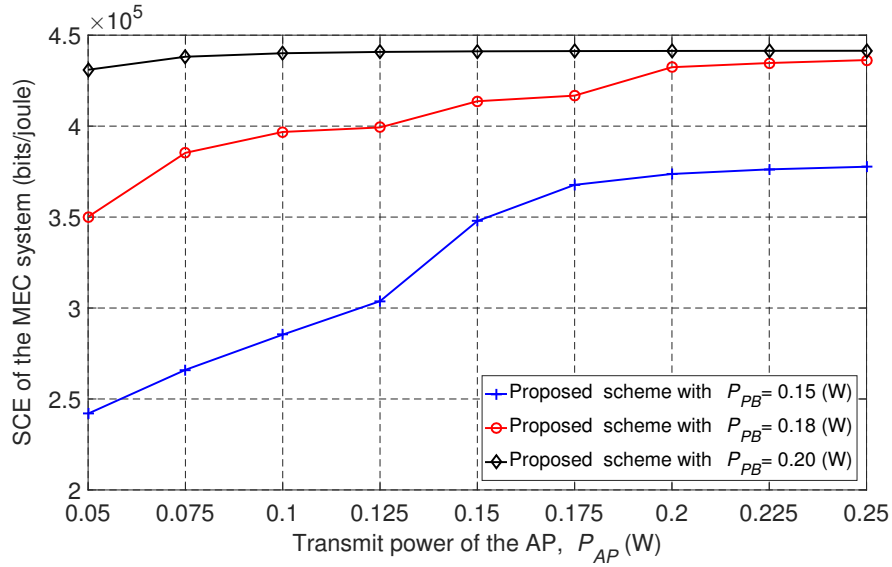
Figure 2.9: SCE based on transmission power of the wireless AP at different transmission power levels for the PB.

energy to be used in the local computing and offloading processes.

Figure 2.10 shows the SCE versus the number of cycles for one bit, C, for the TDMA-MEC baseline scheme and the proposed scheme with two different transmission power levels at the AP. From Figure 2.10, we can observe that the SCE performance decreased as C increased. This is because the relation between the number of locally computed bits of the $m-$th user in local computing mode, γ_m^{loc}, is inversely proportional to C, i.e., γ_m^{loc} decreases as C increases. This relation is indicated in equation (2.3). The main objective in this chapter is to maximize the SCE, and it depends directly on γ_m^{loc}. Consequently, if γ_m^{loc} decreases, the SCE performance also decreases. Moreover, from Figure 2.10, we verify that our proposed scheme outperforms the TDMA-MEC baseline scheme, and SCE is enhanced with higher values for the wireless power transmitted from the AP to users.
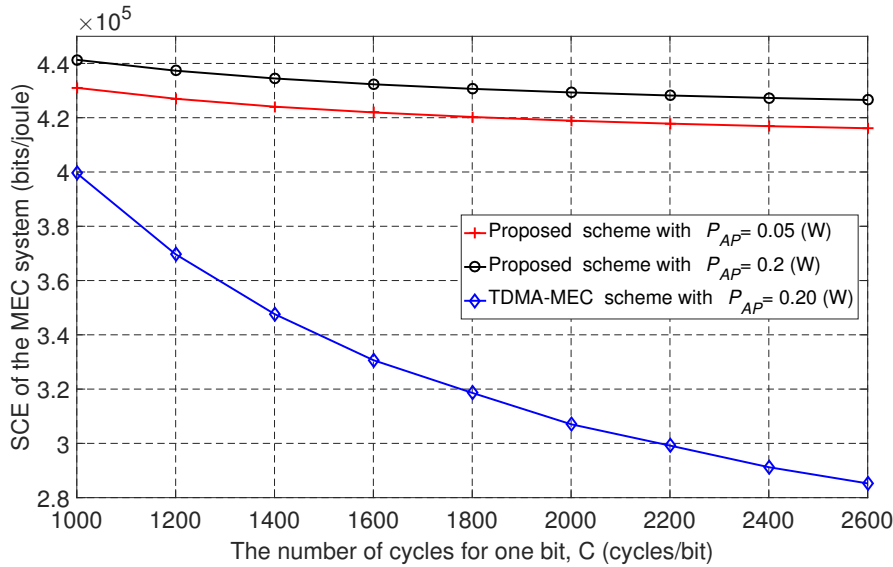
Figure 2.10: The SCE versus the number of cycles for one bit, *C*, at different transmission power levels of the AP.

2.6   Closing Remarks

In this chapter, we considered a wireless-powered NOMA-enabled MEC system assisted by a PB, with an EH user, and in the presence of an eavesdropper. The objective is to maximize the SCE under the constraints of minimum computation bits required by the users, minimum EH required by the EH user, and a limitation on the consumed energy. We proposed a low-complexity approach based on the PSO algorithm, and achieved high performance with a low computation time. Simulation results demonstrated the superiority of the proposed scheme in comparison with fully offloading mode and TDMA-based mode. The advantages of the NOMA technique were proved, compared with the TDMA method, where NOMA permits more efficient utilization of the spectrum resources. Moreover, numerical results showed that the presence of a low-cost and low-complexity PB allows us to improve the SCE in the studied scenarios.

Chapter 3

Joint Beamforming and Artificial Noise Optimization for Secure Transmissions in MISO-NOMA Cognitive Radio System with SWIPT [1]

3.1 Introduction

The rapid development of wireless communications requires advanced communications techniques that can provide massive connectivity, high spectral efficiency, high energy efficiency, and low latency in support of the fast proliferation of the IoT, mobile devices, and so on. Therefore, integration of promising technologies, such as CR and NOMA techniques, has been investigated by the industry and by academics to enable future wireless networks [6, 61]. Specifically, CR tackles spectrum scarcity issues and improves spectrum efficiency based on its strategy of dynamic

---

[1]The study in this chapter is published in Electronics [60]

spectrum access, which permits the use of licensed spectrum by unlicensed users, called SUs, without interfering with licensed users [62, 63]. There are two types of spectrum sharing in accordance with access technology: underlay and overlay spectrum sharing. Underlay spectrum sharing permits SUs to use the licensed spectrum while keeping their power levels below a certain threshold to prevent unacceptable interference with licensed users, also known as PUs [7, 64]. On the other hand, overlay spectrum sharing tries to minimize the risk of any interference with the PUs at the expense of spectrum use, allowing SUs to use the licensed spectrum in the absence of the PUs [8, 65].

Meanwhile, NOMA has surged as another powerful technology to enhance spectrum efficiency while providing high transmission rates and high user densities for future mobile communications [2, 3]. NOMA can be categorized into code-domain and power-domain NOMA. Complex encoding or decoding techniques are required in code-domain NOMA, while the key idea of power-domain NOMA is to assign different power levels to users according to their channel strength, such that higher transmission power is assigned to users with weaker channels. Moreover, on the receiver side, users with stronger channels apply SIC to first decode the signals of the weaker users, and then, they decode their own signals. In this chapter, we focus on power-domain NOMA, which can be further combined with other communications technologies MIMO, cooperative communications) to reach a better yield [29, 58, 66–69].

Furthermore, energy-efficient techniques have been investigated for future wireless networks in support of environmental concerns and battery-limited devices, such as sensors and wearables [70]. In this sense, achieving high energy efficiency and recycling energy are the main goals of energy-efficient techniques, where SWIPT brings technological innovations and plays a key role in energy and information transmission [71–73]. In contrast to the conventional EH technologies that rely on unpredictable natural sources, or where the communications nodes are only able to recharge from electromagnetic radiation, such as wireless power transfer (WPT), SWIPT enables users to perform ID and RF EH simultaneously [74, 75]. Hence, the study of SWIPT in NOMA with CR

networks is of meaningful importance in supporting massive numbers of mobile devices with limited battery power [76–78].

However, a NOMA-CR network assisted by SWIPT technology operates in a wireless transmission environment, which is vulnerable to malicious receivers that can intercept confidential information transmitted from the sources to either the legitimate or the unlicensed users. Therefore, security is a critically challenging issue that must be handled for the suitable deployment of wireless communications networks. In this sense, PLS has emerged as a complementary technology to address the eavesdropping security issue by exploiting the physical characteristics of wireless channels, e.g., propagation delay, multipath fading, and so on. Although traditional cryptographic encryption and decryption techniques have been pointed out to secure communication systems using complex algorithms and encryption keys. They require key management, maintenance and distribution procedures that use network resources and may become an issue in large-scale decentralized and heterogeneous wireless network. Moreover, the encryption keys are prone to being broken by high computational capabilities of an eavesdropper [79, 80]. These drawbacks are the motivations for the study and research on PLS to complement cryptographic techniques. PLS is independent of complex algorithms and key management of which initial idea was investigated in Wyner's work [13]. Wyner et al. explained that it is possible to achieve secure communication between legal users without sharing a secret key if the eavesdropper's channel is a much noisier version than the legitimate user's channel. In addition, PLS metrics include secrecy channel capacity or secrecy rate, secrecy outage probability, secrecy throughput, bit error rate-based and packet error rate-based metrics. One of the most common metric used in various research works is the secrecy channel capacity which indicates the maximum secrecy rate at which the message is retrieved safely at the legitime user while preventing it to be recovered at the eavesdropper. This metric is calculated by the difference between the legitimate and eavesdropper's channel capacities.

3.1.1   Related Work

In the literature, to further improve the secure performance of wireless transmissions, different strategies have been proposed, such as multiple antennas, beamforming designs, AN or jamming, and resource allocation schemes [1, 30, 46]. For instance, security in cooperative single-input single-output (SISO) NOMA networks has been investigated in [30, 46], aiming to maximize the SSR and SEE, respectively, by applying a low-complexity solution based on PSO. Recently, PLS in MEC system was studied in [30] to maximize the secure computation efficiency by jointly optimizing the resource allocations such as the transmission power, the computation time, and the central processing unit frequency. The results showed the superiority of NOMA over the TDMA) conventional scheme. However, none of these studies previously discussed consider MISO and SWIPT technology which can increase the spectral efficiency of the network. Secure NOMA transmission in a MISO scenario was investigated [81–85] via joint beamforming and AN optimization. The authors of both [81, 82] maximized the SSR by using joint precoding optimization, while in [83], the authors provided secure NOMA transmission by maximizing the jamming power, and they applied SIC at the receiver to avoid affecting legitimate transmissions. In [81], the authors considered downlink MISO-NOMA system with the presence of an eavesdropper. The objective was to obtain the optimal precoder vectors to maximize the SSR of the users subject to the constraints of maximum available power and rate requirement in each user. The solution was an iterative algorithm based on the second-order cone programming. However, the authors did not consider the SWIPT technology, EH users, AN along with an underlying CR system, which involves extra constraints related to EH requirements and maximum interference allowed to the primary network. Therefore, the solution proposed in [81] cannot be used to solve the optimization problem proposed in this chapter. Another optimization approach to improve the SSR of a MISO-NOMA network has been studied in [84] which is based on a dynamic user scheduling, grouping strategy, and the application of efficient algorithms such as outer polyblock approximation and Dinkelbach. The authors considered

the zero-forcing (ZF) criteria to define the beamforming vectors and investigated the minimum secrecy rate maximization problem to design the optimal power allocation strategy under three main constrains: QoS requirements, secrecy outage probability (SOP) and maximum available power. However, they did not consider EH users and an underlying CR system, which entails new EH constraints and maximum interference constraints in the optimizations problem. In addition, the proposed approach optimized the beamforming vectors and considered an scheme. Therefore, the algorithm in [84] cannot be used for the proposed system model in this chapter.

Security for the primary network of a NOMA-CR system assisted by SWIPT was studied in [85]. The authors considered SU users with the ability to only decode information and several EH users which are considered to be eavesdropper, where the secondary base station (BS) transmits a jamming signal to increase the security of the primary network. The objective was to minimize the total transmission power under the constraints of minimum secrecy rates and EH requirements, in which the solution was based on the SCA algorithm and the SDR technique. It was shown that application of NOMA consumed lower transmission power than baseline schemes and satisfied QoS requirements such as the minimum secrecy rate of legitimate users. Although this paper opened doors to future secure wireless systems integrated with SWIPT in CR-NOMA networks, the authors did not consider SUs with the ability to simultaneously receive information and harvest energy, and it was assumed that channel vectors to the eavesdroppers are known at the secondary BS, which is not always possible in practical scenarios where eavesdroppers are hidden from the secondary BS. Please note that the PS structure considered in this chapter involves the optimization of PS ratios, which are coupled to the beamforming vectors in the optimization problem.

In general, the mathematical algorithms used to solve optimization problems are problem-dependent. The proposed algorithms to solve the optimization problems in the aforementioned literature are developed based on specific characteristic of the problems such as objective function, type of users, type of constraints and so on. For instance, the procedures and techniques used to

transform non-convex problems to convex ones will differ from system to system and depend on the assumptions and elements considered for the optimization problem. When a system model includes new elements with other applications such as SWIPT users or CR capabilities, the previous proposed algorithms cannot be used anymore directly, and a novel algorithm needs to be developed to solve the new problem. Therefore, previous proposed algorithms for a PLS in MISO-NOMA system cannot be applied for the proposed cognitive MISO SWIPT NOMA system with AN.

None of the research described above was specifically proposed to enhance the security of the secondary network in a SWIPT-assisted NOMA-CR with EH users. In addition, the proposed scheme in the chapter can be applied for the security in different scenarios such as IoT systems with RF EH user where spectrum scarcity is a critical issue due to the massive deployment of IoT devices. Here, NOMA is used to achieve better connectivity and to enhance spectrum use while EH can be used for improving the energy efficiency of IoT systems [86].

Furthermore, in the case that malicious EH users exist in the system as the work in [85], where a secondary transmitter sends information signals to SUs and energy to EH user, the EH user can eavesdrop the information transmitted to SUs because of the broadcast nature of NOMA. In this scenario, a channel state information (CSI) of the EH user is available at the secondary transmitter, which can be used for a more precise beamforming design of the AN to interfere with the malicious EH user. In addition, the SSR for the SUs can be directly maximized in the optimization problem to improve the security in the network. On the other hand, in the chapter we propose a more challenging scenario when the eavesdropper is completely hidden from the secondary transmitter and the CSI of the eavesdropper is not available. In this case, the transmission power for legitimate users is minimized to use the remaining available power to maximize the AN. In addition, there is no any impact on the system even though the eavesdropper performs EH since the eavesdropper is not a legitimate user and the secondary transmitter does not transfer extra energy signals to satisfy some EH requirement at the eavesdropper.

3.1.2 Contributions and Organization

The main contributions of this chapter are summarized as follows.

- Secure transmission for a MISO-NOMA-CR network applying SWIPT and assisted by AN is studied to enhance the security of the secondary network. We jointly optimize the precoder vectors and power-splitting (PS) ratios to minimize the transmit power to the SUs and EH users, subject to the constraints of minimum SINR at the SUs, minimum EH for EH users, maximum available power at the secondary transmitter, denoted as SU-Tx, and maximum permissible interference with the PUs. By minimizing the transmit power for SUs and EH users, we can assign the residual power to AN to generate interference against the eavesdropper, by which the security can be improved in the underlying network.

- The formulated non-convex minimization problem is challenging to solve due to coupling between the PS ratios and transmission beamforming vectors. The proposed solution consists of two steps. First, an SDR-based algorithm converts the formulated problem into a SDP problem. Second, a Gaussian randomization technique is applied to obtain the approximate rank-one solutions for beamforming vectors, and a linear program problem is used to guarantee the feasibility of the candidate solutions of the Gaussian randomization technique.

- The SDMA method and the ZF technique are studied as a comparative schemes to solve the minimization problem in which the solution to the non-convex problems are based on the SDR technique. In addition, a MISO-NOMA-CR without AN is considered to be the baseline scheme to prove the advantages of AN.

- Numerical simulations prove the superiority of the proposed approach based on NOMA with AN for increasing the security of the secondary network, in comparison with NOMA without AN, SDMA and ZF schemes. In particular, the proposed AN method shows a significant improvement in SSR over the no-AN scheme under several studied scenarios.

The rest of this chapter is organized as follows. The MISO-NOMA-CR network model with SWIPT and EH users is described in Section 3.2. In Section 3.3, the beamforming optimization with AN is presented along with the proposed solution, and the comparison SDMA and ZF schemes are formulated. The numerical results are presented in Section 3.4. Finally, the conclusions are presented in Section 3.5.

3.2   System Model

In this chapter, we investigate downlink transmissions in a cognitive MISO SWIPT NOMA system with l-th SUs denoted by SU_l, and m-th EH receivers denoted by EH_m that coexist with k-th PUs denoted by PU_k via the underlay scheme, as shown in Figure 3.1. In the proposed underlying CR system, the secondary network can operate in the same frequency band as the primary network, provided that the interference towards the PUs is kept at a tolerable level. We also consider the presence of one malicious eavesdropper that attempts to intercept confidential information of the SUs. Furthermore, the SU-Tx is equipped with N antennas, while there are single antennas for the PU, SU, and EH receivers, and for the eavesdropper. Moreover, we consider the SUs to be hybrid users capable of decoding information and harvesting energy at the same time by employing a PS structure in the receiver, while energy is harvested by the EH receivers. Moreover, the SU-Tx transmits AN to cause interference with the eavesdropper while improving information secrecy. The SU-Tx is in charge of transmitting the signals towards the SU and the EH receivers, as well as, design the beamforming vectors for the multi-antenna scheme. Then, the signal transmitted from the SU-Tx can be expressed as:

$$\mathbf{x} = \sum_{l=1}^{L} \mathbf{v}_l s_l^{SU} + \sum_{m=1}^{M} \mathbf{w}_m s_m^{EH} + \mathbf{f}r, \tag{3.1}$$

where $\mathbf{v}_l \in \mathbb{C}^{N \times 1}$ represents the beamforming vector for the l-th SU with $l \in \mathbb{Q} \triangleq \{1, 2, .., L\}$, s_l^{SU} is the transmitted signal of the l-th SU with unit power $\left| s_l^{SU} \right|^2 = 1$, $\mathbf{w}_m \in \mathbb{C}^{N \times 1}$ denotes the beamforming
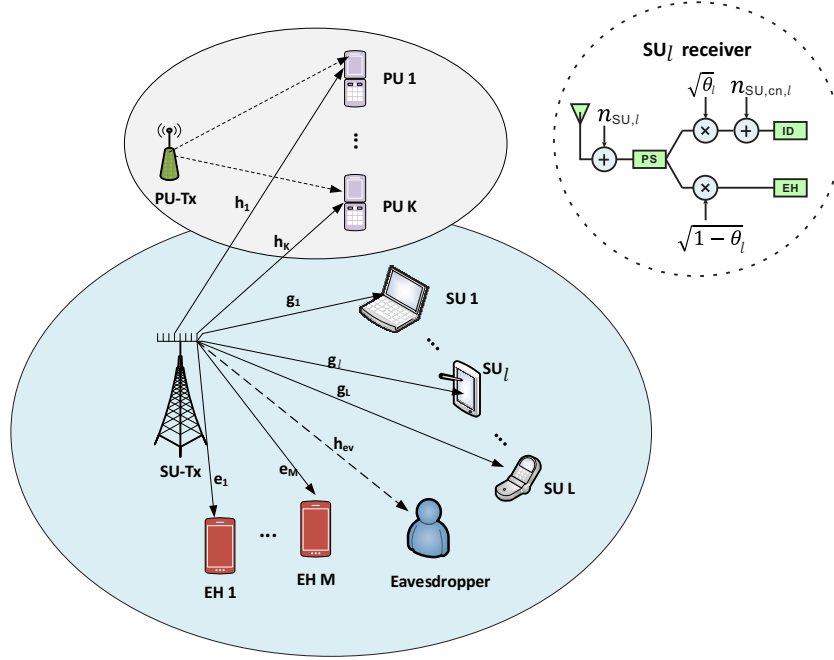
Figure 3.1: Downlink MISO SWIPT CR-NOMA system.

vector for the *m*-th EH receivers with $m = 1, 2, .., M$, s_m^{EH} is the energy signal of the *m*-th EH receiver

with unit power $\left|s_m^{EH}\right|^2 = 1$, $\mathbf{f} \in \mathbb{C}^{N \times 1}$ corresponds to the beamforming vector for the AN, and *r*

is a zero-mean Gaussian random variable with unit power $|r|^2 = 1$, which is artificial jamming.

Beamforming vector $\mathbf{f}$ is used to prevent anything from affecting legal transmissions, and artificial

jamming *r* is randomly generated to effectively disturb any eavesdropping [58].

Accordingly, the received signal at the *l*-th SU is written as

$$y_{SU,l} = \mathbf{g}_l^H \mathbf{v}_l s_l^{SU} + \mathbf{g}_l^H \left(\sum_{l'=1,l'\neq l}^{L} \mathbf{v}_{l'} s_{l'}^{SU} + \sum_{m=1}^{M} \mathbf{w}_m s_m^{EH} + \mathbf{f}r \right) + n_{SU,l}, l \in \mathbb{Q}, \tag{3.2}$$

where $\mathbf{g}_l^H \in \mathbb{C}^{Nx1}$ is the channel vector from the SU-Tx to the *l*-th SU, $n_{SU,l} \sim \mathcal{CN}\left(0, \sigma_l^2\right)$ is the

AWGN at the *l*-th SU, with zero mean and variance denoted as σ^2. In addition, we assume the SU-Tx

has perfect CSI.

Without loss of generality, we consider the first SU to have the strongest channel strength,

whereas the *L*-th SU has the weakest. As such, the order for channel gain between the SU-Tx and the

SUs can be expressed as follows:

$$\|\mathbf{g}_L\|^2 \leq \|\mathbf{g}_{L-1}\|^2 \leq \dots \leq \|\mathbf{g}_1\|^2. \tag{3.3}$$

In NOMA systems, by using the successive interference cancelation procedure, the l-th SU (SU_l) should be capable of successively extracting and decoding the signal intended for the weaker SUs $SU_L, \dots, SU_{l+1}$ from the received signal. Therefore, the following condition for SIC in MISO-NOMA networks with different channel strengths should be satisfied:

$$\left|\mathbf{g}_l^H \mathbf{v}_L\right|^2 \geq \left|\mathbf{g}_l^H \mathbf{v}_{L-1}\right|^2 \geq \dots \geq \left|\mathbf{g}_l^H \mathbf{v}_1\right|^2, l \in \mathbb{Q}. \tag{3.4}$$

The condition expressed in (3.4) will be referred to as the SIC constraint in the rest of the chapter. The condition (3.4) guarantees that at the l-th SU, we have a higher SINR from messages of more distant users since these messages need to be decoded prior to decode the l-th user's own message. Accordingly, the received signal after removing the last $L - l$ user signals can be given by

$$y_{SU,l} = \mathbf{g}_l^H \mathbf{v}_l s_l^{SU} + \mathbf{g}_l^H \sum_{l'=1}^{l-1} \mathbf{v}_{l'} s_{l'}^{SU} + \mathbf{g}_l^H \sum_{m=1}^{M} \mathbf{w}_m s_m^{EH} + \mathbf{g}_l^H \mathbf{f} r + n_{SU,l}, \tag{3.5}$$

where the first term in (3.5) denotes the intended signal for the l-th SU, whereas the second term represents the interference caused by the first $l - 1$ signals intended for the SUs $\{SU_1, \dots, SU_{l-1}\}$. The PS structure at the SUs is based on a PS factor which divides the incoming RF signals into two streams; one to be used for ID and another to harvest energy. It is noteworthy that optimizing the PS factor is required to achieve an optimal trade-off. Then, the achievable SINR for the l-th SU when decoding the signal intended for the i-th SU can be expressed as

$$SINR_l^i = \frac{\theta_l \left|\mathbf{g}_l^H \mathbf{v}_i\right|^2}{\theta_l \left(\sum_{l'=1}^{i-1} \left|\mathbf{g}_l^H \mathbf{v}_{l'}\right|^2 + \sum_{m=1}^{M} \left|\mathbf{g}_l^H \mathbf{w}_m\right|^2 + \left|\mathbf{g}_l^H \mathbf{f}\right|^2 + \sigma_l^2\right) + \sigma_{cn,l}^2}, l \in \mathbb{Q}, \forall_l \leq i, \tag{3.6}$$

where θ_l is the PS factor to divide the incoming signal into the ID and EH modules, and the additive circuit noise in the ID module of the l-th SU is defined as $n_{SU,cn,l} \sim \mathcal{CN}\left(0, \sigma_{cn,l}^2\right)$. It is worth highlighting that (3.6) is true only after performing SIC on the preceding $L - i$ signals.

Moreover, the energy harvested by the EH module in the *l*-th SU can be written as follows:

$$EH_{SU,l} = \eta_{SU,l} (1 - \theta_l) \left(\sum_{l'=1}^{L} \left| \mathbf{g}_l^H \mathbf{v}_{l'} \right|^2 + \sum_{m=1}^{M} \left| \mathbf{g}_l^H \mathbf{w}_m \right|^2 + \left| \mathbf{g}_l^H \mathbf{f} \right|^2 + \sigma_l^2 \right), \forall l. \tag{3.7}$$

In (3.7), $\eta_{SU,l}$ is the energy-harvesting efficiency for the *l*-th SU. For simplicity, we assume that energy-harvesting efficiency is always equal to 1, $\eta_{SU,l} = 1$. The energy harvested by the EH user is given by

$$EH_{EH,m} = \sum_{l=1}^{L} \left| \mathbf{e}_m^H \mathbf{v}_l \right|^2 + \sum_{m'=1}^{M} \left| \mathbf{e}_m^H \mathbf{w}_{m'} \right|^2 + \left| \mathbf{e}_m^H \mathbf{f} \right|^2 + \sigma_{EH,m}^2, \tag{3.8}$$

where $\mathbf{e}_m \in \mathbb{C}^{Nx1}$ is the channel vector from the SU-Tx to the *m*-th EH user, and $\sigma_{EH,m}^2$ is the variance of the antenna noise $n_{EH,m}$ at the m-th EH user, i.e., $n_{EH,m} \sim \mathcal{CN}\left(0, \sigma_{EH,m}^2\right)$.

The power of the SU-Tx causing interference with the *k*-th PU can be defined as

$$PI_k = \sum_{l=1}^{L} \left| \mathbf{h}_k^H \mathbf{v}_l \right|^2 + \sum_{m=1}^{M} \left| \mathbf{h}_k^H \mathbf{w}_m \right|^2 + \left| \mathbf{h}_k^H \mathbf{f} \right|^2, \tag{3.9}$$

where $\mathbf{h}_k^H \in \mathbb{C}^{Nx1}$ is the channel vector from the SU-Tx to the *k*-th PU.

Moreover, the SINR for information signals of the SUs overheard by the eavesdropper is given by

$$SINR_{ev}^l = \frac{\left| \mathbf{h}_{ev}^H \mathbf{v}_l \right|^2}{\sum\limits_{l'=1,l' \neq l}^{L} \left| \mathbf{h}_{ev}^H \mathbf{v}_{l'} \right|^2 + \sum\limits_{m=1}^{M} \left| \mathbf{h}_{ev}^H \mathbf{w}_m \right|^2 + \sigma_{ev}^2}, \tag{3.10}$$

where $\mathbf{h}_{ev}^H \in \mathbb{C}^{Nx1}$ is the channel vector from the SU-Tx to the eavesdropper, and σ_{ev}^2 is the variance of the antenna noise n_{ev} at the eavesdropper i.e., $n_{ev} \sim \mathcal{CN}\left(0, \sigma_{ev}^2\right)$. Moreover, we assume that $\sigma_{EH,m}^2 = \sigma_l^2 = \sigma_{cn,l}^2 = \sigma_{ev}^2 = -80$ dBm.

3.3 Beamforming Optimization with AN

In this chapter, we propose a beamforming optimization scheme to provide security in a MISO SWIPT CR-NOMA network. We consider a practical scenario where the SU-Tx does not have the CSI of the eavesdropper. To further increase the secrecy performance of the network, AN is

generated to tackle eavesdropping and guarantee the security of the confidential information of the unlicensed users. In particular, we minimize the transmit power for the SUs and EH users, subject to the constraints of a minimum SINR for the SUs, minimum EH by the SUs and EH users, maximum available power for the SU-Tx, and maximum interference power to ensure the PUs' legitimate transmissions are not affected. The idea of minimizing transmit power for the SUs and EH users is to use the rest of the available power at the SU-Tx to maximize AN and protect transmitted messages against an eavesdropper. In addition, SDMA and ZF baseline schemes are developed along with MISO CR and SWIPT for comparison purposes.

3.3.1   Beamforming Optimization with AN in the MISO SWIPT CR-NOMA Network

The SU-Tx power for transmitting to SUs and EH users is minimized in the proposed network by satisfying the QoS requirements of each user and in accordance with the decoding order of the SIC indicated in (4), as follows:

$$\min_{\{\mathbf{v}_l, \mathbf{w}_m, \theta_l\}, \mathbf{f}} \quad \sum_{l=1}^{L} \|\mathbf{v}_l\|^2 + \sum_{m=1}^{M} \|\mathbf{w}_m\|^2 \tag{3.11a}$$

$$\text{s.t.} \quad \frac{\theta_l \left|\mathbf{g}_l^H \mathbf{v}_i\right|^2}{\theta_l \left(\sum_{l'=1}^{i-1} \left|\mathbf{g}_l^H \mathbf{v}_{l'}\right|^2 + \sum_{m=1}^{M} \left|\mathbf{g}_l^H \mathbf{w}_m\right|^2 + \left|\mathbf{g}_l^H \mathbf{f}\right|^2 + \sigma_l^2 \right) + \sigma_{cn,l}^2} \geq \gamma_i, \ \forall l, \ i \in \mathbb{Q}, \ l \leq i \tag{3.11b}$$

$$\sum_{l'=1}^{L} \left|\mathbf{g}_l^H \mathbf{v}_{l'}\right|^2 + \sum_{m=1}^{M} \left|\mathbf{g}_l^H \mathbf{w}_m\right|^2 + \left|\mathbf{g}_l^H \mathbf{f}\right|^2 + \sigma_l^2 \geq \frac{\psi_l}{(1-\theta_l)}, \ \forall l \tag{3.11c}$$

$$\sum_{l=1}^{L} \left|\mathbf{e}_m^H \mathbf{v}_l\right|^2 + \sum_{m'=1}^{M} \left|\mathbf{e}_m^H \mathbf{w}_{m'}\right|^2 + \left|\mathbf{e}_m^H \mathbf{f}\right|^2 + \sigma_{EH,m}^2 \geq \xi_m, \ \forall m \tag{3.11d}$$

$$\sum_{l=1}^{L} \|\mathbf{v}_l\|^2 + \sum_{m=1}^{M} \|\mathbf{w}_m\|^2 + \|\mathbf{f}\|^2 = P^{\max}, \tag{3.11e}$$

$$\sum_{l=1}^{L} \left|\mathbf{h}_k^H \mathbf{v}_l\right|^2 + \sum_{m=1}^{M} \left|\mathbf{h}_k^H \mathbf{w}_m\right|^2 + \left|\mathbf{h}_k^H \mathbf{f}\right|^2 \leq \phi_{PU,k}, \ \forall k \tag{3.11f}$$

$$1 > \theta_l > 0, \ \forall l \tag{3.11g}$$

$$\left|\mathbf{g}_l^H \mathbf{v}_L\right|^2 \geq \left|\mathbf{g}_l^H \mathbf{v}_{L-1}\right|^2 \geq \dots \geq \left|\mathbf{g}_l^H \mathbf{v}_1\right|^2, \ \forall l, \tag{3.11h}$$

where γ_i is the minimum targeted SINR for the i-th message, $i \in \mathbb{Q}$, ψ_l is the minimum harvested

energy required by the l-th SU, ξ_m is the minimum harvested energy required by the m-th EH

user, $P^{\max}$ denotes the maximum available power at the SU-Tx, and $\phi_{PU,k}$ denotes the maximum

permissible interference with the k-th PU. Constraint (3.11b) is to guarantee a minimum SINR for

the messages from s_l^{SU} to s_L^{SU} at the l-th SU, while constraints (3.11c) and (3.11d) represent the

minimum harvested energy required by the SUs and the EH users, respectively. Constraint (3.11e)

indicates the maximum available power, $P^{\max}$ that can be consumed by the SUs, the EH users, and

AN. Constraint (3.11f) indicates that the transmit power for the SUs, the EH users, and for AN must

not exceed the maximum permissible interference with the k-th PU, given by $\phi_{PU,k}$. Problem (3.11)

is not convex or challenging to solve due to the coupling between the PS ratios, θ_l, and the precoding

vectors, $\mathbf{v}_l$, $\mathbf{w}_l$, and $\mathbf{f}$, in constraint (3.11b). Therefore, problem (3.11) cannot be solved directly.

We derive an optimal solution via SDR [27] for problem (3.11). Define $\mathbf{V}_l = \mathbf{v}_l \mathbf{v}_l^H$,

$\mathbf{W}_m = \mathbf{w}_m \mathbf{w}_m^H$, $\mathbf{F} = \mathbf{f}\mathbf{f}^H$, $\mathbf{G}_l = \mathbf{g}_l \mathbf{g}_l^H$, $\mathbf{E}_m = \mathbf{e}_m \mathbf{e}_m^H$, and $\mathbf{H}_k = \mathbf{h}_k \mathbf{h}_k^H$, $\forall_l$, $\forall_m$, $\forall_k$. Based on the

properties $\|\mathbf{x}\|^2 = \mathbf{x}^H \mathbf{x}$, $\text{Tr}(\mathbf{AB}) = \text{Tr}(\mathbf{BA})$, and $x = \text{Tr}(x)$, we can derive the following expressions:

$\|\mathbf{v}_l\|^2 = \text{Tr}(\mathbf{V}_l)$, $\|\mathbf{w}_l\|^2 = \text{Tr}(\mathbf{W}_l)$, $\|\mathbf{f}\|^2 = \text{Tr}(\mathbf{F})$, $\left|\mathbf{g}_l^H \mathbf{v}_l\right|^2 = \text{Tr}(\mathbf{G}_l \mathbf{V}_l)$, $\left|\mathbf{g}_l^H \mathbf{w}_m\right|^2 = \text{Tr}(\mathbf{G}_l \mathbf{W}_m)$, and

$\left|\mathbf{g}_l^H \mathbf{f}\right|^2 = \text{Tr}(\mathbf{G}_l \mathbf{F})$. Moreover, a matrix variable, $\mathbf{V}_l = \mathbf{v}_l \mathbf{v}_l^H$, is equivalent to $\mathbf{V}_l$ being a rank-one

symmetric positive semidefinite (PSD) matrix, i.e., $\mathbf{V}_l > 0$, and $\text{rank}(\mathbf{V}_l) = 1$. Thus, we can express

problem (3.11) in the following equivalent form:

$$\min_{\{\mathbf{V}_l, \mathbf{W}_m, \theta_l\}, \mathbf{F}} \sum_{l=1}^{L} \text{Tr}(\mathbf{V}_l) + \sum_{m=1}^{M} \text{Tr}(\mathbf{W}_m) \tag{3.12a}$$

$$\text{s.t.} \left(\sum_{l'=1}^{i-1} \text{Tr}(\mathbf{G}_l \mathbf{V}_{l'}) + \sum_{m=1}^{M} \text{Tr}(\mathbf{G}_l \mathbf{W}_m) + \text{Tr}(\mathbf{G}_l \mathbf{F}) + \sigma_l^2 + \frac{\sigma_{cn,l}^2}{\theta_l} \right) \gamma_i$$

$$- \text{Tr}(\mathbf{G}_l \mathbf{V}_i) \le 0, \ \forall l, \ i \in \mathbb{Q}, \ l \le i \tag{3.12b}$$

$$\frac{\psi_l}{(1 - \theta_l)} - \sum_{l'=1}^{L} \text{Tr}(\mathbf{G}_l \mathbf{V}_{l'}) - \sum_{m=1}^{M} \text{Tr}(\mathbf{G}_l \mathbf{W}_m) - \text{Tr}(\mathbf{G}_l \mathbf{F}) - \sigma_l^2 \le 0, \ \forall_l \tag{3.12c}$$

$$\xi_m - \sum_{l=1}^{L} \text{Tr}\left(\mathbf{E}_m \mathbf{V}_l\right) - \sum_{m'=1}^{M} \text{Tr}\left(\mathbf{E}_m \mathbf{W}_{m'}\right) - \text{Tr}\left(\mathbf{E}_m \mathbf{F}\right) - \sigma_{EH,m}^2 \leq 0, \ \forall m \qquad (3.12\text{d})$$

$$\sum_{l=1}^{L} \text{Tr}\left(\mathbf{V}_l\right) + \sum_{m=1}^{M} \text{Tr}\left(\mathbf{W}_m\right) + \text{Tr}\left(\mathbf{F}\right) = P^{\max}, \qquad (3.12\text{e})$$

$$\sum_{l=1}^{L} \text{Tr}\left(\mathbf{H}_k \mathbf{V}_l\right) + \sum_{m=1}^{M} \text{Tr}\left(\mathbf{H}_k \mathbf{W}_m\right) + \text{Tr}\left(\mathbf{H}_k \mathbf{F}\right) - \phi_{PU,k} \leq 0, \ \forall k \qquad (3.12\text{f})$$

$$\mathbf{V}_l, \mathbf{W}_m, \mathbf{F} \succ 0, \ \forall l, \ \forall m \qquad (3.12\text{g})$$

$$1 > \theta_l > 0, \ \forall l \qquad (3.12\text{h})$$

$$\text{rank}\left(\mathbf{V}_l\right) = 1, \text{rank}\left(\mathbf{W}_m\right) = 1, \text{rank}\left(\mathbf{F}\right) = 1, \ \forall l, \ \forall m \qquad (3.12\text{i})$$

$$\text{Tr}\left(\mathbf{G}_l \mathbf{V}_L\right) \geq \text{Tr}\left(\mathbf{G}_l \mathbf{V}_{L-1}\right) \geq ... \geq \text{Tr}\left(\mathbf{G}_l \mathbf{V}_1\right), \ \forall l. \qquad (3.12\text{j})$$

Problem (3.12) is still non-convex due to the rank-one constraints. Then, we can drop the rank-one constraints to get an SDP problem denoted as (3.12)-SDR, which is convex and can be solved by using the CVX toolbox of MATLAB. To define the computational complexity to solve the (3.12)-SDR problem, we define $\text{T} = L + M + 1$ as the number of matrix variables of size $N \times N$, and $\Upsilon = 3L + M + K + 1$ is the linear constraint. Then, we can denote the computational complexity to solve problem (3.12)-SDR as $O\left(\sqrt{\text{T}\Upsilon}\left(\text{T}^3\Upsilon^6 + \text{T}^2\Upsilon^2\right)\log\left(1/\chi\right)\right)$ with a solution accuracy of $\chi > 0$. The solution to problem (3.12)-SDR is denoted as $\left\{\mathbf{V}_l^*, \mathbf{W}_m^*, \theta_l^*\right\}, \mathbf{F}^*$, which is unlikely to satisfy the following constraints: $\text{rank}\left(\mathbf{V}_l\right) = 1, \text{rank}\left(\mathbf{W}_m\right) = 1, \text{rank}\left(\mathbf{F}\right) = 1, \ \forall l, \ \forall m$. Therefore, we propose a Gaussian randomization technique to obtain the close-to-optimal solutions for problem (3.11).

In the Gaussian randomization technique [29, 58, 87], the first step is to perform eigen decomposition of the precoder matrices obtained from problem (3.12)-SDR, i.e., we evaluate $\mathbf{V}_l = \mathbf{Q}_{SU,l}\mathbf{\Lambda}_{SU,l}\mathbf{Q}_{SU,l}^H$, $\mathbf{W}_m = \mathbf{Q}_{EH,m}\mathbf{\Lambda}_{EH,m}\mathbf{Q}_{EH,m}^H$, and $\mathbf{F} = \mathbf{Q}_f\mathbf{\Lambda}_f\mathbf{Q}_f^H$. Next, we generate candidate solutions based on vectors $\kappa_{SU,l}$, $\kappa_{EH,m}$, and κ_f, where the elements follows a complex, circularly symmetric Gaussian distribution, $\mathcal{CN}(0, 1)$, i.e., $\mathbf{v}_l = \mathbf{Q}_{SU,l}\mathbf{\Lambda}_{SU,l}^{1/2}\kappa_{SU,l}$, $\mathbf{w}_m = \mathbf{Q}_{EH,m}\mathbf{\Lambda}_{EH,m}^{1/2}\kappa_{EH,m}$ and $\mathbf{f} = \mathbf{Q}_f\mathbf{\Lambda}_f^{1/2}\kappa_f$. However, there exists the possibility that the obtained candidate precoder vectors are

not feasible for problem (3.11). Then, we can adjust the value of the candidate precoded vectors based on scalar factors, $\{\tau_{SU,l}, \tau_{EH,m}\}\,\tau_f$, which can be obtained through the solution to the following optimization problem:

$$\min_{\{\tau_{SU,l}, \tau_{EH,m}\}, \tau_f} \quad \sum_{l=1}^{L} \tau_{SU,l} \|\mathbf{v}_l\|^2 + \sum_{m=1}^{M} \tau_{EH,m} \|\mathbf{w}_m\|^2 \tag{3.13a}$$

$$\text{s.t.} \quad \left(\sum_{l'=1}^{i-1} \tau_{SU,l'} \left|\mathbf{g}_l^H \mathbf{v}_{l'}\right|^2 + \sum_{m=1}^{M} \tau_{EH,m} \left|\mathbf{g}_l^H \mathbf{w}_m\right|^2 + \tau_f \left|\mathbf{g}_l^H \mathbf{f}\right|^2 + \sigma_l^2 + \frac{\sigma_{cn,l}^2}{\theta_l} \right) \gamma_i$$

$$- \tau_{SU,i} \left|\mathbf{g}_l^H \mathbf{v}_i\right|^2 \le 0, \; \forall l, \, i \in \mathbb{Q}, \, l \le i \tag{3.13b}$$

$$\frac{\psi_l}{(1 - \theta_l)} - \sum_{l'=1}^{L} \tau_{SU,l'} \left|\mathbf{g}_l^H \mathbf{v}_{l'}\right|^2 - \sum_{m=1}^{M} \tau_{EH,m} \left|\mathbf{g}_l^H \mathbf{w}_m\right|^2 - \tau_f \left|\mathbf{g}_l^H \mathbf{f}\right|^2 - \sigma_l^2 \le 0, \; \forall l \tag{3.13c}$$

$$\xi_m - \sum_{l=1}^{L} \tau_{SU,l} \left|\mathbf{e}_m^H \mathbf{v}_l\right|^2 - \sum_{m'=1}^{M} \tau_{EH,m'} \left|\mathbf{e}_m^H \mathbf{w}_{m'}\right|^2 - \tau_f \left|\mathbf{e}_m^H \mathbf{f}\right|^2 - \sigma_{EH,m}^2 \le 0, \; \forall m \tag{3.13d}$$

$$\sum_{l=1}^{L} \tau_{SU,l} \|\mathbf{v}_l\|^2 + \sum_{m=1}^{M} \tau_{EH,m} \|\mathbf{w}_m\|^2 + \tau_f \|\mathbf{f}\|^2 = P^{\max}, \tag{3.13e}$$

$$\sum_{l=1}^{L} \tau_{SU,l} \left|\mathbf{h}_k^H \mathbf{v}_l\right|^2 + \sum_{m=1}^{M} \tau_{EH,m} \left|\mathbf{h}_k^H \mathbf{w}_m\right|^2 + \tau_f \left|\mathbf{h}_k^H \mathbf{f}\right|^2 - \phi_{PU,k} \le 0, \; \forall k \tag{3.13f}$$

$$1 > \theta_l > 0, \; \forall l \tag{3.13g}$$

$$\tau_{SU,L} \left|\mathbf{g}_l^H \mathbf{v}_L\right|^2 \ge \tau_{SU,L-1} \left|\mathbf{g}_l^H \mathbf{v}_{L-1}\right|^2 \ge \dots \ge \tau_{SU,1} \left|\mathbf{g}_l^H \mathbf{v}_1\right|^2, \; \forall l. \tag{3.13h}$$

Problem (3.13) is a linear program that can be solved with the CVX module of MATLAB. In the Gaussian randomization technique, we generate G_{rand} candidate precoder vectors, where the final solution is the one that achieves the lower transmit power. The proposed algorithm with SDR and the Gaussian randomization technique is summarized in Algorithm 3.1.

3.3.2 Beamforming Optimization with AN in the MISO SWIPT CR-SDMA Network

In this subsection, we describe the baseline scheme based on SDMA for the MISO SWIPT CR system. In SDMA, the messages from other users are considered interference, and no SIC

Algorithm 3.1 The proposed algorithm based on SDR and Gaussian randomization to solve problem (3.11).

1: **inputs**: Number of randomizations, G_{rand}, $\text{Pow}_{\min} = P_{\max}$, optimal solution to the (12)-SDR problem: $\left\{ \mathbf{V}_l^*, \mathbf{W}_m^* \right\}, \mathbf{F}$.

2: Obtain the eigen decomposition of the precoder matrices from the solution to problem (3.12)-SDR $\mathbf{V}_l = \mathbf{Q}_{SU,l}\mathbf{\Lambda}_{SU,l}\mathbf{Q}_{SU,l}^H$, $\mathbf{W}_m = \mathbf{Q}_{EH,m}\mathbf{\Lambda}_{EH,m}\mathbf{Q}_{EH,m}^H$, and $\mathbf{F} = \mathbf{Q}_f\mathbf{\Lambda}_f\mathbf{Q}_f^H$.

3: **For** $i = 1 : 1 : G_{rand}$ **do**

4:     Generate the candidate precoder vectors based on random vectors $\kappa_{SU,l}^i$, $\kappa_{EH,m}^i$, and κ_f^i:

   $\mathbf{v}_l^i = \mathbf{Q}_{SU,l}\mathbf{\Lambda}_{SU,l}^{1/2}\kappa_{SU,l}^i$, $\mathbf{w}_m^i = \mathbf{Q}_{EH,m}\mathbf{\Lambda}_{EH,m}^{1/2}\kappa_{EH,m}^i$, and $\mathbf{f}^i = \mathbf{Q}_f\mathbf{\Lambda}_f^{1/2}\kappa_f^i$.

5:     Use the CVX module to solve problem (3.13) to get scalar factors $\left\{ \tau_{SU,l}^i, \tau_{EH,m}^i \right\} \tau_f^i$.

6:     Use the scalar factors to transform the candidate precoder vectors into feasible solutions to problem (3.11): $\mathbf{v}_l^i = \sqrt{\tau_{SU,l}^i}\mathbf{Q}_{SU,l}\mathbf{\Lambda}_{SU,l}^{1/2}\kappa_{SU,l}^i$, $\mathbf{w}_m^i = \sqrt{\tau_{EH,m}^i}\mathbf{Q}_{EH,m}\mathbf{\Lambda}_{EH,m}^{1/2}\kappa_{EH,m}^i$, and $\mathbf{f}^i = \sqrt{\tau_f^i}\mathbf{Q}_f\mathbf{\Lambda}_f^{1/2}\kappa_f^i$.

7:     Define $ObjF_i = \sum_{l=1}^{L}\left\| \mathbf{v}_l^i \right\|^2 + \sum_{m=1}^{M}\left\| \mathbf{w}_m^i \right\|^2$.

8:     **if** $ObjF_i < \text{Pow}_{\min}$ **then**

9:         $\text{Pow}_{\min} = ObjF_i, \left\{ \mathbf{v}_l^* = \mathbf{v}_l^i, \mathbf{w}_m^* = \mathbf{w}_m^i \right\}, \mathbf{f}^* = \mathbf{f}^i$

10:    **end if**

11: **End for**

12: **Result:** The precoder vectors: $\left\{ \mathbf{v}_l^*, \mathbf{w}_m^* \right\}, \mathbf{f}^*$.

---

procedure exists at the receiver. Therefore, the SINR at the l-th user is as follows:

$$SINR_{SDMA,l} = \frac{\theta_l\left| \mathbf{g}_l^H\mathbf{v}_l \right|^2}{\theta_l\left(\sum\limits_{l'=1,l'\neq l}^{L}\left| \mathbf{g}_l^H\mathbf{v}_{l'} \right|^2 + \sum\limits_{m=1}^{M}\left| \mathbf{g}_l^H\mathbf{w}_m \right|^2 + \left| \mathbf{g}_l^H\mathbf{f} \right|^2 + \sigma_l^2 \right) + \sigma_{cn,l}^2}, \quad \forall l. \qquad (3.14)$$

Although the energy harvested by the SUs and the EH users, as well as the power interfering with the PUs, are expressed in the same way as NOMA, and are defined in (3.7), (3.8) and (3.9), respectively. Then, the minimization of the transmit power for the SUs and EH users under the

constraints of minimum SINR, minimum EH required, and maximum interference with the PUs can
be expressed as follows:

$$\min_{\{\mathbf{v}_l,\mathbf{w}_m,\theta_l\},\mathbf{f}} \quad \sum_{l=1}^{L} \|\mathbf{v}_l\|^2 + \sum_{m=1}^{M} \|\mathbf{w}_m\|^2 \tag{3.15a}$$

$$\text{s.t.} \quad \frac{\theta_l \left|\mathbf{g}_l^H \mathbf{v}_l\right|^2}{\theta_l \left(\sum_{l'=1,l'\neq l}^{L} \left|\mathbf{g}_l^H \mathbf{v}_{l'}\right|^2 + \sum_{m=1}^{M} \left|\mathbf{g}_l^H \mathbf{w}_m\right|^2 + \left|\mathbf{g}_l^H \mathbf{f}\right|^2 + \sigma_l^2 \right) + \sigma_{cn,l}^2} \geq \gamma_l, \ \forall l \tag{3.15b}$$

$$(11c),\ (11d),\ (11e),\ (11f),\ \text{and}\ (11g). \tag{3.15c}$$

Problem (3.15) is non-convex and can be solved by using the SDR technique described in
Section 3.1. Then, problem (3.15) can be reformulated as follows

$$\min_{\{\mathbf{V}_l,\mathbf{W}_m,\theta_l\},\mathbf{F}} \quad \sum_{l=1}^{L} \text{Tr}\left(\mathbf{V}_l\right) + \sum_{m=1}^{M} \text{Tr}\left(\mathbf{W}_m\right) \tag{3.16a}$$

$$\text{s.t.} \quad \left(\sum_{l'=1,l'\neq l}^{L} \text{Tr}\left(\mathbf{G}_l \mathbf{V}_{l'}\right) + \sum_{m=1}^{M} \text{Tr}\left(\mathbf{G}_l \mathbf{W}_m\right) + \text{Tr}\left(\mathbf{G}_l \mathbf{F}\right) + \sigma_l^2 + \frac{\sigma_{cn,l}^2}{\theta_l} \right) \gamma_l$$

$$- \text{Tr}\left(\mathbf{G}_l \mathbf{V}_l\right) \leq 0, \ \forall l \tag{3.16b}$$

$$(12c),(12d),(12e),(12f),(12g),(12h),\text{and}(12i). \tag{3.16c}$$

After removing the rank-one constraints, the problem is denoted as (3.16)-SDR, which is
convex and can be solved with the CVX toolbox of MATLAB. Then, the Gaussian randomization
technique can be used if the precoder matrices, $\left\{\mathbf{V}_l^*, \mathbf{W}_m^*\right\}, \mathbf{F}$, do not satisfy the rank-one condition.

3.3.3   Beamforming Optimization with an in the MISO SWIPT CR-ZF Network

In this section, we include a comparative scheme based on ZF to solve the power minimiza-
tion problem in the cognitive MISO SWIPT system. The ZF scheme allows the nullification of the
interference signals from other users, which is considered to be a common approach used to simplify
the system design [82, 88]. At the *l*-th SU user, we design the ZF scheme to null the interference
from other SU's messages and from the energy signals. At the *k*-th PU user, the ZF scheme nulls

the interference from the SU's messages and from the energy signals. However, to increase the

harvested energy at the EH users, we allow interference signals at the EH users. Then, we define

$A_l = [\mathbf{g}_1, ..., \mathbf{g}_{l-1}, \mathbf{g}_{l+1}, ..., \mathbf{g}_L, \mathbf{h}_1, ..., \mathbf{h}_K] \in \mathbb{C}^{N \times (L+K-1)}$ and $B_m = [\mathbf{g}_1, ..., \mathbf{g}_L, \mathbf{h}_1, ..., \mathbf{h}_K] \in \mathbb{C}^{N \times (L+K)}$.

Therefore, we denote the beamforming vectors as follows:

$$\tilde{\mathbf{v}}_l = \frac{\mathbf{\Omega}_{A,l}\mathbf{\Omega}_{A,l}^H \mathbf{g}_l}{\left\|\mathbf{\Omega}_{A,l}\mathbf{\Omega}_{A,l}^H \mathbf{g}_l\right\|}, \tag{3.17}$$

$$\mathbf{v}_l = \sqrt{p_{SU,l}}\tilde{\mathbf{v}}_l, \tag{3.18}$$

$$\tilde{\mathbf{w}}_m = \frac{\mathbf{\Omega}_{B,m}\mathbf{\Omega}_{B,m}^H \mathbf{e}_m}{\left\|\mathbf{\Omega}_{B,m}\mathbf{\Omega}_{B,m}^H \mathbf{e}_m\right\|}, \tag{3.19}$$

$$\mathbf{w}_m = \sqrt{p_{EH,m}}\tilde{\mathbf{w}}_m, \tag{3.20}$$

where $p_{SU,l}$ and $p_{EH,m}$ are the power variables to be optimized, $\mathbf{\Omega}_{A,l} \in \mathbb{C}^{N \times (N-(L+K-1))}$ is the orthogo-

nal basis of the null space of A_l and $\mathbf{\Omega}_{B,m} \in \mathbb{C}^{N \times (N-(L+K))}$ is the orthogonal basis of the null space of

$\mathbf{B}_m$. Based on the ZF scheme, the transmit power minimization problem (3.11) can be transformed

into the following problem:

$$\min_{\{p_{SU,l}, p_{SU,m}, \theta_l\}, \mathbf{f}} \quad \sum_{l=1}^{L} p_{SU,l} + \sum_{m=1}^{M} p_{EH,m} \tag{3.21a}$$

$$\text{s.t.} \quad \frac{\theta_l p_{SU,l}\left|\mathbf{g}_l^H \tilde{\mathbf{v}}_l\right|^2}{\theta_l\left(\left|\mathbf{g}_l^H \mathbf{f}\right|^2 + \sigma_l^2\right) + \sigma_{cn,l}^2} \geq \gamma_l, \forall l \tag{3.21b}$$

$$p_{SU,l}\left|\mathbf{g}_l^H \tilde{\mathbf{v}}_l\right|^2 + \left|\mathbf{g}_l^H \mathbf{f}\right|^2 + \sigma_l^2 \geq \frac{\psi_l}{(1-\theta_l)}, \forall l \tag{3.21c}$$

$$\sum_{l=1}^{L} p_{SU,l}\left|\mathbf{e}_m^H \tilde{\mathbf{v}}_l\right|^2 + \sum_{m'=1}^{M} p_{EH,m'}\left|\mathbf{e}_m^H \tilde{\mathbf{w}}_{m'}\right|^2 + \left|\mathbf{e}_m^H \mathbf{f}\right|^2 + \sigma_{EH,m}^2 \geq \xi_m, \forall m \tag{3.21d}$$

$$\sum_{l=1}^{L} p_{SU,l} + \sum_{m=1}^{M} p_{EH,m} + \|\mathbf{f}\|^2 = P^{\max}, \tag{3.21e}$$

$$\left|\mathbf{h}_k^H \mathbf{f}\right|^2 - \phi_{PU,k} \leq 0, \forall k \tag{3.21f}$$

$$1 > \theta_l > 0, \forall l. \tag{3.21g}$$

Next, we solve the problem (3.21) by using the SDR technique. We denote $\mathbf{F} = \mathbf{f}\mathbf{f}^H$, $\mathbf{G}_l = \mathbf{g}_l\mathbf{g}_l^H$, $\mathbf{E}_m = \mathbf{e}_m\mathbf{e}_m^H$, $\mathbf{H}_k = \mathbf{h}_k\mathbf{h}_k^H$, $\|\mathbf{f}\|^2 = \mathrm{Tr}(\mathbf{F})$, $\left|\mathbf{g}_l^H\mathbf{f}\right|^2 = \mathrm{Tr}(\mathbf{G}_l\mathbf{F})$, $\left|\mathbf{e}_m^H\mathbf{f}\right|^2 = \mathrm{Tr}(\mathbf{E}_m\mathbf{F})$ and $\left|\mathbf{h}_k^H\mathbf{f}\right|^2 = \mathrm{Tr}(\mathbf{H}_k\mathbf{F})$.

$$\min_{\{p_{SU,l}, p_{SU,m}, \theta_l\}, \mathbf{F}} \quad \sum_{l=1}^{L} p_{SU,l} + \sum_{m=1}^{M} p_{EH,m} \tag{3.22a}$$

$$\text{s.t.} \quad \gamma_l\left(\mathrm{Tr}\left(\mathbf{G}_l\mathbf{F}\right) + \sigma_l^2 + \frac{\sigma_{cn,l}^2}{\theta_l}\right) - p_{SU,l}\kappa_{SU,l} \leq 0, \; \forall l \tag{3.22b}$$

$$\frac{\psi_l}{(1-\theta_l)} - p_{SU,l}\kappa_{SU,l} - \mathrm{Tr}\left(\mathbf{G}_l\mathbf{F}\right) - \sigma_l^2 \leq 0, \; \forall l \tag{3.22c}$$

$$\xi_m - \sum_{l=1}^{L} p_{SU,l}\kappa_{SU-EH,l} - \sum_{m'=1}^{M} p_{EH,m'}\kappa_{EH,m'} - \mathrm{Tr}\left(\mathbf{E}_m\mathbf{F}\right) - \sigma_{EH,m}^2 \leq 0, \; \forall m \tag{3.22d}$$

$$\sum_{l=1}^{L} p_{SU,l} + \sum_{m=1}^{M} p_{EH,m} + \mathrm{Tr}\left(\mathbf{F}\right) = P^{\max}, \tag{3.22e}$$

$$\mathrm{Tr}\left(\mathbf{H}_k\mathbf{F}\right) - \phi_{PU,k} \leq 0, \; \forall_k \tag{3.22f}$$

$$1 > \theta_l > 0, \forall l \tag{3.22g}$$

$$\mathbf{F} > 0, \tag{3.22h}$$

$$\mathrm{rank}\left(\mathbf{F}\right) = 1, \tag{3.22i}$$

where $\kappa_{SU,l} = \left|\mathbf{g}_l^H\tilde{\mathbf{v}}_l\right|^2$, $\kappa_{SU-EH,l} = \left|\mathbf{e}_m^H\tilde{\mathbf{v}}_l\right|^2$ and $\kappa_{EH,m} = \left|\mathbf{e}_m^H\tilde{\mathbf{w}}_m\right|^2$. Then, we drop the constraint (3.22i) and obtain an SDP problem denoted as (3.22)-SDR, which is convex. The solution of (3.22)-SDR can be obtained through the CVX toolbox. The Gaussian randomization technique, detailed in Section 3.3.1, is used to obtain the approximate rank-one solution for the ZF-based problem (3.21).

3.4   Numerical Results

In this section, simulation results are provided to assess the performance of the proposed MISO-NOMA-CR aided by SWIPT with EH users, in comparison with an SDMA approach and with

a scheme without AN. We used MATLAB software on a Core i7-6700K CPU with 16 GB of main

memory to perform the simulations over several channel realizations. The simulation parameters

listed in Table 3.1 were selected based on the work in [68, 89, 90]. More specifically, the transmission

power of the SU-Tx is set to 30 dBm since it is a common value used in the literature for CR

systems [46, 89]. In addition, the channel vectors parameters such as the channel gain and the Rician

factor were set to 10^{-3} and 5 dB, respectively, based on the work in [68]. The number of SUs and the

value for the path-loss exponent are stablished according to the reference [90].

In the considered chapter, we consider a quasi-static channel condition, which is usually

assumed for indoor channels where the degree of time variation in the signal strength is small

compared with the symbol duration. The channel model used in the simulations considers different

distances from the SU-TX to the users, as well as different angle directions. The channel vectors were

modeled based on an independent Rician fading, which is composed of a line-of-sight component

and scattering components, and it is given as follows [68]:

$$\mathbf{g}_l = \sqrt{L_o \left(d_{SU,l}^{-\alpha} \right)} \left(\sqrt{\frac{K_R}{1 + K_R}} \mathbf{g}_l^{LOS} + \sqrt{\frac{1}{1 + K_R}} \mathbf{g}_l^{NLOS} \right), \tag{3.23}$$

where $\mathbf{g}_l^{NLOS}$ is the Rayleigh fading component, which follows a circularly symmetric complex

Gaussian random variable with zero mean and unit variance, and $\mathbf{g}_l^{LOS}$ is the line-of-sight component.

The line-of-sight component is based on a uniform linear array from [69] with a wavelength equal to

the double of the spacing between successive antenna elements, and it is given as follows:

$$\mathbf{g}_l^{LOS} = \left[1 \ e^{-j\pi \sin(\phi_{SU,l})} \ e^{-j2\pi \sin(\phi_{SU,l})} \ ... \ e^{-j(N-1)\pi \sin(\phi_{SU,l})} \right]^T, \tag{3.24}$$

where $\phi_{SU,l}$ denotes the direction from the SU-Tx to the l-th SU, set at $\phi_{SU,1}$ and $\phi_{SU,2}$. Channel

vectors $\mathbf{e}_m$ from the SU-Tx to the m-th EH user were generated by following the aforementioned

procedure, with the directions $\phi_{EH,1}$ and $\phi_{EH,2}$ pointed out in Table 3.1. Moreover, channels vectors

$\mathbf{h}_k$ and $\mathbf{h}_{ev}$ follow Rayleigh fading with an attenuation equal to $L_o \left(d_{PU,k}^{-\alpha} \right)$ and the distances from the

SU-Tx to SUs, EH users, PUs, and the eavesdropper are defined in Table 3.1.

Table 3.1: Simulation parameters.

Parameter	Notation	Value
Number of SUs	L	2
Number of EH users	M	2
Number of PUs	K	2
Number of SU-Tx antennas	N	8
Maximum SU-Tx transmission power	P^{max}	30 dBm
Channel gain	L_o	10^{-3}
Path-loss exponent	α	2
Rician factor	K_R	5
Distance from the SU-Tx to the SU 1	$d_{SU,l}$	10
Distance from the SU-Tx to the SU 2	$d_{SU,2}$	15
Distance from the SU-Tx to the EH user 1	$d_{EH,1}$	5
Distance from the SU-Tx to the EH user 2	$d_{EH,2}$	5
Distance from the SU-Tx to the PU 1	$d_{PU,1}$	20
Distance from the SU-Tx to the PU 2	$d_{PU,2}$	20
Distance from the SU-Tx to the eavesdropper	d_{ev}	13
Direction from the SU-Tx to the SU 1	$\phi_{SU,1}$	30^0
Direction from the SU-Tx to the SU 2	$\phi_{SU,2}$	40^0
Direction from the SU-Tx to the EH user 1	$\phi_{EH,1}$	-15^0
Direction from the SU-Tx to the EH user 2	$\phi_{EH,2}$	-25^0

Furthermore, the proposed model can be adapted to several scenarios since we do not consider a fixed number of users. Instead we assume that there exist L SUs and M EH receivers. It

is worth highlighting that the proposed approach is valid for other channel model because in a real deployment the inputs are channel state information (CSI), which can be obtained by a feedback process between the transmitter and the users and by cooperation between the primary and secondary network.

The simulation results in this section are the average over several independent channel realizations, where the Rayleigh fading component of the channel vectors varies in each channel realization. Please note that new beamforming vectors and PS ratios should be obtained each time the channel conditions changes, which is not the best solution in fast time-varying channels because of the computational complexity of solving the optimization problem.

First, we investigated the results for problem (3.11) by using the SDR technique. Furthermore, we compared the results with the SDMA scheme, ZF technique and with the scheme without using AN.

Figure 3.2 shows AN power, $\|\mathbf{f}\|^2$ according to the minimum SINR required at the SUs when minimum EH requirements of the SUs and EH users are given as $\psi_l = \xi_m = -25$ dBm and $\psi_l = \xi_m = -30$ dBm, respectively. We observed that the radiated AN power is decreased as the minimum required SINR increases, because the SU-Tx needs to allocate more power to satisfy the SINR constraint while reducing the available power for the artificial noise. In addition, the proposed scheme based on the NOMA technique outperforms the SDMA method and ZF scheme for two considered cases of minimum EH. The improvement from the NOMA technique is due to the ability to decode part of the interference from other messages via the SIC procedure, which allows an increase in the achievable SINR at the SUs while reducing the required transmit power to satisfy the minimum SINR constraint. Subsequently, the NOMA technique can provide a high level of PLS, because the interference with the eavesdropper increases as the AN power increases, which makes it difficult for the eavesdropper to decode the SU's messages. The SDMA method outperforms the ZF scheme because ZF nulls the interference from other SU's and EH's messages at the l-th SU
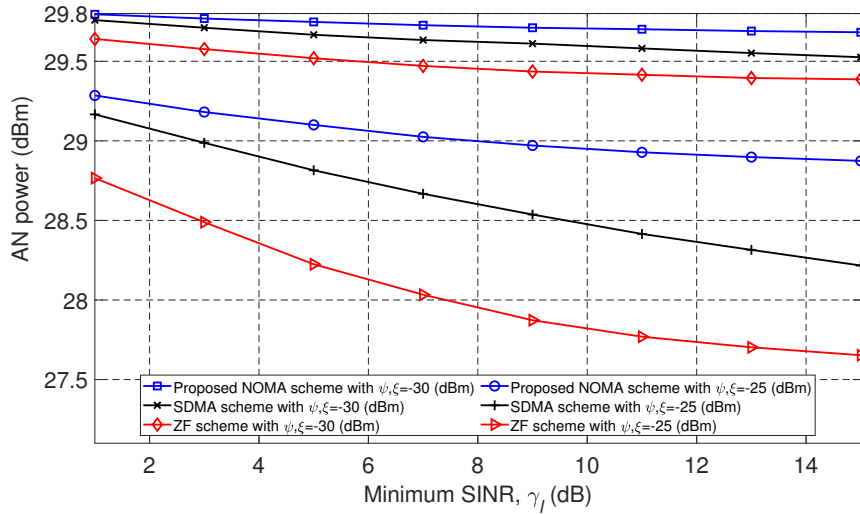
Figure 3.2: AN power according to the minimum SINR required at the SUs.

which permits an increase of the SINR but affects the harvested energy. Subsequently, the ZF scheme harvests lower energy than that harvested by the SDMA approach, which makes that the SU-Tx increases the transmission power to satisfy the EH constraint while reducing the available power to allocate to the AN.

Figure 3.3 illustrates the SSR achieved with the proposed approach and with the scheme without AN, according to the minimum SINR and minimum EH requirements, with maximum permissible interference with the PUs equal to $\phi_{PU} = -60$ dBm. From Figure 3.3, we can observe the benefit of the proposed approach with AN on increasing the achievable SSR, because AN can effectively generate interference with the eavesdropper while the beamforming technique minimizes that interference at the SUs. We note that the SSR grows as the minimum SINR increases, and this trend coincides with previous research [58, 69] because the achievable transmission rate at the SUs increases. In addition, the SSR reduces as the minimum EH requirement increases because more power needs to be allocated to satisfy the EH requirements while reducing the available power for AN.

Figure 3.4 shows AN power according to the minimum harvested energy by the SUs and
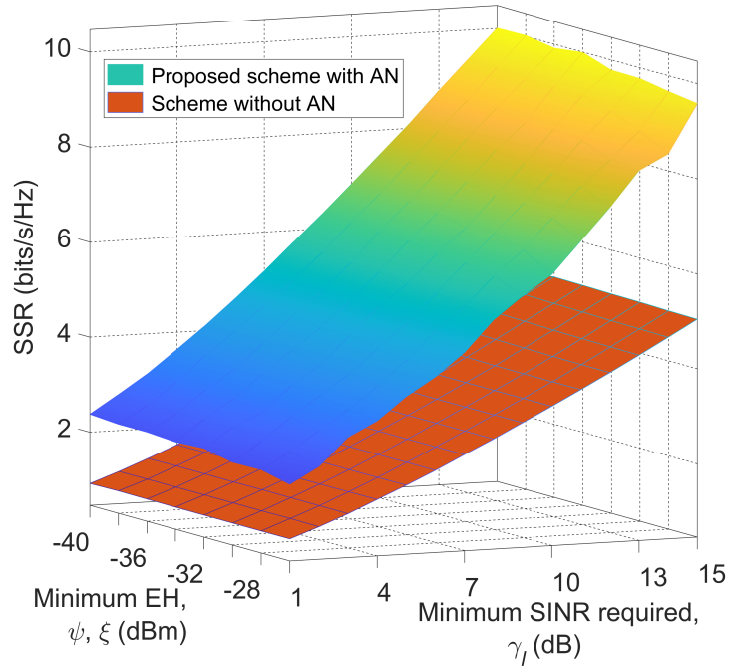
Figure 3.3: SSR performance comparison between the proposed approach and the scheme without AN, in accordance with the minimum harvested energy at the SU and EH users, and the minimum SINR at the SUs.

the EH users when the minimum SINR of the SUs is given as $\gamma_l = 5$ dB and $\gamma_l = 10$ dB, respectively. From Figure 3.4, we can see that AN power decreases for all the considered schemes as the minimum EH requirement increases. The reason is because as the minimum EH increases, more transmission power should be allocated to the users to satisfy their EH requirements. Subsequently, less power is assigned for the AN. Furthermore, we can see that the proposed scheme outperforms SDMA and ZF, since NOMA can achieve higher values of AN power due to the SIC application to nullify interference with other users while causing interference with the eavesdropper to improve network security. Similar to Figure 3.2, the ZF condition of canceling the interference makes it necessary to transmit more power to satisfy the EH requirements at SUs.

Figure 3.5 shows the AN power according to the interference threshold when the minimum
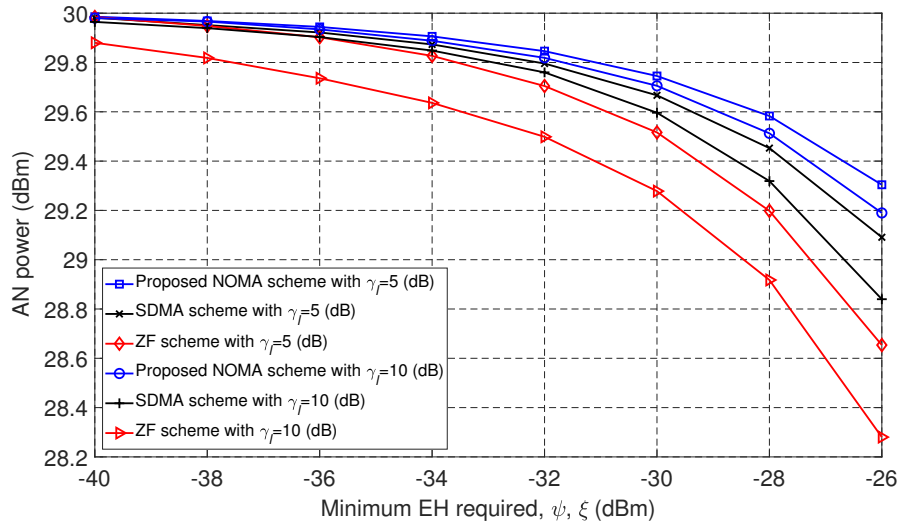
Figure 3.4: AN power versus the minimum harvested energy at the EH users and SUs.

EH requirements of the SUs and EH users are given as $\psi_l = \xi_m = -25$ dBm, and the minimum SINR for the SUs are $\gamma_l = 5$ dB and $\gamma_l = 10$ dB. From Figure 3.5, we can see that the AN power increases along with increasing interference threshold values for the PUs. As the interference threshold increases, the SU-Tx can transmit more power to the SUs and EH users that includes AN power to tackle the eavesdropper's wiretap. Moreover, Figure 3.5 also verifies that the proposed scheme outperforms the other baseline schemes. This can be explained as follows: Unlikely to SDMA and ZF, NOMA can perform SIC to decode part of the interference caused by other users, which allows transmitting less power to satisfy the QoS requirements of the users and more AN power which results in better PLS in the network. The results obtained by ZF are due to the condition of designing the beamforming vectors to null the interference at the PUs, where the constraint (3.21f) of maximum interference allowed to the PUs only depends on the beamforming vector of the AN.
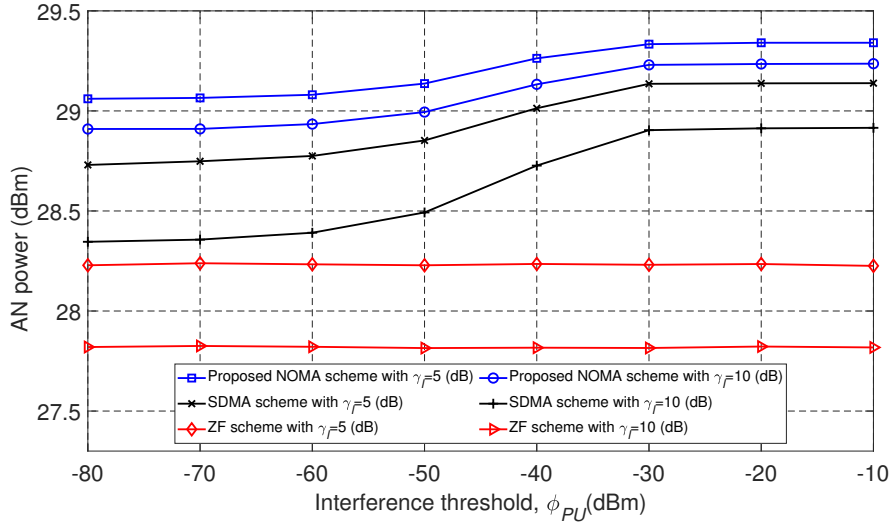
Figure 3.5: AN power versus the interference threshold, $\phi_{PU,k}$.

3.5   Closing Remarks

In this chapter, we consider a MISO-NOMA-CR network assisted by SWIPT with the presence of EH users and an eavesdropper. To improve the security of the secondary network, we investigate a beamforming design and optimal PS ratios to minimize the transmit power of the secondary transmitter. Moreover, AN is considered in the proposed scheme to disrupt eavesdropping. The formulated non-convex optimization problem is subject to satisfying QoS constraints of the SUs and EH users, and maximum allowable power of the SU-Tx and maximum acceptable interference with the PUs. We provide a solution based on SDR, and develop performance comparison with baseline schemes such as SDMA, ZF, and a conventional approach without AN. Numerical results show that the proposed AN-aided beamforming and PS-ratio design furnishes secure transmissions of confidential information, and provides better secrecy than that obtained by the scheme without AN. Furthermore, it was shown that the application of NOMA in the proposed network overcomes the drawbacks of the traditional SDMA and ZF baseline schemes.

Chapter 4

Low-Complexity PSO-based Resource Allocation Scheme for Cooperative Non-linear SWIPT-enabled NOMA[1]

4.1 Introduction

Currently, the limited spectrum and energy resource utilization problem is one of the main concerns for the development of future wireless technologies that permit proliferation of the IoT, device-to-device (D2D) communications, spectrum sharing, massive machine-type communications, and so on [91]. To enhance spectrum efficiency, NOMA is an emerging technique enabling multiple users to share the same time–frequency resource block. NOMA can be classified into power and code domains. In this chapter, we focus on power-domain NOMA where the transmitter sends all the messages of the users by utilizing different power levels for each user in accordance with their channel conditions, i.e., the messages of users with weaker channel conditions are transmitted with

---

[1]The study in this chapter is published in IEEE Access [16]

73

more power than messages of users with stronger channel conditions. At the receiver, users with better channel conditions perform SIC to remove interference caused by users with stronger channel conditions, and users with the weakest channel conditions decode messages by treating the other messages as noise [30].

Moreover, EH techniques have been investigated to improve energy efficiency in limited-processing-power and low-power energy-constrained communication networks, such as wireless body area networks, IoT devices, and wireless sensor networks [92–95]. Particularly with small communication devices, one of the main challenges is to autonomously maintain connectivity and maximize network lifetime. In this regard, the RF EH technique is capable of receiving RF signals and converting them to electricity to extend the battery lifetime of communications devices and avoid wasted power [95]. Indeed, through the application of EH technology, conventional batteries can be eliminated, which entails cost reductions, eliminating wires, and promoting environmentally friendly technologies [96]. One main application of the RF-EH technique is SWIPT. SWIPT technology allows users to receive information and harvest energy from the received RF signal at the same time [97]. SWIPT appears to be a powerful technique, providing energy-efficient green communications, especially in emergency situations. For instance, in [98], SWIPT was integrated into a D2D system to assist natural disaster communications where replacing or recharging batteries is a critical issue.

Among the benefits of SWIPT is prolonging the lifetime of energy-constrained networks since SWIPT users can serve as cooperative relays to edge nodes. Furthermore, SWIPT-enabled NOMA systems have demonstrated meaningful yields over the conventional OMA scheme in terms of spectral efficiency [99], energy efficiency [10, 99, 100], power consumption [6, 73, 101], and secrecy sum rate [11]. For instance, the authors in [99, 100], and [102] maximized energy efficiency in NOMA SWIPT systems subject to the QoS by utilizing analytical approaches. The results showed that SWIPT-enabled NOMA systems satisfactorily outperformed the conventional OMA. Moreover,

energy-saving designs are crucial to establishing eco-friendly communication systems. Therefore, optimization problems have been addressed to minimize the power in wireless networks [6, 101]. In this sense, the authors in [101] designed a deep learning scheme to find an approximately optimal solution for minimizing total transmission power in a SWIPT NOMA network. In [6], the authors derived a closed-form solution to minimize the total transmission power of a cooperative system aided by a collaborative SWIPT user. The outcomes of these studies verified the superiority of NOMA over baseline multiple access schemes. It is worth noting that not one of the previous articles considered non-linear EH, which greatly increases the difficulty in solving the optimization problem due to coupled variables involved in problem resolution.

To suitably design a SWIPT system, a fundamental requirement is to accurately model the EH circuit that allows transforming the received RF signal into a direct current (DC) signal. Although the employment of linear EH models still prevails in most of the literature, recent investigations have highlighted the importance of including realistic models of EH circuits in the analysis of communications systems [103, 104]. Indeed, practical EH reveals a non-linear relation between the stored energy and the received RF power because of physical impairments, such as non-ideal energy conversion efficiency, storage imperfections, non-linear circuits, etc [105, 106]. Consequently, to leverage the advantages of SWIPT and acquire more-accurate results, the application of realistic EH models must be integrated into wireless SWIPT systems.

Although nonlinear EH models consider a more realistic environment, reluctance to adopt them still exists because of the complexity in solving the optimization problems. Conventional optimization methods attempting to find the optimal solution may entail high computational complexity, and a closed-form solution is inflexible to change since it needs to be reformulated after a change in the network [6]. Therefore, the metaheuristic branch of AI algorithms has opened doors to dealing with complex computational problems. Metaheuristics generate possible solutions to optimization problems and select the best one with low complexity and high accuracy. Overall, the

most popular metaheuristic algorithms in the fields of science and engineering include the genetic algorithm [107], the CS [20], and PSO [18]. For instance, the authors in [20] discussed different metaheuristic algorithms and identified which ones work the best to optimize the placement of tasks for network-on-chip cores. The paper concluded that CS is more suitable for placement with a low computational overhead. Moreover, hybrid schemes have been developed by combining two or more characteristics of the original metaheuristic algorithms to enhance optimization results [108].

Motivated by the advantages provided by metaheuristic algorithms for solving complex optimization problems, this chapter investigates the application of swarm intelligence schemes for solving resource allocation optimization problems in a nonlinear SWIPT NOMA green communication system. Among them, we propose the PSO-based scheme as a potential solution that achieves high accuracy with low complexity. To evaluate the performance of the proposed network even further, we formulated two different optimization problems: power transmission minimization and energy efficiency maximization. The main contributions of this chapter can be summarized as follows.

- The goal is to optimize total transmission power and energy efficiency in a cooperative, non-linear, SWIPT-enabled NOMA system with a non-linear EH user while satisfying the constraints on minimum data rates, minimum harvested energy at the terminal, time fraction, and power splitting ratio range.

- The optimization problems considered are non-convex involving joint optimization of the time transmission fraction, power-splitting ratio, and power allocation and are thus difficult to solve directly. To tackle this issue, we propose a low-computational-complexity scheme based on PSO. Moreover, we compare the performance of five swarm intelligence-based baseline schemes and develop a low-complexity solution based on CS [17, 109, 110]. To validate the performance of the proposed PSO scheme, we provide an analytical approach based on convex

optimization with the ES method, denoted as CVX+ES.

- Furthermore, we analyze the effect from linearity of EH on the transmit power and energy efficiency of the proposed scheme (SWIPT NOMA cooperative communication optimizing the power variables, time factor, and the power-splitting ratio) and the following baseline schemes: SWIPT NOMA cooperative communication with a time fixed (TF) scheme, and SWIPT NOMA cooperative communication with equal power splitting (EPS). Moreover, we investigate the conventional OMA baseline scheme for comparison purposes. To our satisfaction, simulation results demonstrated that the proposed cooperative non-linear SWIPT-NOMA system reduces more transmission power and can obtain higher energy efficiency than the benchmark schemes.

- Numerical results show that the outcomes obtained by PSO reach near-optimal performance, compared to those obtained by optimal (but time- and energy-consuming) convex optimization with the ES method [109]. In addition, we provide a complexity comparison between the optimal scheme (CVX+ES) and the swarm intelligence schemes in terms of computation time. Thus, we validated PSO as achieving convergence faster than the CS-based framework and with less computational time.

The rest of the chapter is organized as follows. The system model is described in Section 4.2. In Section 4.3, we formulate the optimization problems of total transmission power minimization and energy efficiency maximization, and we present the proposed PSO-based solution and comparison approaches. Finally, numerical results and the conclusion are presented in Section 4.4 and Section 4.5, respectively.

4.2   System Model

We propose a cooperative, non-linear, SWIP-enabled NOMA system composed of three users and one transmitter, as shown in Figure 4.1, where all nodes have one single antenna. Moreover,
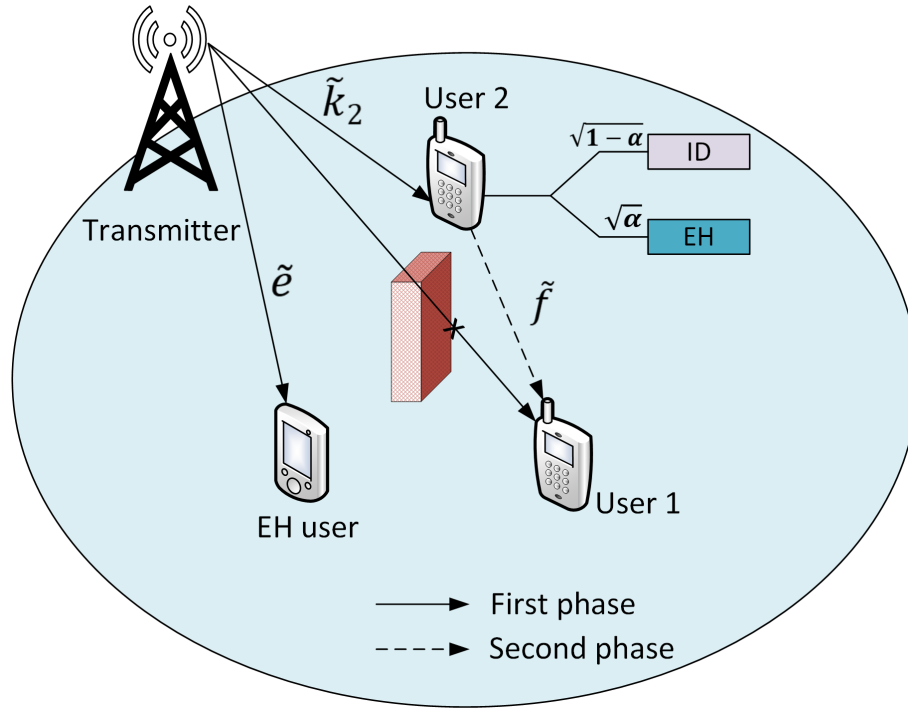
Figure 4.1: Cooperative non-linear SWIPT-enabled NOMA system.

the user close to the transmitter, denoted by u_2, acts as a cooperative DF relay that provides SWIPT

to aid a distant user, u_1, to receive messages. Assume there is no direct transmission link between

the transmitter and distant user u_1 because of the shadowing effect and obstacles. User 3 acts as

a non-linear RF EH user (denoted by u_3) capable of providing an alternative power supply for

electronic devices where conventional energy sources are costly or difficult to implement because of

remote locations, areas of catastrophic damage, or toxic environments.

A transmission is completed in two phases, as shown in Figure 4.2. In the first phase,

the transmitter performs superposition coding according to the NOMA principles by sending the

messages of u_1 and u_2 to nearby user u_2, while u_3 extracts RF power by receiving the superimposed

signal from the transmitter. In the second phase, u_2 forwards message 1 to u_1 by utilizing the stored

energy obtained during the first phase. More details on the first and second phases are in the following

subsections.

First phase	Second phase
Data transmission from the transmitter to user 2 while harvesting energy at user 3.	Cooperative data transmission from user 2 to user 1.

$$\longleftarrow\!\!\!-\!\!\!-\!\!\!-\!\!\!-\!\tau\!-\!\!\!-\!\!\!-\!\!\!-\times\!\!\!-\!\!\!-\!(1\text{-}\tau)\!-\!\!\!-\!\!\!-\longrightarrow$$
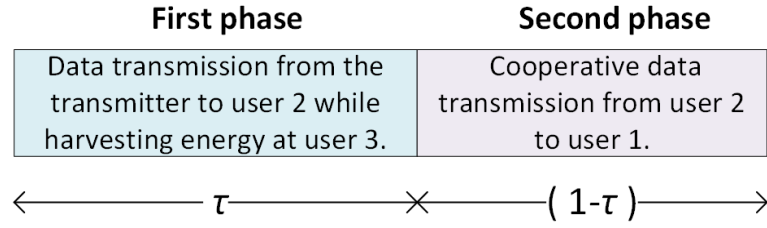
Figure 4.2: Frame structure of the considered cooperative non-linear SWIPT enabled NOMA system.

4.2.1   First Phase

In the first phase, the transmitter conveys a superimposed signal denoted by x, $x = m_1 x_1 + m_2 x_2$, where $x_1, x_2 \in \mathbb{C}$ are the independent and identically distributed (*i.i.d*) messages for u_1 and u_2, respectively. Moreover, the transmitted symbol is normalized as $\mathbb{E}\left(|x_1|^2\right) = \mathbb{E}\left(|x_2|^2\right) = 1$, and the power variables are denoted by m_1 and m_2, for u_1 and u_2, respectively. At the receiver, u_2 provides SWIPT by dividing the superimposed received signal into two parts according to power-splitting ratio α, one for information decoding and the other for energy harvesting. Accordingly, the received signal for information decoding at u_2 can be given by

$$y_2^{(1)} = \sqrt{1-\alpha}\,\widetilde{k_2}\,(m_1 x_1 + m_2 x_2) + z_2^{(1)}, \tag{4.1}$$

where $\widetilde{k_2}$ is the channel coefficient between the transmitter and user 2, $z_2^{(1)} \sim \mathcal{CN}\left(0, \sigma_2^2\right)$ is the AWGN, and $\alpha \in (0, 1)$ is the power-splitting ratio.

In accordance with NOMA principles, since u_2 has the strongest channel conditions, it employs SIC to first decode the message of u_1 and then subtracts this message from the received signal to decode its message, x_2, without interference. Consequently, the SINR of u_2 when decoding message 1, x_1, is described in equation (4.2), and the SNR of u_2 when decoding its own message, x_2, is equation (4.3):

$$SINR_{2,x_1}^{(1)} = \frac{(1-\alpha)\,k_2 m_1^2}{(1-\alpha)\,k_2 m_2^2 + \sigma_2^2}, \tag{4.2}$$

where $k_2 = \left| \widetilde{k_2} \right|^2$,

$$SNR^{(1)}_{2,x_2} = \frac{(1 - \alpha)\, k_2 m_2^2}{\sigma_2^2}. \tag{4.3}$$

Hence, the rate for the distant user's data and the rate for the nearby user's data at u_2 can be given by (4.4) and (4.5), respectively:

$$R^{(1)}_{x_1,u_2} = \tau \log_2 \left(1 + SINR^{(1)}_{2,x_1} \right), \tag{4.4}$$

and

$$R_{u_2} = \tau \log_2 \left(1 + SNR^{(1)}_{2,x_2} \right), \tag{4.5}$$

where $\tau \in (0, 1)$ is the transmission time fraction for the first phase.

Furthermore, in the theoretical linear model of an EH circuit, the users harvest all the power of the incoming signal. For instance, the linear model of the energy harvested by u_2 can be written as:

$$Eh^{(1)}_{2\_linear} = \tau \eta \alpha k_2 \left(m_1^2 + m_2^2 \right), \tag{4.6}$$

where η is the energy harvesting efficiency. However, the practical non-linear EH model is given by the logistic function that includes the saturated harvested power and circuit specifications. Therefore, the energy stored by u_2 follows the nonlinear EH model in [97], and can be calculated as follows:

$$Eh^{(1)}_2 = \tau \frac{\psi_{u_2} - L\Omega}{1 - \Omega}, \tag{4.7}$$

where $\Omega = \frac{1}{1+\exp(ab)}$ and $\psi_{u_2} = \frac{L}{1+\exp\left(-a\left(p_{\text{int}_{u2}} - b\right)\right)}$, in which $p_{\text{int}_{u2}}$ denotes the input power. In this case, $p_{\text{int}_{u2}} = \alpha k_2 \left(m_1^2 + m_2^2 \right)$. L is a constant that sets the maximum harvested power at the EH receiver when the EH circuit is saturated. Parameters a and b are constants depending on the detailed circuit specifications, for example, capacitance, resistance, and diode turn-on voltage. We consider the values adopted in [97], which are $L = 3.9mW$, $a = 1500$, and $b = 0.0022$. For simplicity, we assume the energy stored by user 2 is only utilized for transmitting information to user 1, and energy

consumption for signal processing and maintaining the circuit can be ignored [100]. Therefore, the

transmit power at user 2 can be given by

$$P_{sw} = \frac{Eh_2^{(1)}}{1 - \tau}.$$

(4.8)

Finally, the energy harvested by u_3 utilizes the nonlinear EH model described in [97] and

can be expressed by

$$Eh_3^{(1)} = \tau \frac{\psi_{u_3} - L\Omega}{1 - \Omega}.$$

(4.9)

Here, $\psi_{u_3} = \frac{L}{1+\exp\left(-a\left(p_{\text{int}_{u3}}-b\right)\right)}$, and $p_{\text{int}_{u3}} = |\tilde{e}|^2 \left(m_1^2 + m_2^2\right)$, where $\tilde{e}$ is the channel coefficient

from the transmitter to user 3. Note that the ideal linear EH model for u_3 can be expressed as

$$Eh_{3\_linear}^{(1)} = \tau \eta |\tilde{e}|^2 \left(m_1^2 + m_2^2\right).$$

(4.10)

4.2.2   Second Phase

In this phase, nearby user u_2 utilizes its stored energy to forward message x_1 to u_1. Thus,

the received signal at u_1 is

$$y_1^{(2)} = \sqrt{P_{sw}} \widetilde{f} x_1 + z_1^{(2)},$$

(4.11)

where $\widetilde{f}$ is the channel coefficient from u_2 to u_1, and $z_1^{(2)} \sim \mathcal{CN}\left(0, \sigma_1^2\right)$ is AWGN at u_1. Then, the

SNR to decode x_1 is expressed by

$$SNR_{1,x_1}^{(2)} = \frac{P_{sw}|\tilde{f}|^2}{\sigma_1^2} = \frac{Eh_2^{(1)} \cdot f}{(1 - \tau)},$$

(4.12)

where $f = \frac{|\tilde{f}|^2}{\sigma_1^2}$. Then, the rate for the distant user's data at u_1 can be written as seen in (4.13):

$$R_{x_1,u_1}^{(2)} = (1 - \tau) \log_2 \left(1 + SNR_{1,x_1}^{(2)}\right).$$

(4.13)

4.3   PROBLEM FORMULATION AND SOLUTION

4.3.1   Transmission Power Optimization Problem

In this problem, we aim to minimize the total transmission power of the cooperative non-linear SWIPT-enabled NOMA system with a nonlinear EH user by jointly optimizing the transmission time fraction, τ, the power-splitting ratio, α, and power allocation variables m_1^2 and m_2^2 while satisfying the QoS constraints from all users. For simplicity, let us define $m_1^2 = p_1$ and $m_2^2 = p_2$. Then, the resource allocation problem to minimize the total transmission power is equivalent to the minimization of $p_1 + p_2$, which can be formulated as follows:

$$\min_{p_1,p_2,\tau,\alpha} p_1 + p_2 \tag{4.14a}$$

$$\text{s.t. } \tau \log_2 \left(1 + \frac{(1-\alpha)\,k_2 p_1}{(1-\alpha)\,k_2 p_2 + \sigma_2^2} \right) \geq \gamma_1, \tag{4.14b}$$

$$(1-\tau)\log_2 \left(1 + f\tau \frac{\psi_{u_2} - L\Omega}{(1-\Omega)(1-\tau)} \right) \geq \gamma_1 \tag{4.14c}$$

$$\tau \log_2 \left(1 + \frac{(1-\alpha)\,k_2 p_2}{\sigma_2^2} \right) \geq \gamma_2, \tag{4.14d}$$

$$\tau \frac{\psi_{u_3} - L\Omega}{1-\Omega} \geq \phi, \tag{4.14e}$$

$$p_1 + p_2 \leq P^{\max} \tag{4.14f}$$

$$0 < \alpha < 1, \tag{4.14g}$$

$$0 < \tau < 1, \tag{4.14h}$$

where (4.14b) and (4.14c) guarantee that the rate of distant-user data at u_2 and u_1, respectively, can reach the minimum rate requirement constraint, γ_1. Equation (4.14d) corresponds to the minimum rate constraint for u_2, in which γ_2 denotes the minimum rate target. Equation (4.14e) corresponds to the minimum harvested power constraint for u_3, in which ϕ denotes the minimum harvested power requirement. Constraint (4.14f) guarantees that the power to transmit message 1 and message 2 does not exceed the maximum available power at the transmitter. Constraint (4.14g) indicates that the

power splitting ratio, α, is between 0 and 1. Constraint (4.14h) points out that the time factor, τ, is between 0 and 1.

We can see that this problem is non-convex because of constraints (4.14b) to (4.14e). Specifically, (4.14b) is non-convex due to coupled power allocation variables p_1 and p_2, power-splitting ratio α, and time fraction τ. Moreover, (4.14c) is non-convex due to the coupled fraction time, τ, and due to ψ_{u_2}, which is challenging because ψ_{u_2} involves the sum of the power allocation variables p_1 and p_2 multiplied by power splitting ratio α. Similarly, constraint (4.14e) is non-convex due to the coupled fraction time, τ, and ψ_{u_3}. In (4.14e), ψ_{u_3} involves the sum of the power allocation variables p_1 and p_2. Thus, optimization problem (4.14) is difficult to solve directly. Conventional optimization techniques and ES methods are used to solve resource allocation problems when searching for the optimal solution. However, these techniques involve high complexity due to a high computational load that entails undesired delays in updating the optimal solution. Moreover, if an additional element is involved in the network, a closed-form solution should be reformulated. Therefore, we investigate low-complexity solutions to solve the proposed resource allocation problems more efficiently with much lower complexity and without degrading the network performance. We particular studied the potential PSO framework to obtain a low-complexity solution in the proposed cooperative non-linear SWIPT-enabled NOMA system. Moreover, we investigated CS and CVX+ES-based frameworks for comparison purposes. In addition, we considered two baseline schemes based on an EPS ratio and a TF scheme.

Analytical Solution For Transmission Power Minimization

Since problem (4.14) is non-convex and cannot be directly solved, let us fix the value of variable τ for any given $\tau \in (0, 1)$ to transform non-convex optimization problem (4.14). Then, after some derivations, problem (4.14) is transformed into a convex problem as follows:

$$\min_{p_1, p_2, \alpha} p_1 + p_2 \tag{4.15a}$$

$$\text{s.t. } \nu_{u1,2}k_2p_2 + \frac{\nu_{u1,2}\sigma_2^2}{(1-\alpha)} - k_2p_1 \leq 0, \tag{4.15b}$$

$$\frac{\kappa_{u2}}{\alpha} - k_2(p_1 + p_2) \leq 0, \tag{4.15c}$$

$$\frac{\nu_{u2}\sigma_2^2}{(1-\alpha)} - k_2p_2 \leq 0, \tag{4.15d}$$

$$\kappa_{u3} - |\tilde{e}|^2(p_1 + p_2) \leq 0, \tag{4.15e}$$

$$p_1 + p_2 \leq P^{\text{max}} \tag{4.15f}$$

$$0 < \alpha < 1, \tag{4.15g}$$

where $\nu_{u1,2} = \left(2^{\frac{\gamma_1}{\tau}} - 1\right)$, $\nu_{u2} = \left(2^{\frac{\gamma_2}{\tau}} - 1\right)$, $\kappa_{u3} = b - \frac{1}{a}\ln\left(\frac{L}{L\Omega + (1-\Omega)\frac{\phi}{\tau}} - 1\right)$, $\kappa_{u2} = b - \frac{1}{a}\ln\left(\frac{L}{L\Omega + (1-\Omega)\chi_{u2}} - 1\right)$, $\chi_{u2} = \frac{\nu_{u1,1}(1-\tau)}{f\tau}$, and $\nu_{u1,1} = \left(2^{\frac{\gamma_1}{1-\tau}} - 1\right)$.

Problem (4.15) is convex and can be solved by the CVX toolbox in MATLAB [111]. The optimal value of τ is obtained with a one-dimensional ES method. For each candidate value of τ, problem (4.15) needs to be solved to evaluate the objective function. The ES method gives the optimal value of τ but entails high computational complexity. Then, this method can be considered the optimal solution for comparative analysis. In addition, a near-optimal value of τ can be obtained by using metaheuristic methods, such as PSO or CS, to reduce the load computational complexity. Therefore, in Subsection 4.3.1, we propose PSO and CS-based approaches for transmission power minimization.

Proposed PSO-based Framework For Transmission Power Minimization

PSO is a potential optimization scheme based on a population called the swarm, which is composed of particles that move together in a search space, with the objective being to find the optimal solution. Each particle contains the variables to be optimized, and its position is updated each iteration towards the local and global best positions. The global best position indicates the position in which a particle has reached the best yield in the population, whereas the local best position indicates

the position in which the particle has reached its own best yield so far. In this chapter, each particle position is denoted by $\mathbf{q}_r$, which is a vector of four elements ($p_1, p_2, \alpha,$ and τ) that correspond to the set of variables to be optimized, and it can be written as follows:

$$\mathbf{q}_r = \left\{ q_{p_1,r}, q_{p_2,r}, q_{\alpha,r}, q_{\tau,r} \right\}, \tag{4.16}$$

where $r = 1, 2, 3, ..., R_p$, in which R_p denotes the number of particles in the swarm. Moreover, the feasible search region for each element of the particle's position, $q_{p_1,r}, q_{p_2,r}$, is denoted as $[0, P^{\max}]$, where $P^{\max}$ is the maximum transmission power at the transmitter. The search region for the particle's position, $q_{\alpha,r}$ and $q_{\tau,r}$, is the range $(0, 1)$.

Since proposed problem (4.14) is a constrained optimization problem, a method to deal with constraints is required. Therefore, we utilize the penalty method, where fitness function $f(\mathbf{q}_r) = f(p_1, p_2, \alpha, \tau)$ is based on the objective function of problem (4.14) as follows:

$$f(\mathbf{q}_r) = p_1 + p_2 + \varsigma \sum_{i=1}^{4} \xi(g_i), \tag{4.17}$$

where ς is the penalty value, g_i is the i-th constraint of problem (4.14), and $\xi(g_i) = 0$ if g_i is satisfied, whereas $\xi(g_i) = 1$, otherwise. If all constraints are satisfied, $f(\mathbf{q}_r)$ is the objective function without penalty.

Furthermore, the search strategy to find the optimal solution is based on updating each particle's velocity and position. Based on [6], the velocities of the particles are updated as follows:

$$\mathbf{v}_r^{t+1} = Ine^t \mathbf{v}_r^t + j_1 c_1 \left(\mathbf{lb}_r^t - \mathbf{q}_r^t \right) + j_2 c_2 \left(\mathbf{gb}^t - \mathbf{q}_r^t \right), \tag{4.18}$$

where Ine^t denotes the inertia weight for the velocity update, v_r^t is the velocity of the r-th particle in the t-th iteration, $\mathbf{lb}_r^t$ denotes the local best position of the r-th particle, $\mathbf{q}_r^t$ denotes the position of the r-th particle in the t-th iteration, and $\mathbf{gb}^t$ denotes the global best position of all particles in the t-th iteration; j_1 and j_2 are random numbers between 0 and 1, and c_1 and c_2 are the cognitive and social parameters, respectively.

Then, to update the *r*-th particle's position for each of the elements described in (4.16), the previous particle position plus the updated velocity indicated in (4.18) are considered as follows:

$$\mathbf{q}_r^{t+1} = \mathbf{q}_r^t + \mathbf{v}_r^{t+1}. \tag{4.19}$$

The procedure of the proposed PSO-based algorithm in solving the power minimization problem (4.14) is described in Algorithm 4.1, where the input parameters correspond to the maximum transmission power at the transmitter, P^{max}; the target rate of user 1, γ_1; the target rate value of user 2, γ_2; the minimum energy harvesting at user 3, ϕ; the maximum number of iterations, denoted by I_{PSO}^{total}; the number of particles, R; the inertia weight for the velocity update, *Ine*; random numbers j_1, j_2, and cognitive and social parameters c_1 and c_2. Moreover, the initial global best position is allocated in accordance with the objective function, wherein this chapter the initial **gb** selects the minimum objective value from among all the initial particle positions.

Moreover, the computational complexity of PSO is based on the number of particles, R_p, and the total number of iterations, I_{PSO}^{total} [112]. Thus, the total complexity of the proposed PSO scheme is $O\left(R_p \cdot I_{PSO}^{total}\right)$.

CS-based Framework With Lévy Flights For Transmission Power Minimization

The CS algorithm was inspired by the brood parasitism of the cuckoo species, laying their eggs in the nests of other birds. However, when a host bird realizes the eggs are not its own, it will either leave its nest and build a new one or push the intruding cuckoo's eggs out of the nest. This action can be represented by probability $p_a \in [0, 1]$.

Some cuckoo species are able to mimic the pattern and color of the eggs of a few select host species. This is a key feature that increases cuckoo chick reproduction and prevents them from being abandoned. Overall, the advantage is that the cuckoo eggs hatch slightly earlier than the host eggs, and once the first cuckoo chick emerges, its first act is to dislodge the host species' eggs. This increases its access to feeding opportunities [113].

Algorithm 4.1 The proposed PSO-based algorithm to solve problem (4.14).

1: Establish the input parameters of PSO. Set iteration counter $t = 1$.

2: Initialize particle positions that are randomly selected according to the feasible search region

$[0, P^{\max}]$, and $(0, 1)$. $\mathbf{q}^t = \left\{ \left(q^t_{p_1,1}, q^t_{p_2,1}, q^t_{\alpha,1}, q^t_{\tau,1} \right), ..., \left(q^t_{p_1,R_p}, q^t_{p_2,R_p}, q^t_{\alpha,R_p}, q^t_{\tau,R_p} \right) \right\}$

3: Initialize the particles' velocities: $\mathbf{v}^t = \left(\mathbf{v}^t_1, \mathbf{v}^t_2, ..., \mathbf{v}^t_r \right)$

4: Calculate minimum transmission power $f(\mathbf{q}^t_r)$ by evaluating (4.17) for each r-th particle.

5: Set the initial best particles' positions, $\forall r$, $\mathbf{lb}^t_r = \mathbf{q}^t_r$.

6: Set the initial global best position, $\mathbf{gb}^t = \underset{1 \le r \le R_p}{\arg \min} f(\mathbf{lb}^t_r)$.

7: **For** each particle r **do**

8:     From (4.18), update the particles' velocities.

9:     From (4.19), update the particles' positions.

10:     Update the best particles' positions,

   if $f\left(\mathbf{q}^{t+1}_r\right) < f(\mathbf{lb}^t_r)$ **then** $\mathbf{lb}^{t+1}_r = \mathbf{q}^{t+1}_r$

      else

         $\mathbf{lb}^{t+1}_r = \mathbf{lb}^t_r$

      end if

11: **end for**

12: Update the global best particles' positions, $\mathbf{gb}^{t+1} = \underset{1 \le r \le R_p}{\arg \min} f\left(\mathbf{lb}^{t+1}_r\right)$.

13: **if** $t < I^{total}_{PSO}$, **then** $t = t + 1$ and go to Step 8

   else

      go to Step 15

   end if

14: **Return:** the best values of resource allocation variables, $\left\{ p^*_1, p^*_2, \alpha^*, \tau^* \right\} = \mathbf{gb}$, to obtain the

   minimum value of total transmission power indicated in problem (4.14).

The main idea is that each egg in a nest represents a solution, and the nests with high-quality eggs, i.e., those with potentially the best solutions, will replace a not-so-good solution in the nest and will be carried over to the next generation. In this chapter, we assume each nest has one egg.

Then, each egg is a vector of four elements, p_1, p_2, α, and τ, that are the variables to be optimized, $\mathbf{q}_n = \{p_{1,n}, p_{2,n}, \alpha_n, \tau_n\}$, where $n = 1, 2, 3, ..., N$, in which N denotes the number of nests. Similar to equation (4.17), indicated in the PSO-based algorithm, we use a penalty function to deal with constraints, as follows:

$$f(\mathbf{q}_n) = p_1 + p_2 + \varsigma \sum_{i=1}^{4} \xi(g_i). \tag{4.20}$$

Then, each solution, $f(\mathbf{q}_n)$, is based on the objective function of problem (4.14), which aims to minimize total transmission power. After that, the generation of new solutions is carried out by Lévy flights [104–106]. For instance, the procedure in Lévy flights to generate a new solution for power allocation variable p_1 can be expressed as follows:

$$p_1^{t,new} = p_1^t + R \cdot \beta \cdot L(s, \lambda)\left(p_1^t - p_{1,g}^t\right), \tag{4.21}$$

where R is random number $\mathcal{N}(0, 1)$, $p_{1,g}^t$ is the nest with the best fitness function, $L(s, \lambda) = \frac{\lambda \Gamma(\lambda) \sin(\pi\lambda/2)}{\pi} \frac{1}{s^{1+\lambda}}$, $\beta > 0$ is the step size, and factor $1 < \lambda \leq 3$ we consider to have a value of $\lambda = 3/2$. Parameter s denotes the step length based on Mantegna's algorithm [14], and it can be calculated by

$$s = \frac{u}{|v|^{1/\beta}}, \tag{4.22}$$

where $u \sim \mathcal{N}\left(0, \sigma_u^2\right)$, $v \sim \mathcal{N}\left(0, \sigma_v^2\right)$, $\sigma_u^2 = \left\{\frac{\Gamma(1+\lambda)\sin(\pi\lambda/2)}{\Gamma[(1+\lambda)/2]\lambda 2^{(\lambda-1)/2}}\right\}$, $\sigma_v^2 = 1$.

Similarly, the process to compute the new solution for power allocation variables p_2, α, and τ can be written as

$$p_2^{t,new} = p_2^t + R \cdot \beta \cdot L(s, \lambda)\left(p_2^t - p_{2,g}^t\right), \tag{4.23}$$

$$\alpha^{t,new} = \alpha^t + R \cdot \beta \cdot L(s, \lambda)\left(\alpha^t - \alpha_g^t\right), \tag{4.24}$$

and

$$\tau^{t,new} = \tau^t + R \cdot \beta \cdot L(s, \lambda) \left(\tau^t - \tau_g^t\right). \tag{4.25}$$

For simplicity, we denote that $\mathbf{q}_g^t = \left\{p_{1,g}^t, p_{2,g}^t, \alpha_g^t, \tau_g^t\right\}$. It is worth mentioning that in this chapter, we implement an improved CS version described in [109]. In the conventional CS algorithm, the probability, p_a, and the step size, β, are fixed parameters. However, fine-tuning these parameters can be essential to enhancing the convergence rate and the performance of the algorithm. Therefore, we implemented the improved CS version, which dynamically changed the parameters, p_a and β, based on the number of generations. Accordingly, probability p_a was modified as follows:

$$p_a = p_a^{\max} - \frac{t}{I_{CS}^{total}} \left(p_a^{\max} - p_a^{\min}\right), \tag{4.26}$$

where t denotes the current iteration, and I_{CS}^{total} denotes the total number of iterations. According to the experiment results, we consider $p_a^{\max} = 0.5$, and $p_a^{\min} = 0.25$.

Moreover, step size parameter β is modified as follows:

$$\beta = \beta_{\max} \exp\left(q \cdot t\right), \tag{4.27}$$

where $q = \frac{1}{I_{CS}^{total}} \ln\left(\frac{\beta_{\min}}{\beta_{\max}}\right)$. A fraction of the worst nests, p_a, are abandoned and their positions are updated as follows [110]:

$$p_1^{t,new} = p_1^t + R \cdot \left(p_{1,g}^t - p_{1,u}^t\right), \tag{4.28}$$

$$p_2^{t,new} = p_2^t + R \cdot \left(p_{2,g}^t - p_{2,u}^t\right), \tag{4.29}$$

$$\alpha^{t,new} = \alpha^t + R \cdot \left(\alpha_g^t - \alpha_u^t\right), \tag{4.30}$$

$$\tau^{t,new} = \tau^t + R \cdot \left(\tau_g^t - \tau_u^t\right), \tag{4.31}$$

where $\mathbf{q}_u^t = \left\{ p_{1,u}^t, p_{2,u}^t, \alpha_u^t, \tau_u^t \right\}$ is a randomly selected nest.

The procedure of the CS-based algorithm in solving power minimization problem (4.14) is described in Algorithm 4.2. The input parameters are the maximum transmission power at the transmitter, $P^{\max}$; the target rate value of user 1, γ_1; the target rate value of user 2, γ_2; the minimum energy harvesting at user 3, ϕ; the maximum iteration number, I_{CS}^{total}; the number of nests, denoted by N; the probability that a host bird discovers the intruder cuckoo's egg, p_a; step size β, factor λ, and step length s. In addition, as input parameters, the lower and upper boundaries of the variables to be optimized are considered. Then, power allocation variables p_1 and p_2 are within the range $[0, P^{\max}]$, while variables for fraction transmission time τ and power splitting ratio β fall within $(0, 1)$. Moreover, the computational complexity of the CS depends on the number of nests, N, and the total number of iterations, I_{CS}^{total} [114]. Thus, the total complexity of the CS scheme is $O\left(N \cdot I_{CS}^{total}\right)$.

4.3.2   Energy Efficiency Optimization Problem

In this problem, we aim to maximize the total energy efficiency of the proposed cooperative non-linear SWIPT-enabled NOMA system that also considers an additional nonlinear EH user. Here, we jointly optimized the transmission time fraction, τ, the power-splitting ratio, α, and the power allocation variables, p_1 and p_2, while satisfying the QoS constraints of all users. The energy efficiency is defined as the ratio of total rate to power consumption, as shown in the objective function of the problem, and it can be formulated as follows:

$$\max_{p_1, p_2, \tau, \alpha} \frac{R_{u_1} + R_{u_2}}{\tau \left(p_1 + p_2 + p_{c1}\right) + \left(1 - \tau\right)\left(P_{sw} + p_{c2}\right)} \tag{4.32a}$$

$$\text{s.t.}\ \ (14b), (14c), (14d), (14e), (14f), (14g), (14h),$$

where $R_{u1} = \min\left(R_{x_1, u_2}^{(1)}, R_{x_1, u_1}^{(2)}\right)$, p_{c1} and p_{c2} are the circuit power variables at user 1 and user 2, respectively.

It is worth highlighting that the energy efficiency maximization problem is more challeng-

---

Algorithm 4.2 CS-based framework to solve power minimization problem (4.14).

1: Input parameters of CS scheme, define objective function $f(\mathbf{q}_n)$ in (4.20).

2: Initialize a population of N host nests for each variable to be optimized, $\mathbf{q}_n = \{p_{1,n}, p_{2,n}, \alpha_n, \tau_n\}$,

   $n \in \{1, .2, ..., N\}$.

3: Initialize $t = 0$.

4: Evaluate fitness function for each nest, $F_n^t = f(\mathbf{q}_n^t)$, $\forall n$, and find $\mathbf{q}_g^t$.

5: **For** $t < I_{CS}^{total}$ **do**

6:     Calculate β with (4.27) and obtain new position $\mathbf{q}_n^{t,new} = \left\{p_{1,n}^{t,new}, p_{1,n}^{t,new}, \alpha_{1,n}^{t,new}, \tau_n^{t,new}\right\}$

       for each nest via Lévy flights with (4.21), (4.23), (4.24), and (4.25).

7:     Evaluate the fitness function for each nest, $F_n^{t,new}$, $\forall n$.

8:     For all nests do:

         if $F_n^{t,new} < F_n^t$ **then** $F_n^{t+1} = F_n^{t,new}$, $\mathbf{q}_n^{t+1} = \mathbf{q}_n^{t,new}$

         else $F_n^{t+1} = F_n^t$, $\mathbf{q}_n^{t+1} = \mathbf{q}_n^t$

         end if

9:     Calculate the value of p_a with (4.26).

10:    A fraction, p_a, of the worst nests are abandoned, and the corresponding positions of the nests

       are updated based on (4.28)-(4.31).

11:    Evaluate fitness of new nests and execute Step 8; rank all solutions and find the current

12:     best nest.

13:    $t = t + 1$

14: **end for**

15: **Return:** the best values, $\left\{p_1^*, p_2^*, \alpha^*, \tau^*\right\} = $ **best_nest**, to obtain the minimum transmission power

    indicated in problem (4.14).

---

ing to solve since the cost function is in fractional form and constraints are non-convex. Therefore,

in Subsection 4.3.2, we propose a swarm-intelligence-based scheme called PSO to reduce the com-

putational complexity. In addition, we develop a CS-based benchmark scheme for comparison purposes.

Proposed PSO-based Framework For Energy Efficiency Maximization

Similar to (4.16), we define the objective function as follows:

$$f(\mathbf{q}_n) = \frac{R_{u_1} + R_{u_2}}{\tau(p_1 + p_2 + p_{c1}) + (1 - \tau)(P_{sw} + p_{c2})} - \varsigma \sum_{i=1}^{4} \xi(g_i). \tag{4.33}$$

Then, the PSO algorithm to solve problem (4.32) is based on Algorithm 4.1 with the following modifications: (a) the objective function is evaluated with (4.33); (b) the global best position is obtained with $\mathbf{gb}^t = \arg\max\limits_{1 \le r \le R_p} f(\mathbf{lb}_r^t)$; (c) in Step 11, the condition to update the local best position is $f(\mathbf{q}_r^{t+1}) > f(\mathbf{lb}_r^t)$.

Cuckoo-Search-Based Framework with Lévy Flights For Energy Efficiency Maximization

To maximize the energy efficiency of the proposed NOMA SWIPT network based on CS with Lévy flights, we follow Algorithm 4.2 with minor modifications. Since the current optimization problem is one of maximization, in Step 9 of Algorithm 4.2, we replace inequality $F_n^{t,new} < F_n^t$ with $F_n^{t,new} > F_n^t$. In addition, the objective function is given in (4.33). Then, we obtain the best values, $\{p_1^*, p_2^*, \alpha^*, \tau^*\} = \mathbf{best\_nest}$, to achieve the maximum energy efficiency indicated in (4.32a).

4.4   NUMERICAL RESULTS

In this section, we present the simulation results programmed into MATLAB software, of the proposed cooperative non-linear SWIPT-enabled NOMA system. The results are averaged over several channel realizations. More specifically, we present a performance comparison between the optimal scheme provided by the convex optimization with the ES method, denoted as CVX+ES,

and the proposed PSO-based scheme. Moreover, we assess the performance of the following swarm intelligence-based baseline algorithms: CS, the ALO method, the BOA, the firefly algorithm (FA), and the BA. In addition, we compare the performances between NOMA and OMA transmission cooperative communication with a TF scheme ($\tau = 0.5$) [115–119], and SWIPT NOMA cooperative communication with the EPS scheme ($\alpha = 0.5$) [6].

Rayleigh fading channels $\widetilde{k_2}, \widetilde{f}, \widetilde{e}$ have i.i.d. complex Gaussian entries with zero mean and a certain variance, i.e, $\widetilde{k_2} \sim \mathcal{CN}\left(0, d_{t_r u_2}^{-pl}\right), \widetilde{f} \sim \mathcal{CN}\left(0, d_{u_1 u_2}^{-pl}\right)$, and $\widetilde{e} \sim \mathcal{CN}\left(0, d_{t_r u_3}^{-pl}\right)$, respectively, where d_{ij} denotes the distance between nodes i and j, and pl is the path-loss exponent; index t_r indicates the transmitter. In the simulations, we assume the path-loss exponent is $pl = 2$ for channels $\widetilde{k_2}, \widetilde{f}, \widetilde{e}$, and noise power is $\sigma_1^2 = \sigma_2^2 = -60$ dBm. The distances in meters between the nodes are $d_{t_r u_2} = 15$, $d_{u_1 u_2} = 18$, and $d_{t_r u_3} = 6$. Moreover, the maximum transmission power at the transmitter is $P^{\max} = 30$ dBm.

4.4.1 Transmission Power Minimization

In this subsection, we analyze the numerical results obtained for transmission power minimization. Figure 4.3 shows the total transmit power of the proposed PSO-based scheme compared with those of the following swarm intelligence algorithms: CS, ALO, BAO, FA, and BA. The parameters of each algorithm in Table 4.1 are set based on the best results achieved through several experiments. The description of these baseline swarm algorithms and their parameters are explained in [120]. From Figure 4.3, it is observed that the trend of all schemes rises as the minimum rate at user 1 increases. However, the proposed PSO scheme outperforms the comparison swarm intelligent algorithms in terms of total transmit power. It is noteworthy that the performance of CS is very close to that obtained by PSO. Thus, to validate the superiority of PSO, we evaluate the convergence behavior between PSO and CS. In addition, we compare the average (central processing unit) CPU running time of the proposed PSO-based framework, the optimal CVX+ES method, and
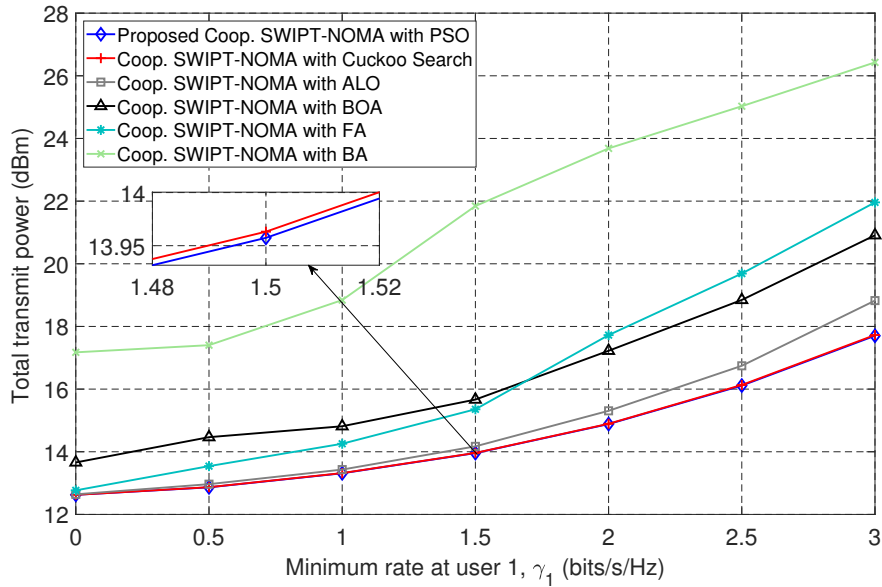
Figure 4.3: Total transmit power of the proposed PSO-based scheme, CS, ALO, BOA, FA, and BA according to the minimum rate at user 1, γ_1.

the performance of five benchmark swarm intelligence algorithms.

Figure 4.4 illustrates the convergence behavior of the proposed low-complexity PSO algorithm and the CS baseline algorithm according to the number of iterations. We can see that as the number of iterations increases, the total transmission power is minimized. Moreover, Figure 4.4 shows that for the PSO-based scheme, the transmit power converges within about 60 iterations. Therefore, we fix the number of iterations, I_{PSO}^{total}, equal to 60 at other simulations. Moreover, we also set the number of particles at $R_p = 30$, the inertia weight to $Ine = 0.7$, along with the scaling factors, $c_1 = 1.494$, and $c_2 = 1.494$. Meanwhile, for the CS-based scheme, Figure 4.4 shows that the transmit power converges within about 250 iterations, which is a bit more than double that of PSO and entails higher complexity. After the fine-tuning process for CS, we set its parameters: number of nests, $N = 35$, and total iterations, $I_{CS}^{total} = 250$. Furthermore, we can see that total transmission power increases as the minimum requirement for EH at u_3, and the minimum target rates, γ_1 and

Table 4.1: Simulation parameters for transmission power minimization

Algorithm	Simulation parameters
PSO	$I_{PSO}^{total} = 60$, $R_p = 30$, $Ine = 0.7$, $c_1 = 1.494$, $c_2 = 1.494$
CS	$I_{CS}^{total} = 250$, $N = 35$, $\beta_{min} = 0.01$, $\beta_{max} = 0.5$
ALO	Number of iterations, $I_{ALO}^{total} = 120$, Number of ants, $N_{ALO} = 30$
BOA	Number of generations, $G_{BOA} = 250$, Number of agents, $S_{BOA} = 35$ Sensory modality, $sm = 0.01$, Power exponent, $pe = 0.01$ Switch probability, $sp = 0.5$
FA	Number of iterations, $I_{FA}^{total} = 500$, Number of fireflies, $N_{FA} = 40$ Randomness strength, $R_{str} = 1$, Attractiveness constant, $Atc = 1$ Absorption coefficient, $ac = 0.01$, Randomness reduction factor, $R_{rf} = 0.97$
BA	Number of iterations, $I_{BA}^{total} = 200$, Number of bats, $N_{BA} = 40$ Pulse emission rate, $p_{BA} = 0.001$, Maximum frequency, $f_{BA}^{max} = 2$ Minimum frequency, $f_{BA}^{min} = 0$, Constant for loudness, $l_{BA} = 0.5$ Constant for emission rate, $l_{er} = 0.5$

γ_2, respectively, increases. This is because more power must be allocated to users as the QoS requirements increase.

To validate the optimality of the proposed low-complexity PSO-based framework, Figure 4.5 shows the performance comparison between the optimal scheme, CVX+ES, the PSO-based scheme, the CS-based scheme, and cooperative SWIPT-OMA for transmission power minimization. Note that CVX with the ES method corresponds to the analytical solution indicated in subsection III.A. Figure 4.5 shows the transmission power when the minimum EH requirement is $\phi = -23$dBm, and target rate at u_2 is $\gamma_2 = 1$ bit/s/Hz. From Figure 4.5, we verify that the proposed PSO and
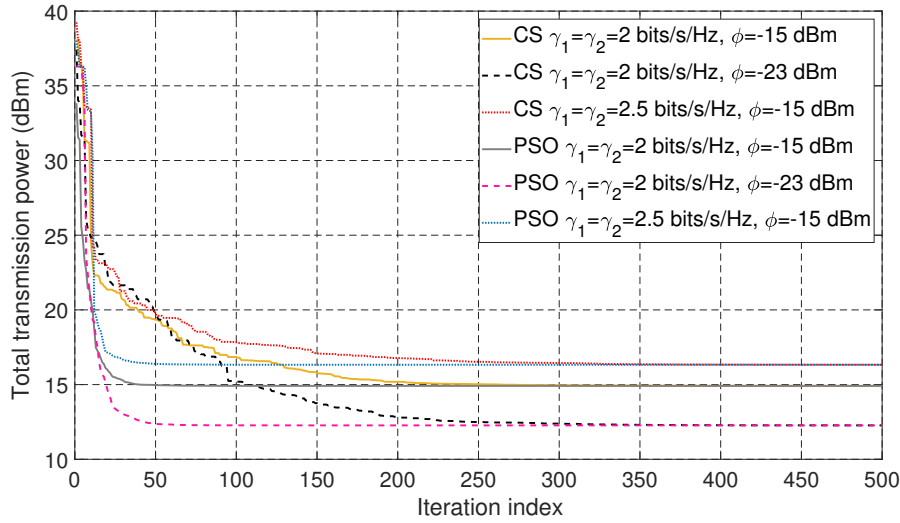
Figure 4.4: Convergence of the proposed PSO-based algorithm and CS with different required rates γ_1, γ_2, and minimum harvested energy, ϕ, for transmission power minimization.

CS-based frameworks provide near-optimal performance, compared with the CVX+ES method. In addition, it is worth highlighting that the PSO-based scheme can reach a result closer to the optimal solution provided by CVX+ES in fewer iterations than under the CS, which means that less time is needed to compute a solution with higher performance. Therefore, in this chapter, we propose the PSO-based framework as the most suitable low-complexity solution in the cooperative non-linear SWIPT-NOMA network.

Furthermore, the average CPU running times are compared in Table 4.2 among the proposed PSO-based framework, the optimal CVX+ES method, and five benchmark swarm intelligence algorithms. The results are obtained by using a computer with a 4 GHz i7-6700K CPU and 16 GB RAM. Firstly, we can observe that CVX+ES requires the most computation time. By contrast, the low-complexity solutions provided by the proposed PSO-based scheme and the swarm intelligence-based baseline algorithms can reduce the CPU running time to obtain a sub-optimal solution. However, it is remarkable that the PSO scheme requires the least CPU running time to reach a solution than
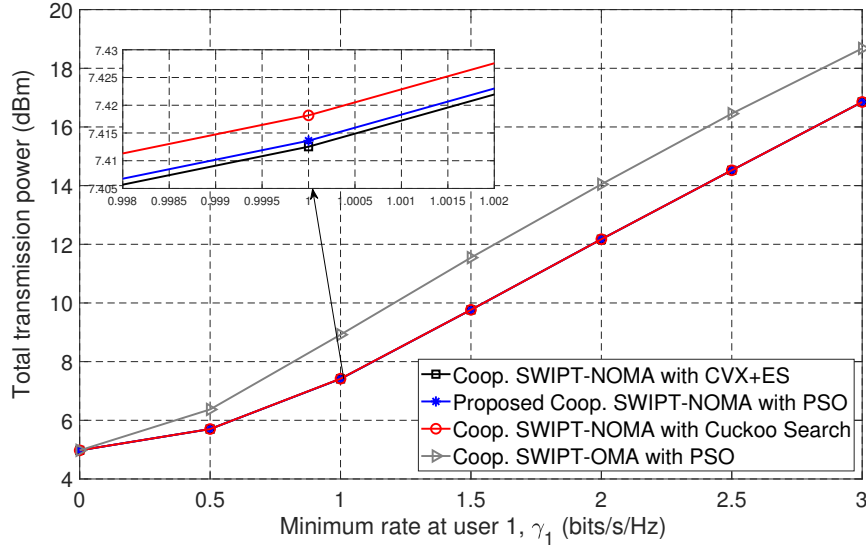
Figure 4.5: Performance comparison among the optimal scheme (CVX+ES), the PSO-based scheme, the CS-based scheme, and cooperative SWIPT-OMA for transmission power minimization.

their counterparts to reach a solution. This is because PSO requires fewer iterations compared to the benchmark swarm intelligence schemes, as shown in Table 4.1. Particularly, from Figure 4.5, we can observe that CS and PS achieve a very close performance to the optimal CVX+ES method. However, we can also see that CS needs more time than PSO to reach a solution. This is because PSO requires fewer iterations to achieve convergence compared to the CS method. Moreover, the number of particles, R_p, utilized in PSO is lower than the number of nests, N, required under CS. Recall that the computation complexity depends on the number of iterations and the number of particles used by each algorithm. Specifically, the computational complexity of PSO is computed by $O\left(R_p \cdot I_{PSO}^{total}\right)$ while the computation complexity of CS is computed by $O\left(N \cdot I_{CS}^{total}\right)$. In this sense, since the PSO-based scheme requires fewer iterations and a lower number of particles than that required by CS, the least computational complexity with the highest accuracy is achieved by the proposed PSO-based solution. Regarding CVX+ES, the problem (4.15) should be solved for each possible time value for τ and it is needed to check if the candidate solution satisfies all the constraints.

Table 4.2: CPU running time

Scheme	CPU time (sec)
PSO	0.671
CVX+ES	3584
CS	6.017
ALO	3.495
BOA	25.106
FA	119.641
BA	2.784

Next, the candidate solution with the lowest objective function is defined as the best solution. Then, the CVX+ES method cannot have a convergence behavior like the presented in Figure 4.4 for PSO and CS because the possible values of τ are tested in order from 0 to 1 with a predefined step. For instance, we considered increments of 0.0001 for τ, and thus, solved the problem (4.15) a total of 10,000 times, whereas the average time to solve the problem (4.15) is 0.358 sec.

Moreover, we considered the total power minimization problem for the cooperative non-linear SWIPT-enabled OMA benchmark. We used the TDMA technique in which three phases are required to complete transmission in the comparison SWIPT-OMA scheme. Specifically, TDMA allocates a fraction of time τ_1 and τ_2 to u_1 and u_2, respectively. Moreover, a fraction of time τ_3 is assigned to the cooperative transmission from u_2 to u_1. From Figure 4.5, we observed that the proposed cooperative SWIPT-NOMA scheme outperforms the conventional OMA strategy in the cooperative network since OMA increases the total transmission power compared with the proposed cooperative NOMA scheme. This is because, in NOMA, the users share the same frequency at the same time, which improves the spectral efficiency of the system. By contrast, OMA requires more

resources to complete a transmission because users share the same frequency channel at different times.

Figure 4.6 and Figure 4.7 illustrate the effect from linearity of EH on the transmit power of the proposed scheme (cooperative SWIPT NOMA communication optimizing resource allocation variables p_1, p_2, τ, and α) and the following baseline schemes: SWIPT NOMA cooperative communication with TF, and SWIPT NOMA cooperative communication with EPS. In cooperative non-linear SWIP-NOMA, we used the non-linear EH model at u_2 specified in (4.7) and the non-linear EH model at u_3 specified in (4.9). On the other hand, for application of the ideal linear EH model in the cooperative SWIPT-enabled NOMA system, we used the linear EH model at u_2 specified in (4.6) and the linear EH model at u_3 specified in (4.10). Moreover, we considered $\eta = 1$ for the linear EH models. Overall, we verified that the cooperative SWIPT-NOMA scheme with a linear EH model achieved lower transmission power since it considers the users to be storing all the power of the incoming signal. By contrast, the non-linear EH model considers a more realistic environment where the relationship between stored energy and received RF power is non-linear because of physical impairments, saturated harvested power, and circuit specifications. Moreover, from Figure 4.6 and Figure 4.7, we can see that the proposed cooperative non-linear SWIPT-NOMA scheme outperforms the EPS and TF baseline schemes. This verifies that including the power splitting ratio and time fraction variables in the optimization problem improves the performance of the network. Recall that the EPS and TF schemes considered the power splitting ratio to be $\alpha = 0.5$, and the time transmission fraction to be set at $\tau = 0.5$, respectively.

4.4.2 Energy Efficiency Maximization

In this subsection, we assess the results for energy efficiency maximization in the proposed nonlinear SWIPT NOMA system.

Figure 4.8 shows energy efficiency among the proposed PSO-based scheme and the

Figure 4.6: Transmit power comparison between the proposed cooperative non-linear SWIPT-NOMA and cooperative linear SWIPT-NOMA according to different required rate, γ_1, $\gamma_2 = 1$ bit/s/Hz, $\phi = -15$ dBm.

following swarm intelligence algorithms: CS, ALO, the BAO, FA, and BA. The parameters of each algorithm in Table 4.3 are set based on the best results achieved through several experiments. From Figure 4.8, it is observed that the energy efficiency of all schemes diminishes as the minimum rate at user 1 increases. However, the proposed PSO scheme outperforms the other swarm intelligent algorithms by utilizing fewer iterations to obtain the maximum energy efficiency which entails less computational time. Similar to the transmit power problem, the performance of CS is very close to that obtained by PSO. Thus, to validate the superiority of PSO, we evaluate the convergence behavior and the CPU time between PSO and CS.

Figure 4.9 illustrates the convergence behavior of energy efficiency of the proposed low-complexity PSO-based algorithm and the CS baseline scheme. As the number of iterations increases, energy efficiency is maximized. Moreover, Figure 4.9 shows that in the case of PSO, the energy efficiency is converged within about 125 iterations. Therefore, we set the number of iterations, I_{PSO}^{total},
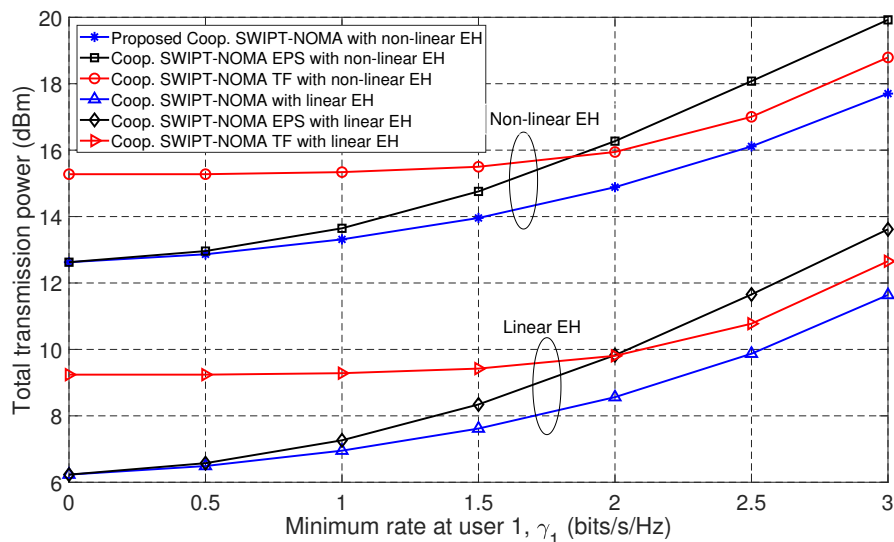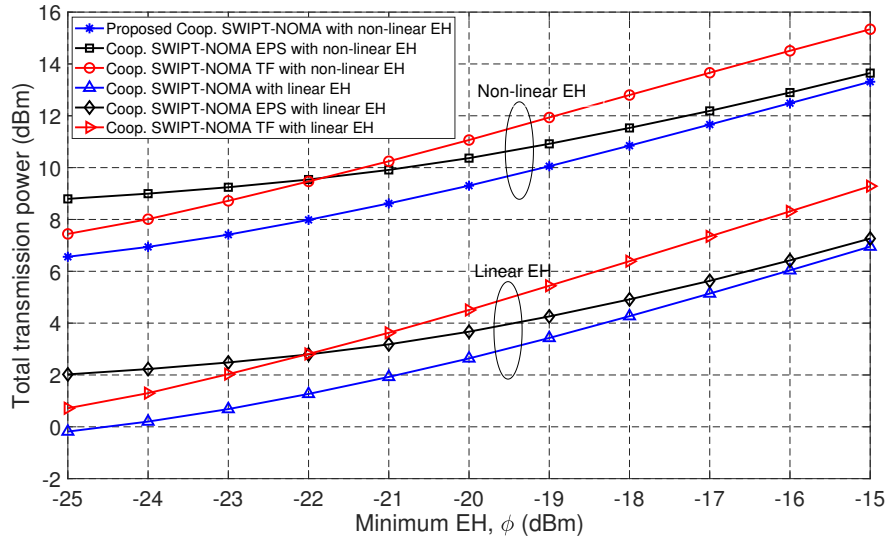
Figure 4.7: Transmit power comparison between the proposed cooperative non-linear SWIPT-NOMA and cooperative linear SWIPT-NOMA according to different required EH, ϕ, $\gamma_1 = 1$ bit/s/Hz, $\gamma_2 = 1$ bit/s/Hz.

Figure 4.8: Energy efficiency comparison among the proposed PSO-based scheme, CS, ALO, BOA, FA, and BA according to the minimum rate at user 1, γ_1.

Table 4.3: Simulation parameters for energy efficiency

Algorithm	Simulation parameters
PSO	$I_{PSO}^{total} = 125$, $R_p = 35$, $Ine = 0.7$ $c_1 = 1.494$, $c_2 = 1.494$
CS	$I_{CS}^{total} = 400$, $N = 35$, $\beta_{\min} = 0.01$ $\beta_{\max} = 0.5$
ALO	$I_{ALO}^{total} = 250$, $N_{ALO} = 35$
BOA	$G_{BOA} = 250$, $S_{BOA} = 60$, $sm = 0.01$ $pe = 0.01$, $sp = 0.5$
FA	$I_{FA}^{total} = 500$, $N_{FA} = 60$, $R_{str} = 1$ $Atc = 1$, $ac = 0.01$, $R_{rf} = 0.97$
BA	$I_{BA}^{total} = 250$, $N_{BA} = 50$, $p_{BA} = 0.001$ $f_{BA}^{\max} = 2$, $f_{BA}^{\min} = 0$, $l_{BA} = 0.5$ $l_{er} = 0.5$

at 125. Moreover, we set the number of particles to $R_p = 35$, the inertia weight to $Ine = 0.7$, and for the scaling factors, $c_1 = 1.494$, and $c_2 = 1.494$. Regarding CS, from Figure 4.9, we can see that the energy efficiency is converged within about 400 iterations. Similar to the convergence behavior for the power minimization problem, the number of iterations for energy efficiency is also more than double that of PSO, which entails higher complexity. After performing various experiments with CS, we selected the parameters for the number of nests, $N = 35$, and the total iterations, $I_{CS}^{total} = 400$. Moreover, from Figure 4.11, we can see that the energy efficiency decreases as the minimum requirements for EH at u_3, and for the minimum target rates, γ_1 and γ_2, increase. This is because when QoS requirements increase, more power needs to be allocated to users. Accordingly,
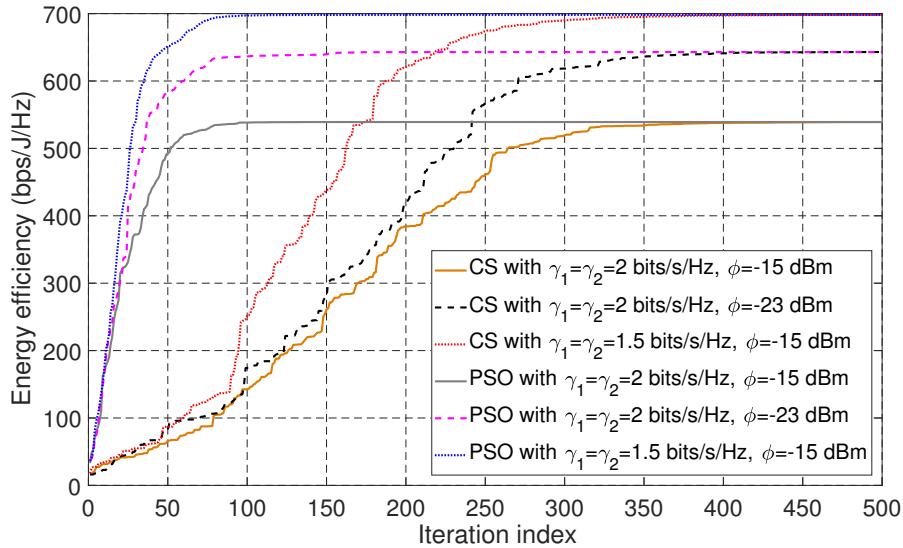
Figure 4.9: Convergence of the proposed PSO-based algorithm and CS with different required rates, γ_1, γ_2, and minimum harvesting energy, ϕ, for energy efficiency maximization.

energy efficiency is reduced, since its relationship to power consumption is inversely proportional.

From Figure 4.10, we verified that the energy efficiency performances obtained by the proposed PSO- and CS-based frameworks are close to that by the ES method with the minimum EH requirement, $\phi = -23$ dBm, and for the target rate at u_2, $\gamma_2 = 1$ bit/s/Hz. In contrast to the ES method, the low-complexity solutions provided by PSO and CS can lessen the time needed to achieve an approximately optimal solution with low computational complexity. It is worth noting that the proposed PSO-based scheme can reach a result closer to the optimal solution provided by ES in fewer iterations than the CS-based scheme. This means less time is needed to compute a solution with higher performance. Therefore, we propose the PSO-based scheme as a powerful low-complexity solution in cooperative non-linear SWIPT-NOMA networks. Moreover, from Figure 4.10, we verify that the proposed cooperative SWIPT-NOMA network outperforms the OMA scheme in terms of energy efficiency.

Figure 4.11 and Figure 4.12 illustrate the effect from linearity of EH on energy efficiency
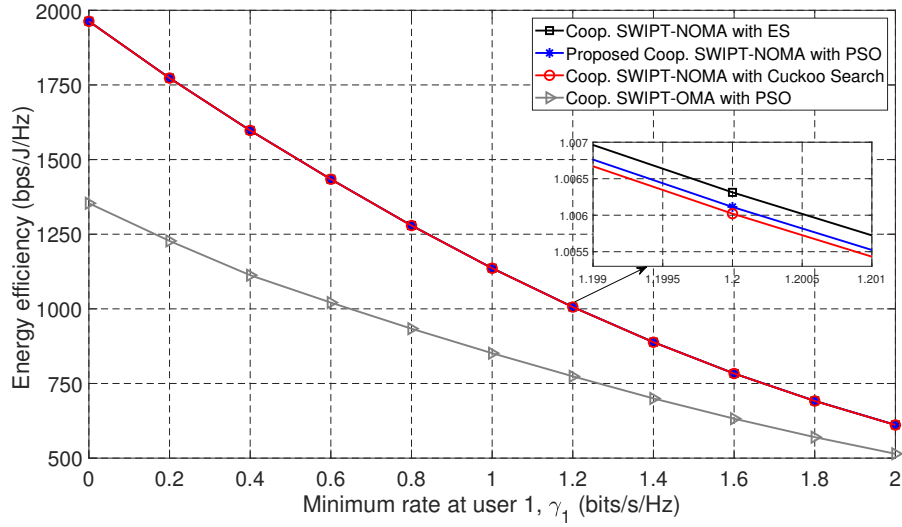
Figure 4.10: Energy efficiency performance of ES, cooperative non-linear SWIPT-NOMA with PSO, cooperative non-linear SWIPT-NOMA with CS, and cooperative non-linear SWIPT-OMA with PSO.

in the proposed cooperative SWIPT NOMA communication that optimizes the variables p_1, p_2, τ, and α, and on the following baseline schemes: SWIPT NOMA cooperative communications with a TF scheme, and SWIPT NOMA cooperative communications with EPS. Besides, we consider $\eta = 1$. From Figure 4.11 and Figure 4.12, we verify that the cooperative SWIPT-NOMA scheme with the ideal linear EH model achieves higher energy efficiency. This is due to a linear relationship between the stored energy and the received RF power. Thus, users can store all the power of the incoming signal. This differs from the proposed non-linear EH model, which considers a more realistic environment that involves saturated harvested power and circuit specifications. Furthermore, from Figure 4.11 and Figure 4.10, we can see that the proposed cooperative non-linear SWIPT-NOMA scheme outperforms the EPS and TF baseline schemes in terms of energy efficiency.
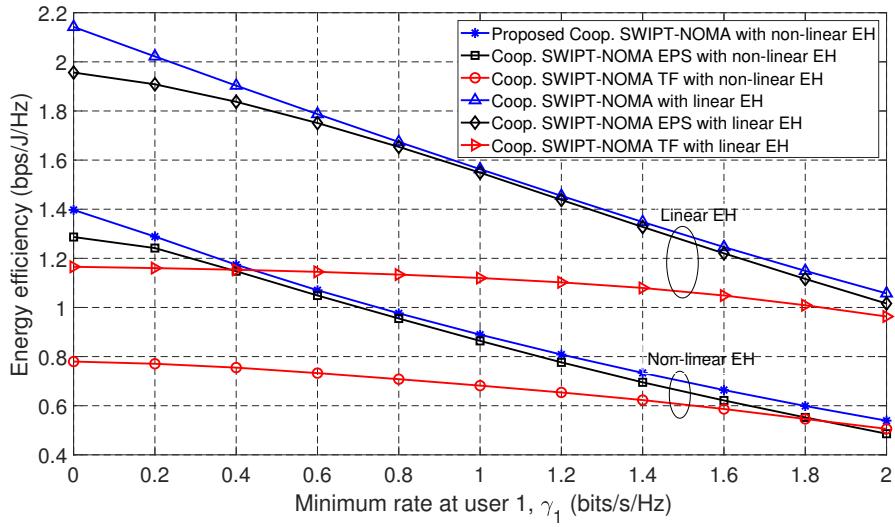
Figure 4.11: Energy efficiency comparison between the proposed cooperative non-linear SWIPT-NOMA, and cooperative linear SWIPT-NOMA according to different required rates, γ_1, $\gamma_2 = 1$ bit/s/Hz, $\phi = -15$ dBm.
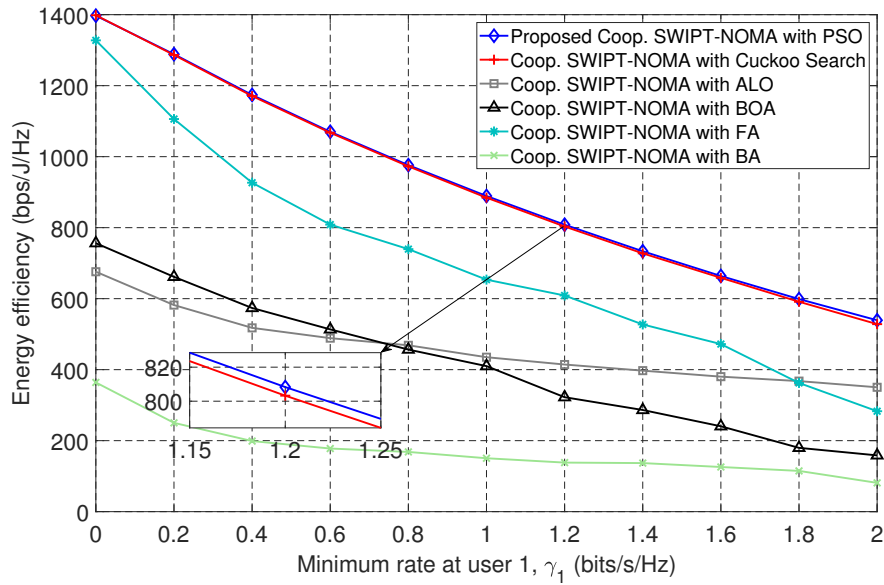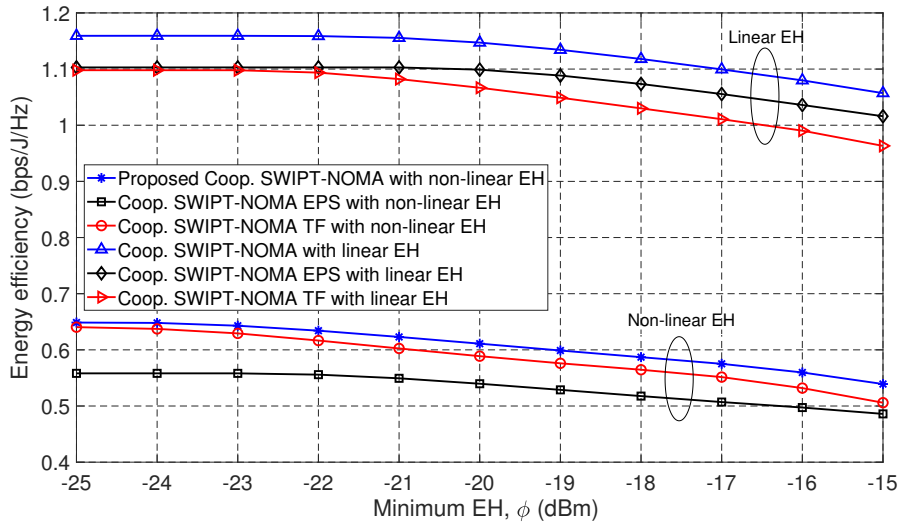

Figure 4.12: Energy efficiency comparison between the proposed cooperative non-linear SWIPT-NOMA, and cooperative linear SWIPT-NOMA according to different required EH, ϕ, $\gamma_1 = 1$ bit/s/Hz, $\gamma_2 = 1$ bit/s/Hz.

4.5   Closing Remarks

In this chapter, we propose to optimize transmission power and energy efficiency in a collaborative non-linear SWIPT-NOMA system with a non-linear EH user while satisfying constraints on minimum target rate at the users and minimum harvested energy at the terminal. The considered optimization problems are non-convex, involving joint optimization of the transmission time fraction, the power splitting ratio, and power allocation, and are thus difficult to solve directly. To tackle this issue, we propose a PSO–based solution with low computational complexity where results reach performance near-optimal to those obtained by the optimal but time- and energy-consuming convex optimization and ES methods. In addition, we also study and develop a CS-based benchmark as an alternative low-complexity solution and evaluate the performance of five swarm intelligence benchmark schemes. Simulation results showed that PSO requires fewer iterations than the swarm intelligence baseline schemes to achieve convergence, which leads to the least CPU time for PSO. Furthermore, we investigate cooperative non-linear SWIPT-OMA, EPS, and TF benchmark schemes for performance comparison with the proposed cooperative non-linear SWIPT-NOMA system. Results showed that the proposed cooperative non-linear NOMA with SWIPT can reduce transmit power and achieved higher spectral efficiency compared to the OMA, EPS, and TF baseline schemes. It is worth highlighting that the optimization of the time variable provided a significant performance improvement, but it is conventionally kept as a constant in the literature. Furthermore, we analyzed the application of a non-linear EH model with the ideal linear EH. The developed schemes with linear EH achieved lower transmission power and high energy efficiency because they consider an ideal case where the receiver harvests all the power of the incoming signal.

Chapter 5

Ensemble Learning aided QPSO–Based Framework for Secrecy Energy Efficiency in FD CR-NOMA Systems[1]

5.1 Introduction

Cooperative communications integrating full-duplex (FD) operation mode, CR, and NOMA are emerging technologies for deployment of IoT networks, and 5G-and-beyond wireless systems [121]. These technologies enable a vast variety of applications with a diverse set of requirements that strain orthogonal technology resources to their limits. Therefore, among the recognized promising multiple access techniques to support massive connectivity and combat spectrum scarcity, NOMA holds a significant role. Different from the conventional multiple access technologies, such as FDMA, TDMA, and code division multiple access, NOMA simultaneously serves multiple users on the same channel, and thus increases the spectral efficiency of wireless networks. For instance, power-domain

---

[1]The study in this chapter is published in IEEE Transactions on Green Communications and Networking [22]

NOMA conveys superposition signals to receivers at the same frequency and time but with different transmit power levels. Power level assignment is realized according to the user's channel conditions, i.e., more power will be allocated to users with poor channel conditions while less power will be assigned to those with better channel conditions. On the receiver side, NOMA users employ SIC to eliminate multi-user interference and extract the desired signal [122, 123].

To further tackle and relieve the spectrum resource–shortage issue, CR-inspired NOMA promotes intelligent use of spectrum sharing. In particular, CR allows unlicensed users to access licensed communication channels in an opportunistic or non-interfering manner [60]. In addition, FD systems have gained attention from the research community owing to their main benefits—high velocity, diverse gain, and low delay in data transmission. Theoretically, FD achieves spectral efficiency that is twice that of a HF system because, in FD systems, messages can be transmitted and received simultaneously. Moreover, SIC techniques assist FD systems to significantly diminish the power self-interference because of the simultaneous transmissions [124]. On the other hand, security is still a serious concern that limits the development of next-generation communications due to the open wireless communications environments. To tackle this issue, conventional encryption security techniques implemented at the upper layers of the network protocol stack are utilized to ensure secure information transmission. Although these security techniques employ complex cryptographic keys, with the breakthrough of quantum computing and the constant improvement of computational methods, encryption techniques become more untrustworthy. The main drawback of these traditional techniques is that their encryption algorithms can be broken by the high computational capabilities of malicious users [125]. In this regard, PLS is considered a potent choice to complement the use of conventional secure technologies. The core idea of PLS is to leverage the inherent randomness of wireless communication channels to avoid malicious users from successfully decoding data addressed to others. It is worth noting that, in the information-theoretic approach, PLS has proven trustworthy.

Research developments in PLS techniques are of meaningful importance for future wireless

networks, including collaborative relay nodes and FD, NOMA, and CR networks. In the literature, an effective research direction relied on the integration of PLS and cooperative networks has attracted meaningful interest to enhance secure communications (e.g., [12, 126–130]). For instance, CR networks employing a collaborative relay have been proposed to potentially improve reception reliability in cooperative NOMA networks [126, 127]. Moreover, different relay networks employing NOMA were investigated in [128, 129] to improve secrecy affected by external eavesdroppers. The authors of these papers analyzed security performance through closed-form expressions of secrecy outage probability (SOP) and confirmed the superiority of NOMA over OMA. Furthermore, rate-splitting multiple access (RSMA) has drawn the attention of the academy because it is considered a powerful transmission scheme in wireless communications [131, 132], especially in MIMO systems. The authors in [132] stated that in a SISO broadcast channel (BC) system, there is no need to employ the RSMA technique since the NOMA scheme can achieve the capacity region.

In [12, 130], the authors studied PLS for a NOMA network with collaborative relays exposed to eavesdroppers in terms of SOP and secrecy sum rate, respectively. The results showed that relays can aid in forwarding signals from source to destination in the challenging scenario of multiple eavesdroppers. However, it is worth highlighting that conventional relay selection techniques rely on closed-form expressions that entail high latency and communication overhead, which is not appropriate for practical networks [133, 134]. For instance, in [12], the relay selection process is performed by applying the ES technique, which requires a lot of computational time searching for the optimal relay from all available relays that permit maximizing the objective function. Therefore, in this chapter, we propose a smart relay selection technique based on a ML approach that greatly reduces the computational time.

A smart resource-allocation scheme is a prominent and useful strategy in wireless networks with collaborative relay nodes because it alleviates trouble from high complexity, and reduces latency in communications systems [124]. Thus, AI holds a key position in resource allocation design and in

solving challenges linked to various aspects of wireless networks [133]. ML leads the most popular AI technologies, and is widely used in the telecommunications engineering field. For instance, ML-based relay selection in IoT networks can significantly reduce selection complexity, which further achieves low latency. Therefore, different ML algorithms have been proposed in cooperative relay networks [133–136],. In [135], the authors proposed a low-complexity iterative algorithm along with a deep neural network (DNN) method to solve the relay selection problem and to predict throughput in an IoT network. The results showed that the proposed DNN-based solution achieved high accuracy with a short execution time. Similarly, the authors in [136] investigated a regression problem based on a DNN scheme to predict sum throughput and energy efficiency. Meanwhile, a supervised ML technique was studied in [137] to enable a relay selection scheme that requires two relay nodes to retransmit signals on multiple subcarriers. The paper concluded that ML reached optimal performance close to that provided by the optimal ES method but with lower computing latency. To the best of our knowledge, the aforementioned research articles did not consider PLS and the application of FD technology. In this regard, although HD relays are frequently used in cooperative wireless networks, FD-enabled relays can considerably enhance the data rate and reduce communication latency by utilizing the SIC technique [133, 138, 139]. Moreover, network security is an essential research topic to promote continuous technological advancement in a safe manner.

To further reduce the computational complexity and provide suitable resource management in the implementation of innovative wireless communications systems while ensuring secrecy performance, AI-based solutions integrated by ML [140–142] and heuristic approaches [12, 30, 46] have attracted a great deal of interest in the industry and research community. For instance, in [142], the authors designed a power allocation (PA) scheme with the aid of a neural network model for enhancing PLS. The paper concluded that the proposed ML method can improve the security sum rate by optimizing PA at the relay node. Similarly, in [139, 142], the authors developed PA assignments in NOMA networks based on a PSO algorithm to maximize secure computational efficiency and

SEE, respectively. To this end, PSO is among the AI techniques that aim to find approximate solutions to acutely tough optimization problems [143]. PSO is a potent optimization algorithm that iteratively attempts to enhance a candidate solution based on updating positions and velocities of the swarm [144]. However, the limitations in PSO arise when constraints and restrictions increase or when the network becomes more complex. As a result, its convergence behavior is severely degraded in trying to reach the desired optimal solution. Therefore, it is essential to find alternative optimization techniques that provide low complexity, deal with complex environments, and ensure high reliability in wireless communications.

Computational complexity reduction and low processing latency are among the major objectives of network models [124, 135]. Therefore, in this chapter, we propose a novel AI-based framework to maximize the SEE in FD cooperative relay CR-NOMA networks in the presence of multiple eavesdroppers. Specifically, we investigate QPSO to perform power allocation assignment while smart relay selection is performed by EL algorithms. To this end, QPSO [145] is a PSO variant inspired by quantum mechanics. Different from the standard PSO, QPSO overcomes the problem of slow convergence, which considerably reduces processing time. Moreover, EL schemes belong to a subset of ML algorithms that integrate multiple classifiers to improve the prediction accuracy. The proposed EL is composed of RF and Stagewise Additive Modeling using a Multi-class Exponential loss function (SAMME) algorithms. In this context, RF utilizes a multiple decision–tree-based bagging approach, whereas SAMME uses the boosting technique to sequentially build a tree-based ensemble model.

Our aim is to build an AI framework to maximize the SEE in a low-complexity manner that can converge faster than optimization techniques like the ES method. To this end, ES (a brute force technique) is used to search for the best solution to optimization problems by searching over all possible candidate options. It entails high computational complexity, and it increases when more nodes are attached to the communication network. The goal is to solve the SEE optimization problem,

which is first transformed into a challenging bi-level optimization task, where the inner problem corresponds to optimizing the power allocation real-value variables, and the outer problem solves relay selection. The relay selection procedure is based on an EL module. Hence, in this chapter, we investigate joint relay-selection and power-allocation problems for SEE maximization in the proposed FD cooperative CR-NOMA network. Furthermore, we compare the SEE performance of the proposed system with that of OMA, RSMA, and the conventional HD operation mode.

The main contributions of this chapter are summarized as follows.

- We formulate the optimization problem to maximize SEE in the proposed FD cooperative relay CR-NOMA system with imperfect SIC to prevent multiple-eavesdropper wiretapping. The optimization solution satisfies QoS requirements corresponding to the minimum rate for SUs, the maximum interference threshold, and maximum transmission power at the secondary transmitter (ST) and relay. It is worth noting that the proposed optimization problem is non-convex and challenging to solve because the objective function is in fractional form, and constraints are non-convex.

- We designe the AI framework based on EL and QPSO modules to provide a low-complexity solution. First, we start with construction of the EL module, which is composed of the potent RF and SAMME algorithms. This module is in charge of solving the relay selection issue because RF and SAMME were shown to be efficient and robust ML classifier algorithms in complex network environments.

- After construction of the EL module, we investigate swarm intelligence methods to design a power allocation scheme based on QPSO. The efficient and low-complexity QPSO module is used to complement the proposed AI framework. The proposed QPSO method is capable of maximizing the non-convex SEE of the proposed system with fewer iterations than needed by the standard PSO method.

- We assemble the EL and QPSO modules to build the AI framework. Therefore, we designed the EL module for smart relay selection. Then, we use the best relay as one of the input parameters for the QPSO algorithm to efficiently solve the formulated optimization problem.

- Finally, according to simulation results, we verify that the proposed AI-based solution can reach near-optimal performance with much lower complexity, compared with an ES-based scheme. Moreover, convergence behavior is significantly improved by the proposed QPSO, which results in computational complexity reduction. Furthermore, we include results on the performance of more swarm intelligence-based baseline algorithms in terms of SEE, converge behavior and computational complexity. The swarm intelligence-based baseline algorithms [16, 120] include the standard PSO, CS, the ALO method, and the BOA. In addition, in Appendix A, we provide a mathematical solution based on the SCA [146, 147] method aided by PSO.

- In addition, for comparison purposes in terms of wireless network design, we describe the conventional OMA, RSMA, and HD mode in the considered cooperative relay CR network affected by various eavesdroppers. Satisfactorily, the proposed FD CR system with the aid of the NOMA transmission strategy improves the security of the network and outperforms comparison approaches in terms of SEE. Moreover, we analyze the scenario of multiple antennas at eavesdroppers.

The remainder of this chapter is organized as follows. The system model of the proposed FD cooperative relay CR-NOMA network and the HD comparison approach are described in Section 5.2. The problem formulation for SEE maximization is discussed in Section 5.3. The AI framework is described in Section 5.4, and the baseline OMA and RSMA transmission strategies are described in Section 5.5. Simulation results of the proposed scheme and the comparison approaches are presented in Section 5.6. Finally, the conclusion is Section 5.7.
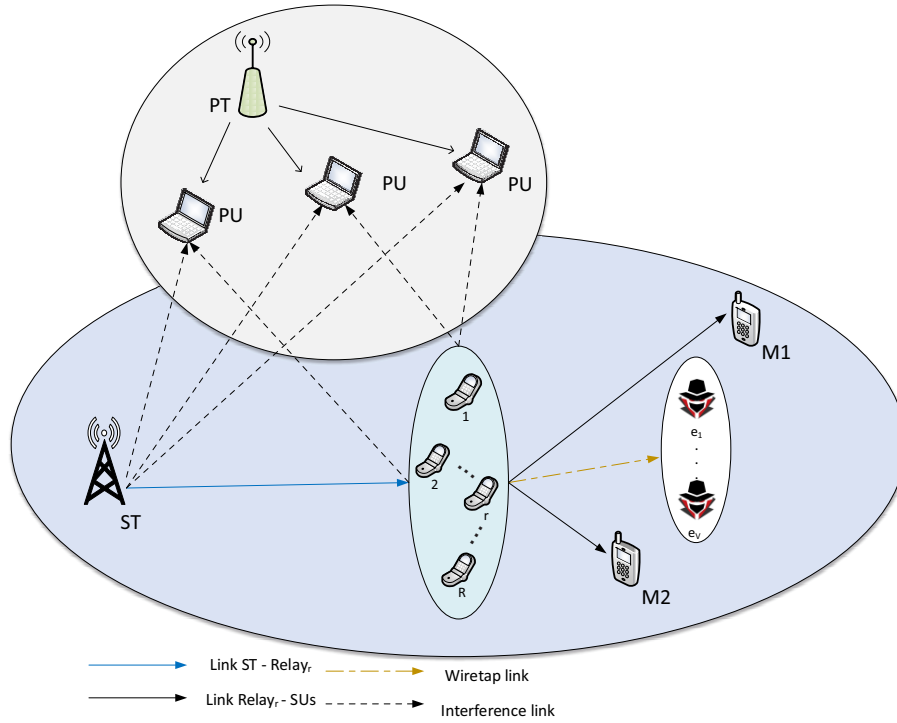
Figure 5.1: The considered FD cooperative relay CR-NOMA network with imperfect SIC.

5.2　System Model

In this chapter, we propose a FD cooperative relay CR-NOMA network consisting of a ST, two SUs denoted as M1 and M2, R relays, K PUs, and multiple eavesdroppers ($e_v, v = \{1, ..., V\}$) as illustrated in Figure 5.1. All nodes are equipped with a single antenna. Without loss of generality, we consider the distance of the ST–R–M1 link is significantly longer than the ST–R–M2 link, and this means the ST–M1 link can support a lower QoS than ST–M2 [12]. Therefore, the M1 user is considered the weak user, and M2 is considered the strong user.

The proposed FD CR-NOMA network is assisted by an intermediate DF relay since it is assumed there is no direct link between the ST and the SUs. The relay is selected from the R available relays; it is denoted as r and operates in FD mode. Based on [130], we consider the eavesdroppers to be located in the neighborhood of the target users, and as such, eavesdroppers overhear messages

only from the relay.

In this section, we describe both the proposed cooperative relay CR-NOMA network in FD mode and its counterpart based on HD technology.

5.2.1   Full-Duplex Operation

First, let us describe FD mode in the proposed CR-NOMA system. Because of FD transmission, the ST and the relay transmit their messages simultaneously to the intended destinations.

Then, the ST sends the superimposed signal, $m = m_1 \sqrt{p_1} + m_2 \sqrt{p_2}$, where $m_1, m_2 \in \mathbb{C}$ are independent and identically distributed (i.i.d.) information-bearing messages for M1 and M2. The power of the transmitted symbol is normalized, i.e., $\mathbb{E}\left(|m_1|^2\right) = \mathbb{E}\left(|m_2|^2\right) = 1$, and p_1 and p_2 are the corresponding transmit-power control variables. Accordingly, the received signal at relay r can be given by

$$y_r = h_r \left(\sqrt{p_1} m_1 + \sqrt{p_2} m_2 \right) + n_r, \tag{5.1}$$

where h_r is the channel coefficient between the ST and relay r while $n_r \sim \mathcal{CN}\left(0, \sigma_r^2\right)$ is additive Gaussian noise with zero mean and σ_r^2 variance.

The relay, r, first decodes message m_1 by treating message m_2 as noise, and it then executes SIC to decode m_2. Consequently, the received SINR for M1 and M2 at relay r can be described by (5.2) and (5.3), respectively, as follows:

$$\text{SINR}_{m_1}^r = \frac{|h_r|^2 p_1}{|h_r|^2 p_2 + \rho\left(p_{r,M1} + p_{r,M2}\right) + \sigma_r^2}, \tag{5.2}$$

and

$$\text{SINR}_{m_2}^r = \frac{|h_r|^2 p_2}{\zeta |h_r|^2 p_1 + \rho\left(p_{r,M1} + p_{r,M2}\right) + \sigma_r^2}, \tag{5.3}$$

where ζ is the remaining residual noise interference due to imperfect SIC. When the signal intended for weaker user M1 is decoded without error, the remaining residual noise interference is $\zeta = 0$. Otherwise, $\zeta > 0$. Moreover, $\rho\left(p_{r,M1} + p_{r,M2}\right)$ represents the residual self-interference at the relay, in

which ρ denotes the level of self-interference cancellation [148]. The power allocations assigned to M1 and M2 from the relay are denoted as $p_{r,M1}$ and $p_{r,M2}$, respectively.

Based on (5.2) and (5.3), the rates of the weak-user data and the strong-user data at the relay are formulated by (5.4) and (5.5), respectively:

$$\gamma_{r,M1} = \log_2\left(1 + \text{SINR}^r_{m_1}\right), \tag{5.4}$$

$$\gamma_{r,M2} = \log_2\left(1 + \text{SINR}^r_{m_2}\right), \tag{5.5}$$

Moreover, (5.6) and (5.7) are conditions to guarantee that relay r can successfully decode messages m_1 and m_2:

$$\log_2\left(1 + \text{SINR}^r_{m_1}\right) \geq \phi_1, \tag{5.6}$$

and

$$\log_2\left(1 + \text{SINR}^r_{m_2}\right) \geq \phi_2, \tag{5.7}$$

where ϕ_1 and ϕ_2 are the target data rates for SUs, M1 and M2, respectively.

Assuming relay r can decode both signals, the SUs, Mi, $i \in \{1, 2\}$, receive the following signal from the relay:

$$y_{r,Mi} = f_{r,Mi}\left(\sum_{j=1}^{2} \sqrt{p_{r,Mj}}m_j\right) + n_{Mi}, \ i \in \{1, 2\}, \tag{5.8}$$

where $f_{r,Mi}$ is the channel coefficient between relay r and the SU, Mi, $i \in \{1, 2\}$. $n_{Mi} \sim \mathcal{CN}\left(0, \sigma^2_{Mi}\right)$ denotes the additive Gaussian noise at M1 and M2.

According to NOMA principles, weak-user M1 decodes its own message, m_1, by treating m_2 as noise. Therefore, the SINR at M1 to decode message m_1 takes into consideration the interference caused by SU, M2 and can be described as follows:

$$\text{SINR}^r_{m_1,M1} = \frac{\left|f_{r,M1}\right|^2 p_{r,M1}}{\left|f_{r,M1}\right|^2 p_{r,M2} + \sigma^2_{M1}}. \tag{5.9}$$

Furthermore, in accordance with NOMA principles, strong-user M2 subtracts the message of weak-user M1 by applying SIC. In this chapter, we consider imperfect SIC for more realistic conditions. Therefore, the SINR for M2 to decode its message can be written as follows:

$$\text{SINR}^r_{m_2,M2} = \frac{|f_{r,M2}|^2 p_{r,M2}}{\zeta |f_{r,M2}|^2 p_{r,M1} + \sigma^2_{M2}}. \tag{5.10}$$

Accordingly, the rates of the weak-user data at M1 and M2 can be described with (5.11) and (5.12), respectively:

$$\gamma_{m_1,rM1} = \log_2\left(1 + \text{SINR}^r_{m_1,M1}\right), \tag{5.11}$$

$$\gamma_{m_1,rM2} = \log_2\left(1 + \frac{|f_{r,M2}|^2 p_{r,M1}}{|f_{r,M2}|^2 p_{r,M2} + \sigma^2_{M2}}\right). \tag{5.12}$$

The rate of the strong-user data at user M2 can be expressed as

$$\gamma_{m_2,rM2} = \log_2\left(1 + \text{SINR}^r_{m_2,M2}\right). \tag{5.13}$$

Furthermore, the maximum rate of SUs' data at the eavesdroppers can be expressed as

$$\gamma^{Mi}_{r,E} = \log_2\left(1 + \text{SINR}^{Mi}_{r,ev}\right), i \in \{1, 2\}, \tag{5.14}$$

where $\text{SINR}^{Mi}_{r,ev} = \max\limits_{v \in \{1,2,...V\}, j \neq i} \frac{p_{r,Mi}|g_{r,e_v}|^2}{p_{r,Mj}|g_{r,e_v}|^2 + \sigma^2_{e_v}}$, g_{r,e_v} is the channel coefficient between relay r and eavesdropper v, and $\sigma^2_{e_v}$ denotes the variance in the additive Gaussian noise at the eavesdropper.

The achievable data rate for the message of SU, M1 should satisfy the minimum rate at the relay and at SUs, M1 and M2 because the relay applies the DF protocol, and strong user M2 employs SIC:

$$\gamma_{m_1,\min} = \min\left(\gamma_{m_1,rM1}, \gamma_{m_1,rM2}, \gamma_{r,M1}\right). \tag{5.15}$$

Similarly, the achievable data rate of the message for SU, M2 should meet the minimum rate at the relay and at SU, M2, as follows:

$$\gamma_{m_2,\min} = \min\left(\gamma_{m_2,rM2}, \gamma_{r,M2}\right). \tag{5.16}$$

Accordingly, the secrecy rates of SU, M1 and M2 are given by their achievable rates minus their corresponding maximum rates at the eavesdroppers, which can be expressed as (5.17) and (5.18), respectively:

$$\gamma_{\text{sec},M1} = \left[\gamma_{m_1,\min} - \gamma_{r,E}^{M1}\right]^+,$$ (5.17)

and

$$\gamma_{\text{sec},M2} = \left[\gamma_{m_2,\min} - \gamma_{r,E}^{M2}\right]^+,$$ (5.18)

where $[x]^+ = \max(0, x)$.

Eavesdroppers equipped with multiple antennas   If we consider the scenario where the eavesdroppers are equipped with $N_{eve} \geq 2$ antennas. Then, the maximum SINR of the i-th message at the eavesdroppers is given by

$$\text{SINR}_{r,ev}^{Mi} = \max_{v \in \{1,2,\dots V\},} \frac{p_{r,Mi}\left|\mathbf{q}_{e_v}^H \mathbf{g}_{r,e_v}\right|^2}{\mathbf{q}_{e_v}^H\left(p_{r,Mj\neq i}\mathbf{g}_{r,e_v}\mathbf{g}_{r,e_v}^H + \sigma_{e_v}^2 I\right)\mathbf{q}_{e_v}} \forall i, i \in \{1, 2\},$$ (5.19)

where $\mathbf{q}_{e_v}$ is the receiver beamforming vector at the v-th eavesdropper and $\mathbf{g}_{r,e_v} \in C^{N_{eve}\times 1}$ is the channel vector between relay r and eavesdropper v. Based on the maximum-ratio combining method, the beamforming vector is defined by $\mathbf{q}_{e_v} = \frac{\mathbf{g}_{r,e_v}}{\|\mathbf{g}_{r,e_v}\|}$ [149]. Therefore, we can simplify (5.19) into the following expression:

$$\text{SINR}_{r,ev}^{Mi} = \max_{v \in \{1,2,\dots V\},} \frac{p_{r,Mi}\left\|\mathbf{g}_{r,e_v}\right\|^2}{p_{r,Mj\neq i}\left\|\mathbf{g}_{r,e_v}\right\|^2 + \sigma_{e_v}^2}, \forall i, i \in \{1, 2\}.$$ (5.20)

Note that the solution to the SEE maximization problem when the eavesdroppers are equipped with multi antennas follows the proposed scheme detailed in Section 5.4 by replacing the $\text{SINR}_{r,ev}^{Mi}$ in (5.14) with (5.20).

5.2.2   Half-Duplex Mode Baseline Scheme

In this subsection for comparison purposes, we describe the cooperative relay CR-NOMA system by applying HD technology. In HD mode, transmission is completed in two phases. In Phase

1, the ST conveys messages m_1 and m_2. Then, the relay, r, decodes m_1 by treating m_2 as interference, and applies imperfect SIC to decode m_2. In Phase 2, the relay transmits the superimposed signal composed of m_1 and m_2 to the SUs. In the following subsections, we explain phases 1 and 2 in more detail.

Phase 1: Direct Transmission

In this phase, the received SINR for M1 incorporates the noise caused by M2 while the SINR for M2 incorporates the remaining residual noise interference, ζ, due to imperfect SIC. Therefore, the SINR for M1 and M2 at the relay can be described with (5.21) and (5.22), respectively:

$$\text{SINR}_{m_1}^{r,HD} = \frac{|h_r|^2 p_1}{|h_r|^2 p_2 + \sigma_r^2},$$

(5.21)

$$\text{SINR}_{m_2}^{r,HD} = \frac{|h_r|^2 p_2}{\zeta |h_r|^2 p_1 + \sigma_r^2}.$$

(5.22)

Based on (5.21) and (5.22), the rates of the weak-user data and the strong-user data at the relay are formulated by (5.23) and (24), respectively:

$$\gamma_{M1}^{HD} = \tau \log_2 \left(1 + \text{SINR}_{m_1}^{r,HD} \right),$$

(5.23)

and

$$\gamma_{M2}^{HD} = \tau \log_2 \left(1 + \text{SINR}_{m_2}^{r,HD} \right),$$

(5.24)

where τ is the transmission time fraction allocated for the first phase. For a fixed time, the allocation value is equal to $\tau = 0.5$.

Phase 2: Relay Transmissionn

In Phase 2, the relay conveys the information to intended SUs, M1 and M2. Then, the rates of the weak-user data at M1 and M2 in HD mode can be described with (5.25) and (5.26),

respectively:

$$\gamma_{m_1,rM1}^{HD} = (1 - \tau) \log_2 (1 + \text{SINR}_{m_1,M1}),$$

(5.25)

$$\gamma_{m_1,rM2}^{HD} = (1 - \tau) \log_2 \left(1 + \frac{|f_{r,M2}|^2 p_{r,M1}}{|f_{r,M2}|^2 p_{r,M2} + \sigma_{M2}^2}\right).$$

(5.26)

Moreover, the rate of the strong-user data at SU, M2 can be expressed as

$$\gamma_{m_2,rM2}^{HD} = (1 - \tau) \log_2 (1 + \text{SINR}_{m_2,M2}).$$

(5.27)

The maximum rate for SUs' data at the eavesdroppers in HD mode can be expressed as

$$\gamma_E^{Mi,HD} = (1 - \tau) \log_2 \left(1 + \text{SINR}_{ev}^{Mi}\right), \; i \in \{1, 2\}.$$

(5.28)

Similar to FD mode, the achievable data rate conditions for the messages of SUs, M1 and M2 can be expressed with (5.29) and (5.30), respectively:

$$\gamma_{m_1,\min}^{HD} = \min\left(\gamma_{m_1,rM1}^{HD}, \gamma_{m_1,rM2}^{HD}, \gamma_{M1}^{HD}\right),$$

(5.29)

$$\gamma_{m_2,\min}^{HD} = \min\left(\gamma_{m_2,rM2}^{HD}, \gamma_{M2}^{HD}\right).$$

(5.30)

Accordingly, the secrecy rates of SUs, M1 and M2 can be expressed as (5.31) and (5.32), respectively:

$$\gamma_{sec,M1}^{HD} = \left[\gamma_{m_1,\min}^{HD} - \gamma_E^{M1,HD}\right]^+,$$

(5.31)

$$\gamma_{sec,M2}^{HD} = \left[\gamma_{m_2,\min}^{HD} - \gamma_E^{M2,HD}\right]^+,$$

(5.32)

where $[x]^+ = \max(0, x)$.

5.3   Problem Formulation

In this chapter, our goal is to build an AI framework that provides a low-complexity solution for maximizing SEE in FD cooperative relay CR-NOMA systems. SEE is defined as the ratio of total secrecy rate to power consumption. This maximization of SEE is formulated as bi-level optimization, which can be performed in two steps; the inner stage encompasses the solution search for the transmit power variables, and the outer stage finds the best relay index, as given below:

$$\max_{r} \left(\Upsilon(r) = \max_{p_1, p_2, \{p_{r,M1}, p_{r,M2}\}} \frac{\gamma_{\text{sec},M1} + \gamma_{\text{sec},M2}}{P_{comsup}} \right) \tag{5.33a}$$

$$\text{s.t. } C1 : \gamma_{m_1,\min} \geq \phi_1, \tag{5.33b}$$

$$C2 : \gamma_{m_2,\min} \geq \phi_2, \tag{5.33c}$$

$$C3 : p_1 + p_2 \leq P_{\text{ST}}^{\max}, \tag{5.33d}$$

$$C4 : p_{r,M1} + p_{r,M2} \leq P_r^{\max}, \tag{5.33e}$$

where $P_{comsup} = p_1 + p_2 + p_{c1} + p_{r,M1} + p_{r,M2} + p_{c2}$, and $\Upsilon(r)$ represents the inner optimization problem with respect to the lower-level variables given by the power allocation variables: p_1, p_2, and $p_{r,M1}$, $p_{r,M2}$. Meanwhile, $r \in \{1, 2, ..., R\}$ belongs to the upper-level variable of the outer optimization problem. Moreover, p_{c1} and p_{c2} are constant circuit power for transmit signal processing at the ST and relay, respectively. Constraint C1 and constraint C2 indicate the minimum data rate targeted by ϕ_1 and ϕ_2, which are required by SUs, M1 and M2, respectively. Constraint C3 indicates that the value of the power allocation variables in Phase 1, i.e., p_1 and p_2, should be lower than or equal to the allowed transmission power at the ST. Constraint C4 indicates that the value of the power allocation variables in Phase 2, i.e., $p_{r,M1}$ and $p_{r,M2}$, should be lower than or equal to the allowed transmission power at the relay.

In an underlay CR network, the interference caused by unlicensed users or SUs should stay below a certain threshold on the primary network, since both PUs and SUs, are allowed to perform

transmissions simultaneously. Therefore, transmission powers at the ST and the relay, $P_{ST}^{\max}$ and $P_r^{\max}$ are constrained as shown in (5.34) and (5.35), respectively, as follows:

$$P_{ST}^{\max} = \min \left\{ \frac{Int_{ST}^{\max}}{\max\limits_{k \in \psi_k} |h_{sk}|^2}, P_{ST} \right\}, \tag{5.34}$$

where $Int_{ST}^{\max}$ is the maximum permissible interference power at the PUs from the ST, ψ_k is the set of PUs, P_{ST} is the maximum power at the ST, and h_{sk} is the channel coefficient from the ST to the k-th PU.

$$P_r^{\max} = \min \left\{ \frac{Int_r^{\max}}{\max\limits_{k \in \psi_k} |h_{rk}|^2}, P_r \right\}, \tag{5.35}$$

where $Int_r^{\max}$ is the maximum permissible interference power at the PUs from relay r, P_r is the maximum power at relay r, and h_{rk} is the channel coefficient from relay r to the k-th PU.

5.4   Proposed Artificial Intelligence Framework For SEE Maximization

In this chapter, we design an AI framework based on integration of the EL module and the QPSO algorithm. Figure 5.2 shows the framework of the proposed method, which encompasses two main modules: EL and QPSO. Specifically, the EL module utilizes the RF and SAMME algorithms to select the best relay to achieve the highest SEE. The QPSO module solves the inner optimization problem, detailed in (5.33), for power allocation assignment.

The training dataset, $D_{tr} = \{(\mathbf{q}_i, l_i)\}$ where $i \in \{1, 2, ..., ns\}$, in which ns represents the number of samples and $\mathbf{q_i} = \left(q_i^1, ..., q_i^{dim} \right)^T$, $\mathbf{q_i} \in \mathbb{R}^{dim}$, is composed of the features of channels $|h_r|^2$, $|h_{sk}|^2$, $\left| f_{r,M1} \right|^2$, $\left| f_{r,M2} \right|^2$, $\left| g_{r,e_v} \right|^2$, the strongest channel from the relay to the PUs given by $\max\limits_{k \in \psi_k} |h_{rk}|^2$, and the rate requirement of the users. The notation dim represents the number of features, and l_i is the integer response variable that corresponds to the relay that achieves the highest SEE performance. Hence, response variable l_i is qualitative and assumes values in a finite set, $l_i \in \{1, 2, ..., R\}$, where R is the number of classes (relays). Note that the output variable is the best relay that will be used. The
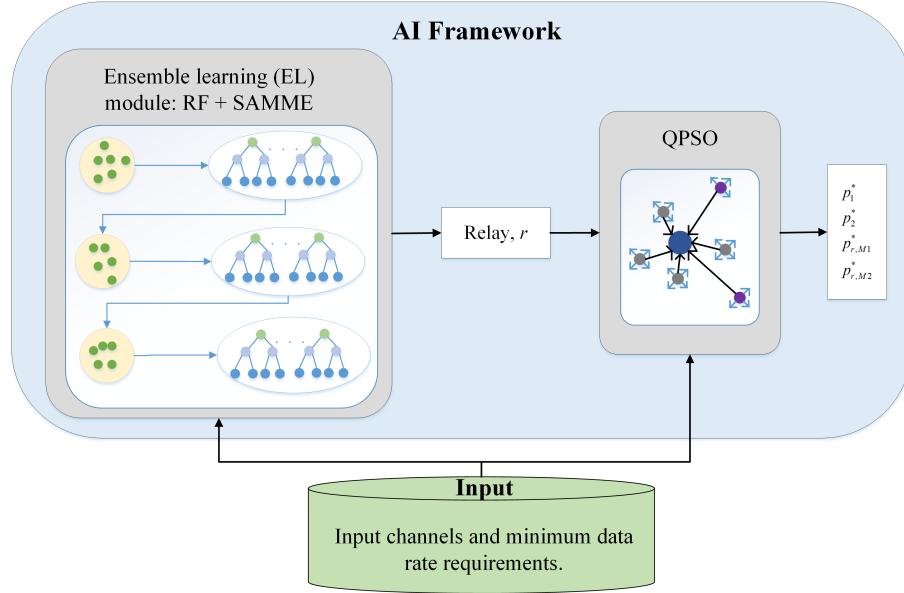
Figure 5.2: General overview of the proposed EL aided QPSO-based scheme.

total dataset contains 52,500 samples or instances. It is divided into 80% for training dataset D_{tr} and 20% for testing dataset D_{ts}. Moreover, to obtain a common scale, we normalize all the features to Z-scores.

5.4.1   EL module

In this subsection, we introduce the proposed EL module comprising RF and SAMME algorithms. Overall, EL methods are composed of multiple learning algorithms that integrate the prediction results in some manner, usually by weighted or unweighted voting, to attain a superior predictive performance than that obtained from any of the integrant single algorithms [21, 150]. For this purpose, EL utilizes different ensemble techniques; among them boosting and bagging are widely used for tree-based ensemble models.

First, RF is an ensemble of *m* decision trees that utilize the bagging technique. According to the bagging approach, the training data are divided into several independent subsets of samples, with replacement. Then, a learning model is applied to each subset, and the most voted class is

selected as the final prediction outcome in classification problems. When the output is categorical data, most voted means the class predicted by the majority in each model. In the case of regression problems, which are outside the scope of this chapter, the result is the average prediction value of all independent learning models. Therefore, in this chapter, RF starts creating each decision tree by randomly selecting samples with replacement. Then, each decision tree calculates an output, and the most voted class is selected as the final result.

Regard the SAMME algorithm [26], it is an extension of AdaBoost with multiclass capabilities. SAMME utilizes the boosting technique to sequentially combine the predictions of other individual learners, in accordance with weight assignment, to indicate the relevance of a specific instance. In this chapter, RF acts as the individual learner to develop the SAMME–aided EL module. In each iteration, SAMME trains a different RF model using all the input data. For the next iteration, the method compensates for incorrectly predicted instances by allocating a greater weight to them. Weights are recomputed after each of the iterations to focus on instances with a higher error in the predicted outcome, such that each individual incoming learner has a redefined dataset to train on, which allows the algorithm to learn from previous mistakes. The final prediction is a weighted majority vote. The proposed EL scheme composed of SAMME with RF is described in Algorithm 1, where the maximum number of iterations is denoted by MI, $lr \leq 1$ is the learning rate, and $\mathbb{I}\left(l \neq \widehat{r}\right)$ is the indicator variable which gets a value of 1 if $l \neq \widehat{r}$, and 0, otherwise.

In the testing stage, test instance $\mathbf{q}$ passes through each individual learner, $RF_{(mi)}\left(\mathbf{q}\right)$, and the prediction outcome of the AdaBoost algorithm is denoted by $AB_f\left(\mathbf{q}\right)$.

In the next subsection, we explain the operation of the QPSO module to complement the solution for optimization problem (5.33), and we build the proposed AI framework. Note that QPSO utilizes the relay obtained by the EL module as one of its inputs to optimize the power allocation assignment.

Algorithm 5.1 SAMME with the RF baseline scheme for relay selection in problem (5.33).

1: Set the inputs: training dataset $D_{tr} = \{(\mathbf{q}_i, l_i)\}$ of size ns, maximum number of iterations MI.

2: Initialize $w_i^1 = 1/ns, \forall_i \in D_{tr}$.

3: **For** $mi = 1, ..., MI$ **do**

4:     Train the mi individual learner with D_{tr} utilizing

    weight vector $\mathbf{w}^{mi}$, and get the $RF_{(mi)}(\mathbf{q})$ model.

5:     Compute the error for each training sample for

    model $RF_{(mi)}(\mathbf{q})$.

    $\in^{(mi)} = \frac{\sum_{i=1}^{ns} w_i^{mi}\mathbb{I}(l_i \neq RF_{(mi)}(\mathbf{q_i}))}{\sum_{i=1}^{ns} w_i^{mi}}.$

6:     Compute the update parameter, $\alpha^{(mi)}$:

    $\alpha^{(mi)} = lr \cdot \log\left(\frac{1-\in^{(mi)}}{\in^{(mi)}}\right) + \log(R-1).$

7:     Update the weights

    $w_i^{mi} \leftarrow w_i^{mi} \cdot \exp\left(\alpha^{(mi)}\mathbb{I}(l_i \neq RF_{(mi)}(\mathbf{q_i}))\right), \forall i.$

8: **End:** the result of SAMME $AB_f(\mathbf{q})$ can be expressed as follows:

$AB_f(\mathbf{q}) = \arg\max_{r \in R} \sum_{mi=1}^{MI} \alpha^{(mi)}\mathbb{I}(RF_{(mi)}(\mathbf{q}) = r).$

5.4.2   QPSO module

To complement the construction of the AI framework, we describe the module with the

QPSO algorithm. QPSO is an extension of PSO, inspired by quantum mechanics, in which a wave

function, $\psi(x, t)$, represents the state of a particle. QPSO came from the hypothesis that each particle

is in a quantum state, and its probability density function, $|\psi(x, t)|^2$, is utilized to determine the

probability of a particle's appearing in position x at any time t [145]. Each n-th particle's position is a

vector composed of J elements that represent the variables to be optimized. Therefore, the dimension

of the proposed optimization problem is denoted by $J = 4$. Accordingly, the vector of a particle's

position can be expressed as follows:

$$\mathbf{x}_n = \left\{ x_{n,p_1}, x_{n,p_2}, x_{n,p_{r,M1}}, x_{n,p_{r,M2}} \right\}, \tag{5.36}$$

where $n = 1, 2, ..., N_P$, N_p indicates the number of particles in the swarm, and $j \in \left\{ x_{n,p_1}, x_{n,p_2}, x_{n,p_{r,M1}}, x_{n,p_{r,M2}} \right\}$ corresponds to the particle's position in transmission power variables p_1, p_2, $p_{r,M1}$, and $p_{r,M2}$, respectively. Moreover, the limits of the search space for each power allocation variable, p_1, p_2, $p_{r,M1}$, and $p_{r,M2}$ are $\left[0, P_{ST}^{\max}\right]$, $\left[0, P_{ST}^{\max}\right]$, $[0, P_r^{\max}]$, and $[0, P_r^{\max}]$, respectively. Based on the SEE obtained with particle $\mathbf{x}_n$ by using (33a), we define $f(\mathbf{x}_n)$ as follows:

$$f(\mathbf{x}_n) = \frac{\gamma_{\text{sec},M1} + \gamma_{\text{sec},M2}}{(p_1 + p_2 + p_{c1} + p_{r,M1} + p_{r,M2} + p_{c2})} - \delta \sum_{i=1}^{4} g_i, \tag{5.37}$$

where δ is a penalty factor, and g_i depends on the i-th constraint in problem (5.33), taking a value of 1 if the i-th constraint is not satisfied, and 0, otherwise.

Then, the position of the particles is updated in accordance with the following equation:

$$x_{n,j}^{t+1} = p_{n,j}^t \pm \beta \left| mbest_{n,j}^t - x_{n,j}^t \right| \ln \left[\frac{1}{u_{n,j}^t} \right], \tag{5.38}$$

where $u_{n,j}^t$ is a random number uniformly distributed in the range $(0, 1)$; β is the contraction expansion coefficient, which is used to control the convergence behavior and provide good balance between the exploration and exploitation search mechanisms. It is set up, according to [19], as follows:

$$\beta = \frac{\sin(1 - rand)}{(1 + t)^{e^{1 - \log(t)}}} - \frac{(QI - t)}{QI}, \tag{5.39}$$

where QI denotes the maximum number of iterations, t is the current iteration index, and $rand$ is a random number uniformly distributed in the range $(0, 1)$. Moreover, $mbest_{n,j}^t$ denotes the mean of the best positions of the particles and can be expressed, according to the equation in [146], as follows:

$$mbest_{n,j}^t = \frac{\left(st_1^t P_{n,j} + st_2^t P_{g,j} \right)}{2}, \tag{5.40}$$

where st_1 and st_2 are the two random numbers generated from the Student's t distribution. $\mathbf{P}_n = \left[P_{n,p_1}, ..., P_{n,p_{r,M2}} \right]$ and $\mathbf{P}_g = \left[P_{g,p_1}, ..., P_{g,p_{r,M2}} \right]$ represent the personal best local position and global

optimal position vectors of each particle, respectively. Furthermore, each particle converges to a local attractor, defined as

$$p_{n,j}^t = \varphi_{n,j}^t P_{n,j} + \left(1 - \varphi_{n,j}^t\right) P_{g,j},$$
(5.41)

where $\varphi_{n,j}^t$ is a random number uniformly distributed in $(0, 1)$. In Algorithm 5.2, we describe the procedure for implementing QPSO along with the EL module to construct the proposed AI framework for maximizing the SEE of proposed optimization problem (5.33).

The computational complexity of the proposed AI framework depends on the complexity of the EL module and the QPSO algorithm. At first, the computational complexity of the EL depends on the size of the ensemble of SAMME denoted as n_{SAMME} and the specific base model utilized in the ensemble, which in this case is RF [151]. The computational complexity of RF is based on the number of used features m_f, the number of trees in RF denoted as m_{RF}, and the depth of the RF tree denoted as d [152]. Therefore, the computational complexity of the proposed EL algorithm is $O\left(n_{SAMME}m_f m_{RF}d\right)$. Note that for the EL module, we consider the computational complexity of the online prediction because the training process is offline. Second, the computational complexity of the QPSO algorithm depends on the number of particles N_P and the number of iterations QI. Hence, the computational complexity of the proposed QPSO-based algorithm is $O\left(N_P QI\right)$ [153]. Accordingly, the computational complexity of the proposed AI framework, which is composed of the EL and QPSO-based technique, is $O\left(n_{SAMME}m_f m_{RF}d\right) + O\left(N_P QI\right)$.

5.5   Multiple-Access Baseline Schemes

In this section, we describe the system model and problem formulation for the comparison-approaches such as FD cooperative relay OMA scheme and RSMA scheme.

Algorithm 5.2 Proposed AI framework to solve problem (5.33).

1: Set the input parameters of the system and selected relay r^* from the SAMME algorithm.

2: Input the population size, N_P and start iteration count, $t = 1$.

3: Initialize the n-th particle's position: $\mathbf{x}_n^t = \left\{ \left(x_{n,p1}^t, x_{n,p2}^t, x_{n,pr,M1}^t, x_{n,pr,M2}^t \right) \right\}, \forall n$.

4: Initialize the best local position, $\mathbf{P}_n = \mathbf{x}_n^t, \forall n$.

5: Obtain the global optimal position, $\mathbf{P}_g = \arg\max\limits_{1 \le n \le N_p} f(\mathbf{P}_n)$.

6: **While** $t \le QI$ **do**

7:   Calculate β with (5.39) and $mbest_{n,j}^t$ with (5.40).

8:   **For** each particle n **do**

9:     **For** $j = 1 : J$ **do**

10:       Compute local attractor $p_{n,j}^t$ according to (5.41).

11:       **if** rand $(0, 1) > 0.5$ **then** $x_{n,j}^{t+1} = p_{n,j}^t + \beta \left| mbest_{n,j}^t - x_{n,j}^t \right| \ln\left[\frac{1}{u_{n,j}^t} \right]$

           else $x_{n,j}^{t+1} = p_{n,j}^t - \beta \left| mbest_{n,j}^t - x_{n,j}^t \right| \ln\left[\frac{1}{u_{n,j}^t} \right]$

           end if

12:     **end for**

13:     **if** $f(\mathbf{x}_n(t+1)) > f(\mathbf{P}_n)$ **then** $\mathbf{P}_n = \mathbf{x}_n(t+1)$

         end if

14:   **end for**

15:   Update the global optimal position, $\mathbf{P}_g = \arg\max\limits_{1 \le n \le N_p} f(\mathbf{P}_n)$.

16:   Increase the counter, $t = t + 1$.

17: **end while**

18: **End QPSO:** for relay r^*, the optimal power allocation values are $\left\{ p_1^*, p_2^*, p_{r,M1,p}^*, p_{r,M2}^* \right\} = \mathbf{P}_g$

    to obtain the maximum value of SEE indicated in problem (5.33).

5.5.1   SEE Maximization in the OMA Baseline Scheme

In OMA, SUs, utilize TDMA such that a time slot is assigned for the transmission infor-
mation of each user. In the proposed network, the application of the traditional such as FD-OMA
scheme involves two phases as following.

In Phase 1, the ST conveys the signal, $m_{1\_OMA} = \sqrt{p_{1\_OMA}} m_1$, to the relay, r, where p_{1_OMA}
is the power allocated to M1 from the ST. Then, the rate for the data of user M1 can be expressed
with (5.42) and should be equal to or higher than the minimum target value, ϕ_1:

$$\gamma_{sm_1\_OMA} = \frac{1}{2}\log_2\left(1 + \frac{|h_r|^2 p_{1\_OMA}}{\rho p_{r,M1\_OMA} + \sigma_r^2}\right) \geq \phi_1, \tag{5.42}$$

where $p_{r,M1\_OMA}$ is the power intended for user M1 from the relay.

Moreover, assuming that relay r successfully decodes the message, m_{1_OMA}, the rate at
user M1 can be expressed as:

$$\gamma_{rm_1\_OMA} = \frac{1}{2}\log_2\left(1 + \frac{|f_{r,M1}|^2 p_{r,M1\_OMA}}{\sigma_{M1}^2}\right). \tag{5.43}$$

Accordingly, the achievable rate for M1 can be given by

$$\gamma_{m_1,\min\_OMA} = \min\left(\gamma_{sm_1\_OMA}, \gamma_{rm_1\_OMA}\right). \tag{5.44}$$

Furthermore, the maximum rate for the data of user M1 at the eavesdroppers can be given
by

$$\gamma_{E\_OMA}^{M1} = \frac{1}{2}\log_2\left(1 + \max_{v \in \{1,2,\dots V\}} \frac{p_{r,M1\_OMA}|g_{r,e_v}|^2}{\sigma_{e_v}^2}\right). \tag{5.45}$$

Consequently, the achievable secrecy rate for M1 can be expressed as

$$\gamma_{\text{sec},M1\_OMA} = \left[\gamma_{m_1,\min\_OMA} - \gamma_{E\_OMA}^{M1}\right]^+. \tag{5.46}$$

In Phase 2, the ST transmits the signal, $m_{2\_OMA} = \sqrt{p_{2\_OMA}} m_2$, to the relay r where p_{2_OMA}
is the power allocated to M2 from the ST. Then, the rate for the data of user M2 can be expressed by

(5.47) and should be equal to or higher than the minimum target value ϕ_2 such that we have

$$\gamma_{sm_2\_OMA} = \frac{1}{2}\log_2\left(1 + \frac{|h_r|^2 p_{2\_OMA}}{\rho p_{r,M2\_OMA} + \sigma_r^2}\right) \geq \phi_2, \tag{5.47}$$

where $p_{r,M2\_OMA}$ is the power intended for user M2 from the relay. Moreover, assuming that relay r successfully decodes message m_{2_OMA}, the rate at M2 can be expressed as

$$\gamma_{rm_2\_OMA} = \frac{1}{2}\log_2\left(1 + \frac{|f_{r,M2}|^2 p_{r,M2\_OMA}}{\sigma_{M2}^2}\right). \tag{5.48}$$

Accordingly, the achievable rate of user M2 can be expressed as

$$\gamma_{m2,\min\_OMA} = \min\left(\gamma_{sm_2\_OMA}, \gamma_{rm_2\_OMA}\right). \tag{5.49}$$

The maximum rate for the data of M2 at the eavesdroppers can be given by

$$\gamma_{E\_OMA}^{M2} = \frac{1}{2}\log_2\left(1 + \max_{v\in\{1,2,\dots V\}} \frac{p_{r,M2\_OMA}|g_{r,e_v}|^2}{\sigma_{e_v}^2}\right). \tag{5.50}$$

Consequently, the achievable secrecy rate of user M2 can be expressed by

$$\gamma_{\sec,M2\_OMA} = \left[\gamma_{m2,\min\_OMA} - \gamma_{E\_OMA}^{M2}\right]^+. \tag{5.51}$$

According to the definition of SEE (the ratio of total secrecy rate to power consumption), then the cost function for the OMA baseline scheme considers the minimum data requirement of the SUs, and the power constraints of the ST and the relay, which are as follows:

$$\max_r\left(\Upsilon(r) = \max_{\substack{p_{1\_OMA},p_{2\_OMA}, \\ \{p_{r,M1\_OMA},p_{r,M2\_OMA}\}}} \frac{\gamma_{\sec,M1\_OMA} + \gamma_{\sec,M2\_OMA}}{\frac{1}{2}(pc_{OMA})}\right) \tag{5.52a}$$

$$\text{s.t. } C1: \gamma_{m_1,\min\_OMA} \geq \phi_1, \tag{5.52b}$$

$$C2: \gamma_{m_2,\min\_OMA} \geq \phi_2, \tag{5.52c}$$

$$C3: p_{1\_OMA} \leq P_{ST}^{\max}, \tag{5.52d}$$

$$C4: p_{2\_OMA} \leq P_{ST}^{\max}, \tag{5.52e}$$

$$C5 : p_{r,M1\_OMA} \leq P_r^{\max}, \tag{5.52f}$$

$$C6 : p_{r,M2\_OMA} \leq P_r^{\max}, \tag{5.52g}$$

where $pc_{OMA} = p_{1\_OMA} + p_{c1} + p_{2\_OMA} + p_{c2} + p_{r,M1\_OMA} + p_{c1} + p_{r,M2\_OMA} + p_{c2}$.

5.5.2   SEE Maximization in the RSMA Baseline Scheme

Recent studies have promoted the application of RSMA as a powerful transmission scheme in wireless communications. Thus, in addition to the NOMA and OMA transmission strategies, we consider the RSMA-based multiple access technique as a comparative approach. RSMA spits the user messages into common and private parts at the transmitter. At the receiver, the common message is decoded by treating all the private messages as interference, and the SIC technique is employed to remove the contribution of the common message. Accordingly, let us describe FD mode operation in the CR-RSMA baseline scheme. In this chapter, we utilize the one-layer rate splitting strategy in which the SIC procedure is applied once by the receivers.

First, since the transmission from the ST is intended to one node identified as the relay device, the messages are sent from the ST by using superposition coding and the relay performs SIC to decode the messages. Therefore, the SINR for M1 and M2 at relay, r, can be described by (53) and (54), respectively, as follows:

$$\text{SINR}_{m_1\_RSMA}^{r} = \frac{|h_r|^2 p_1}{|h_r|^2 p_2 + \rho \left(p_{r,pM1} + p_{r,pM2} + p_{r,cm} \right) + \sigma_r^2} \tag{5.53}$$

$$\text{SINR}_{m_2\_RSMA}^{r} = \frac{|h_r|^2 p_2}{\zeta |h_r|^2 p_1 + \rho \left(p_{r,pM1} + p_{r,pM2} + p_{r,cm} \right) + \sigma_r^2}, \tag{5.54}$$

where the power allocation assigned to the private message M1, the private message M2, and the common message from the relay r are denoted as $p_{r,pM1}$, $p_{r,pM2}$, and $p_{r,cm}$, respectively.

Based on (5.53) and (5.54), the rates of the weak-user data and the strong-user data at the

relay are formulated by (5.55) and (5.56), respectively, as follows:

$$\gamma_{M1\_RSMA} = \log_2\left(1 + \text{SINR}^r_{m_1\_RSMA}\right), \tag{5.55}$$

$$\gamma_{M2\_RSMA} = \log_2\left(1 + \text{SINR}^r_{m_2\_RSMA}\right). \tag{5.56}$$

According to RSMA principles, the original message w_j intended to the user j, is divided into a private and a common part w_j^c, and the private parts are independently encoded into the private stream m_j, $j \in \{1, 2\}$. Therefore, the relay r transmits the signal $m = m_1 \sqrt{p_1} + m_2 \sqrt{p_2} + m_c \sqrt{p_{r,cm}}$, where $\{w_1^c, w_2^c\}$ are jointly encoded into a common stream, m_c, and $p_{r,cm}$ is the power intended for the common message. Then, the received signal at the SUs, M1 and M2 from the r-th relay can be expressed as follows:

$$y^{RSMA}_{r,Mi} = f_{r,Mi}\left(m_c \sqrt{p_{r,cm}} + \sum_{j=1}^{2} \sqrt{p_{r,pMj}}m_j\right) + n_{Mi}, i \in \{1, 2\}. \tag{5.57}$$

Accordingly, the SINR of the common stream m_c at the SUs, M1 and M2 can be formulated by (5.58) and (5.59), respectively, as follows:

$$\text{SINR}^r_{m_c,M1} = \frac{\left|f_{r,M1}\right|^2 p_{r,cm}}{\left|f_{r,M1}\right|^2 \sum\limits_{j=1}^{2} p_{r,pMj} + \sigma^2_{M1}}, \tag{5.58}$$

$$\text{SINR}^r_{m_c,M2} = \frac{\left|f_{r,M2}\right|^2 p_{r,cm}}{\left|f_{r,M2}\right|^2 \sum\limits_{j=1}^{2} p_{r,pMj} + \sigma^2_{M2}}. \tag{5.59}$$

Then, the achievable rate of the common stream at SUs, M1 and M2 can be formulated by (5.60) and (5.61), respectively, as follows:

$$\gamma^r_{m_c,M1} = \log_2\left(1 + \text{SINR}^r_{m_c,M1}\right), \tag{5.60}$$

$$\gamma^r_{m_c,M2} = \log_2\left(1 + \text{SINR}^r_{m_c,M2}\right). \tag{5.61}$$

Moreover, the SINRs to decode the private stream at the SUs, M1 and M2 are given by (5.62) and (5.63), respectively, as follows:

$$\text{SINR}^r_{p,M1} = \frac{\left|f_{r,M1}\right|^2 p_{r,pM1}}{\left|f_{r,M1}\right|^2 p_{r,pM2} + \zeta \left|f_{r,M1}\right|^2 p_{r,cm} + \sigma^2_{M1}}, \tag{5.62}$$

$$\text{SINR}^r_{p,M2} = \frac{\left|f_{r,M2}\right|^2 p_{r,pM2}}{\left|f_{r,M2}\right|^2 p_{r,pM1} + \zeta \left|f_{r,M2}\right|^2 p_{r,cm} + \sigma^2_{M2}}. \tag{5.63}$$

Consequently, the rate of the private stream at M1 and M2 can be expressed by (5.64) and (5.65), respectively, as follows:

$$\gamma^r_{p,M1} = \log_2\left(1 + \text{SINR}^r_{p,M1}\right), \tag{5.64}$$

$$\gamma^r_{p,M2} = \log_2\left(1 + \text{SINR}^r_{p,M2}\right). \tag{5.65}$$

To ensure that the common stream m_c is successfully decoded during the SIC procedure by all the SUs, the super-common rate R_{m_c} should not exceed any $\gamma^r_{m_c,M1}$, $\gamma^r_{m_c,M2}$ i.e., $R_{m_c} \le \gamma^r_{m_c,M1}$, and $R_{m_c} \le \gamma^r_{m_c,M2}$. Moreover, R_{m_c} is given by $R_{m_c} = C_1 + C_2$ where $\{C_1, C_2\}$ are the common rate variables to transmit the common parts of the messages $\{w^c_1, w^c_2\}$, respectively.

Moreover, the SINR of the SUs, M1 and M2 at the eavesdropper to decode the common message can be expressed by

$$\text{SINR}^{mc}_{r,e_v} = \max_{v \in \{1,2,...V\}, j \neq i} \frac{p_{r,mc}\left|g_{r,e_v}\right|^2}{p_{r,pMj}\left|g_{r,e_v}\right|^2 + \sigma^2_{e_v}}, i \in \{1, 2\}. \tag{5.66}$$

Consequently, the maximum rate of the common message at the eavesdroppers when the *r*-th relay is selected is given by

$$\gamma^{mc}_{r,e_v} = \log_2\left(1 + \text{SINR}^{mc}_{r,ev}\right). \tag{5.67}$$

Furthermore, the maximum rate of the private messages of the SUs at the eavesdroppers is

formulated in (68).

$$\gamma_E^{pMi} = \log_2\left(1 + \text{SINR}_{ev}^{Mi}\right), i \in \{1, 2\} \tag{5.68}$$

where $\text{SINR}_{r,ev}^{Mi} = \max\limits_{v \in \{1,2,\dots V\}, j \neq i} \frac{p_{r,pMi}|g_{r,ev}|^2}{(p_{r,pMj}+p_{r,mc})|g_{r,ev}|^2+\sigma_{ev}^2}$.

Hence, the secrecy for the common message is $R_{\text{sec}}^{mc} = \left[C_1 + C_2 - \gamma_E^{mc}\right]^+$. Meanwhile, the

secrecy rates of the private messages of SUs, M1 and M2 are given by their achievable rates minus

their corresponding maximum rates at the eavesdroppers, which can be expressed as (5.69) and

(5.70), respectively, as follows:

$$\gamma_{\text{sec},M1\_RS MA} = \left[\gamma_{p,M1}^r - \gamma_E^{pM1}\right]^+, \tag{5.69}$$

$$\gamma_{\text{sec},M2\_RS MA} = \left[\gamma_{p,M2}^r - \gamma_E^{pM2}\right]^+, \tag{5.70}$$

where $[x]^+ = \max(0, x)$.

Accordingly, the secrecy rate for the RSMA benchmark is given by (71) which considers

the secrecy for the common message plus the secrecy rates of the private messages of SUs, M1 and

M2.

$$R_{\text{sec}}^{total\_RS MA} = R_{\text{sec}}^{mc} + \sum_{i=1}^{2} \gamma_{\text{sec},Mi\_RS MA}. \tag{5.71}$$

Consequently, the SEE problem for RSMA in (5.72) can be given as a bi-level optimization

problem subject to constraints that satisfy the QoS requirements of all nodes.

$$\max_r \left(R\left(r\right) = \max_{p_1,p_2,\{p_{r,pM1},p_{r,pM2},p_{r,mc},C_1,C_2\}} \frac{R_{\text{sec}}^{total-RS MA}}{P_{consump}^{RS MA}}\right) \tag{5.72a}$$

$$\gamma_{M1\_RS MA} \geq \phi_1, \tag{5.72b}$$

$$\gamma_{M2\_RS MA} \geq \phi_2, \tag{5.72c}$$

$$C_1 + \gamma_{p,M1}^r \geq \phi_1, \tag{5.72d}$$

$$C_2 + \gamma^r_{p,M2} \geq \phi_2, \tag{5.72e}$$

$$\gamma_{M1\_RSMA} \geq C_1 + \gamma^r_{p,M1}, \tag{5.72f}$$

$$\gamma_{M2\_RSMA} \geq C_2 + \gamma^r_{p,M2}, \tag{5.72g}$$

$$C_1 + C_2 \leq \gamma^r_{m_c,M1}, \tag{5.72h}$$

$$C_1 + C_2 \leq \gamma^r_{m_c,M2}, \tag{5.72i}$$

$$p_1 + p_2 \leq P^{\max}_{ST}, \tag{5.72j}$$

$$p_{r,pM1} + p_{r,pM2} + p_{r,mc} \leq P^{\max}_r, \tag{5.72k}$$

where $P^{RSMA}_{consump} = p_1 + p_2 + p_{c1} + p_{r,pM1} + p_{r,pM2} + p_{c2} + p_{r,mc}$ and $R\left(r\right)$ represents the inner optimization problem with respect to the lower-level variables such as $p_1, p_2, p_{r,pM1}, p_{r,pM2}, p_{r,mc}, C_1, C_2$. Similarly to NOMA case, constraint (5.72b) and constraint (5.72c) indicate the minimum data rate labeled by ϕ_1 and ϕ_2, which are required by SUs, M1 and M2, respectively. Constraint (5.72d) and constraint (5.72e) indicate that the common rate variables C_1 and C_2, and the rate of the private stream at M1 and M2 should meet the minimum data rate targeted by ϕ_1 and ϕ_2, respectively. Constraint (5.72f) and constraint (5.72g) guarantee that the achievable rate of the messages from the relay to users does not overpass the corresponding achievable rates from the BS to the relay. Constraint (5.72h) and constraint (5.72i) guarantee that the sum of the common rate variables do not exceed the achievable rate of the common stream at SUs, M1 and M2, $\gamma^r_{m_c,M1}$ and $\gamma^r_{m_c,M2}$. Constraint (5.72j) indicates that the value of the power allocation variables transmitted from the ST to the relay should be lower or equal to the permitted transmission power at the ST. Constraint (5.72k) indicates that the value of the power allocation variables transmitted from the relay to the SUs, M1 and M2 should be lower or equal to the permitted transmission power at the relay.

5.6   Simulation Results

In this section, we present the simulation results programmed into MATLAB and Python to validate the proposed AI framework maximizing SEE in the FD cooperative relay CR-NOMA network. We used an Intel Core i7-6700K CPU with 16GB of main memory. Afterward, we present the performance comparison against the proposed EL module. Then,we present the performance comparison against the proposed QPSO module. Next, we present the results obtained by the AI framework in comparison with benchmark schemes. In addition, we exhibit comparison approaches that use HD mode, the conventional OMA scheme, and the RSMA technique.

In the considered network, the channels coefficients follow a circularly symmetric complex Gaussian distribution [154–156] with zero mean and variance that relies on the distance between the nodes, as follows, h_r : $C\mathcal{N}\left(0, d_{ST-r}^{-pa}\right)$, $f_{r,M1}$: $C\mathcal{N}\left(0, d_{r-M1}^{-pa}\right)$, $f_{r,M2}$: $C\mathcal{N}\left(0, d_{r-M2}^{-pa}\right)$, g_{r,e_v} : $C\mathcal{N}\left(0, d_{r-e_v}^{-pa}\right)$, h_{sk} : $C\mathcal{N}\left(0, d_{ST-PU_k}^{-pa}\right)$, and h_{rk} : $C\mathcal{N}\left(0, d_{r-PU_k}^{-pa}\right)$, where d_{i-j} denotes the distance between nodes i and j, and pa is the path-loss exponent. In addition, we set noise variance at $\sigma_{M1}^2 = \sigma_{M2}^2 = \sigma_r^2 = \sigma_{e_v}^2 = -80$dBm and $P_{ST}^{\max} = P_r^{\max} = P_{\max} = 30$dBm. Hence, the channel conditions of the nodes vary for each different channel realization.

Note that in this chapter, we use Gaussian inputs that are optimal in theory [156]. However, the outcomes obtained from the gaussian inputs to the signals with finite-alphabet inputs (FAI) can result in a meaningful performance loss because the practical implementation faces many challenges, for instance, large storage capacity, high computational complexity, and extremely long decoding delay [157]. In this sense, in [158,159], precoding schemes were designed with finite-alphabet signals in MIMO systems to reduce the complexity of the precoder optimization. Although in practical communication systems, FAI attain better practical implementations. In this chapter, the analysis of the capacity for different types of modulations is not feasible due to the lack of closed-form expression for the data rate in the proposed system model. Therefore, we aim to optimize the

resource allocation by considering the theoretical bound of the Shannon capacity, which represents the maximum capacity at zero error rate for an infinitely complex digital modulation/demodulation transmission system [160]. Another option would be to consider the resource allocation in NOMA systems with FAI, e.g., by employing quadrature amplitude modulation (QAM) and phase shift keying (PSK), but this falls outside of the scope of the current chapter and is left for our future investigation.

The values of the network parameters considered in these simulations are listed in Table 5.1. The relays were randomly distributed within transmission range of the ST, the PUs were randomly distributed within transmission range of the ST and the chosen relay, and the eavesdroppers were randomly distributed within transmission range of the relay.

The eavesdroppers were also randomly distributed between the relays and SUs, M1 and M2. The results were averaged over 1750 channel realizations.

For the considered system setup, the dataset was 52,500 samples, with 80% intended for training, to learn the prediction model, and 20% for testing, to measure performance. Note that the testing samples have independent channel realizations, that are different from the ones considered in the training samples. Moreover, we train only one time the EL module to simulate the different scenarios, varying the rate requirements.

5.6.1   Performance comparison against the proposed EL module

In this chapter, we assessed the performance of the relay selection scheme with three error metrics: accuracy, precision, and recall. Accuracy is the ratio of correctly predicted samples to total samples evaluated with the testing data. To understand the definition of precision and recall, let us briefly describe the confusion matrix.

Table 5.2 shows the confusion matrix, which is in a table layout to visualize the performance of a classifier, where each row of the matrix indicates the true class, while each column indicates

Table 5.1: Simulation Parameters of the Network.

Parameter	**Value**	**Parameter**	**Value**
Network area	100m × 60m	ST coordinates	(0,50)
Number of relays, R	4	M1 coordinates	(100,50)
Number of eavesdroppers, V	4	M2 coordinates	(70,42)
Number of PUs, K	3	Relay 1 coordinates	(50,54)
Path-loss exponent, pa [134]	3	Relay 2 coordinates	(50,50)
Maximum power at the ST, P_{ST}	30 dBm	Relay 3 coordinates	(50,46)
Maximum permissible interference power at the PUs from the ST, Int_{ST}^{max} [161]	-10 dBm	Relay 4 coordinates	(50,42)
Maximum permissible interference power at the PUs from the relay, Int_{r}^{max}	-10 dBm	PU1 coordinates	(75,59)
Level of self-interference, ρ [148]	10^{-12}	PU2 coordinates	(25,59)
The remaining residual noise interference due to imperfect SIC, ζ [134]	0.05	PU3 coordinates	(50,37)
Constant circuit power, p_{c1}, p_{c2} [44]	5 dBm		

the predicted class. The true class is obtained by the ES method. ES exhaustively selects each possible relay and chooses the one with the best SEE as the true class. It is worth highlighting that the computational time required by the ES method is significantly higher than that required by the proposed EL module.

Accordingly, the precision and recall scores were assessed in each class, based on the confusion matrix, as follows:

$$\text{Precision}_i = \frac{C_{ii}}{\sum_{j=1}^{4} C_{ji}}, \tag{5.73}$$

Table 5.2: Confusion Matrix.

		Predicted class			
		Relay 1	Relay 2	Relay 3	Relay 4
	Relay 1	C_{11}	C_{12}	C_{13}	C_{14}
True	Relay 2	C_{21}	C_{22}	C_{23}	C_{24}
class	Relay 3	C_{31}	C_{32}	C_{33}	C_{34}
	Relay 4	C_{41}	C_{42}	C_{43}	C_{44}

Table 5.3: Normalized confusion matrix for the proposed scheme.

		Predicted class			
		Relay 1	Relay 2	Relay 3	Relay 4
	Relay 1	0.9221	0.0201	0.0352	0.0226
True	Relay 2	0.0270	0.9303	0.0202	0.0225
class	Relay 3	0.0127	0.0233	0.9089	0.0551
	Relay 4	0.0437	0.0230	0.0391	0.8943

and

$$\text{Recall}_i = \frac{C_{ii}}{\sum_{j=1}^{4} C_{ij}}, \tag{5.74}$$

where i refers to each class, with $i = 1$ for Relay 1, $i = 2$ for Relay 2, $i = 3$ for Relay 3, and $i = 4$ for

Relay 4. Table 5.3 shows the normalized confusion matrix for the proposed scheme.

To simplify the comparison results, Table 5.4 shows the average precision and recall for

the proposed EL scheme and the comparison methods such as AdaBoost, RF, extremely randomized

trees (ERT) [162], and multi-layer perceptron (MLP). From Table 5.4, we can see that the proposed

EL scheme attained the highest accuracy, precision, and recall among the comparison methods. In

the chapter, the hyperparameters of max depth, the number of estimators, and the learning rate of the

Table 5.4: Error Metrics of the ML schemes.

Algorithm	**Accuracy (%)**	**Precision (%)**	**Recall (%)**
RF+SAMME (Proposed EL technique)	91.371	91.349	91.390
AdaBoost	85.657	85.862	85.584
RF	88.467	88.468	88.407
ERT	86.114	86.227	85.964
MLP	85.867	85.869	85.835
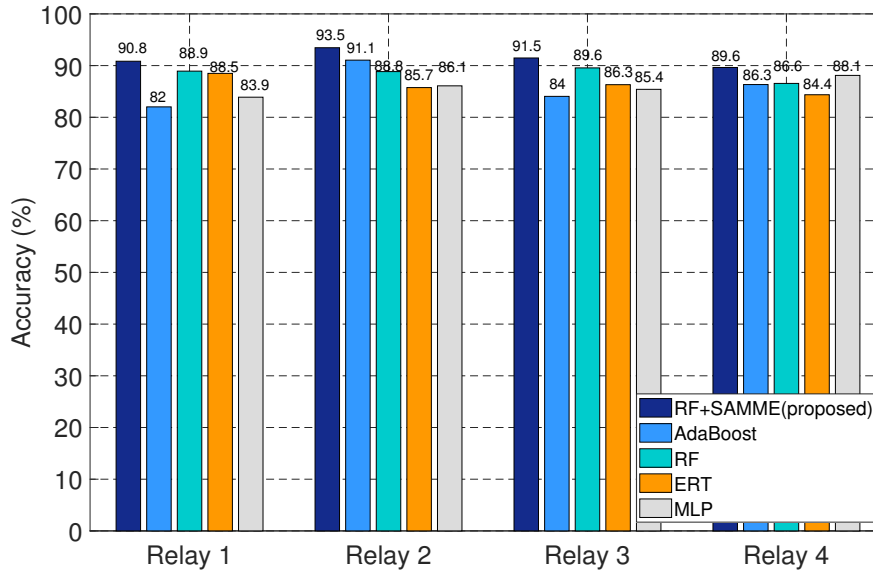
Figure 5.3: Average accuracy in each class.

proposed EL scheme were set to 2, 150, and 0.1, respectively.

Furthermore, Figure 5.3 shows the average accuracy per class for the proposed EL scheme and the baseline schemes. We can see that the proposed scheme outperformed the other algorithms in all classes: Relay 1, Relay 2, Relay 3, and Relay 4. Therefore, we utilized the EL scheme in the construction of the AI framework as an essential module for the relay selection task.

5.6.2 Performance comparison against the proposed QPSO module

In this subsection, we analyze the performances of the proposed QPSO-based technique and more swarming algorithms in terms of SEE, converge behavior, and computational complexity. Moreover, we compare the performance of the proposed QPSO-based scheme with the optimal values obtained by the ES method. To validate the outcomes obtained by the swarm intelligence algorithms, we consider that the relay selection task is performed exhaustively. That is, each algorithm must be executed based on the number of available relays in the network to select the best one that achieves the highest SEE. Thus, in addition to the proposed QPSO-based scheme, we evaluate the performance of the following swarm intelligence-based baseline algorithms: standard PSO algorithm, CS, the ALO algorithm, and the BOA. These benchmark schemes are explained in detail in [120].

The simulation parameters in Table 5.5 for each swarm intelligence algorithm are set according to the best result obtained through several experiments.

Figure 5.4 shows the convergence of the proposed QPSO and the baseline swarm intelligence algorithms to maximize the SEE when the minimum rate of user 1 is equal to $\phi_1 = 1.5$ bits/s/Hz and the minimum rate of user 2 is equal to $\phi_2 = 1.2$ bits/s/Hz. From Figure 5.4, we can observe that as the iteration index increases, the SEE is improved. Moreover, Figure 5.4 shows that the QPSO algorithm achieves convergence in fewer iterations than its counterparts. Therefore, we set the number of iterations equal to $QI = 250$ when the number of particles is equal to $N_p = 45$. By contrast, ALO requires more iterations to obtain the maximum SEE which entails high computational time. After QPSO, PSO achieves the second-best convergence behavior within about 650 iterations when the number of particles is equal to $N_p^{PSO} = 45$. The CS and BOA follow the PSO with 850 and 1000 iterations, respectively.

Figure 5.5 shows the SEE performance of the proposed QPSO algorithms and the following swarm intelligence baseline schemes: PSO, CS, BOA, and ALO when the minimum rate of user 1 is equal to $\phi_1 = 1.5$ bits/s/Hz and the minimum rate of user 2 is equal to $\phi_2 = 1.2$ bits/s/Hz.

Table 5.5: Simulation parameters of swarm intelligence-based algorithms.

| Algorithm	Simulation parameters
Proposed QPSO	Number of iterations $QI = 250$, Number of particles $N_p = 45$
PSO	Number of iterations $It^{PSO} = 650$, Number of particles $N_p^{PSO} = 45$ Minimum inertia weight $Ine_{\min} = 0.4$, Maximum inertia weight $Ine_{\max} = 0.9$ Cognitive component $c_1 = 1.494$, Social component, $c_2 = 1.494$
CS	Number of iterations $It^{CS} = 850$, Number of nests $N^{CS} = 45$ Minimum step size factor $\beta_{\min} = 0.01$, Maximum step size factor $\beta_{\max} = 0.5$
ALO	Number of iterations $It^{ALO} = 1000$, Number of ants $N^{ALO} = 50$
BOA	Number of generations $G^{BOA} = 950$, Number of agents $S^{BOA} = 55$ Sensory modality $sm = 0.01$, Power exponent $pe = 0.01$ Switch probability $sp = 0.5$
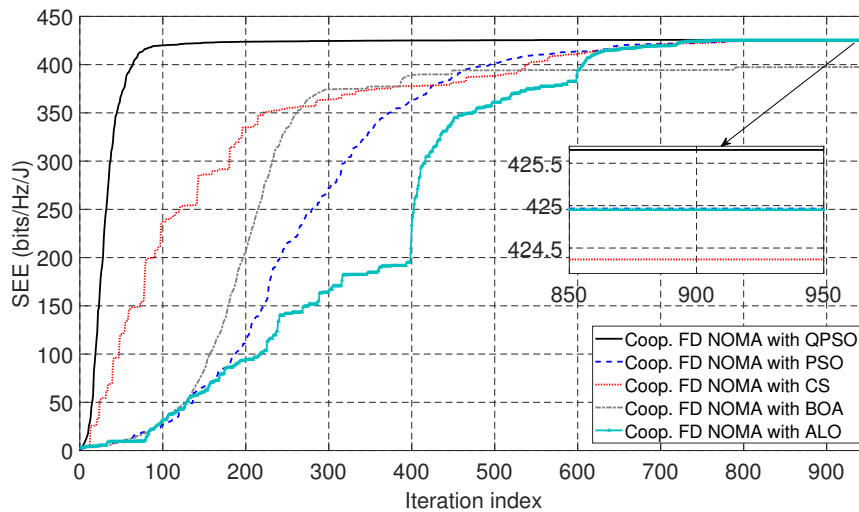
Figure 5.4: Convergence of the proposed QPSO scheme and the swarm intelligence baseline schemes.
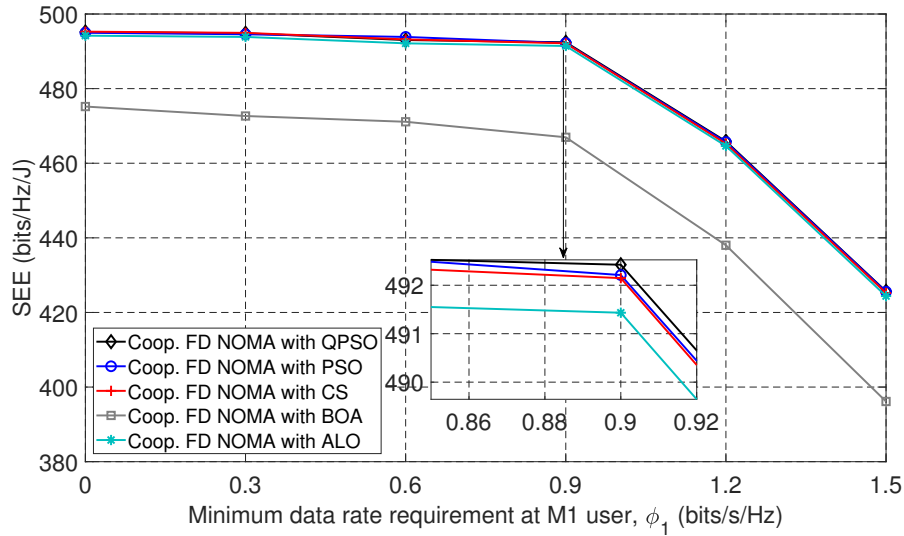
Figure 5.5: SEE performance of the proposed QPSO scheme and the swarm intelligence baseline schemes.

From Figure 5.5, it can be observed that the proposed QPSO outperforms the benchmark schemes. Although the outcome of PSO is very near to that of QPSO as shown in Figure 5.5, PSO requires more iterations and more particles as shown in Figure 5.4 and Table 5.5. Furthermore, it is worth highlighting that the computational complexity of the swarm intelligence-based schemes relies on the number of iterations and the number of particles. Particularly, the computational complexities of QPSO and PSO, which achieve the best outcomes in terms of SEE and convergence behavior, are computed by $O\left(QI \cdot N_p\right)$ and $O\left(It^{PSO} \cdot N_p^{PSO}\right)$, respectively. Accordingly, QPSO achieves the least computational complexity with the highest performance since it requires fewer iterations and a lower number of particles.

To further validate the superiority of the proposed QPSO algorithm over PSO technique in the proposed optimization problem (5.33), Figure 5.6 presents the convergence behavior of the QPSO algorithm and the baseline PSO scheme when the maximum available powers at the ST and the relay are all 30 dBm, and when the minimum rate requirements of user M2, ϕ_2, and user M1,
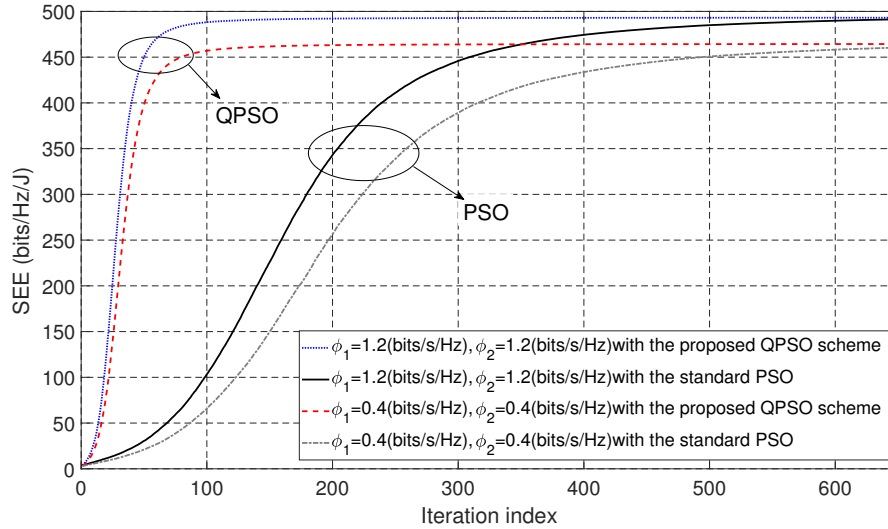
Figure 5.6: Convergence behavior of the proposed QPSO-based algorithm and PSO baseline scheme.

ϕ_1, are 1.2 and 0.4. The results were averaged over 1750 channel realizations. We can see that the

proposed QPSO algorithm converges faster than the standard PSO method. QPSO achieved a stable

condition after 200 iterations, whereas PSO reached convergence within about 600 iterations. Then,

the maximum iteration value and number of particles for QPSO were set to $QI = 250$ and $N_P = 45$,

respectively, for the rest of the simulations. Moreover, it is observed that increases in the minimum

data rate resulted in decreasing the SEE. This is because, as the minimum data rate increases, more

power needs to be allocated from the ST and the relay to satisfy the requirements; Subsequently,

the multiple eavesdroppers can detect these messages with more power, and leverage them to trap

information, which results in the reduction of SEE.

5.6.3   Performance comparison against the proposed AI model

Figure 5.7 shows total SEE versus the minimum required rate of user M1, ϕ_1, when the

minimum data rate requirement of M2 is $\phi_2 = 0.8$ bits/s/Hz. In Figure 5.7, it is observed that the

proposed EL aided QPSO-based framework achieves performance close to the optimal ES method.

Table 5.6: Computational time and absolute error of the proposed and baseline schemes.

Scheme	CPU time (s)	Absolute error
EL-QPSO (Proposed scheme)	1.0041	0.0023678
QPSO-ES	2.1487	0.0005587
Standard PSO-ES	3.7288	0.0008678

The main drawback of ES is the high computational complexity and computational time, since it systematically searches all possible options to find the best values for the optimal solution. Therefore, the computational complexity of ES increases when more receivers are aggregated to the network. Under QPSO-ES, the main issue is that QPSO must be executed based on the number of available relays in the network, and then, the QPSO algorithm selects the relay that achieves the highest SEE. Thus, the benefit of the proposed AI framework is the reduction of computational complexity since it avoids executing QPSO for each available relay in the network. Instead, the proposed AI framework utilizes the EL technique to directly predict the best relay, which is used as an input parameter in the QPSO framework to maximize SEE. Table 5.6 shows the computational time and absolute error of the proposed EL aided QPSO-based scheme, QPSO-ES, and the standard PSO-ES baseline scheme. The absolute error was evaluated by taking into account the SEE obtained by the ES method.From Table 5.6, we can see that the proposed scheme achieved the lowest CPU running time. The absolute error of the proposed scheme was slightly greater than those of the baseline schemes. In particular, the standard PSO-ES slightly gets a higher absolute error than the QPSO-ES, and the corresponding CPU running time is around four times that of the investigated QPSO-EL scheme. Similarly, the accuracy obtained by QPSO-ES requires two times more computational time than the developed QPSO-EL scheme.

Moreover, from Figure 5.7, we can see that adopting the EL module in the proposed AI framework achieved superior performance in terms of SEE than the random relay–selection
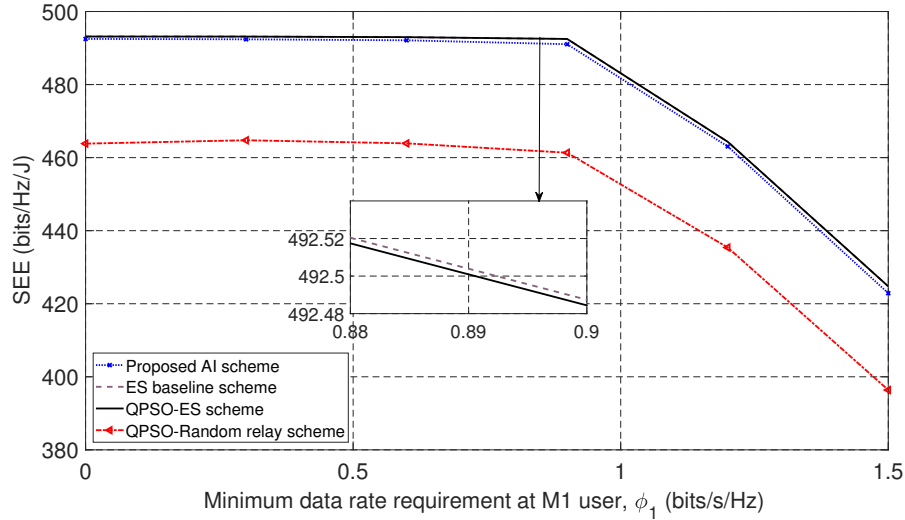
Figure 5.7: Total SEE versus the minimum rate requirement.

technique, even though this comparison approach also utilizes QPSO for SEE maximization. This is because the random relay selection baseline scheme selects any available relay in the network, which is not necessarily the best one that allows achieving the highest SEE.

In addition, in Appendix A, we provide a mathematical solution based on the SCA method aided by PSO to solve the proposed optimization problem (5.33). Accordingly, Figure 5.8 shows the SEE performance of the proposed QPSO-EL scheme and the SCA-PSO baseline scheme according to the minimum data rate at user M1, ϕ_1, when the rate requirement for user M2 is equal to $\phi_2 = 1.2$ bits/s/Hz. In the simulation, the number of particles for the comparative SCA-PSO scheme is equal to $N_{PSO} = 10$, the number of iterations of the PSO algorithm is equal to $I_{PSO} = 30$, and the number of iterations of the SCA-based scheme is equal to $N_{\max} = 20$. From Figure 5.8, we observe that the proposed QPSO-EL achieves a higher SEE compared with the baseline scheme SCA-PSO. The reason is that the SCA-based scheme is composed of different convex approximation methods and depends on initial feasible points. Since the initial feasible points are not guaranteed to be optimal, the SCA-based method may converge to sub-optimal solutions. Note that in the SCA-PSO algorithm, the problem (A.11) should be solved a total time of $N_{PSO} \times I_{PSO} \times N_{\max}$, which is equal to 7161 s.
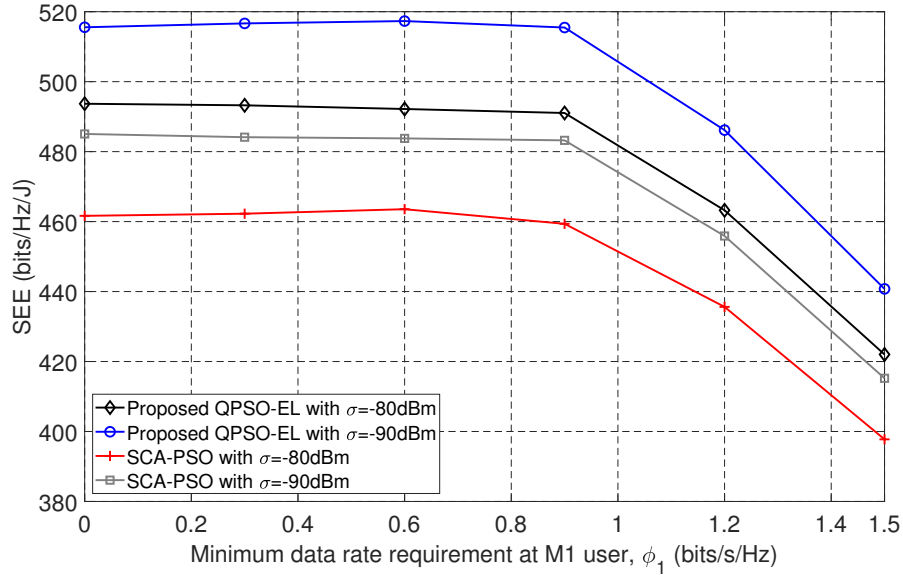
Figure 5.8: SEE performance comparison between the proposed QPSO-EL scheme with the baseline SCA-PSO scheme.

Thus, SCA-PSO method leads to a significant higher computational time and lower performance compared with the proposed QPSO-EL.

Figure 5.9 shows the SEE performance versus the minimum data rate requirement, ϕ_1, of our proposed cooperative FD CR-NOMA system and the HD CR-NOMA baseline approach when the minimum rate requirement of user M2 is $\phi_2 = 0.8$ bits/s/Hz. We developed two scenarios for the HD-NOMA scheme. The first considers optimizing time, and the other uses fixed time. Then, from Figure 5.9, we can see that the performance of FD-NOMA, in terms of SEE, is superior to its counterpart, HD-NOMA. This is because FD mode can receive and transmit data simultaneously, which greatly increases spectrum utilization. On the other hand, HD mode utilizes the same medium to receive and transmit data, but at different times. Furthermore, from Figure 5.9 we can see that the proposed FD CR-NOMA network reaches a higher SEE when the selection of the relay is optimized, compared to the case that the relay is selected randomly.

Figure 5.10 shows SEE performance versus the minimum data rate requirements for ϕ_1 and

Figure 5.9: SEE performance comparison between the FD cooperative relaying CR-NOMA network and the HD cooperative relaying CR-NOMA network.

ϕ_2 in our proposed scheme using FD-NOMA and the conventional FD-OMA scheme in accordance with two different values of noise: $\sigma = -80$ dBm and $\sigma = -90$ dBm. From Figure 5.10, we can see that the performance from the NOMA transmission strategy overcomes the OMA benchmark. This is because NOMA users can share the same frequency at the same time, which improves utilization of resources, and thus, in the proposed cooperative FD-NOMA scheme, a complete transmission requires only one phase. Meanwhile, the comparison FD-OMA scheme needs to allocate its resources to a different frequency or time. In this chapter, we utilize the TDMA technique. Therefore, two phases are required to complete the transmission under OMA, which degrades the performance of the network in terms of SEE. Furthermore, we can see that SEE performance diminishes as noise power increases. This is because the power of noise is inversely proportional to the SINR of M1 and M2. Subsequently, the secrecy rate is reduced at higher power for noise.

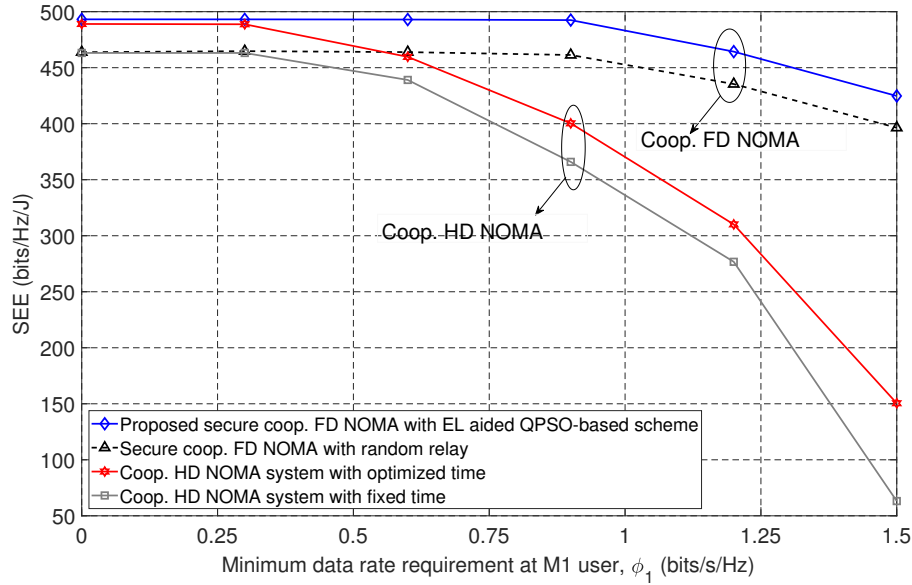Figure 5.11 shows the convergence behavior of the proposed secure cooperative FD NOMA
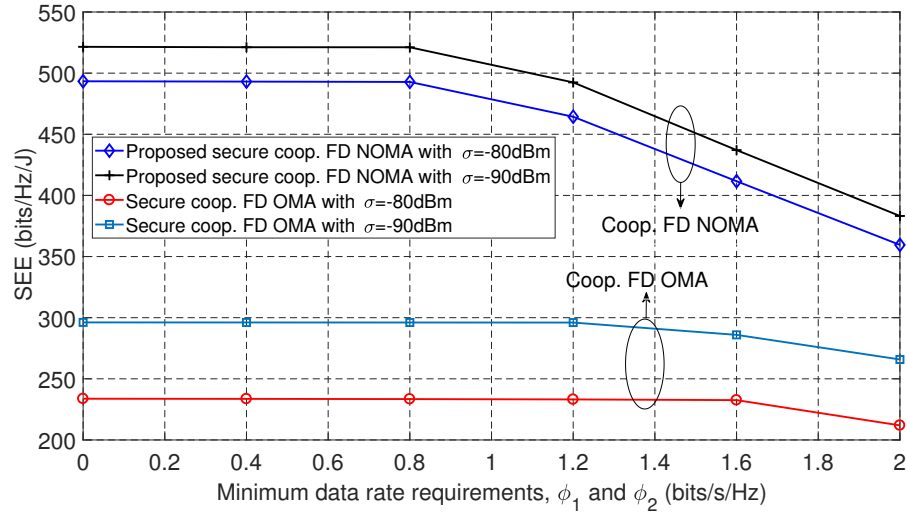
Figure 5.10: SEE performance comparison between the FD cooperative relay CR-NOMA network and the FD cooperative relay CR-OMA network.

scheme and the RSMA method with a different number of antennas at the eavesdroppers when the number of particles of the QPSO algorithm used for the NOMA scheme is set to 45 and the number of particles of the PSO algorithm used for the RSMA algorithm is set to 100. From Figure 5.11, we observe that the proposed secure cooperative FD NOMA method converges within 200 iterations while the RSMA method requires more than 1500 iterations. The significant increase in the number of iterations required by the RSMA method is due to the greater number of variables and constraints compared with the NOMA method which is necessary to satisfy the QoS requirements of the system. In particular, in RSMA, three extra variables $\{p_{r,mc}, C_1, C_2\}$ and four extra constraints are added per relay compared with the NOMA method, which significantly increases the computational complexity required to solve the problem. Furthermore, from Figure 5.11, it can be observed that the NOMA method achieves a higher SEE compared with the RSMA scheme, which is in concordance with the results obtained in [132]. According to [132], in a SISO BC system, there is not necessary to implement the RSMA scheme because the NOMA method can achieve the capacity region. Then, in SISO BC, the benefits of RSMA are only focused on reducing the number of SIC required at
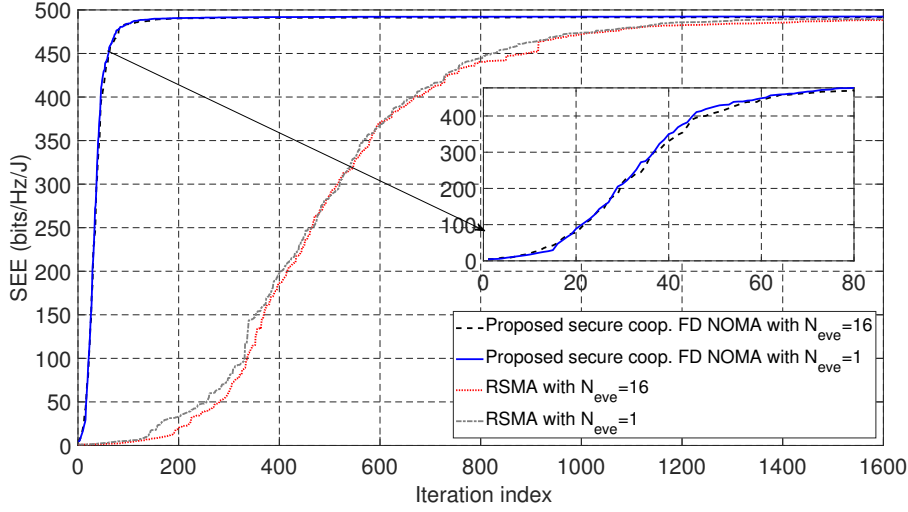
Figure 5.11: Convergence behavior between the proposed secure coop. FD NOMA and the secure coop. FD RSMA baseline scheme.

the receiver. However, our system is composed of two users, where only one SIC is required at the receiving. Therefore, there is no advantage to using the RSMA method in our proposed system model.

For the scenario of multiple antennas at eavesdroppers described in Subsection 5.2.1, the channel from the relay to the eavesdroppers is modeled based on the Rician fading [54] as follows: $\mathbf{g}_{r,e_v} = \sqrt{\frac{K_R}{1+K_R}}\mathbf{g}_{r,e_v}^{LOS} + \sqrt{\frac{1}{1+K_R}}\mathbf{g}_{r,e_v}^{NLOS}$, where K_R is the Rician factor equal to 3, $\mathbf{g}_{r,e_v}^{LOS}$ represents the line-of-sight (LOS) component with $\left\|\mathbf{g}_{r,e_v}^{LOS}\right\|^2 = d_{r-e_v}^{-pa}$, and $\mathbf{g}_{r,e_v}^{NLOS}$ denotes the Rayleigh fading component defined by $\mathbf{g}_{r,e_v}^{NLOS} \sim \mathcal{CN}\left(0, d_{r-e_v}^{-pa}\mathbf{I}\right)$. Moreover, the model in [69] is applied to model the LOS component. Accordingly, from Figure 5.11 and Figure 5.12, we can observe that as the number of antennas in the eavesdropper increases, the SEE decreases. The reason is that the received signals from the antennas are added together while increasing the SINR at the eavesdroppers, which decreases the SEE of the system. Particularly, Figure 5.12 shows the SEE performance comparison for the scenario of multi-antenna eavesdroppers when the rate requirement for M2 user is equal to $\phi_2 = 2$ bits/s/Hz. Similar to Figure 5.11, we observe that the proposed NOMA-based scheme
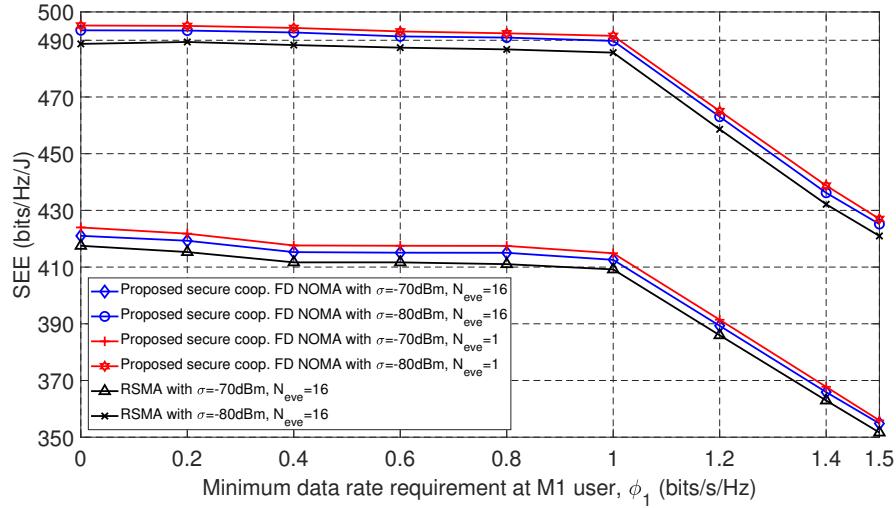
Figure 5.12: SEE performance between the proposed QPSO-EL scheme and the benchmark RSMA-based scheme with multi-antenna eavesdroppers.

achieves a higher SEE compared with the RSMA-based scheme. Moreover, a greater SEE is achieved with a lower number of antennas at the eavesdroppers.

5.7 Closing Remarks

In this article, we proposed a new method based on AI to maximize the SEE of a cooperative relay FD CR-NOMA in the presence of multiple eavesdroppers. In particular, we designed an AI framework for the considered system setup, where the EL was developed for the relay selection problem, and QPSO was investigated for power allocation assignment. Simulation results showed that the proposed EL scheme overcame the state-of-the-art ML techniques in all error metrics (accuracy, precision, and recall). Moreover, the QPSO algorithm improved the convergence behavior more than the swarm intelligence baseline schemes without affecting performance. Satisfactorily, the proposed AI design achieved a performance very close to the optimal ES method with low computational complexity. In addition, the proposed FD CR-NOMA network outperformed its counterpart HD,

OMA, and RSMA baseline schemes. As potential future work, an interesting study can be conducted by integrating simultaneous wireless information and transfer technology in the relays, as well as NOMA users, to enhance the network lifetime and provide sustainability.

Chapter 6

Summary of contributions and further works

6.1 Introduction

In this chapter, the primary focus is to highlight the dissertation's key findings and outline potential avenues for future research. The previous chapters (Chapters 2 to 5) presented the dissertation's motivation, research techniques, and results. The first Subsection 6.2 summarizes the primary contributions of these studies, while the second Subsection (6.3) explores effective and significant areas for future investigation.

6.2 Summary of Contributions

This dissertation investigated and proposed close-optimal solution methods focusing on resource allocation in NOMA with underlying CR and SWIP technologies by considering different EH users and security. The main contributions of this dissertation, in the context of resource optimization for cooperative NOMA-based 5G systems with consideration of CR and security is

appended below:

- Firstly, we investigated the SCE maximization problem in a wireless-powered NOMA-enabled MEC network assisted by a PB under the partial offloading mode, where a practical nonlinear EH and power amplifier coefficient are considered in the design of the system. The problem was formulated and solved by a low-complexity PSO-based solution, which maximizes SCE by satisfying the QoS requirements of NOMA users and meeting the minimum energy harvested by non-linear EH users. Specifically, we jointly optimized the local computing frequency, the computation time for local computing, and the power allocation variables involved in the network. Moreover, we determined the limits of the search range of each variable to be optimized through mathematical procedures to properly find the global best particle's position. Numerical showed that the SCE obtained under our proposed wireless-power NOMA-enabled MEC scheme is superior to that of other baseline schemes. Moreover, the numerical results showed that a system with a PB improves SCE performance.

- Secondly, we considered the secure transmission for a MISO-NOMA-CR network applying SWIPT and assisted by AN to enhance the security of the secondary network. The goal of this work was to optimize the precoder vectors and PS ratios to minimize the transmit power to the SUs and EH users, subject to the constraints of minimum SINR at the SUs, minimum EH for EH users, maximum available power at the ST, and maximum permissible interference with the PUs. The key point of the proposed scheme is that by minimizing the transmit power for SUs and EH users, we can assign the residual power to AN to generate interference against the eavesdropper, by which the security can be improved in the underlying network. The proposed solution consists of two steps. First, an SDR-based algorithm converted the formulated problem into a SDP problem. Second, a Gaussian randomization technique was applied to obtain the approximate rank-one solutions for beamforming vectors, and a linear program problem is

used to guarantee the feasibility of the candidate solutions of the Gaussian randomization technique. Numerical simulations proved the superiority of the proposed approach based on NOMA with AN for increasing the security of the secondary network, in comparison with NOMA without AN, SDMA, and ZF schemes. In particular, the proposed AN method showed a significant improvement in SSR over the no-AN scheme under several studied scenarios.

- Thirdly, we studied the optimization of total transmission power and energy efficiency problems in a cooperative, non-linear, SWIPT-enabled NOMA system using a practical non-linear EH user. The optimization problems considered are non-convex involving joint optimization of the time transmission fraction, power-splitting ratio, and power allocation, and are thus difficult to solve directly. To tackle this issue, we proposed a low-computational-complexity scheme based on PSO. Moreover, we compared the performance of five swarm intelligence-based baseline schemes and developed an alternative solution based on CS. In addition to the metaheuristics baseline schemes, to confirm the effectiveness of the proposed PSO scheme, we provided an analytical approach based on convex optimization with the ES denoted as CVX+ES. Moreover, we analyzed the effect from linearity of EH on the transmit power and energy efficiency of the proposed system (SWIPT NOMA cooperative communication optimizing the power variables, the time factor, and the power-splitting ratio) and the following baseline schemes: SWIPT NOMA cooperative communication with a TF scheme, and SWIPT NOMA cooperative communication with EPS. Simulation results demonstrated that the proposed cooperative non-linear SWIPT-NOMA system reduces transmission power and can obtain higher energy efficiency than the benchmark schemes. Furthermore, numerical results showed that PSO can reach a near-optimal performance, compared to those obtained by the optimal (but time- and energy-consuming) CVX+ES method. In addition, we validated that the proposed PSO achieves a convergence faster than the CS-based framework and with less computational time.

- Finally, we raised a solution based on AI techniques that integrated EL and QPSO modules for solving the optimization problem to maximize SEE in the proposed FD cooperative relay CR-NOMA system with imperfect SIC to prevent multiple-eavesdropper wiretapping. First, we started with the construction of the EL module, which is composed of the potent RF and SAMME algorithms. This module is in charge of solving the relay selection issue because RF and SAMME were shown to be efficient and robust ML classifier algorithms in complex network environments. Second, we investigated swarm intelligence methods to design a power allocation scheme based on QPSO. The efficient and low-complexity QPSO module is used to complement the proposed AI framework. Accordingly, we assembled the EL and QPSO modules to build the AI framework. Therefore, we designed the EL module for smart relay selection. Then, we use the best relay as one of the input parameters for the QPSO algorithm to efficiently solve the formulated optimization problem. Simulation results showed that the proposed AI-based solution can reach near-optimal performance with much lower complexity, compared with an ES-based scheme. Moreover, convergence behavior is significantly improved by the proposed QPSO, which results in computational complexity reduction. Furthermore, we include results on the performance of the standard PSO, cuckoo search (CS), the ant lion optimization (ALO) method, and the butterfly optimization algorithm (BOA) baseline algorithms in terms of SEE, converge behavior, and computational complexity. To further prove the effectiveness of the proposed AI framework, we provided a mathematical solution based on the SCA method aided by PSO. In addition, for comparison purposes in terms of wireless network design, we described the conventional OMA, RSMA, and HD mode in the considered cooperative relay CR network affected by various eavesdroppers. Satisfactorily, the proposed FD CR system with the aid of the NOMA transmission strategy improved the security of the network and outperforms comparison approaches in terms of SEE. Moreover, we analyzed the scenario of multiple antennas at eavesdroppers. In addition, simulation results

showed that the proposed AI design achieved a performance very close to the optimal ES method with low computational complexity.

6.3   Future Direction

The primary focus of this dissertation is to enhance the resource optimization of collaborative NOMA systems by optimizing the total transmission power and secrecy energy efficiency while satisfying the minimum QoS requirements. To achieve this objective, we proposed resource allocation-based optimization techniques as discussed in Chapters 2 to 5. The research carried out in this dissertation suggests several interesting further directions that need to be explored in the future. This study ends by outlining future research directions as follows:

- To fully utilize the benefits of NOMA technique, NOMA can be extended to support massive IoT applications, which require low power consumption, high reliability, and high connectivity. NOMA-based solutions can enable massive IoT devices to share the same resources efficiently and increase the network capacity and coverage. However, several challenges need to be addressed, such as user mobility, interference management, and synchronization. It is worth highlight that massive IoT devices entails the integration of more nodes in the network which increases the difficulty to solve the resource optimization problem. Therefore, innovative schemes that provide a close-optimal solutions with low computational complexity are essential challenges to be investigated.

- Recently, hybrid beamforming has been proposed as an effective approach to improve the security of cooperative NOMA systems. Moreover, by using hybrid beamforming in NOMA systems, the number of RF chains required can be significantly reduced compared to fully digital beamforming. This can lead to cost savings in hardware and power consumption while still achieving the benefits of beamforming. Therefore, the design of secure beamforming

algorithms for hybrid beamforming architectures in cooperative NOMA systems is a promising research direction.

- AI techniques has shown great potential in addressing complex problems in wireless communication systems. In the context of cooperative NOMA, ML-based approaches can be combined with metaheuristic algorithms to optimize resource allocation, interference management, and relay selection. In particular, reinforcement learning algorithms, deep learning methods and nature-inspired algorithms can be promising solutions to replace traditional optimization techniques.

- As potential future work, an interesting study can be conducted by integrating physical layer authentication. This technique is a security mechanism that utilizes the characteristics of wireless communication channels such as the path loss, channel fading, and multipath propagation to verify the identity of communicating devices. It relies on the fact that wireless communication channels have unique and random features that can be used to identify the transmitting device. In this sense, physical layer authentication provides an additional layer of security to NOMA systems that can prevent unauthorized access to the system and protect against eavesdropping and other attacks.

- The enhancement of physical layer security (PLS) through the use of RSMA is a meaningful area of investigation. Although RSMA-aided PLS is in its initial research stages, it is anticipated to become a potential research area in the future, especially in multi-antenna wireless systems.

Publications

International journal papers

[1] C. E. Garcia, M. R. Camana, and I. Koo, "Particle Swarm Optimization-Based Secure Computation Efficiency Maximization in a Power Beacon-Assisted Wireless-Powered Mobile Edge Computing NOMA System," *Energies*, vol. 13, no. 21, pp. 5540, Oct. 2020.

[2] C. E. Garcia, M. R. Camana, and I. Koo, "Joint Beamforming and Artificial Noise Optimization for Secure Transmissions in MISO-NOMA Cognitive Radio System with SWIPT," *Electronics*, vol. 9, no. 11, pp. 1948, Nov. 2020.

[3] C. E. Garcia, M. R. Camana, and I. Koo,"Machine learning-based scheme for multi-class fault detection in turbine engine disks Machine Learning–based Scheme for Multi-class Fault Detection in Turbine Engine Disks," *ICT Express*, vol. 7, pp. 15–22, Mar. 2021.

[4] C. E. Garcia, M. R. Camana, and I. Koo, "Relay selection and power allocation for secrecy sum rate maximization in underlying cognitive radio with cooperative relaying NOMA," *Neurocomputing*, vol. 452, no. 4, pp. 756–767, Sep. 2021.

[5] C. E. Garcia, M. R. Camana, and I. Koo, "Low-Complexity PSO-based Resource Allocation Scheme for Cooperative Non-linear SWIPT-enabled NOMA," *IEEE Access*, vol. 10, pp. 34207--34220, March. 2022.

[6] C. E. Garcia, M. R. Camana, and I. Koo, "Ensemble Learning aided QPSO–Based Framework for Secrecy Energy Efficiency in FD CR-NOMA Systems," *IEEE Transactions on Green Communications and Networking*, pp. 1–1, Nov. 2022.

Journal paper under preparation (Excluded thesis)

[7] C. E. Garcia, and I. Koo, "Extremely Randomized Trees Regressor Scheme for Mobile Network Coverage Prediction and REM Construction," submitted to *IEEE Access*, March 2023.

[8] C. E. Garcia, M. R. Camana and I. Koo, "Enhancing Security in an RSMA-based MISO CR System with Non-Linear SWIPT and EH Users: A Robust Beamforming Optimization Scheme with Artificial Noise," 2023.

[9] S. U. Khan, C. E. Garcia, T. Hwang and I. Koo, "A Federated Learning-based Approach to Construct Indoor Radio Environment Maps for PLC-Wi-Fi Networks," 2023.

[10] T. Aziz, M. R. Camana, C. E. Garcia, T. Hwang , and I. Koo, "Supervised Learning for Indoor Localization Prediction based on REM," 2023.

[11] M. R. Camana, C. E. Garcia, and I. Koo, "Beamforming Optimization Assisted with Deep Learning in an RSMA SWIPT System with a PB," 2023.

International conference

[12] C. E. Garcia, M. R. Camana, and I. Koo, "Machine learning-based Scheme for Fault Detection for Turbine Engine Disk," *The 11th International Conference on Information and Communication Technology Convergence (ICTC)*, Jeju, S. Korea, Oct. 11–16, 2020.

[13] C. E. Garcia, M. R. Camana, and I. Koo, "Cuckoo Search based-Scheme for Power Minimization in a Green SWIPT NOMA System," *KICS Winter Conference 2022*, Pyeongchang, S. Korea, Feb. 9–11, 2022.

[14] C. E. Garcia, M. R. Camana, and I. Koo, "DNN aided PSO based-scheme for a Secure Energy Efficiency Maximization in a cooperative NOMA system with a non-linear EH," *The 13th International Conference on Ubiquitous and Future Networks (ICUFN)*, Barcelona, Spain, Jul. 5–8, 2022.

[15] C. E. Garcia, and I. Koo, "Coverage Prediction and REM Construction for 5G networks in Band n78, Sidney, Australia," *2023 15th International Conference on Computer and Automation Engineering (ICCAE)*, Sydney, Australia, March. 3–5, pp. 125-129, 2023.

Bibliography

[1] C. Garcia, M. Camana, I. Koo, and R. Md Arifur, "Particle swarm optimization-based power allocation scheme for secrecy sum rate maximization in NOMA with cooperative relaying," in *Intelligent Computing Theories and Application*. Springer International Publishing, 2019, pp. 1–12.

[2] S. Singh, D. Mitra, and R. Baghel, "Analysis of NOMA for future cellular communication," in *2019 3rd International Conference on Trends in Electronics and Informatics (ICOEI)*. IEEE, 2019.

[3] G. Liu, Z. Wang, J. Hu, Z. Ding, and P. Fan, "Cooperative NOMA broadcasting/multicasting for low-latency and high-reliability 5g cellular v2x communications," *IEEE Internet of Things Journal*, vol. 6, no. 5, pp. 7828–7838, 2019.

[4] K. K. Gurrala and S. Das, "Hybrid decode-amplify-forward (HDAF) scheme in distributed alamouti-coded cooperative network," *International Journal of Electronics*, vol. 102, no. 5, 2014.

[5] L. Xu, H. Zhang, and T. A. Gulliver, "Joint TAS and power allocation for DF relaying m2m cooperative system," *International Journal of Electronics*, pp. 1–14, 2016.

[6] C. Garcia, P. Tuan, M. Camana, and I. Koo, "Optimized power allocation for a coopera-

tive NOMA system with SWIPT and an energy-harvesting user," *International Journal of Electronics*, vol. 107, no. 10, pp. 1704–1733, 2020.

[7] S. Arzykulov, G. Nauryzbayev, T. A. Tsiftsis, and B. Maham, "Performance analysis of underlay cognitive radio nonorthogonal multiple access networks," *IEEE Transactions on Vehicular Technology*, vol. 68, no. 9, pp. 9318–9322, 2019.

[8] K. Zheng, X.-Y. Liu, X. Liu, and Y. Zhu, "Hybrid overlay-underlay cognitive radio networks with energy harvesting," *IEEE Transactions on Communications*, vol. 67, no. 7, pp. 4669–4682, 2019.

[9] M. Song, C. Xin, Y. Zhao, and X. Cheng, "Dynamic spectrum access: from cognitive radio to network radio," *IEEE Wireless Communications*, vol. 19, no. 1, pp. 23–29, 20128.

[10] Y. Yuan, Y. Xu, Z. Yang, P. Xu, and Z. Ding, "Energy efficiency optimization in full-duplex user-aided cooperative SWIPT NOMA systems," *IEEE Transactions on Communications*, vol. 67, no. 8, pp. 5753–5767, 2019.

[11] J. Tang, T. Dai, M. Cui, X. Y. Zhang, A. Shojaeifard, W. Kai-Kit, and Z. Li, "Optimization for maximizing sum secrecy rate in SWIPT-enabled NOMA systems," *IEEE Access*, vol. 6, pp. 43 440–43 449, 2018.

[12] C. E. Garcia, M. R. Camana, and I. Koo, "Relay selection and power allocation for secrecy sum rate maximization in underlying cognitive radio with cooperative relaying NOMA," *Neurocomputing*, vol. 452, pp. 756–767, 2021.

[13] A. D. Wyner, "The wire-tap channel," *Bell System Technical Journal*, vol. 54, no. 8, pp. 1355–1387, 1975.

[14] X.-S. Yang, *Nature-Inspired Optimization Algorithms*.   Elsevier, 2014.

[15] M. O. Okwu and L. K. Tartibu, *Metaheuristic Optimization: Nature-Inspired Algorithms Swarm and Computational Intelligence, Theory and Applications*. Springer International Publishing, 2021.

[16] C. E. Garcia, M. R. Camana, and I. Koo, "Low-complexity PSO-based resource allocation scheme for cooperative non-linear SWIPT-enabled NOMA," *IEEE Access*, vol. 10, pp. 34 207–34 220, 2022.

[17] E. Valian, S. Mohanna, and S. Tavakoli, "Improved cuckoo search algorithm for feed forward neural network training," *International Journal of Artificial Intelligence & Applications*, vol. 2, no. 3, pp. 36–43, 2011.

[18] J. Kennedy and R. Eberhart, "Particle swarm optimization," in *Proceedings of ICNN'95 - International Conference on Neural Networks*. IEEE, 1995.

[19] S. Tu, O. U. Rehman, S. U. Rehman, S. Ullah, M. Waqas, and R. Zhu, "A novel quantum inspired particle swarm optimization algorithm for electromagnetic applications," *IEEE Access*, vol. 8, pp. 21 909–21 916, 2020.

[20] M. M. Junaid, N. K. Baloch, F. Hussain, S. Saleem, Y. B. Zikria, and H. Yu, "Application mapping using cuckoo search optimization with lévy flight for NoC-based system," *IEEE Access*, vol. 9, pp. 141 778–141 789, 2021.

[21] T. G. Dietterich, "Ensemble methods in machine learning," in *Multiple Classifier Systems*. Springer Berlin Heidelberg, 2000, pp. 1–15.

[22] C. E. Garcia, M. R. Camana, and I. Koo, "Ensemble learning aided QPSO–based framework for secrecy energy efficiency in FD CR-NOMA systems," *IEEE Transactions on Green Communications and Networking*, pp. 2605–2619, 2022.

[23] ——, "Prediction of digital terrestrial television coverage using machine learning regression," *IEEE Transactions on Broadcasting*, vol. 65, no. 4, pp. 702–712, 2019.

[24] H. Phan, M. Maas, R. Mazur, and A. Mertins, "Random regression forests for acoustic event detection and classification," *IEEE/ACM Transactions on Audio, Speech, and Language Processing*, vol. 23, pp. 20–31, 2015.

[25] L. Dery and E. Shmueli, "BoostLR: A boosting-based learning ensemble for label ranking tasks," *IEEE Access*, vol. 8, pp. 176 023–176 032, 2020.

[26] T. Hastie, S. Rosset, J. Zhu, and H. Zou, "Multi-class AdaBoost," *Statistics and Its Interface*, vol. 2, no. 3, pp. 349–360, 2009.

[27] Z.-q. Luo, W.-K. Ma, A. So, Y. Ye, and S. Zhang, "Semidefinite relaxation of quadratic optimization problems," *IEEE Signal Processing Magazine*, vol. 27, no. 3, pp. 20–34, 2010.

[28] A. H. Phan, H. D. Tuan, H. H. Kha, and D. T. Ngo, "Nonsmooth optimization for efficient beamforming in cognitive radio multicast transmission," *IEEE Transactions on Signal Processing*, vol. 60, no. 6, pp. 2941–2951, 2012.

[29] E. Karipidis, N. D. Sidiropoulos, and Z.-Q. Luo, "Quality of service and max-min fair transmit beamforming to multiple cochannel multicast groups," *IEEE Transactions on Signal Processing*, vol. 56, no. 3, pp. 1268–1279, 2008.

[30] C. E. Garcia, M. R. Camana, and I. Koo, "Particle swarm optimization-based secure computation efficiency maximization in a power beacon-assisted wireless-powered mobile edge computing NOMA system," *Energies*, vol. 13, no. 21, p. 5540, 2020.

[31] H. Lin, Y. Cao, Y. Zhong, and P. Liu, "Secure computation efficiency maximization in NOMA-enabled mobile edge computing networks," *IEEE Access*, vol. 7, pp. 87 504–87 512, 2019.

[32] W. Wu, F. Zhou, R. Q. Hu, and B. Wango, "Energy-efficient resource allocation for secure NOMA-enabled mobile edge computing networks," *IEEE Transactions on Communications*, vol. 68, no. 1, pp. 493–505, 2020.

[33] Z. Ding, J. Xu, O. A. Dobre, and H. V. Poor, "Joint power and time allocation for NOMA-MEC offloading," *IEEE Transactions on Vehicular Technology*, vol. 68, no. 6, pp. 6207–6211, 2019.

[34] Q. Cheng, L. Li, Y. Sun, D. Wang, W. Liang, X. Li, and Z. Han, "Efficient resource allocation for NOMA-MEC system in ultra-dense network: A mean field game approach," in *2020 IEEE International Conference on Communications Workshops (ICC Workshops)*.   IEEE, jun 2020.

[35] A. Kiani and N. Ansari, "Edge computing aware NOMA for 5g networks," *IEEE Internet of Things Journal*, vol. 5, no. 2, pp. 1299–1306, 2018.

[36] W. Wu, F. Zhou, P. Li, P. Deng, B. Wang, and V. C. M. Leung, "Energy-efficient secure NOMA-enabled mobile edge computing networks," in *ICC 2019 - 2019 IEEE International Conference on Communications (ICC)*.   Hindawi Limited, May. 2019.

[37] Y. Wu, K. Ni, C. Zhang, L. P. Qian, and D. H. K. Tsang, "NOMA-assisted multi-access mobile edge computing: A joint optimization of computation offloading and time allocation," *IEEE Transactions on Vehicular Technology*, vol. 67, no. 12, pp. 12 244–12 258, 2018.

[38] F. Wang, J. Xu, X. Wang, and S. Cui, "Joint offloading and computing optimization in wireless powered mobile-edge computing systems," *IEEE Transactions on Wireless Communications*, vol. 17, no. 3, pp. 1784–1797, 2018.

[39] S. Bi and Y. J. Zhang, "Computation rate maximization for wireless powered mobile-edge computing with binary computation offloading," *IEEE Transactions on Wireless Communications*, vol. 17, no. 6, pp. 4177–4190, 2018.

[40] F. Zhou, Y. Wu, R. Q. Hu, and Y. Qian, "Computation rate maximization in UAV-enabled wireless-powered mobile-edge computing systems," *IEEE Journal on Selected Areas in Communications*, vol. 36, no. 9, pp. 1927–1941, 2018.

[41] L. Ji and S. Guo, "Energy-efficient cooperative resource allocation in wireless powered mobile edge computing," *IEEE Internet of Things Journal*, vol. 6, no. 3, pp. 4744–4754, 2019.

[42] F. Wang, J. Xu, and S. Cui, "Optimal energy allocation and task offloading policy for wireless powered mobile edge computing systems," *IEEE Transactions on Wireless Communications*, vol. 19, no. 4, pp. 2443–2459, 2020.

[43] M. R. Camana, P. V. Tuan, and I. Koo, "Optimised power allocation for a power beacon-assisted SWIPT system with a power-splitting receiver," *International Journal of Electronics*, vol. 106, no. 3, pp. 415–439, 2018.

[44] F. Zhou and R. Q. Hu, "Computation efficiency maximization in wireless-powered mobile edge computing networks," *IEEE Transactions on Wireless Communications.*, vol. 19, no. 5, pp. 3170–3184, 2020.

[45] K. Huang and V. K. N. Lau, "Enabling wireless power transfer in cellular networks: Architecture, modeling, and deployment," *IEEE Transactions on Wireless Communications*, vol. 13, no. 2, pp. 902–912, 2014.

[46] C. E. Garcia, M. R. Camana, and I. Koo, "Secrecy energy efficiency maximization in an underlying cognitive radio NOMA system with a cooperative relay and an energy-harvesting user," *Applied Sciences*, vol. 10, no. 10, p. 3630, 2020.

[47] C. You, K. Huang, and H. Chae, "Energy efficient mobile cloud computing powered by wireless energy transfer," *IEEE Journal on Selected Areas in Communications*, vol. 34, no. 5, pp. 1757–1771, 2016.

[48] J. Xu, L. Chen, and S. Ren, "Online learning for offloading and autoscaling in energy harvesting mobile edge computing," *IEEE Transactions on Cognitive Communications and Networking*, vol. 3, no. 3, pp. 361–373, 2017.

[49] Y. Mao, J. Zhang, and K. B. Letaief, "Dynamic computation offloading for mobile-edge computing with energy harvesting devices," *IEEE Journal on Selected Areas in Communications*, vol. 34, no. 12, pp. 3590–3605, 2016.

[50] X. Hu, K.-K. Wong, and K. Yang, "Wireless powered cooperation-assisted mobile edge computing," *IEEE Transactions on Wireless Communications*, vol. 17, no. 4, pp. 2375–2388, 2018.

[51] S. Mao, S. Leng, K. Yang, X. Huang, and Q. Zhao, "Fair energy-efficient scheduling in wireless powered full-duplex mobile-edge computing systems," in *GLOBECOM 2017 - 2017 IEEE Global Communications Conference*.   IEEE, 2017.

[52] S. Mao, S. Leng, K. Yang, Q. Zhao, and M. Liu, "Energy efficiency and delay tradeoff in multi-user wireless powered mobile-edge computing systems," in *GLOBECOM 2017 - 2017 IEEE Global Communications Conference*.   IEEE, 2017.

[53] S. Wang, M. Xia, K. Huang, and Y.-C. Wu, "Wirelessly powered two-way communication with nonlinear energy harvesting model: Rate regions under fixed and mobile relay," *IEEE Transactions on Wireless Communications*, vol. 16, no. 12, pp. 8190–8204, 2017.

[54] Y. Wang, M. Sheng, X. Wang, L. Wang, and J. Li, "Mobile-edge computing: Partial computation offloading using dynamic voltage scaling," *IEEE Transactions on Communications*, vol. 64, pp. 4268–4282, 2016.

[55] C.-F. Liu, M. Bennis, and H. V. Poor, "Latency and reliability-aware task offloading and

resource allocation for mobile edge computing," in *2017 IEEE Globecom Workshops (GC Wkshps)*. IEEE, 2017, pp. 1–7.

[56] K. E. Parsopodos and M. N. Vrahatis, "Particle swarm optimization method for constrained optimization problems," in *Intelligent Technologies—Theory and Applications: New Trends in Intelligent Technologies*, no. 76. IOS Press, 2002, pp. 214–220.

[57] Y. He, W. J. Ma, and J. P. Zhang, "The parameters selection of PSO algorithm influencing on performance of fault diagnosis," *MATEC Web of Conferences*, vol. 63, no. 02019, 2016.

[58] M. Camana, P. Tuan, C. Garcia, and I. Koo, "Joint power allocation and power splitting for MISO SWIPT RSMA systems with energy-constrained users," *Wireless Networks*, vol. 26, no. 3, pp. 2241–2254, 2019.

[59] P. Cazzaniga, M. S. Nobile, and D. Besozzi, "The impact of particles initialization in PSO: Parameter estimation as a case in point," in *2015 IEEE Conference on Computational Intelligence in Bioinformatics and Computational Biology (CIBCB)*. IEEE, 2015, pp. 1–8.

[60] C. E. Garcia, M. R. Camana, and I. Koo, "Joint beamforming and artificial noise optimization for secure transmissions in MISO-NOMA cognitive radio system with SWIPT," *Electronics*, vol. 9, no. 11, p. 1948, 2020.

[61] J. Cui, Z. Ding, and P. Fan, "Beamforming design for MISO non-orthogonal multiple access systems," *IET Communications*, vol. 11, no. 5, pp. 720–725, 2017.

[62] A. Sharmila and P. Dananjayan, "Spectrum sharing techniques in cognitive radio networks—a survey," in *2019 IEEE International Conference on System, Computation, Automation and Networking (ICSCAN)*. IEEE, 2019, pp. 1–4.

[63] L. G. M. Riveros, F. B. S. de Carvalho, and R. S. de Marinho, "Spectrum management based

on genetic algorithm for cognitive networks," in *2020 43rd International Conference on Telecommunications and Signal Processing (TSP)*.   IEEE, 2020, pp. 569–572.

[64] W. Lee, "Resource allocation for multi-channel underlay cognitive radio network based on deep neural network," *IEEE Communications Letters*, vol. 22, no. 9, pp. 1942–1945, 2018.

[65] D. M. Alias and R. G. K., "Cognitive radio networks: A survey," in *2016 International Conference on Wireless Communications, Signal Processing and Networking (WiSPNET)*. IEEE, 2016, pp. 1981–1986.

[66] J.-M. Kang and I.-M. Kim, "Optimal user grouping for downlink noma," *IEEE Wireless Communications Letters*, vol. 7, no. 5, pp. 724–727, 2018.

[67] M. Salehi, H. Tabassum, and E. Hossain, "Meta distribution of SIR in large-scale uplink and downlink NOMA networks," *IEEE Transactions on Communications*, vol. 67, no. 4, pp. 3009–3025, 2019.

[68] L. Liu, R. Zhang, and K.-C. Chua, "Multi-antenna wireless powered communication with energy beamforming," *IEEE Transactions on Communications*, vol. 62, no. 12, pp. 4349–4361, 2014.

[69] E. Karipidis, N. D. Sidiropoulos, and Z.-Q. Luo, "Far-field multicast beamforming for uniform linear antenna arrays," *IEEE Transactions on Signal Processing*, vol. 55, no. 10, pp. 4916–4927, 2007.

[70] N. John and A. Jyotsna, "A survey on energy efficient tree-based data aggregation techniques in wireless sensor networks," in *2018 International Conference on Inventive Research in Computing Applications (ICIRCA)*.   IEEE, 2018, pp. 461–465.

[71] F. Zhou, N. C. Beaulieu, Z. Li, J. Si, and P. Qi, "Energy-efficient optimal power allocation for fading cognitive radio channels: Ergodic capacity, outage capacity, and minimum-rate

capacity," *IEEE Transactions on Wireless Communications*, vol. 15, no. 4, pp. 2741–2755, 2016.

[72] D. Feng, C. Jiang, G. Lim, L. Cimini, G. Feng, and G. Li, "A survey of energy-efficient wireless communications," *IEEE Communications Surveys & Tutorials*, vol. 15, no. 1, pp. 167–178, 2013.

[73] S. Mao, S. Leng, J. Hu, and K. Yang, "Power minimization resource allocation for underlay MISO-NOMA SWIPT systems," *IEEE Access*, vol. 7, pp. 17 247–17 255, 2019.

[74] T. D. P. Perera, D. N. K. Jayakody, S. K. Sharma, S. Chatzinotas, and J. Li, "Simultaneous wireless information and power transfer (SWIPT): Recent advances and future challenges," *IEEE Communications Surveys & Tutorials*, vol. 20, no. 1, pp. 264–302, 2018.

[75] K. W. Choi, S. I. Hwang, A. A. Aziz, H. H. Jang, J. S. Kim, D. S. Kang, and D. I. Kim, "Simultaneous wireless information and power transfer (SWIPT) for internet of things: Novel receiver design and experimental validation," *IEEE Internet of Things Journal*, vol. 7, no. 4, pp. 2996–3012, 2020.

[76] M. Hedayati and I.-M. Kim, "On the performance of NOMA in the two-user SWIPT system," *IEEE Transactions on Vehicular Technology*, vol. 67, no. 11, pp. 11 258–11 263, 2018.

[77] Z. Song, X. Wang, Y. Liu, and Z. Zhang, "Joint spectrum resource allocation in NOMA-based cognitive radio network with SWIPT," *IEEE Access*, vol. 7, pp. 89 594–89 603, 2019.

[78] Q. N. Le, N.-P. Nguyen, A. Yadav, and O. A. Dobre, "Outage performance of full-duplex overlay CR-NOMA networks with SWIPT," in *2019 IEEE Global Communications Conference (GLOBECOM)*.   IEEE, 2019, pp. 1–6.

[79] A. Mukherjee, "Physical-layer security in the internet of things: Sensing and communication

confidentiality under resource constraints," *Proceedings of the IEEE*, vol. 103, no. 10, pp. 1747–1761, 2015.

[80] J. M. Hamamreh, H. M. Furqan, and H. Arslan, "Classifications and applications of physical layer security techniques for confidentiality: A comprehensive survey," *IEEE Communications Surveys & Tutorials*, vol. 21, no. 2, pp. 1773–1828, 2019.

[81] N. Zhao, D. Li, M. Liu, Y. Cao, Y. Chen, Z. Ding, and X. Wang, "Secure transmission via joint precoding optimization for downlink MISO NOMA," *IEEE Transactions on Vehicular Technology*, vol. 68, no. 8, pp. 7603–7615, 2019.

[82] N. Zhao, W. Wang, J. Wang, Y. Chen, Y. Lin, Z. Ding, and N. C. Beaulieu, "Joint beamforming and jamming optimization for secure transmission in miso-noma networks," *IEEE Transactions on Communications*, vol. 67, no. 3, pp. 2294–2305, 2019.

[83] P. Zhao, M. Zhang, H. Yu, H. Luo, and W. Chen, "Robust beamforming design for sum secrecy rate optimization in MU-MISO networks," *IEEE Transactions on Information Forensics and Security*, vol. 10, no. 9, pp. 1812–1823, 2015.

[84] H.-M. Wang, X. Zhang, Q. Yang, and T. A. Tsiftsis, "Secure users oriented downlink MISO NOMA," *IEEE Journal on Selected Topics in Signal Processing*, vol. 13, no. 3, pp. 671–684, 2019.

[85] Z. Zhou, Fuhuiand Chu, H. Sun, R. Q. Hu, and L. Hanzo, "Artificial noise aided secure cognitive beamforming for cooperative MISO-NOMA using SWIPT," *IEEE Journal on Selected Areas in Communications*, vol. 36, no. 4, pp. 918–931, 2018.

[86] V. N. Vo, C. So-In, H. Tran, D.-D. Tran, S. Heng, P. Aimtongkham, and A.-N. Nguyen, "On security and throughput for energy harvesting untrusted relays in IoT systems using NOMA," *IEEE Access*, vol. 7, pp. 149 341–149 354, 2019.

[87] M. R. Camana, C. E. Garcia, and I. Koo, "Joint power allocation and power splitting for MISO-RSMA cognitive radio systems with SWIPT and information decoder users," *IEEE Systems Journal*, vol. 15, no. 4, pp. 5289–5300, 2020.

[88] Q. Shi, C. Peng, W. Xu, M. Hong, and Y. Cai, "Energy efficiency optimization for MISO SWIPT systems with zero-forcing beamforming," *IEEE Transactions on Signal Processing*, vol. 64, no. 4, pp. 842–854, 2016.

[89] K. Umebayashi, J. Lehtomäki, and I. M. Suliman, "Analysis of transmit power setting technique for cognitive radio networks," *EURASIP Journal on Wireless Communications and Networking*, vol. 2016, no. 144, 2016.

[90] Z. Yang, Z. Ding, P. Fan, and G. K. Karagiannidis, "On the performance of non-orthogonal multiple access systems with partial channel information," *IEEE Transactions on Communications*, vol. 64, no. 2, pp. 654–667, 2016.

[91] G. Chen, J. Tang, and J. Coon, "Optimal routing for multihop social-based D2D communications in the internet of things," *IEEE Internet of Things Journal*, vol. 5, no. 3, pp. 1880–1889, 2018.

[92] H. Visser and R. Vullers, "RF energy harvesting and transport for wireless sensor network applications: Principles and requirements," *Proceedings of the IEEE*, vol. 101, no. 6, pp. 1410–1423, 2013.

[93] M.-L. Ku, W. Li, Y. Chen, and K. J. R. Liu, "Advances in energy harvesting communications: Past, present, and future challenges," *IEEE Communications Surveys andTutorials*, vol. 18, no. 2, pp. 1384–1412, 2016.

[94] P. Kaur, B. S. Sohi, and P. Singh, "Recent advances in MAC protocols for the energy harvesting

based WSN: A comprehensive review," *Wireless Personal Communications*, vol. 104, no. 1, pp. 423–440, 2018.

[95] X. Lu, P. Wang, D. Niyato, D. Kim, and Z. Han, "Wireless networks with RF energy harvesting: A contemporary survey," *IEEE Communications Surveys & Tutorials*, vol. 17, no. 2, pp. 757–789, 2015.

[96] A. Pop-Vadean, P. P. Pop, T. Latinovic, C. Barz, and C. Lung, "Harvesting energy an sustainable power source, replace batteries for powering WSN and devices on the IoT," *IOP Conference Series: Materials Science and Engineering*, vol. 200, p. 012043, 2017.

[97] K. Xiong, B. Wang, and K. J. R. Liu, "Rate-energy region of SWIPT for MIMO broadcasting under nonlinear energy harvesting model," *IEEE Transactions on Wireless Communications*, vol. 16, no. 8, pp. 5147–5161, 2017.

[98] K. Ali, H. X. Nguyen, Q.-T. Vien, P. Shah, and Z. Chu, "Disaster management using d2d communication with power transfer and clustering techniques," *IEEE Access*, vol. 6, pp. 14 643–14 654, 2018.

[99] J. Tang, J. Luo, M. Liu, D. K. C. So, E. Alsusa, G. Chen, K.-K. Wong, and J. A. Chambers, "Energy efficiency optimization for NOMA with SWIPT," *IEEE Journal of Selected Topics in Signal Processing*, vol. 13, no. 3, pp. 452–466, 2019.

[100] Z. Wang and Q. Zhu, "Energy efficiency optimization algorithm of CR-NOMA system based on SWIPT," *Mathematical Problems in Engineering*, vol. 2020, pp. 1–13, 2020.

[101] J. Luo, J. Tang, D. K. C. So, G. Chen, K. Cumanan, and J. A. Chambers, "A deep learning-based approach to power minimization in multi-carrier NOMA with SWIPT," *IEEE Access*, vol. 7, pp. 17 450–17 460, 2019.

[102] A. N. Uwaechia and N. M. Mahyuddin, "Spectrum and energy efficiency optimization for hybrid precoding-based SWIPT-enabled mmWave mMIMO-NOMA systems," *IEEE Access*, vol. 8, pp. 139 994–140 007, 2020.

[103] P. Nezhadmohammad, M. Abedi, M. J. Emadi, and R. Wichman, "SWIPT-enabled multiple access channel: Effects of decoding cost and non-linear EH model," *IEEE Transactions on Communications*, vol. 70, no. 1, pp. 306–316, 2022.

[104] N. Shanin, L. Cottatellucci, and R. Schober, "Markov decision process based design of SWIPT systems: Non-linear EH circuits, memory, and impedance mismatch," *IEEE Transactions on Communications*, vol. 69, no. 2, pp. 1259–1274, 2021.

[105] X. Xu, A. Ozcelikkale, T. McKelvey, and M. Viberg, "Simultaneous information and power transfer under a non-linear RF energy harvesting model," in *2017 IEEE International Conference on Communications Workshops (ICC Workshops)*.   IEEE, 2017, pp. 179–184.

[106] M. Varasteh, B. Rassouli, and B. Clerckx, "On capacity-achieving distributions for complex AWGN channels under nonlinear power constraints and their applications to SWIPT," *IEEE Transactions on Information Theory*, vol. 66, no. 10, pp. 6488–6508, 2020.

[107] J. H. Holland, "Outline for a logical theory of adaptive systems," *Journal of the ACM*, vol. 9, no. 3, pp. 297–314, 1962.

[108] W.-S. Zhao, B.-X. Wang, D.-W. Wang, B. You, Q. Liu, and G. Wang, "Swarm intelligence algorithm-based optimal design of microwave microfluidic sensors," *IEEE Transactions on Industrial Electronics*, vol. 69, no. 2, pp. 2077–2087, 2022.

[109] I. Pavlyukevich, "Lévy flights, non-local search and simulated annealing," *Journal of Computational Physics*, vol. 226, no. 2, pp. 1830–1844, 2007.

[110] Z. Cui, B. Sun, G. Wang, Y. Xue, and J. Chen, "A novel oriented cuckoo search algorithm to improve DV-hop performance for cyber–physical systems," *Journal of Parallel and Distributed Computing*, vol. 103, pp. 42–52, 2017.

[111] M. Grant and S. Boyd, "CVX: MATLAB software for disciplined convex programming, version 2.2," Jan 2020.

[112] T. T. Vu, H. H. Kha, T. Q. Duong, and N.-S. Vo, "Particle swarm optimization for weighted sum rate maximization in MIMO broadcast channels," *Wireless Personal Communications*, vol. 96, no. 3, pp. 3907–3921, 2017.

[113] X.-S. Yang and S. Deb, "Cuckoo search via lévy flights," in *2009 World Congress on Nature and Biologically Inspired Computing (NaBIC)*. IEEE, 2009.

[114] R. Salgotra, U. Singh, and S. Saha, "New cuckoo search algorithms with enhanced exploration and exploitation properties," *Expert Systems with Applications*, vol. 95, pp. 384—420, 2018.

[115] X. Chen, G. Liu, Z. Ding, F. R. Yu, and P. Fan, "Power allocation for full-duplex cooperative non-orthogonal multiple access systems," in *GLOBECOM 2017 - 2017 IEEE Global Communications Conference*. IEEE, 2017, pp. 1–6.

[116] Q. Liu, T. Lv, and Z. Lin, "Energy-efficient transmission design in cooperative relaying systems using NOMA," *IEEE Communications Letters*, vol. 22, no. 3, pp. 594–597, 2018.

[117] M. Wu, Q. Song, L. Guo, and A. Jamalipour, "Joint user pairing and resource allocation in a SWIPT-enabled cooperative NOMA system," *IEEE Transactions on Vehicular Technology*, vol. 70, no. 7, pp. 6826–6840, 2021.

[118] Q. N. Le, A. Yadav, N.-P. Nguyen, O. A. Dobre, and R. Zhao, "Full-duplex non-orthogonal multiple access cooperative overlay spectrum-sharing networks with SWIPT," *IEEE Transactions on Green Communications and Networking*, vol. 5, no. 1, pp. 322–334, 2021.

[119] X. Li, Q. Wang, M. Liu, J. Li, H. Peng, M. J. Piran, and L. Li, "Cooperative wireless-powered NOMA relaying for b5g IoT networks with hardware impairments and channel estimation errors," *IEEE Internet of Things Journal*, vol. 8, no. 7, pp. 5453–5467, 2021.

[120] M. O. Okwu and L. K. Tartibu, "Future of nature inspired algorithm, swarm and computational intelligence," in *Metaheuristic Optimization: Nature-Inspired Algorithms Swarm and Computational Intelligence, Theory and Applications*. Springer International Publishing, 2020, vol. 927, pp. 147–151.

[121] C. Wu, Z. Liu, T. Yoshinaga, F. Liu, Y. Ji, and J. Li, "Collaborative learning of communication routes in edge-enabled multi-access vehicular environment," *IEEE Transactions on Cognitive Communications and Networking*, vol. 6, no. 4, pp. 1155–1165, 2020.

[122] M.-J. Youssef, C. A. Nour, X. Lagrange, and C. Douillard, "A deep q-learning bisection approach for power allocation in downlink NOMA systems," *IEEE Communications Letters*, vol. 26, no. 2, pp. 316–320, 2022.

[123] D.-H. Ha, T. T. Duy, P. N. Son, T. Le-Tien, and M. Voznak, "Security-reliability trade-off analysis for rateless codes-based relaying protocols using NOMA, cooperative jamming and partial relay selection," *IEEE Access*, vol. 9, pp. 131 087–131 108, 2021.

[124] H. Liu, Y. Xiao, P. Yang, J. Fu, S. Li, and W. Xiang, "Transmit antenna selection for full-duplex spatial modulation based on machine learning," *IEEE Transactions on Vehicular Technology*, vol. 70, no. 10, pp. 10 695–10 708, Oct 2021.

[125] K. Jiang and H. Wang, "Secrecy performance for full-duplex jamming-aided uplink NOMA system," *IEEE Transactions on Vehicular Technology*, vol. 70, no. 10, pp. 10 409–10 419, 2021.

[126] S. Jia, J. Zhang, H. Zhao, and R. Zhang, "Relay selection for improved security in cognitive relay networks with jamming," *IEEE Wireless Communications Letters*, vol. 6, no. 5, pp. 662–665, 2017.

[127] L. Lv, J. Chen, Q. Ni, Z. Ding, and H. Jiang, "Cognitive non-orthogonal multiple access with cooperative relaying: A new wireless frontier for 5g spectrum sharing," *IEEE Communications Magazine*, vol. 56, no. 4, pp. 188–195, 2018.

[128] L. Yang, J. Chen, H. Jiang, S. A. Vorobyov, and H. Zhang, "Optimal relay selection for secure cooperative communications with an adaptive eavesdropper," *IEEE Transactions on Wireless Communications*, vol. 16, no. 1, pp. 26–42, 2017.

[129] D.-T. Do, M.-S. Van Nguyen, T.-A. Hoang, and M. Voznak, "NOMA-assisted multiple access scheme for IoT deployment: Relay selection model and secrecy performance improvement," *Sensors*, vol. 19, no. 3, p. 736, 2019.

[130] Y. Feng, S. Yan, C. Liu, Z. Yang, and N. Yang, "Two-stage relay selection for enhancing physical layer security in non-orthogonal multiple access," *IEEETransactions on Information Forensics and Security*, vol. 14, no. 6, pp. 1670–1683, 2019.

[131] M. R. Camana, C. E. Garcia, and I. Koo, "Deep learning-assisted power minimization in underlay MISO-SWIPT systems based on rate-splitting multiple access," *IEEE Access*, vol. 10, pp. 62 137–62 156, 2022.

[132] Y. Mao, B. Clerckx, and V. O. Li, "Rate-splitting multiple access for downlink communication systems: bridging, generalizing, and outperforming SDMA and NOMA," *EURASIP Journal on Wireless Communications and Networking*, vol. 2018, no. 1, 2018.

[133] U. Uyoata, J. Mwangama, and R. Adeogun, "Relaying in the internet of things (IoT): A survey," *IEEE Access*, vol. 9, pp. 132 675–132 704, 2021.

[134] Y. Wu, L. p. Qian, L. Huang, and X. Shen, "Optimal relay selection and power control for energy-harvesting wireless relay networks," *IEEE Transactions on Green Communications and Networking*, vol. 2, no. 2, pp. 471–481, 2018.

[135] T.-V. Nguyen, T.-N. Tran, K. Shim, T. Huynh-The, and B. An, "A deep-neural-network-based relay selection scheme in wireless-powered cognitive IoT networks," *IEEE Internet of Things Journal*, vol. 8, no. 9, pp. 7423–7436, 2021.

[136] T.-H. Vu, T.-V. Nguyen, and S. Kim, "Cooperative NOMA-enabled SWIPT IoT networks with imperfect SIC: Performance analysis and deep learning evaluation," *IEEE Internet of Things Journal*, vol. 9, no. 3, pp. 2253–2266, 2022.

[137] S. Dang, J. Tang, J. Li, M. Wen, S. Abdullah, and C. Li, "Combined relay selection enabled by supervised machine learning," *IEEE Transactions on Vehicular Technology*, vol. 70, no. 4, pp. 3938–3943, 2021.

[138] T. N. Nguyen, D.-H. Tran, V.-D. Phan, M. Voznak, S. Chatzinotas, B. Ottersten, and H. V. Poor, "Throughput enhancement in FD- and SWIPT-enabled IoT networks over nonidentical rayleigh fading channels," *IEEE Internet of Things Journal*, vol. 9, no. 12, pp. 10 172–10 186, 2022.

[139] Q. T. Ngo, K. T. Phan, W. Xiang, A. Mahmood, and J. Slay, "Two-tier cache-aided full-duplex hybrid satellite–terrestrial communication networks," *IEEE Transactions on Aerospace and Electronic Systems*, vol. 58, no. 3, pp. 1753–1765, 2022.

[140] A. Ly and Y.-D. Yao, "A review of deep learning in 5g research: Channel coding, massive MIMO, multiple access, resource allocation, and network security," *IEEE Open Journal of the Communications Society*, vol. 2, pp. 396–408, 2021.

[141] M. Zhu, K. Ye, and C.-Z. Xu, "Network anomaly detection and identification based on deep learning methods," in *Lecture Notes in Computer Science*.   Springer International Publishing, 2018, pp. 219–234.

[142] J. Xing, T. Lv, and X. Zhang, "Cooperative relay based on machine learning for enhancing physical layer security," in *2019 IEEE 30th Annual International Symposium on Personal, Indoor and Mobile Radio Communications (PIMRC)*.   IEEE, 2019.

[143] M. E. C. Bento, "A hybrid particle swarm optimization algorithm for the wide-area damping control design," *IEEE Transactions on Industrial Informatics*, vol. 18, no. 1, pp. 592–599, 2022.

[144] X. Mu, A. Ottino, F. M. Ferreira, and G. Zervas, "Optimization of 125-um heterogeneous multi-core fibre design using artificial intelligence," *IEEE Journal of Selected Topics in Quantum Electronics*, vol. 28, no. 4, pp. 1–13, 2022.

[145] W. Fang, J. Sun, Y. Ding, X. Wu, and W. Xu, "A review of quantum behaved particle swarm optimization," *IETE Technical Review*, vol. 27, no. 4, pp. 336–348, 2010.

[146] A. A. Nasir, H. D. Tuan, T. Q. Duong, and H. V. Poor, "Secrecy rate beamforming for multicell networks with information and energy harvesting," *IEEE Transactions on Signal Processing*, vol. 65, no. 3, pp. 677–689, 2017.

[147] Y. Xu, C. Shen, Z. Ding, X. Sun, S. Yan, G. Zhu, and Z. Zhong, "Joint beamforming and power-splitting control in downlink cooperative SWIPT NOMA systems," *IEEE Transactions on Signal Processing*, vol. 65, no. 18, pp. 4874–4886, 2017.

[148] D. Li, Y. Cao, Z. Yang, Y. Chen, S. Zhang, N. Zhao, and Z. Ding, "Secrecy analysis in NOMA full-duplex relaying networks with artificial jamming," *IEEETransactions on Vehicular Technology*, vol. 70, no. 9, pp. 8781–8794, 2021.

[149] L. Liu, R. Zhang, and K.-C. Chua, "Multi-antenna wireless powered communication with energy beamforming," *IEEE Transactions on Communications*, vol. 62, no. 12, pp. 4349–4361, 2014.

[150] C. Zhu, Z. Zhu, Y. Xie, W. Jiang, and G. Zhang, "Evaluation of machine learning approaches for android energy bugs detection with revision commits," *IEEE Access*, vol. 7, pp. 85 241–85 252, 2019.

[151] Z. Ma and Q. Dai, "Selected an stacking ELMs for time series prediction," *Neural Processing Letters*, vol. 44, no. 3, pp. 831–856, 2016.

[152] M. Abdar, U. R. Acharya, N. Sarrafzadegan, and V. Makarenkov, "NE-nu-SVC: A new nested ensemble clinical decision support system for effective diagnosis of coronary artery disease," *IEEE Access*, vol. 7, pp. 167 605–167 620, 2019.

[153] S. Zheng, X. Zhou, X. Zheng, and M. Ge, "Improved quantum-behaved particle swarm algorithm based on levy flight," *Mathematical Problems in Engineering*, vol. 2020, pp. 1–10, 2020.

[154] T. Assaf, A. J. Al-Dweik, M. S. E. Moursi, H. Zeineldin, and M. Al-Jarrah, "Exact bit error-rate analysis of two-user NOMA using QAM with arbitrary modulation orders," *IEEE Communications Letters*, vol. 24, no. 12, pp. 2705–2709, 2020.

[155] B. K. Ng and C.-T. Lam, "Joint power and modulation optimization in two-user non-orthogonal multiple access channels: A minimum error probability approach," *IEEE Transactions on Vehicular Technology*, vol. 67, no. 11, pp. 10 693–10 703, Nov. 2018.

[156] Y. Wu, C.-K. Wen, C. Xiao, X. Gao, and R. Schober, "Linear precoding for the MIMO multiple access channel with finite alphabet inputs and statistical CSI," *IEEE Transactions on Wireless Communications*, vol. 14, no. 2, pp. 983–997, 2015.

[157] X. Pei, Y. Chen, M. Wen, H. Yu, E. Panayirci, and H. V. Poor, "Next-generation multiple access based on NOMA with power level modulation," *IEEE Journal on Selected Areas in Communications*, vol. 40, no. 4, pp. 1072–1083, 2022.

[158] T. Ketseoglou and E. Ayanoglu, "Linear precoding gain for large MIMO configurations with QAM and reduced complexity," in *2016 IEEE Global Communications Conference (GLOBECOM)*.   IEEE, 2016, pp. 1–7.

[159] Y. Wu, D. W. K. Ng, C.-K. Wen, R. Schober, and A. Lozano, "Low-complexity MIMO precoding for finite-alphabet signals," *IEEE Transactions on Wireless Communications*, vol. 16, no. 7, pp. 4571–4584, 2017.

[160] R. L. Freeman, *Radio System Design for Telecommunications*.   Wiley, 2006.

[161] H. Soury, F. Bader, M. Shaat, and M.-S. Alouini, "Joint sub-carrier pairing and resource allocation for cognitive networks with adaptive relaying," *EURASIP Journal on Wireless Communications and Networking*, vol. 2013, no. 1, 2013.

[162] M. R. Camana, S. Ahmed, C. E. Garcia, and I. Koo, "Extremely randomized trees based scheme for stealthy cyber-attack detection in smart grid networks," *IEEE Access*, vol. 8, pp. 19 921–19 933, 2020.

Appendix A

Proof in Chapter 5

A.1 SCA-PSO method to solve the proposed optimization problem (5.33)

In this appendix, we develop a comparative scheme based on the SCA method and the PSO algorithm to solve the problem (5.33). First, let us rewrite the objective function (5.33a) as follows:

$$\max_{r} \left(h\left(r \right) = \max_{p_1,p_2,\{p_{r,M1},p_{r,M2}\}} \frac{\log_2 \left(1 + t_1 \right) - \log_2 \left(1 + d_1 \right)}{w} + \right.$$

$$\left. \frac{\log_2 \left(1 + t_2 \right) - \log_2 \left(1 + d_2 \right)}{w} \right), \tag{A.1a}$$

$$\text{s.t. } C1 : (p_1 + p_2 + p_{c1} + p_{r,M1} + p_{r,M2} + p_{c2}) \leq w, \tag{A.1b}$$

$$C2 : \max_{v \in \{1,2,\dots V\},} \frac{p_{r,Mi} \left| g_{r,e_v} \right|^2}{p_{r,Mj \neq i} \left| g_{r,e_v} \right|^2 + \sigma_{e_v}^2} \leq d_i, \forall i, i \in \{1, 2\}, \tag{A.1c}$$

$$C3 : \frac{\left| f_{r,M1} \right|^2 p_{r,M1}}{\left| f_{r,M1} \right|^2 p_{r,M2} + \sigma_{M1}^2} \geq t_1, \tag{A.1d}$$

$$C4 : \frac{\left| f_{r,M2} \right|^2 p_{r,M1}}{\left| f_{r,M2} \right|^2 p_{r,M2} + \sigma_{M2}^2} \geq t_1, \tag{A.1e}$$

$$C5 : \frac{\left| h_r \right|^2 p_1}{\left| h_r \right|^2 p_2 + \rho \left(p_{r,M1} + p_{r,M2} \right) + \sigma_r^2} \geq t_1, \tag{A.1f}$$

$$C6 : \frac{\left|f_{r,M2}\right|^2 p_{r,M2}}{\zeta \left|f_{r,M2}\right|^2 p_{r,M1} + \sigma_{M2}^2} \geq t_2, \tag{A.1g}$$

$$C7 : \frac{|h_r|^2 p_2}{\zeta |h_r|^2 p_1 + \rho \left(p_{r,M1} + p_{r,M2}\right) + \sigma_r^2} \geq t_2 \tag{A.1h}$$

Next, from [146], $-\ln\left(1+t\right) \geq -\ln\left(1+\hat{t}\right) - \frac{t-\hat{t}}{1+\hat{t}}$ is used to approximate $-\log_2\left(1+d_1\right)$

into the following:

$$-\frac{\ln\left(1+d_1\right)}{\ln(2)} \geq -\left(\ln\left(1+d_1^{(n)}\right) + \frac{d_1 - d_1^{(n)}}{1 + d_1^{(n)}}\right)/\ln(2), \tag{A.2}$$

where $d_1^{(n)}$ is the value of the variable d_1 at the n-th iteration. By using the aforementioned inequality

over $-\log_2\left(1+d_2\right)$, the objective function (A.1a) can be approximated as:

$$\frac{\delta_1}{w} = \Omega^{(n)}\left(t_1, t_2, d_1, d_2\right), \tag{A.3}$$

where $\delta_1 = \log_2\left(1+t_1\right) - \left(\ln\left(1+\hat{d}_1\right) + \frac{d_1 - \hat{d}_1}{1+\hat{d}_1}\right)/\ln(2) + \log_2\left(1+t_2\right) - \left(\ln\left(1+\hat{d}_2\right) + \frac{d_2 - \hat{d}_2}{1+\hat{d}_2}\right)/\ln(2)$.

To deal with the non-convex constraint (A.1d), we can approximate (A.1d) as below

$$\left|f_{r,M1}\right|^2 p_{r,M1} \geq t_1 b_1, \tag{A.4}$$

$$\left|f_{r,M1}\right|^2 p_{r,M2} + \sigma_{M1}^2 \leq b_1. \tag{A.5}$$

Next, the AGM inequality [147] is used to approximate the non-convex term $xy \leq z$ into

the convex expression $2xy \leq (ax)^2 + \left(\frac{y}{a}\right)^2 \leq 2z$ with $a = \sqrt{y/x}$. Then, constraint (A.4) can be

approximated as

$$\left(a_{t1,U1}^{(n)} t_1\right)^2 + \left(\frac{b_1}{a_{t1,U1}^{(n)}}\right)^2 \leq 2\left|f_{r,M1}\right|^2 p_{r,M1}, \tag{A.6}$$

where the value of $a_{t1,U1}^{(n+1)}$ is updated in each n-th iteration and can be described by

$$a_{t1,U1}^{(n+1)} = \sqrt{\frac{b_1^{(n)}}{t_1^{(n)}}}. \tag{A.7}$$

By using the aforementioned AGM inequality procedure, the constraint (A.1c) can be approximated as follows:

$$\left(a_{d_i,e_v}^{(n)}\left(p_{r,Mi}|g_{r,e_v}|^2\right)\right)^2 + \left(\frac{r_i}{a_{d_i,e_v}^{(n)}}\right)^2 \le 2\left(p_{r,Mj\ne i}|g_{r,e_v}|^2 + \sigma_{e_v}^2\right), \forall i, \forall v \tag{A.8}$$

$$\frac{1}{d_i} \le r_i, \tag{A.9}$$

where the value of $a_{d_i,e_v}^{(n+1)}$ can be update by

$$a_{d_i,e_v}^{(n+1)} = \sqrt{\frac{r_1^{(n)}}{p_{r,Mi}^{(n)}|g_{r,e_v}|^2}}, \forall i, \forall v. \tag{A.10}$$

Moreover, the constraints (A.1e)-(A.1h) are approximated by following the same procedure used in (A.6). Therefore, given the value of the variable w, the problem (5.33) can be reformulated as follows:

$$\max_{\substack{p_1,p_2,\{p_{r,M1},p_{r,M2}\},t_1,t_2,b_1,b_2,b_3,\\c_1,c_2,d_1,d_2,r_1,r_2}} \Omega^{(n)}\left(t_1,t_2,d_1,d_2\right) \tag{A.11a}$$

$$\text{s.t. } \left(a_{t1,U2}^{(t)}t_1\right)^2 + \left(\frac{b_2}{a_{t1,U2}^{(t)}}\right)^2 - 2|f_{r,M2}|^2 p_{r,M1} \le 0, \tag{A.11b}$$

$$|f_{r,M2}|^2 p_{r,M2} + \sigma_{M2}^2 - b_2 \le 0, \tag{A.11c}$$

$$\left(a_{t1,T}^{(t)}t_1\right)^2 + \left(\frac{b_3}{a_{t1,T}^{(t)}}\right)^2 - 2|h_r|^2 p_1 \le 0, \tag{A.11d}$$

$$|h_r|^2 p_2 + \rho\left(p_{r,M1} + p_{r,M2}\right) + \sigma_r^2 - b_3 \le 0, \tag{A.11e}$$

$$\left(a_{t2,U2}^{(t)}t_2\right)^2 + \left(\frac{c_1}{a_{t2,U2}^{(t)}}\right)^2 - 2|f_{r,M2}|^2 p_{r,M2} \le 0, \tag{A.11f}$$

$$\zeta|f_{r,M2}|^2 p_{r,M1} + \sigma_{M2}^2 - c_1 \le 0, \tag{A.11g}$$

$$\left(a_{t2,T}^{(t)}t_2\right)^2 + \left(\frac{c_2}{a_{t2,T}^{(t)}}\right)^2 - 2|h_r|^2 p_2 \le 0, \tag{A.11h}$$

$$\zeta|h_r|^2 p_1 + \rho\left(p_{r,M1} + p_{r,M2}\right) + \sigma_r^2 - c_2 \le 0, \tag{A.11i}$$

$$\left(2^{\phi_1} - 1\right)\left(\left|f_{r,M1}\right|^2 p_{r,M2} + \sigma_{M1}^2\right) - \left|f_{r,M1}\right|^2 p_{r,M1} \le 0, \tag{A.11j}$$

$$\left(2^{\phi_1} - 1\right)\left(\left|f_{r,M2}\right|^2 p_{r,M2} + \sigma_{M2}^2\right) - \left|f_{r,M2}\right|^2 p_{r,M1} \le 0, \tag{A.11k}$$

$$\left(2^{\phi_1} - 1\right)\left(\left|h_r\right|^2 p_2 + \rho\left(p_{r,M1} + p_{r,M2}\right) + \sigma_r^2\right)$$

$$- \left|h_r\right|^2 p_1 \le 0, \tag{A.11l}$$

$$\left(2^{\phi_2} - 1\right)\left(\zeta\left|f_{r,M2}\right|^2 p_{r,M1} + \sigma_{M2}^2\right) - \left|f_{r,M2}\right|^2 p_{r,M2} \le 0, \tag{A.11m}$$

$$\left(2^{\phi_2} - 1\right)\left(\zeta\left|h_r\right|^2 p_1 + \rho\left(p_{r,M1} + p_{r,M2}\right) + \sigma_r^2\right)$$

$$- \left|h_r\right|^2 p_2 \le 0 \tag{A.11n}$$

$$(75b), (79), (80), (82), (83), (33d), (33e).$$

The constraints (A.11b)-(A.11i) are obtained based on the AGM inequality following a similar procedure used in (A.6). Constraints (A.11b) and (A.11c) are derived from (A.1e). Constraints (A.11d) and (A.11e) are obtained from (A.1f). Constraints (A.11f) and (85g) are derived from (75g). Constraints (A.11h) and (A.11i) are obtained from (A.1h). Constraints (A.11j), (A.11k), and (A.11l) are derived from (33b). Constraints (A.11m) and (A.11n) are obtained from (33c). Finally, the value of the $a_x^{(t)}$ is updated in each n-th iteration with (A.7), (A.10), and the following equations:

$$a_{t1,U2}^{(t+1)} = \sqrt{\frac{b_2^{(t)}}{t_1^{(t)}}}, \tag{A.12a}$$

$$a_{t1,T}^{(t+1)} = \sqrt{\frac{b_3^{(t)}}{t_1^{(t)}}}, \tag{A.12b}$$

$$a_{t2,U2}^{(t+1)} = \sqrt{\frac{c_1^{(t)}}{t_2^{(t)}}}, \tag{A.12c}$$

$$a_{t2,T}^{(t+1)} = \sqrt{\frac{c_2^{(t)}}{t_2^{(t)}}}, \tag{A.12d}$$

where the initial value of $a_x^{(t)}$ is set to be one. Note that the problem (A.11) is convex and can be solved based on the CVX module in MATLAB. The iterative SCA-based algorithm is presented

---

Algorithm A.1 Comparative SCA-based scheme to solve problem (A.11).

1: **Inputs:** $w, a_{d_i,e_v}^{(0)}, a_{t1,U1}^{(0)}, a_{t1,U2}^{(0)}, a_{t1,T}^{(0)}, a_{t2,U2}^{(0)}, a_{t2,T}^{(0)}, d_1^{(0)}, d_2^{(0)}$.

2: Start $n = 1$.

3: **while** $n \leq N_{\max}$ **do**

4:    Solve problem (5.85) with CVX to obtain

   $$p_1^*, p_2^*, \left\{ p_{r,M1}^*, p_{r,M2}^*, q_{i,E_v}^* \right\}, t_1^*, t_2^*, b_1^*, b_2^*, b_3^*, c_1^*, c_2^*, d_1^*, d_2^*.$$

5:    Update the auxiliary values of $a_x^{(t)}$ based on (A.7),

   (A.10), (A.12a), (A.12b), (A.12c), (A.12d).

6:    Update $d_1^{(n+1)} = d_1^*$ and $d_2^{(n+1)} = d_2^*$.

7:    Update the counter $n = n + 1$.

8: **end while**

9: **outputs:** The close-optimal transmit power variables $p_1^*, p_2^*, p_{r,M1}^*, p_{r,M2}^*$, which are used to evaluate the objective function (5.33a).

---

in Algorithm 3. The PSO algorithm is used to update the value of the variable w in an iterative manner. First, the initial positions of the particles in PSO are randomly initialized in the range of $\left[p_{c1} + p_{c2}, P_{ST}^{\max} + P_R^{\max} + p_{c1} + p_{c2} \right]$. Then, the fitness function for each particle is obtained by solving the problem (A.11) with Algorithm A.1. Next, the obtained fitness function is used to update the position and velocity of the particles. Finally, the fitness function of the updated particles is obtained by solving the problem (A.11) with Algorithm A.1. The aforementioned procedure is repeated until convergence is being reached. Moreover, the relay selection is performed by the ES method.